Application of targeted contrast nanoparticles for human multiple myeloma imaging

Dorota Kozlowska

Ph.D. 2012

Application of targeted contrast nanoparticles for human multiple myeloma imaging

A thesis submitted for the degree of

Doctorate of Philosophy

by

Dorota Kozlowska M.Sc. (Hons).

Based on research carried out

in

The Applied Biochemistry Group,

School of Biotechnology,

Dublin City University,

Dublin 9,

Ireland.

February 2012

Under the supervision of Professor Richard O'Kennedy

Declaration:

I hereby certify that this material, which I now submit for assessment on the programme of study leading to the award of Doctorate of Philosophy is entirely my own work, that I have exercised reasonable care to ensure that the work is original, and does not to the best of my knowledge breach any law of copyright, and has not been taken from the work of others save and to the extent that such work has been cited and acknowledged within the text of my work.

Signed: _____ (Candidate) ID No.: _____ Date: _____

This thesis is dedicated
to my parents.

Abstract

Magnetic resonance imaging (MRI) is capable of three dimentional non-invasive imaging of opaque tissues at near cellular resolution. Among the imaging techniques available, MRI has, perphaps, the greatest potential to exploit the possibilities that molecular imaging presents. Nanoparticles (1-100 nm and 100-2500 nm in size) are the focus of intense interest, due their potential applications in the biomedicine and especially as labelling agents in imaging. This research is based on development of nanoparticles (immunoliposomes) as targeted contrast agents for molecular magnetic imaging of human multiple myeloma. It uses an application of antibody (CD138; syndecan-1) to target liposomes and other particles for delivery of MRI contrast agents to cell-surface based biomarkers. The use of gadolinium-loaded polychelating amphiphilic polymer (PAP) for incorporation into liposome membranes, and for conjugation with CD138 antibody was also examined. The diagnosis of human multiple myeloma currently requires the performance of a range of tests and the assessment of marrow specimens derived from invasive biopsy. The strategy undertaken in this research should provide an alternative and potentially more beneficial way of addressing this problem.

Table of Contents

List of Figures

List of Tables

Abbreviations

34A	antibody against mouse pulmonary gp112 endothelial cells
anti-CD166	single chain antibody mediating intracellular delivery
anti-VEGFR-2	anti-vascular endothelial growth factor receptor-2
Ab	antibody
AbII	secondary antibody
ADCC	antibody-dependent cell cytotoxicity
AP	alkaline phosphatase
BSA	bovine serum albumin
BMSC	bone marrow stromal cells
CBZ	ε-carbobenzyoxy-l-lysine
cDNA	complementary deoxyribonucleic acid
CLL	chronic lymphocytic leukaemia
cRGD	cyclic Arg-Gly-Asp peptide
DC101	murine antibody against VEGFR-2
DCC	N,N'-dicyclohexylcarbodiimide
dH_2O	distilled water
DNA	deoxyribonucleic acid
dNTP	deoxyribonucleotide trophosphate
DDAB	dimethyldioctadecylammonium
DOC	deoxycholate
DOPE	1,2-dioleoyl-*sn*-glycero-3-phosphoethanolamine
DOTA	1,4,7,10-tetra-azacyclododecane-1,4,7,10-tetraacetic acid

DOTA-DSA	2-{4,7-bis-carboxymethyl-10-[(N,N'-distearylamido-methyl]-1,4,7,10-tetra-azacyclododec-1-yl}-acetic acid
DOTAP	1,2-dioleoyl-3-trimethylammonium-propane
DSMZ	Deutsche Sammlung von Mikroorganismen und Zellkulturen
DSPC	1,2-distearoyl-*sn*-glycero-3-phosphocholine
DTT	dithiothreitol
EDC	1-ethyl-3-(3-dimethylaminopropyl)carbodiimide) hydrochloride
EDTA	ethylenediaminetetraacetic acid
e.g.	from the latin 'exempli gratia'
EGTA	ethylene glycol tetraacetic acid
ELISA	enzyme-linked immunosorbent assay
EPR	enhanced permeability and retention
FACS	Fluorescence-Activated Cell Sorting
Fab'	fragment antibody binding
FBS	foetal bovine serum
FCS	foetal calf serum
FITC	fluorescein isothiocyanate
FLISA	fluophore-linked immunosorbent assay
GAG	glycosaminoglycan
GAH	human monoclonal antibody recognizes non-muscle myosin expresses by gastic, colorectal and mammary cancer cells

Gd-DTPA-BSA	diethylenetriaminepentaacetic acid α,ω-bis(8-stearoyla-mido-3,6-dioxaoctyl-amide) gadolinium salt
Gd-DTPA	gadolinium-diethylenetriaminepentaacetic acid
GM1	ganglioside, a glycolipid
gp80	glycoprotein 80
gp130	glycoprotein 130
HER2	human epidermal growth factor receptor 2
HEPES	4-(2-hydroxyethyl)-1-piperazinethanesulfonic acid
HPH	high pressure homogenisation
HPMA	N-(2-hydroxypropyl)-methacrylamide
HUVEC	human umbilical vein endothelial cells
ICAM	intracellular adhesion molecule
ICP-AES	Inductively-Coupled Plasma-Atomic Emission Spectroscopy
IgG	Immunoglobulin class G
IL	immunoliposome
IL-6	interleukin-6
IMAC	immobilized-metal affinity chromatography
IMS	industrial methylated spirits
IPTG	isopropyl-ß-D-1-thiogalactopyranoside
JAK	jun-activated kinase
kDa	kilodaltons
mAb	monoclonal antibody
LDH	lactate dehydrogenase
LFA-1	leukocyte-associated antigen-1

Lon	mitochondrial protease inhibiting protein expression by binding to promotor
LUV	large unilamellar vesicles
MAPK	mitogen-activated protein kinase
MES	2-(N-morpholino)-ethanesulfonic acid
MGUS	monoclonal gammopathy of undetermined significance
MLV	multilamellar vesicles
MM	multiple myeloma
MOPS	3-morpholinopropane-1-sulfonic acid
MR	magnetic resonance
MRI	magnetic resonance imaging
MPS	mononuclear phagocyte system
MTT	1-(4,5-dimethylthiazol-2-yl)-3,5-diphenylformazan
NGPE	1,2-dioleoyl-*sn*-glycero-3-phosphoethanolamine-N-(glutaryl)
NHS	N-hydroxysulfosuccinimide
NMR	Nuclear Magnetic Resonance
OmpT	outer membrane protease
OX26	monoclonal antibody against the transferrin receptor
PAGE	Polyacrylamide gel electrophoresis
PAP	polychelating amphiphilic polymer
PBS	Phosphate buffered saline
PC	L-α-phosphatidylcholine (egg, chicken)
PEG	polyethylene glycol

PEG-DSPE	polyethylene glycol-1,2-distearoyl-s*n*-glycero-3-phosphatidylethanolamine
PET	positron emission tomography
PI3K	phosphatidyl-3-kinase
poly(CBZ)-lysine	poly(ε-carbobenzyoxy-l-lysine)
RES	reticuloendothelial system
REV	reverse-phase evaporation
RT	room temperature
R_1	longitudinal relaxation rate
R_2	transverse relaxation rate
r_1	longitudinal relaxivity
r_2	transverse relaxivity
scFv	single chain variable fragment (of an antibody)
SATA	succinimidyl-S-acetyl thioacetate
SB	super broth
SDS	sodium dodecyl sulphate
SLN	solid lipid nanoparticles
SMM	smoldering multiple myeloma
SPDP	N-succinimidyl-pyridyl-dithiopropionate
SPECT	single photon emission computed tomography
SPIO	superparamagnetic iron oxide
STAT1	nuclear transcription factor 1 upregulating interferon stimulated genes by binding to the promoter
STAT3	nuclear transcription factor 3 upregulating interferon stimulated genes by binding to the promoter

NF-κB	nuclear transcription factor
SUV	small unilamellar vesicles
t_r	rotational correlation time
t_D	translational diffusion time
t_M	water residence time
TCA	trichloroacetic acid
TfR	transferrin receptor
T_1	longitudinal relaxation time
T_2	transverse relaxation time

Units

µg	microgram
(k)Da	(kilo) Daltons
µL	microlitre
µM	micromoles
°C	degrees Celcius
cm	centimetres
g	grams (mass)
h	hours
kg	kilogram
L	litre
m	metre
M	molar
mg	milligram
min	minute
mL	millilitre
mm	millimetres
ms	millisecond
nm	nanometre
mol	molar
rpm	revolutions per minute
s	seconds
v/v	volume per unit volume
w/v	weight per unit volume

Publications and Presentations

Publications:

Kozlowska, D., Foran, P., MacMahon, P., Shelly, MJ., Eustace, S. and O'Kennedy, R. (2009) Molecular and magnetic resonance imaging: The value of immunoliposomes, Adv. Drug. Deliv. Rev., **61**(15):1402-11.

Posters:

MacMahon, P., **Kozlowska, D.**, Eustace, S. and O'Kennedy R. (2007) CD138 targeted superparamagnetic nanoparticles: A potential multiple myeloma-specific MR Contrast Agent, Radiological Society of North America Connecting Radiology, November 25-30th , Chicago, USA.

Foran, P., **Kozlowska, D.**, MacMahon, P., Shelly, M., Eustace, S. and O'Kennedy R. (2009) Targeting gadolinium to the HER2 receptor using immunoliposomes, Annual Breast Cancer Meeting, Mater Misericordiae University Hospital, 14-15th May, Dublin, Ireland.

Presentations:

Foran, P., **Kozlowska, D.**, MacMahon, P., Shelly, M., Eustace, S. and O'Kennedy R. (2009) Molecular magnetic resonance imaging: the value of immunoliposomes, Annual Scientific Meetings, RCSI (Royal College Surgeons in Ireland), Faculty of Radiologists, 24-26th September, Dublin, Ireland.

Foran, P., **Kozlowska, D.**, MacMahon, P., Shelly, M., Eustace, S. and O'Kennedy R. (2009) Molecular Magnetic Resonance Imaging of Multiple Myeloma and HER2-positive Breast Cancer, Annual Scientific Meetings, RCSI (Royal College Surgeons in Ireland), Faculty of Radiologists, 24-26th September, Dublin, Ireland.

External collaboration:

- Pharmaceutical Biotechnology and Nanomedicine Centre, Northeastern University, Boston, USA.

Internal collaboration:

- Mater Misericordiae Hospital, Radiology Department, Dublin, Ireland.
- Cappagh National Orthopaedic Hospital, Radiology Department, Dublin, Ireland.
- Chemical Sciences, Dublin City University, Dublin, Ireland.

Chapter 1

Introduction

1.1 Introduction

Molecular imaging is a relatively new and exciting area in diagnostic imaging. It can be defined as the *in vivo* characterisation and measurement of biological processes at the cellular and subcellular level (Allport and Weissleder, 2001). Magnetic Resonance Imaging (MRI) is achieved through a combination of imaging and active targeting of a contrast agent to disease-specific markers enabling minimally non-invasive, specific detection of biochemical markers. Molecular imaging differs from 'traditional' imaging approaches, which rely primarily on registering and interpreting differences in image contrast between tissues, normal or pathological, which represent the anatomical expression of disease. In contrast, molecular imaging looks to improve diagnostic accuracy through the visualisation of processes or components that cause disease (Lanza *et al.,* 2003). Thus, the development of molecular imaging can be seen as complementary to well-established imaging techniques rather than a potential replacement for them.

The most commonly used techniques for molecular imaging have been nuclear methods (positron emission tomography - PET and single positron emission computed tomography - SPECT) (Phelps 2000) and MRI (Weissleder *et al.,* 1997). In more recent times ultrasound (Liang and Blomley, 2003) and optical techniques (Baeten *et al.,* 2009) have also been applied. Each modality has advantages and disadvantages, some of which are outlined in Table 1.1. For example, nuclear methods (SPECT and PET) have high sensitivity but low spatial resolution and poor definition of anatomy. MRI, in contrast, exhibits good spatial resolution but low sensitivity, though this can be improved by the use of contrast agents with

high relaxivity. Ultimately, the specific molecular process that is being targeted will determine the choice of technique. However, among the approaches outlined MRI alone combines the benefits of high spatial resolution with the capacity to extract physiological and anatomical information (Smith *et al.,* 1994; Phelps, 2000) and in this introduction the focus is on this particular modality's role in molecular imaging.

Table 1.1 Summary of the differences between imaging modalities and their possibilities for nanoparticle applications.
Adapted from Kairemo *et al.* (2008).

MODALITY	SPATIAL RESOLUTION	DEPTH	TEMPORAL RESOLUTION	SENSITIVITY (mol/L)
PET	1-2 mm	No limit	10s-min	10^{-11}-10^{-12}
SPECT	0.5-1 mm	No limit	min	10^{-10}-10^{-11}
MRI	25-100 μm	No limit	min-h	10^{-3}-10^{-5}
CT	50-200 μm	No limit	min	10^{-2}-10^{-4}
Ultrasound	50-500 μm	mm-cm	s-min	10^{-3}-10^{-4}

1.2 Magnetic Resonance Imaging

MRI exploits the remarkable range of physical and chemical properties of water protons e.g. hydrogen nuclei (Mulder *et al.,* 2004) and has emerged as one of the leading minimally non-invasive imaging modalities (Aime *et al.,* 2002). The signal detected in MRI is created through the interaction of total water signal (proton density) and the magnetic properties of the tissues

being imaged (Caravan *et al.,* 1999). The magnetic properties in question are the longitudinal relaxation time, T_1, and transverse relaxation time, T_2. The reciprocal of these values represent the longitudinal and transverse relaxation rates (1/s), R_1 and R_2, respectively. Signal tends to increase with increasing R_1 and decrease with increasing R_2. Pulse sequences that emphasise changes in R_1 are referred to as T_1-weighted, those that emphasise changes in R_2 T_2-weighted scans. Proton longitudinal and transverse relaxation times are dependent upon the physiochemical environment of a given tissue and are modified in the presence of a pathological state (Aime *et al.,* 2002). Hence, MRI enables differentiation between various tissues in the body as well as between normal and pathological tissues.

1.2.1 Nuclear spin behaviour in a magnetic field

When a nucleus with magnetic moment μ is placed in a uniform external magnetic field, B_0, the nuclear spin, which are otherwise randomly oriented, will align in definite directions relative to the direction of B_0. There are only two possible orientations of the magnetic moments allowed for a proton nucleus with spin ½. The moments can either be aligned parallel or antiparallel to the direction of B_0, corresponding to a lower energy α-state or higher energy β-state, respectively. The population ratio between the number of nuclei in the higher and lower energy levels is described by the Boltzmann relationship:

$$\frac{N_\alpha}{N_\beta} = e^{\frac{\Delta E}{k_B T}}$$

The number of nuclei in the higher and lower energy level is dependent upon the absolute temperature of the sample, T, the strength of the magnetic field, and the nuclear magnetic moment. The value of ΔE is very low. The resulting slight excess of nuclei in the lower spin state produces a small net macroscopic nuclear magnetisation, aligned with B_0, called the equilibrium magnetisation (Figure 1.1).

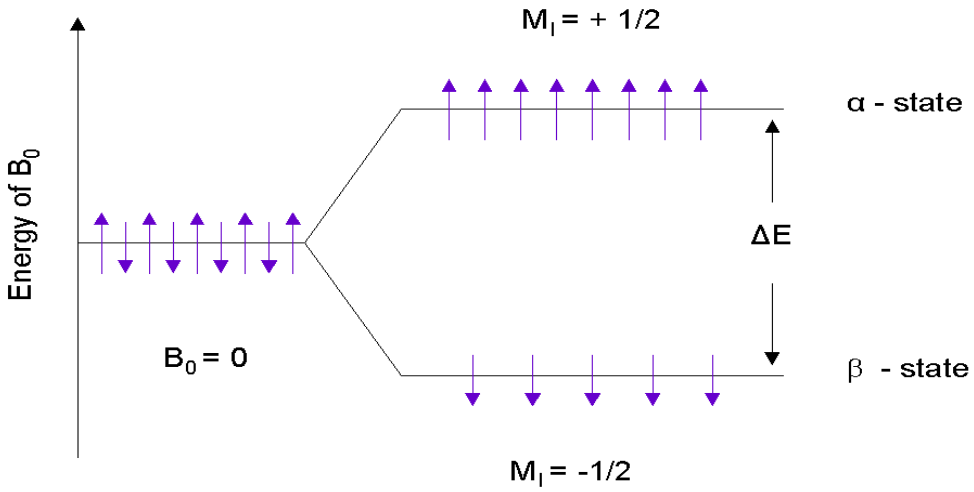

Figure 1.1 Representation of the equilibrium distribution of nuclear spins in the presence of magnetic field, B_0.

Before applying the rf (radiofrequency pulse), the magnetic moments are in the α- or β-states each precesses around the z-axis. The frequency of precession, known as the Larmor frequency, is proportional to the field strength and the nuclear magnetic moment. The equilibrium magnetisation

vector M_0 is the vector sum of all the individual moments of the proton nuclei and is aligned along B_0 (Figure 1.2).

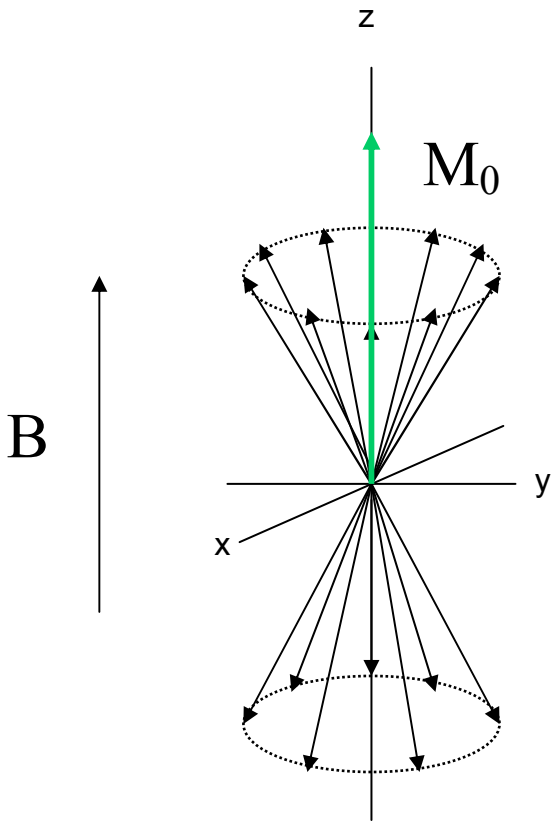

Figure 1.2 Representation of ensemble of nuclear spins in the presence of a magnetic field applied along the z-axis.

When a radiofrequency pulse (rf) is applied into the plane perpendicular to B_0. Transitions between the spin states are induced. The perturbation will rotate the magnetisation away from its original position. The new magnetisation vector M_{xy} now precesses about the z-axis but produces a non-zero magnetisation component in the xy plane. After the rf pulse is switched off the individual nuclei begin to undergo relaxation by releasing the absorbed rf energy, re-establishing the thermal equilibrium Boltzmann population of nuclear spins. The RF coil, which acts as an antenna, is only sensitive to magnetisation in the xy-plane. The relaxation process can occur by two different mechanisms.

First, when the excitation pulse is discontinued, the individual nuclei can begin to undergo relaxation by releasing the absorbed rf energy to the surrounding lattice. This mechanism is known as longitudinal or spin-lattice relaxation (Figure 1.3). This corresponds to the sample magnetisation the return to its equilibrium position (to z-axis from y-axis).

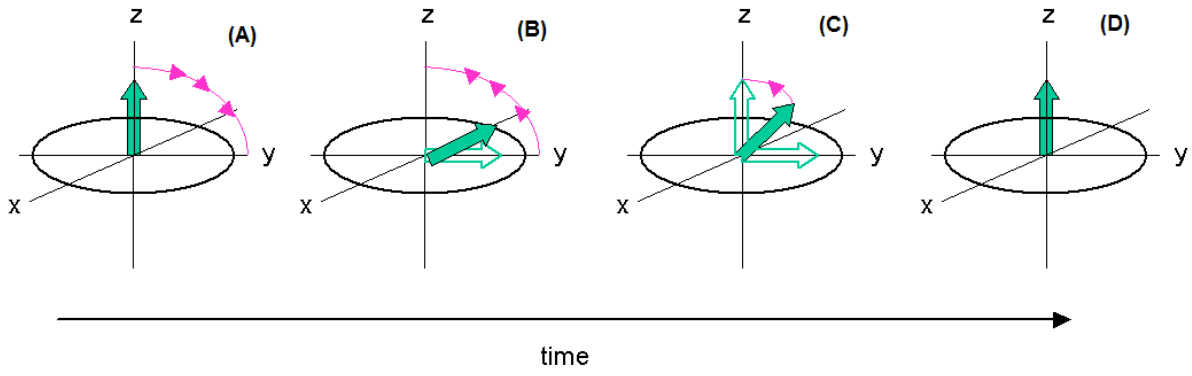

Figure 1.3 Schematic of magnetization undergoing longitudinal (spin-lattice) relaxation in time followed the radiofrequency (rf) pulse.

T_1, the longitudinal (spin-lattice) relaxation time, is the characteristic time required for the magnetisation to return to equilibrium.

The second type of relaxation mechanism is called transverse relaxation, or spin-spin relaxation (Figure 1.4). The nuclear spins slowly lose their phase coherence or order. This occurs, due to mutual simultaneous spin transitions, e.g. α to β and at the same time β to α. The T_2 process can be more rapid than T_1 process in some situations, but not reverse.

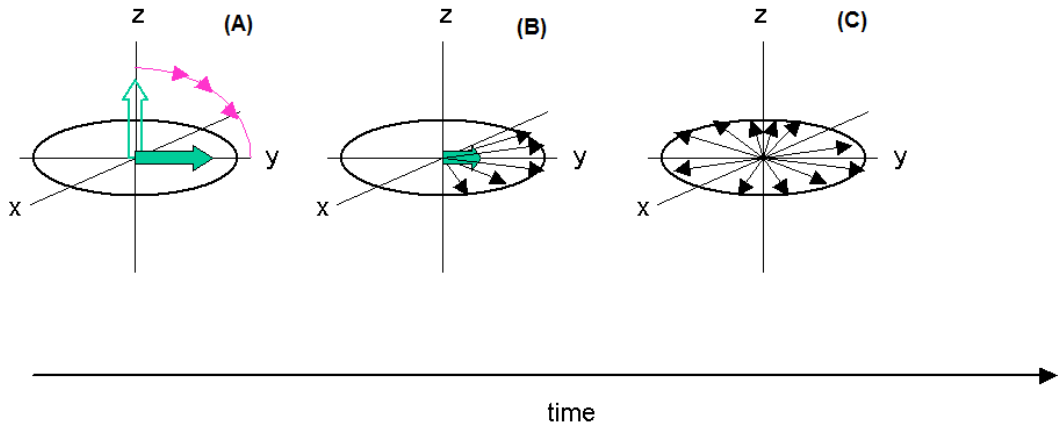

Figure 1.4 Schematic of magnetization undergoing tranverse (spin-spin) relaxation in time.

1.2.2 T_1-weighted imaging

Organs containing gadolinium ions will have increased ‘H NMR signal intensity if the image is recorded with T_1-weighting. That means that T_1-weighting images can be obtained by reducing time between successive scans. By performing successive scans without allowing full relaxation the signal obtained is weighted to that fraction at the ‘H magnetisation with shorter T_1.

1.2.3 Contrast Agents in MRI

Contrast agents are used in imaging to increase the signal difference between the area of interest and the background. Currently, approximately 35% of MRI examinations involve the use of contrast agents, but this percentage can be expected to increase further following the development of more effective and specific contrast media than those currently commercially available.

The contrast agents used in MRI act through, hereby the water proton relaxation, thus increasing longitudinal and transverse relaxation rates (R_1

and R_2) and, therefore, the intensity of the MR signal, in the regions where they are distributed (Aime *et al.,* 2002). Contrast agents increase both longitudinal and transverse rates but to varying degrees, depending on their nature as well as the applied magnetic field.

There are two main classes of contrast agents for MRI: paramagnetic complexes and superparamagnetic iron oxide particles. The former class includes mainly chelates of Mn(II), Mn(III) and Gd(III) ions, with gadolinium-based agents being the most commonly used. Paramagnetic agents increase R_1 and R_2 by similar amounts but are best visualised using T_1-weighted images since the percentage change in R_1 in tissue is much greater than that in R_2. Nanoparticulate contrast agents generally lead to a much larger increase in R_2 than in R_1 and are best seen with T_2-weighted scans. The ability of a contrast agent to increase R_1 and R_2 per millimolar of agent is defined as its longitudinal or transverse relaxivity, r_1 or r_2, respectively, and is expressed in $s^{-1}.mM^{-1}$ (Caravan *et al.,* 1999). T_1 agents usually have r_2/r_1 ratios of 1-2, whereas the value for T_2 agents, such as iron oxide particles, is as high as 10 or more. Paramagnetic agents directly affect water protons in their close vicinity and are highly dependent on local water flux. Hence, the influence of these agents is very local and they should ideally be in contact with water with adequate exchange rates. In contrast, superparamagnetic agents affect the magnetic field independent of their environment and, thus, their influence in terms of contrast extends well beyond their immediate surroundings (Lanza *et al.,* 2004).

However, MRI contrast agents are limited by their lack of specificity. Targeting of MRI contrast agents to distinct molecules associated with

tissue pathology would enable more specific diagnosis by MRI and provide the potential to characterise disease at the molecular level *in vivo*. The gadolinium contrast agents currently on the market require a tissue concentration in the order of 10^{-7} mol/g to obtain sufficient contrast in the resulting image (Gupta and Weissleder, 1996; Lanza *et al.,* 2004). Such a number is too high to be able to image sparse molecular biomarkers expressed in the living body since typical receptors are normally present in low concentrations of 10^{-9} to 10^{-13} mol/g (Strijkers *et al.,* 2005). An amplification strategy is required to overcome these sensitivity problems. One solution is to use nanoparticles since a high payload of a contrast agent can be incorporated in a single particle, thus increasing the effective relaxivity per particle; consequently, the signal detected during imaging increases (Glogard *et al.,* 2002).

1.3 Fast Field-Cycling NMR

Fast Field-Cycling NMR (FFC NMR) is a technique used to obtain longitudinal relaxation times, T_1 (R_1, relaxation rate-reciprocal of T_1) over a wide range of magnetic field strenghts. A plot of r_1 (relaxivity) as a function of frequency is known as a nuclear magnetic relaxation dispersion (NMRD) profile.

1.4 Nanoparticles

Nanoparticles are small clusters of atoms, approximately 10 to 100 nm in diameter, and they present an opportunity to improve drug delivery as well as targeting of contrast agents. Many varieties of nanoparticles are available. A short overview of some that are relevant to medical diagnostics

and therapeutics is given here. A more in-depth analyses of the advances made in the field of nanomedicine, with a particular focus on molecular magnetic resonance imaging are described in two excellent reviews by Mody *et al*. (Mody *et al.,* 2009) and Sun *et al.* (Sun *et al.,* 2008).

Lipid-based nanoparticles are among the most intensively studied group of nanoparticles, having been investigated since the 1970's. Liposomes are closed vesicles composed of one or more amphiphilic bilayers. Lipids used to create such bilayers are amphiphilic phospholipids with hydrophilic heads and hydrophobic tails (Figure 1.5). These bilayered membrane vesicles can range from 50 nm up to 5μm in size and have been utilized for the delivery of small molecules (Dass and Choong, 2006), proteins (Meldrum *et al.,* 2003), peptides (Torchilin *et al.,* 2001), DNA (Reimer *et al.,* 1999) and MR imaging contrast agents (Torchilin, 2005). The *in vivo* behaviour of liposomes is well established with modifications such as PEGylation resulting in longer circulation times. Liposomes will be discussed in greater detail in section 1.5.

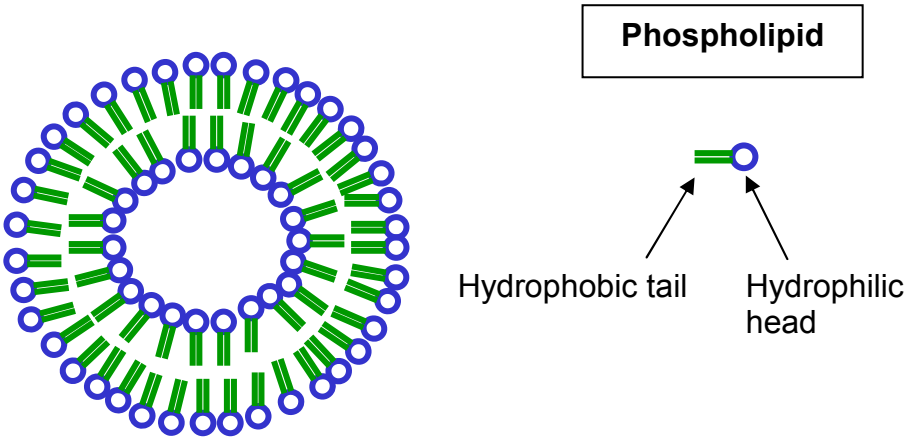

Figure 1.5 Illustration of a liposome.
Liposomes are composite structures made of phospholipids, which are composed of hydrophilic head and hydrophobic tail.

Solid lipid nanoparticles (SLN) represent an alternative lipid-based carrier system. They are colloidal particles of a lipid matrix that is solid at body temperature and may be stabilized by surfactant (Pardeike *et al.,* 2009) (Figure 1.6). They have potential as carriers for parenteral administration of hydrophobic drugs and also for improving oral absorption of drugs such as cyclosporin A (Müller *et al.,* 2000). SLN are commonly produced by high pressure homogenisation (HPH) or diluting warm micro-emulsions. Advantages of SLNs above other colloidal carriers include the use of physiological lipids in the lipid matrix (decreasing the danger of acute and chronic toxicity), production without use of organic solvents, prolonged physical stability and the possibility of protection of chemically labile active substances inside the particles.

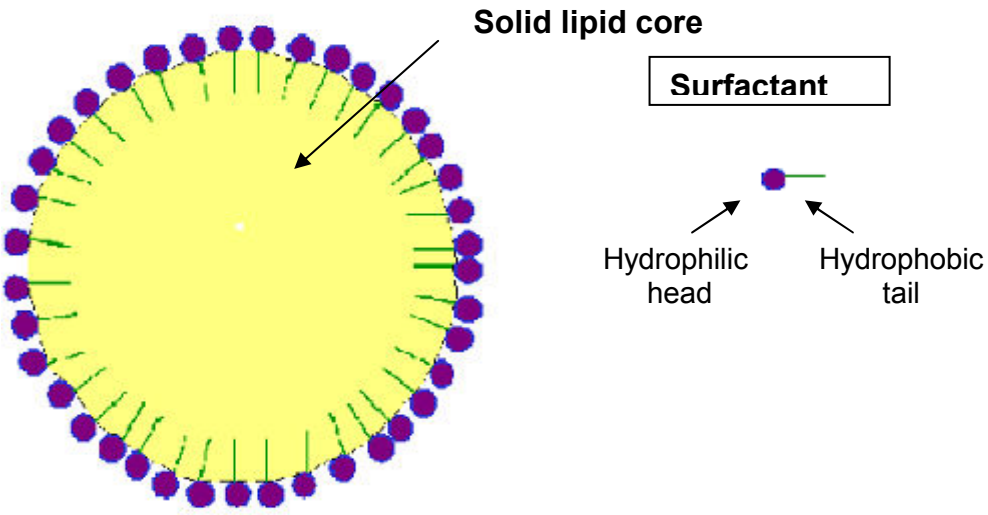

Figure 1.6 Diagram of solid lipid matrix stabilized by surfactant.
Solid lipid nanoparticles possess a solid lipid core matrix that can solubilize lipophilic molecules. The lipid core is stabilized by surfactants (emulsifiers), with hydrophilic heads and hydrophobic tails.

Another type of colloidal carrier is the polymeric nanoparticle. Research has focussed on conjugating drugs with polymers to form co-polymers (Debbage *et al.,* 2008) which are prepared as nanospheres or nanocapsules that generally increase the stability of volatile pharmaceutical agents and are easily and cheaply fabricated in large quantities. A polymeric coating of nanoparticles provides a steric barrier to prevent agglomeration and avoid opsonization. Furthermore, such coating provides a means to tailor the surface properties of nanoparticles such as surface charge and chemical functionality. Dextran, a polysaccharide, is one of the most widely utilized and successful polymer coatings in terms of *in vivo* applications (Gref *et al.,* 2000). Previously, many types of polymers were used as water-soluble drug carriers, e.g. Poly(ethylene glycol) (PEG) (Corot *et al.,* 2006), poly (L-glutamic acid) and N-(2-hydroxypropyl)methacrylamide (HPMA)

copolymers. HPMA copolymer-drug conjugates have been used in clinical trials (Vasey *et al.,* 1999) and HPMA polymer-drug conjugates, bearing a combination of two anti-cancer drugs differing in their mechanism of action, effectively inhibited growth of melanoma, solid tumours and metastases in mice (Poucková *et al.,* 2001) (Soucek *et al.,* 2002). Recently, HPMA copolymer-Gd-RGDfK conjugates demonstrated potential as effective targetable MR contrast agents for tumour imaging (Zarabi *et al.,* 2009).

Alternatively, polymeric micelles are nanocarriers that can water-solubilize hydrophobic drug molecules and/or contrast agents. These polymers are constructed with a branched, hydrophobic interior (core) and hydrophilic exterior (shell) to maintain physical properties characteristic of conventional micelles, but with enhanced thermodynamic stability. One example of polymeric micelles are the multifunctional cancer ligand-targeting polymeric micelles for controlled drug delivery and MRI contrast characterisation (Nasongkla *et al.,* 2006). The micelles harbour the chemotherapeutic agent doxorubicin, which is released through a pH-dependent mechanism. To enable MRI detection, a cluster of superparamagnetic iron oxide (SPIO) nanoparticles is loaded inside the hydrophobic core of the micelles. In addition, a cRGD ligand that targets $\alpha_v\beta_3$ integrin on tumor endothelial cells and induces receptor-mediated endocytosis is incorporated to direct micelles to their appropriate target.

Nanocrystals are single crystalline nanoparticles consisting of aggregates of hundreds of molecules combined in a single crystal with a thin coating as a surfactant. They are produced according to a technique called nanonization using dispersion in an aqueous surfactant solution (Möschwitzer *et al.,*

2006); nanocrystals are being developed to improve the bioavailability of poorly soluble drugs.

More complex structures, such as dendrimers and carbon nanotubes, are under development for targeted delivery of drugs. *Dendrimers* are synthetic, three-dimensional molecules with branching parts (see Figure 1.7). The branches are structured around a designed central core and, like a tree, expand outward *via* polymerisation reactions, which allow for exact shaping of the nanoparticle. The branched structure makes it possible to attach other molecules such as drugs and contrast agents (Tomalia *et al.,* 2007). They are formed using a nano-scale, multistep fabrication process.

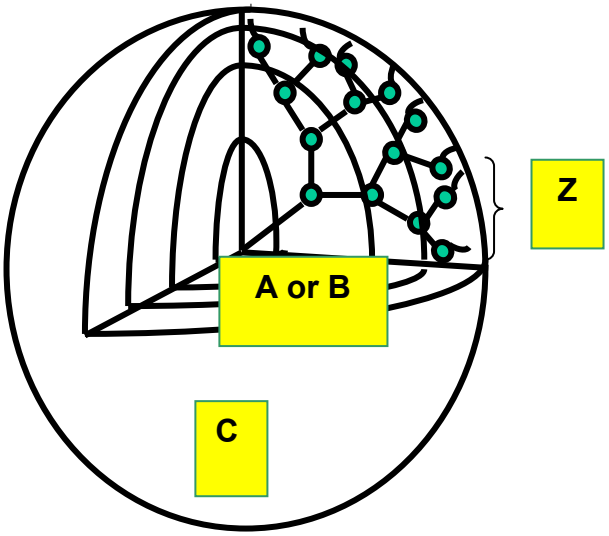

Figure 1.7 Illustration of general dendrimer architectural topology. Imaging moieties (A) or small molecular therapeutic components (B) may be incorporated into the interior. Receptor-mediated targeting groups (C) may be attached to the surface for active targeting. Low-toxicity surface groups (Z), such as PEG-DSPE-carboxylic acid, may also be attached.

Carbon nanotubes are sheets of atoms in the form of tubes, resembling tiny drinking straws (Martin *et al.,* 2003) (see Figure 1.8). They are considered optimal vehicles for the delivery of genes, peptides and proteins (Bianco *et al.,* 2005), although currently only used under experimental conditions.

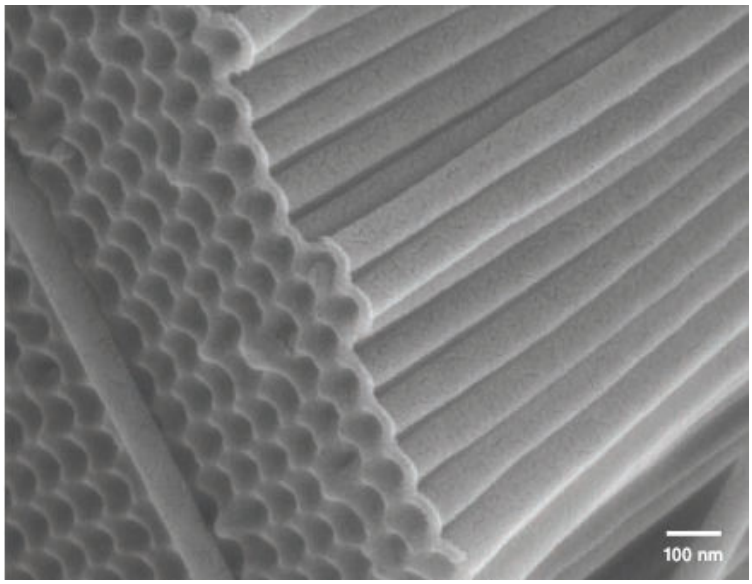

Figure 1.8 Scanning electron micrograph of an array of carbon nanotubes (Adapted from Bianco *et al.* (2005)).

1.4.1 Targeting of Nanoparticles

A key feature in using nanoparticles as targeted contrast agents is the ability of the particles to accumulate in or be directed to the area of interest. Such targeting may be passive or active.

1.4.1.1 Passive Targeting of Nanoparticles

The small size of a nanoparticle allows preferential extravasation in many solid tumours because of abnormal vascular membranes associated with tumour angiogenesis (Huang *et al.,* 1992). This is known as the enhanced permeability and retention (EPR) effect. It describes a phenomenon whereby relatively high molecular weight (40 kDa or higher), long circulating macromolecules, as well as various long-circulating nanoparticles, are capable of spontaneous accumulation in various pathological sites, e.g. solid tumors. Accumulation is due to 'leaky' vasculature at such sites, e.g., it

can be penetrated by large molecules and even small particles (Maeda *et al.,* 2001). In general this 'leakiness' of endothelial barriers in newly vascularised tumours is due to wide inter-endothelial junctions, large numbers of fenestrations and transendothelial channels, and discontinuous or absent basement membranes. Pore sizes in such tumours vary from 100 to 780 nm. By comparison, normal tissues outside the reticuloendothelial system (RES) generally have continuous and non-fenestrated vascular endothelia, and extravasation of liposomes is very limited (Ishida *et al.,* 2001); pore size is <2 nm in most tissues, 6 nm in post capillary venules, 40-60 nm for the kidney glomerulus, and up to 150 nm for sinusoidal epithelium of the liver and spleen (Seymour, 1992). This phenomenon allows for the extravasation and accumulation of nanoparticles in an interstitial tumour. Also, in many tumors, the absence of any lymphatic system, which is responsible for draining macromolecules from normal tissues, contributes to accumulation. The enhanced permeability and retention effect allows for passive targeting of nanoparticles to tumors based on the 'cut-off' size of the leaky vasculature (see Figure 1.9).

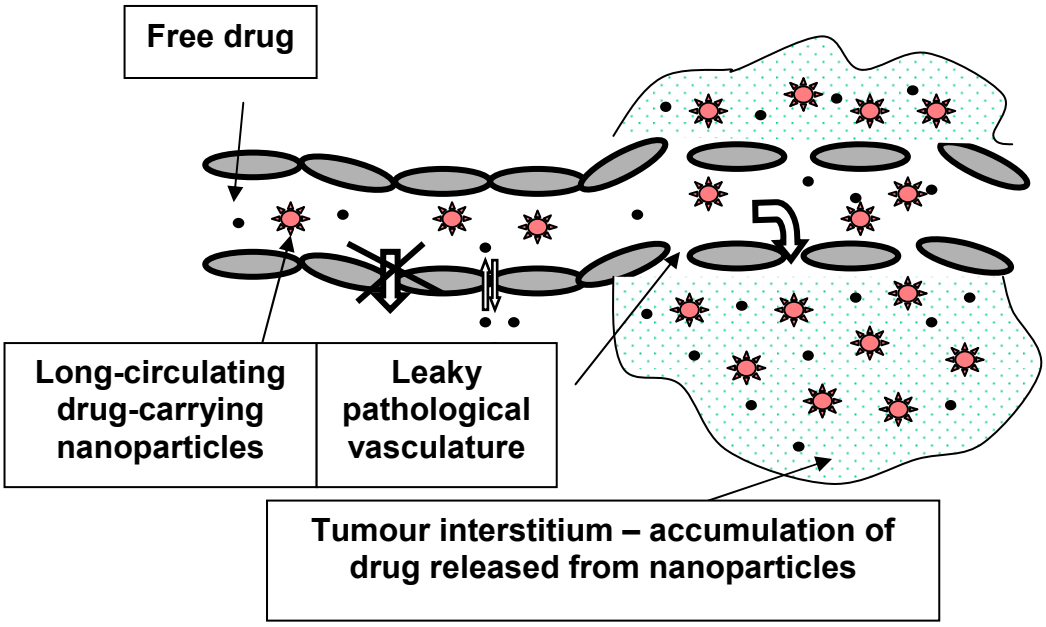

Figure 1.9 Passive tumour targeting with nanoparticles.
Long-circulating nanoparticles accumulate passively in solid tumor tissue by the enhanced permeability and retention effect. The hyperpermeable angiogenic tumour vasculature allows preferential extravasation of circulating nanoparticles.

1.4.1.2 Active Targeting of Nanoparticles

Although passive targeting mechanisms will increase the accumulation of nanoparticles in a tumor, however, they are unlikely to be sufficient to achieve the concentrations necessary for successful molecular magnetic resonance imaging. Furthermore, larger tumors show poor vascularization, especially inside necrotic areas, preventing the localisation of nanoparticles in the tumor. Hence, improved targeting of nanoparticles to tumors is necessary. This may be achieved by conjugating the nanoparticles to biological recognition moieties (ligands) that recognize cell surface antigens or receptors in the target tissue (Mulder *et al.,* 2006). A wide variety of ligands can potentially be used to target cellular biomarkers including

antibodies (Park *et al.,* 2002), other proteins (Yang *et al.,* 2009), peptides (Chang *et al.,* 2009) and polysaccharides (Sihorkar *et al.,* 2001).

Nanoparticles require certain characteristics to facilitate molecular imaging: their circulating half-life should be in on the order of hours to allow sufficient exposure and interaction with the binding site (cellular biomarker), they should bind specifically to the epitope chosen for their visualization, they should have an acceptable toxicity profile and they should fit easily into the clinical routine (Lanza *et al.,* 2004).

Perhaps the most common method for targeting such cellular epitopes is the use of monoclonal antibodies. These antibodies have been investigated extensively for cancer cell recognition and have been used successfully in the treatment of certain cancers especially non-solid tumours such as Non-Hodgkin's lymphoma (Wang *et al.,* 2008). Many factors need to be taken into consideration when using monoclonal antibodies, including proper choice of target antigen, antibody function and antibody-nanoparticle linkage (Park *et al.,* 1997). Thus, an appropriate tumor antigen must be identified and interaction with a given antibody determined.

Identification of tumor-specific antigens has proven difficult because most tumors do not possess unique antigens, but express the same antigens as normal tissue but in greater quantities. Additionally, many tumors do not overexpress the antigens homogeneously throughout the primary tumour or may not express them in metastases. Some antigens may be shed or secreted, leading to potentially high levels of soluble antigen that could interfere with cell targeting.

Despite the potential difficulties, successful use of monoclonal antibodies (mAbs) such as herceptin® (Trastuzumab, antibody to the HER2 receptor) in immunotherapy suggests that antibody targeting may represent a viable approach. This antibody has been used to target liposomes carrying the chemotherapeutic agent doxorubicin, to breast cancer cells in mice. Doxorubicin encapsulated in herceptin®-targeted liposomes was found to be more effective than free doxorubicin or herceptin® alone in inhibiting the growth of cancer cells (Park *et al.,* 2002). Similarly Fab^1 fragments of the monoclonal rat anti-VEGFR-2 antibody DC101 were used to target liposomes carrying doxorubicin to tumor endothelium. These immunoliposomes caused a significant delay in tumor growth compared to empty DC101-conjugated immunoliposomes, free doxorubicin and HEPES/glucose, and resulted in a higher amount of necrotic areas in the tumors (Roth *et al.,* 2007). Immunoliposomes conjugated to an antibody against CD166 scFv (single chain variable fragment) successfully delivered the chemotherapeutic agent topotecan to prostate cancer cells. Targeted delivery of liposomal topotecan achieved significantly greater cell killing than either non-targeted liposomes or free topotecan (Roth *et al.,* 2007).

Monoclonal antibodies have also been used to develop targeted contrast agents. Gold nanoparticles conjugated with monoclonal antibodies to three different proteins (the epidermal growth factor receptor, matrix metalloproteinases and E7 oncoprotein) were used successfully to optically image their target proteins (Sokolov *et al.,* 2004). Qiao *et al.* (2011) demonstrated that Gd^{3+}-chelated protein-based (ProCA1) MRI contrast moiety HER2-targeted affibody-conjugated showed higher relaxivity value

than non-targeted moiety in ovarian cancer (SKOV-3) and breast cancer (MDA-MB-231) cell lines *in vivo*. Further, Wang *et al.* (2011) prepared a *novel* monoclonal anti-BRCAA1 (protein overexpressed in 64% gastric cancer tissue) FMNPs (silica-coated quantum dots and super-paramagnetic nanopatricles) nanoprobes, which are effective for *in vivo* two modal imaging such as fluorescent imaging and magnetic resonance imaging.

Endogenous chemicals, for which receptors are present in increased numbers in specific tissues, can be used for nanoparticle targeting. An example of this phenomenon is folate, which was used successfully to target nanoparticles to folate receptor-expressing cells (Hilgenbrink and Low, 2005). Significant tumor regression of a folate receptor-expressing cancer in mice was observed after doxorubicin-carrying micelles, with folate attached, were administered to the mice (Yoo and Park, 2004). Transferrin has also been used in this manner to target cancer as most tumor cells overexpress the transferrin receptor. Paclitaxel-loaded biodegradable nanoparticles were shown to have greater anti-tumor activity compared to the free form of the drug in the murine model of prostate cancer following conjugation to transferrin (Sahoo *et al.,* 2004).

1.5 Liposomes

Liposomes are defined, quasi-spherical, self-closed structures formed by one or more concentric lipid bilayers containing an aqueous phase inside and between the bilayers (Torchilin, 2005) (see Figure 1.1). The lipids used in the formation of liposomes are usually comprised of a hydrophilic

headgroup and two hydrophobic fatty acyl chains. These amphiphilic molecules spontaneously assemble into aggregates in an aqueous environment. Water-soluble molecules occupy the aqueous compartment, whereas molecules of a more lipophilic character occupy the lipid bilayers. Liposomes can vary substantially in size and lamellarity. They are subdivided into multilamellar vesicles (MLV) consisting of several concentric bilayers, large unilamellar vesicles (LUV) and small unilamellar vesicles (SUV) that are less than 150 nm in diameter.

Liposomes can be formed by a variety of methods. When they are prepared by hydration of the dried lipid mixture, they spontaneously form MLVs. Other procedures, such as prolonged exposure to ultrasound or pressure-driven filtration through small-pore filters, cause MLVs to form SUVs.

Other procedures lead to the formation of LUVs (Sulkowski *et al.,* 2005). For instance, large vesicles are prepared from an initial phosphatidylserine aqueous solution, which, when sonicated and subjected to ultrasound, produces small unilamellar vesicles (SUV) with diameters of 200-500 Å. After adding 1 to 10 mM (threshold 1-2 mM) calcium ion (Ca^{2+}) and incubating for 30-60 min at a room temperature above 10°C (preferably 37°C), intermediate cochleate (spiral-shaped) lipid cylinders form. Finally, addition of a calcium-chelating agent, such as EDTA or EGTA to these cochleate cylinders produces the desired large closed spherical unilamellar vesicles (LUV) by fusion (United States Patent 4078052).

Liposomes (LUVs), with a large internal aqueous space and high capture capacity, are produced by reverse-phase evaporation (REV). The procedure is based on the formation of ‘inverted micelles’ - small water droplets which

are stabilized by a phospholipid monolayer and dispersed in excess of organic solvent. Slow removal of the organic solvent leads to transformation of these inverted micelles into a viscous gel-like state. At a critical point in this procedure, the gel state collapses and some of the inverted micelles disintegrate. The resulting excess of phospholipid contributes to the formation of a complete bilayer around the remaining micelles, leading to the formation of LUVs.

1.5.1 Pharmacokinetics of liposomes

The pharmacokinetics of liposomes depend on their physiochemical characteristics such as size, surface charge, membrane lipid packing, steric stabilization, dose and route of administration (Barenholz, 2003). In general, larger liposomes are eliminated from the blood circulation more rapidly than smaller ones (Senior *et al.,* 1982). Binding of opsonins to liposomes depends on liposome size; consequently, the reticuloendothelial (RES) uptake of liposomes by the liver is size-dependent (Harashima *et al.,* 1994). The action of the reticuloendothelial system results in rapid removal from the blood and accumulation in tissues such as liver and spleen.

In vivo behaviour of liposomes is also determined by their constituent parts, viz., phospholipids and other amphiphilic molecules, cholesterol and molecules bound to the liposome surface. The circulatory half-life of liposomes can be significantly increased through use of sterically shielded lipids in their construction. ‘Steric stabilization’ refers to the colloidal stability resulting from the attachment of hydrophilic polymers or glycolipids on to the

liposome surface (see Figure 1.10). These liposomes are less reactive toward serum proteins and less susceptible to RES uptake than non-stabilized liposomes (Allen *et al.,* 1995). Hence, such liposomes show prolonged life-times in the circulation. The putative mechanism by which sterically stabilized liposomes are thought to decrease RES-mediated places the stabilizer in the space immediately adjacent to the liposomal surface effectively excluding other macromolecules from this space. Consequently, access to and binding of blood plasma opsonins to the liposome surface are hindered, preventing interactions with RES macrophages.

Polyethylene glycol (PEG) is the most widely used polymeric steric stabilizer. PEG is a linear polyether diol with many useful properties. It is highly soluble in aqueous and organic media and possesses very low immunogenicity and antigenicity (Dreborg *et al.,* 1990) and is non-toxic. It can be attached to the liposome surface in various ways, but the most widely used method is to anchor the polymer in the liposome membrane *via* a cross-linked lipid (PEG-DSPE) (Allen *et al.,* 1995). The grafted polymer moiety extends about 50 Å from the lipid surface and exerts a strong inter-membrane repulsive force (Needham *et al.,* 1992). It was shown that steric stabilisation of liposomes with PEG increases their longevity in the circulation (Drummond *et al.,* 1999). In a similar fashion, the glycolipid ganglioside, GM1, also prolongs circulatory life-time of liposomes when attached to the exterior wall (Gabizon *et al.,* 1988).

A supplementary method to ensure long circulation times involves adding cholesterol to the lipid bilayer. Cholesterol acts as a spacer between

phospholipids of the liposome membrane because of its inflexible structure, thus preventing demixing of the lipids and reducing PEG chain-chain interactions. This results in improved steric stabilization of the liposomes. Most optimal formulations for long circulation times contain more than 30% (w/v) cholesterol and low concentrations (5 mol%) of PEG (Strijkers *et al.,* 2005).

The phospholipids used while concentrating liposomes affect the circulatory life-time of liposomes by altering membrane fluidity. This is most likely caused by increased protein binding to hydrophobic domains exposed by packing defects in gel-phase membranes (Drummond *et al.,* 2008). The presence of charged lipids in liposome construction also tends to increase clearance from the circulation, though the relationship is complex (Drummond *et al.,* 1999). However, charged lipids can be useful in attaching therapeutic substances to liposomes.

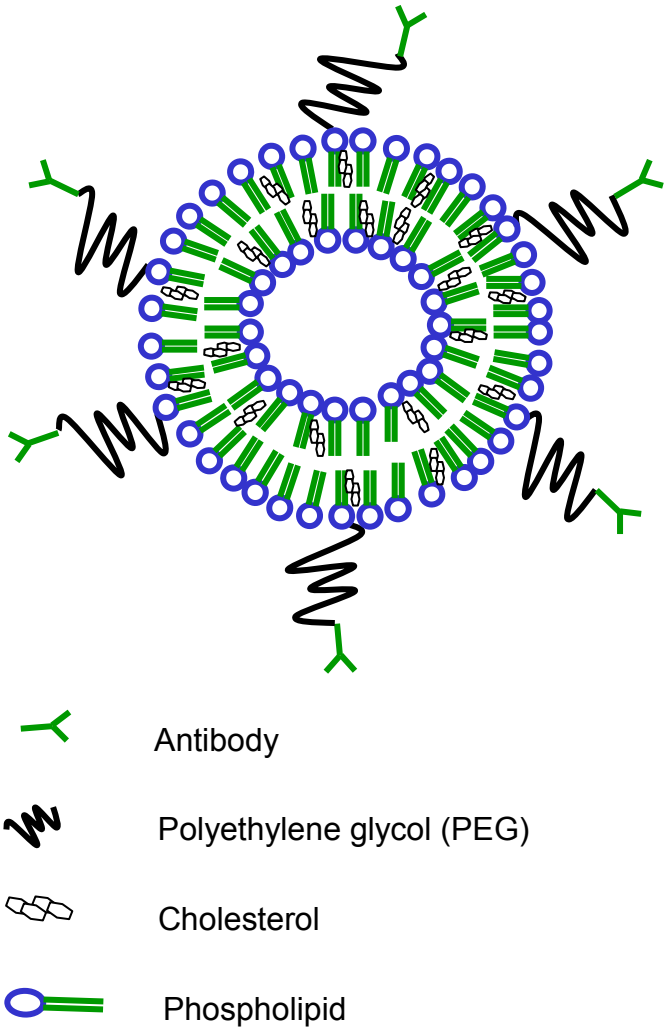

Figure 1.10 Sterically stabilized PEGylated paramagnetic immunoliposome.
This schematic representation shows antibodies coupled to the distal end of the PEG-chains.

1.6 Targeting of liposomes to cells or tissues

The use of targeted liposomes was suggested to increase liposomal accumulation in desired tissues. This involves the coupling of ligands to liposomes leading to specific binding to the required target cells.

1.6.1 Immunoliposomes

The term immunoliposome was coined to describe a liposome conjugated to an antibody or portions of an antibody (Siwak *et al.,* 2002). Immunoliposomes appear to have immunogenic potential that is attributed to the constant region of the immunoglobulin (Harding *et al.,* 1997). The use of chimeric or humanized monoclonal antibodies or antibody fragments can reduce or minimise a host's immunologic response against the therapeutic antibody/fragment (Winter and Harris, 1993).

Conjugation of the antibody to the liposome presents a challenge in the construction of immunoliposomes. The location of the linkage is first considered. Studies on usage of conventional ('PEG-free') immunoliposomes (Type A in Figure 1.11) show that there is enhanced uptake by the RES (Aragnol *et al.*, 1986). These immunoliposomes are effective in specific binding to target cells *in vitro* but their targeting efficiency *in vivo* is relatively low.

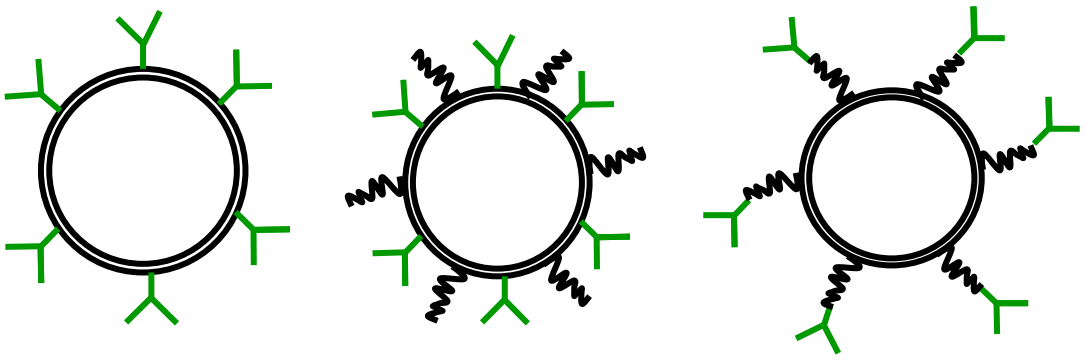

TYPE A *TYPE B* *TYPE C*

Figure 1.11 Illustration of the conjugation of antibodies to liposomes. Type A: 'PEG-free' immunoliposomes with antibody directly linked to the lipid; Type B: PEG-immunoliposomes with antibody directly linked to the lipid; Type C: Pendant PEG-immunoliposomes with antibody conjugated to the distal end of the PEG chain.

PEGylated liposomes are sterically stabilized with PEG, as discussed earlier, thus reducing RES uptake and consequently, prolonging their circulatory life-times. Such steric stabilization has been combined with antibody targeting of liposomes *via* attachment directly to the lipid bilayer (see Type B in Figure 1.9). However, the steric barrier of PEG decreases the protein coupling efficiency at the liposome surface as well as the target recognition, especially where higher concentrations of PEG (with high molecular weight) are used (Aragnol *et al.*, 1986).

In order to overcome these problems, antibodies were coupled to the terminal ends of PEG to increase antibody accessibility. A pendant-type PEG-immunoliposome was developed with monoclonal antibodies or their fragments attached at the distal ends of the PEG chains (see Type C in Figure 1.9) (Maruyama *et al.,* 1995). These liposomes showed improved binding to their specific target when compared to both Type A and Type B due to the combined benefits of steric stabilization by PEG and improved antibody accessibility.

1.6.2 Conjugation of Antibodies to Liposomes

Various types of linkages can be used to attach antibodies, entire units or fragments, to liposomes in order to create immunoliposomes. Antibodies can be attached to lipids, such as phosphatidylamine (PE), either before or after liposome formation depending on the particular strategy employed. The bonds formed fall into two main categories, noncovalent and covalent.

1.6.2.1 Non-covalent conjugation

Liposomes incorporating biotin-modified lipids can be easily prepared and used to attach a variety of avidin/streptavidin-linked targeting proteins. The primary advantage of this technique is that many different site-directing ligands can be used with a single well-defined liposome preparation. Examples of non-covalent conjugation procedures include the use of biotinylated ligands bound to streptavidin-conjugated liposomes (Pan *et al.,* 2008) or antibody bound to protein A - bearing liposomes (Machy *et al.,* 1984). Ligands such as avidin, streptavidin, protein A or protein G can be attached to liposomes by use of covalent conjugation procedures on section 1.6.2.2.

1.6.2.2 Covalent conjugation

Two efficient and selective methodologies for conjugating antibodies to liposomes are examined here.

a) Attachment of proteins and peptides to liposomes *via* amino groups

An amide bond is formed in two stages to achieve conjugation. In the first stage, free carboxylates on the terminal end of a PEG chain are activated with water-soluble N,N'-dicyclohexylcarbodiimide (DCC). In the second stage, protein or peptide solutions are added at pH 8.0; the activated carboxyl groups react with amino groups on the protein to produce an amide bond (see Figure 1.12).

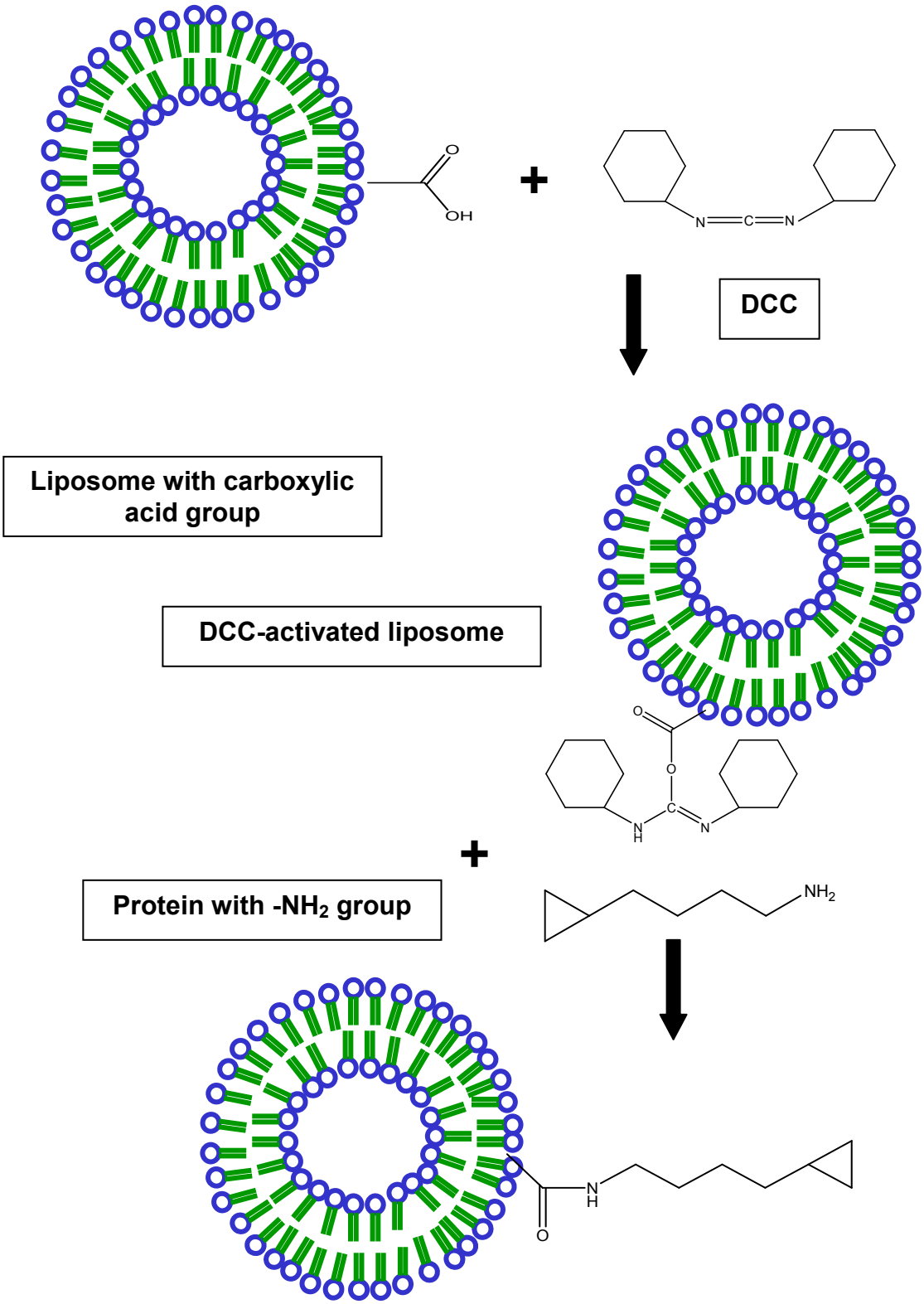

Figure 1.12 Amide bond formation
Free carboxylated group on the terminal end of the phospholipid is activated with DCC reagent. Activated carboxyl group reacts with amino groups on the protein producing an amide bond.

b) Attachment of proteins to liposomes *via* maleimide derivatives

Sulfhydryl groups present on proteins, peptides and other compounds are important in protein chemistry. SATA (N-hydroxysuccinimide S-acetylthioacetate) is used in the formation of stable thioether bonds (R^1-S-R^2) through a two-step reaction. In the first step, a stable covalent amide bond is formed from the reaction of the NHS esters present in SATA with primary amines on proteins. The amine reacts with the NHS ester by the nucleophilic attack, with consequent release of NHS as a by-product. In the second step, hydroxylamine is used to deacetylate the sulphur, resulting in a sulfhydryl group.

Maleimide's double bond on the terminal end of a PEG chain can undergo an alkylation reaction with sulfhydryl groups to form stable thioether bonds. Maleimide reactions are specific for sulfhydryl groups at pH 6.5-7.5. At pH 7.0 the reaction of maleimide with sulfhydryl proceeds at a rate 1,000 times greater that its reactions with amines (see Figure 1.13).

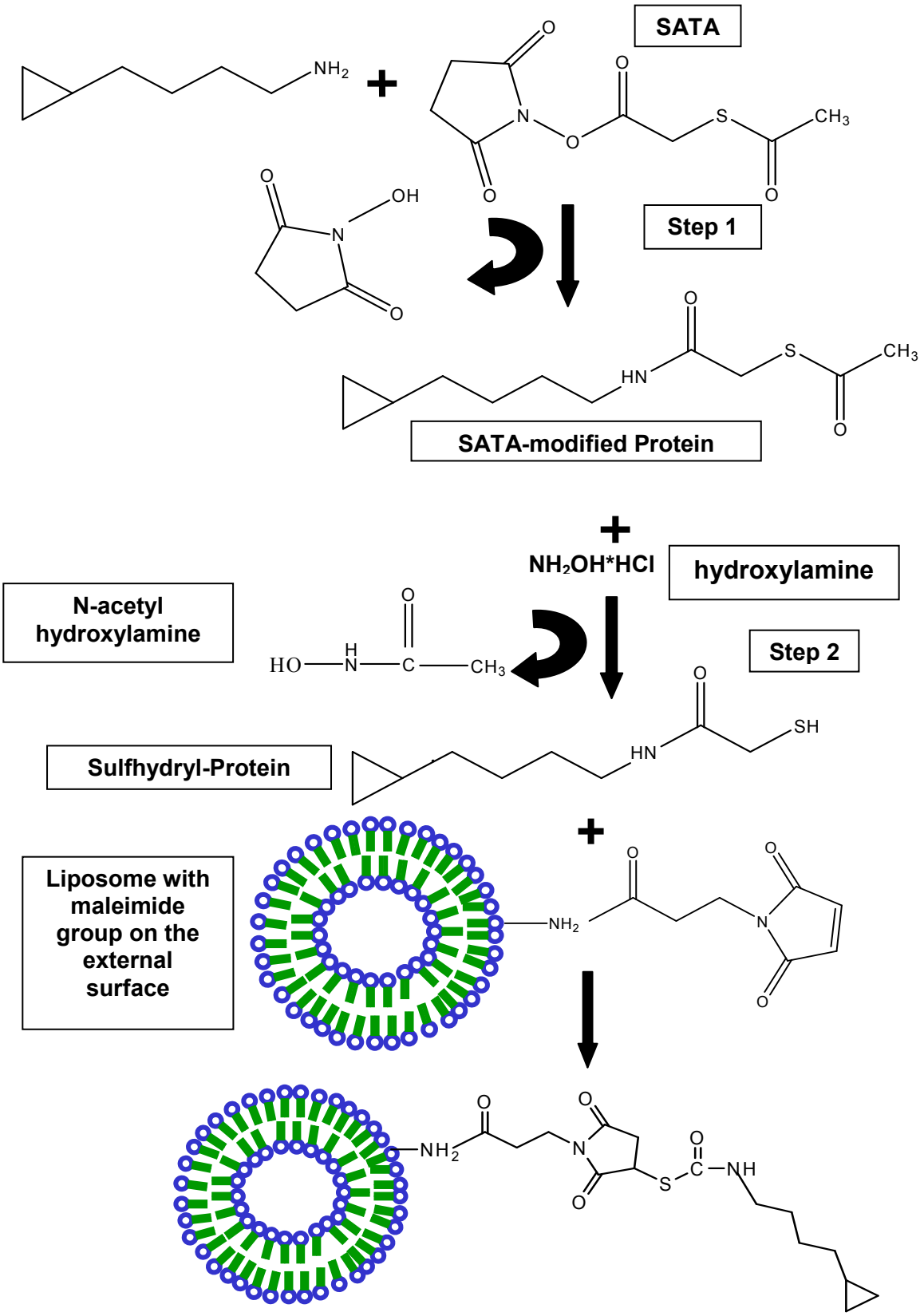

Figure 1.13 Thioeter bond formation.
Step 1 is the reaction of N-hydroxysuccinimide S-acetylthioacetate with a primary amine and step 2 is the deprotection with hydroxylamine to generate a sulfydryl. The sulfhydryl can subsequently react with maleimide group on PEG to form a thioether bond.

1.7 Gadolinium (Gd) - loading of liposomes for MR imaging

In developing targeted contrast agents for molecular magnetic resonance imaging, paramagnetic or superparamagnetic ions need to be targeted in sufficient quantities to a relevant tissue-specific target. Gadolinium, a paramagnetic ion, is the most commonly used contrast agent in MRI and the use of this ion in the development of immunoliposomes for molecular MRI will be described.

Loading liposomes with gadolinium presents a challenge in the development of targeted contrast agents. Three major methods have been explored:

1) Gd encapsulated in the aqueous space of the liposome
2) Gd incorporated into the lipid bilayer
3) Gd carried on exterior of the liposome *via* polymerizable amphiphilic polymers

Each of these methods will be examined in turn.

1.7.1 Encapsulation of gadolinium within liposomes

The first type of liposomal MRI contrast agents contain paramagnetic entities entrapped in the aqueous interior phase. Paramagnetic agents such as $MnCl_2$ (Unger *et al.,* 1993; Yang *et al.,* 2009), Gd-DTPA (Devoisselle *et al.,* 1988), Mn-DTPA (Caride *et al.,* 1984) and macromolecular contrast agents, such as Mn^{2+} bound to serum proteins, can be encapsulated in liposomes (Navon *et al.,* 1986). Results have been largely unsuccessful because of poor encapsulation efficiency, poor stability, toxicity and poor relaxivity. Contrast agents of this type have been used successfully to improve the detection of tumors in the liver of rats with hepatic metastases

(Unger *et al.,* 1989). A more in-depth analysis of the advances made in development of manganese-based nanoparticles as contrast probes for magnetic resonance imaging is described in review by Zhen *et al.* (Zhen *et al.*, 2012). Application of the freeze-thaw extrusion process to the synthesis of Gd-DTPA liposomes has helped overcome problems with encapsulation efficiency and stability. This method creates small liposomes, which yield greater contrast enhancement because of their larger surface-area-to-volume ratio, and, as a result, exchange with bulk water is improved (Caride *et al.,* 1984). This suggests that small liposomes with a permeable bilayer are desirable. However, permeable liposomes (created by varying the nature of lipids used in their production) are usually less stable (with reduced longevity in the circulation) in serum than liposomes with a more rigid bilayer (Mulder *et al.,* 2006). Also, leakage of gadolinium from such liposomes reduces their efficacy as targeted contrast agents.

1.7.2 Incorporation of gadolinium into the lipid bilayer

Gadolinium-DTPA can be bound to two fatty acid chains to form an amphiphilic molecule that can be incorporated into the lipid bilayer of liposomes, thus making gadolinium an integral part of the liposome surface (Kabalka *et al.,* 1987). Gadolinium (Gd)-DTPA can be incorporated as a hydrophilic segment accompanying hydrophobic stearate (Schwendener *et al.,* 1990) or acryl chains (Kabalka *et al.,* 1991). A schematic representation of this scenario, along with antibodies attached to the terminal end of the PEG chains, is displayed in Figure 1.14. This approach results in improved relaxivity of the metal compared to encapsulation of the paramagnetic

molecules in the liposomal lumen (Strijkers *et al.,* 2005). Gadolinium-incorporating liposomes also pose less risk of leakage of potentially toxic metals in the body (Torchilin, 2007). The addition of considerable amounts of gadolinium-containing lipid apparently does not negatively affect the stability of the cholesterol-containing liposomes. The membrane permeability of liposomes with and without gadolinium-containing lipid was shown to be equivalent when measured with a calcein-leakage assay (Mulder *et al.,* 2004).

The application of this kind of liposomal contrast agent is broad. For example, Trubetskoy *et al.* used PEGylated liposomes to detect of lymph nodes (Trubetskoy *et al.,*1995) and to achieve sustained contrast enhancement in tumors (Bertini *et al.,* 2004). Also, the biodistribution of cationic liposomes bound to DNA was analysed over time using liposomes incorporating Gd-lipid amphiphiles (Leclercq *et al.,* 2003). Neointimal lesions in mice were effectively detected using liposomes incorporating gadolinium in the lipid bilayer (Leclercq *et al.,* 2003).

More recently, a novel paramagnetic lipid molecule, Gd-DOTA-DSPE, was developed (Hak *et al.,* 2009). The ionic relaxivity of the Gd(III)DOTA-DSPE incorporated in liposomes was shown to be significantly higher than that of Gd(III)DTPA-BSA in liposomes. It is thought that water molecules have greater access to the paramagnetic complex since the Gd-DOTA moiety extends from the liposomal membrane; contrarily, Gd-DTPA-BSA, when incorporated into liposomes, lies at the liposomal membrane-bulk water interface. This development could dramatically improve the detection of low concentration biomarkers in MRI-based molecular imaging studies.

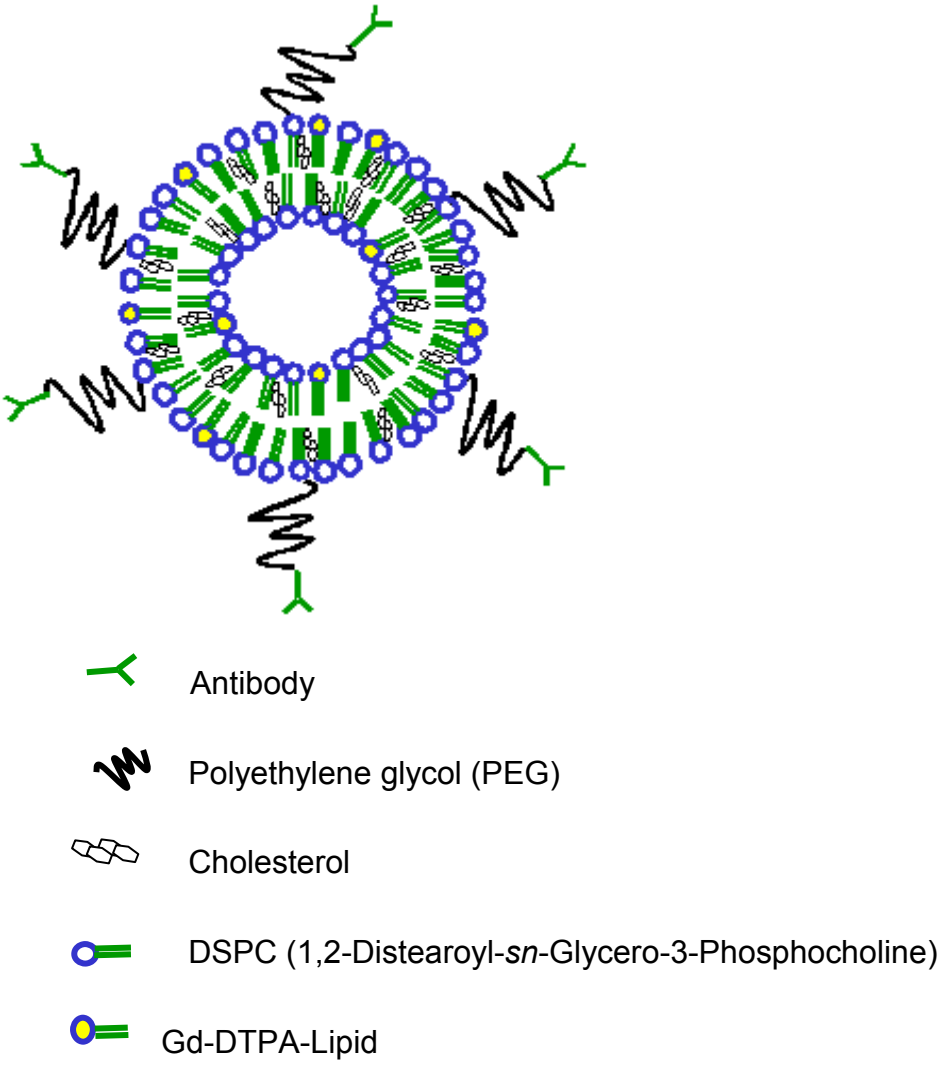

Figure 1.14 Immunoliposome with gadolinium-DTPA incorporated into the amphiphile bilayer *via* conjugation with two fatty acid chains.

1.7.3 Gadolinium carried on the exterior of liposomes

Another method of loading gadolinium into liposomes is through the use of polychelating amphiphilic polymers (PAPs). These molecules are capable of carrying multiple gadolinium ions and can be incorporated into the liposome structure by binding to an amphiphilic molecule, such as N-glutaryl-phosphatidylethanolanime (NGPE) (see Figure 1.10). In contrast to amphiphilic gadolinium-containing molecules described in the previous section, PAPs carry gadolinium on the exterior of liposomes. PAPs consist

of a main hydrophilic chain with multiple chelating side groups capable of binding many gadolinium atoms and a hydrophobic terminal group that anchors the molecule into the liposome membrane (Torchilin, 2000; Torchilin, 2007) (see Figure 1.15). This technique increases the number of gadolinium atoms per vesicle, which significantly increases the relaxivity of PEGylated liposomes. The contrast properties of the liposomes are enhanced as a result (Torchilin, 2007). An interesting example of the application of PAP-nanoparticles *in vivo* is the MR imaging of lymphatic system components with the Gd-loaded nanocarriers (investigating metastases in lymph nodes). Trubetskoy and Torchillin have studied liposomes and micelles as delivery vesicles to the lymphatic system. Tumors have also been targeted successfully using this method. Gd-loaded PAP-containing immuno-liposomes carrying the monoclonal antibody 2C5 delivered elevated amounts of Gd to the surface of various cancer cells *in vitro* compared to 'antibody-free' Gd-liposomes or Gd-liposomes modified with non-specific antibody (Erdogan *et al.,* 2006). In a separate study, using mouse models of cancer, these immunoliposomes allowed for fast and specific tumor imaging *in vivo* (Erdogan *et al.,* 2008).

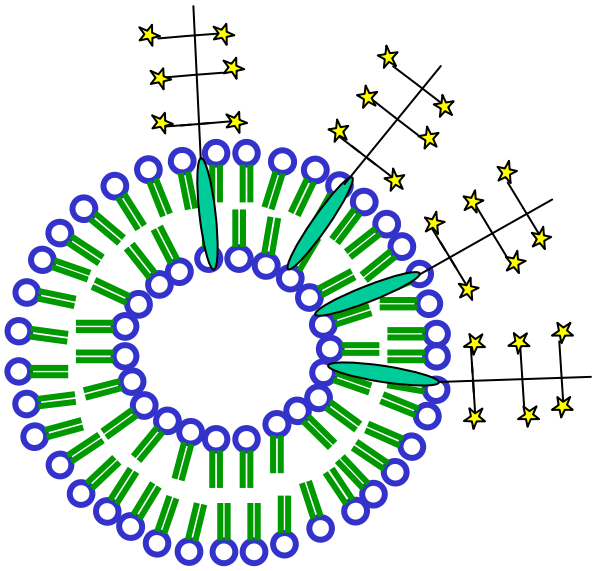

Polychelating amphiphilic polymer with multiple chelating groups

N-glutaryl-phosphatidylethanolanime (hydrophobic tail)

Figure 1.15 The incorporation of the amphiphilic polychelating polymer into the liposome membrane.
Each polychelating chain contains multiple chelating groups carrying gadolinium and a hydrophobic tail to anchor with the liposome.

1.7.4 Motions of gadolinium-containing lipid incorporated into liposomes

There are various parameters that can influence the relaxation rate of water molecules within contrast agent's vicinity. τ_M is the average time (nanoseconds) a water molecule remains co-ordinated to the metal ion in the first inner spher. τ_r is how fast the contrast agent tumbles in water, which is measured by the rotational correlation time and τ_D is the translational diffusion time of the outer sphere water molecules. The relaxivity of paramagnetic liposomes has been shown to be mainly effected by the

exchange rate (τ_M) of the coordinated water molecule to the Gd metal centre of the membrane anchored paramagnetic lipid. In addition to the exchange rate, the coordination number and the rotational correclation time (τ_r) are also factors that affect the relaxivity of macromolecular contrast agents (Mulder *et al*., 2006). Possible motions of the Gd chelate head group are displayed in Figure 1.16. As all these dynamic proccesses will change depending on the composition of the agent, the nature of the liposome formulation can be used to determine the relaxivity.

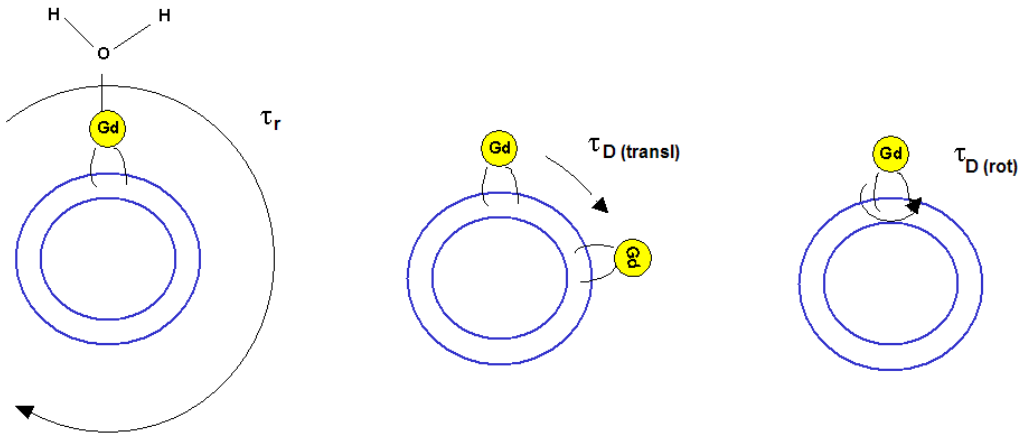

Figure 1.16 Possible motions of Gd lipid chelate head.
τ_r represents the rotational motion of the whole paramagnetic liposome in water; $\tau_{D(transl)}$ – the translational diffusion of individual Gd chelates protruding from the paramagnetic liposome surface; $\tau_{D(rot)}$ – the rotational diffusion of the entire Gd lipid in the paramagnetic liposome membrane. Figure was based on Mulder *et al.* (2006).

1.8 Challenges encountered in the use of immunoliposomes as targeted molecular MRI contrast agents

Immunoliposomes show huge promise in targeted drug and contrast agent delivery to tumors. Park *et al.* indicated that doxorubicin-loaded anti-p185^{HER2} immuno-liposomes are markedly and specifically cytotoxic against

$p185^{HER2}$-overexpressing tumor cells *in vitro* and demonstrated it is a promising therapeutic vehicle for the treatment of $p185^{HER2}$-overexpressing human cancers. A PEGylated liposome encapsulating doxorubicin and attached to a monoclonal antibody fragment named GAH showed superior cytotoxic activity against several human stomach cancer cells compared with doxorubicin or doxorubicin-incorporated PEG liposomes with any antibody fragment (Matsumura *et al.,* 2004). However, major challenges lie ahead before this promise can be transformed into improved clinical outcomes.

Issues pertinent to MRI include sensitivity and target specificity. Sensitivity can be improved by maximising the payload of gadolinium per liposome. Target specificity can be achieved through identification of suitable target antigens and receptors and subsequent development of suitable targeting moieties such as antibodies.

Immunogenicity of immunoliposomes is a problem as it increases their clearance from the circulation. Thus, if repeated administration of the immunoliposome is planned, the targeting ligand should not be immunogenic. Immunoliposomes prepared using full IgG molecules were shown to succumb to an increased rate of clearance compared to non-targeted liposomes (Drummond *et al.,* 2008). This is due to recognition of the Fc portion of the antibody by Fc receptors on the surface of macrophages. Use of antibody fragments such as Fabs or scFvs does not appear to increase liposomal uptake by macrophages. Also, human or humanised antibodies are preferred as xenogenic protein sequences may result in immunogenicity in humans.

Achieving optimal liposome size represents another challenge. Smaller liposomes have longer circulatory life-times and increased access to tumors. However, below a certain size, suggested to be 80 nm, any advantage is lost since liposomes of diminutive sizes are cleared more quickly from the tumor. Liposome sizes between 100-120 nm appear to be optimal for accumulation in solid tumors (Drummond *et al.,* 2008).

Clearly, despite the enormous strides made in the development of immunoliposomes as targeted contrast agent for molecular magnetic resonance imaging, there remain significant challenges to be overcome before this exciting field delivers significantly improved clinical outcomes.

1.9 CD138 (syndecan-1) protein and multiple myeloma malignancy

Multiple myeloma is the second most common form of haematological malignancy in the Western World after non-Hodgkin's lymphoma. The most common symptoms of multiple myeloma can be summarised as the tetrad, *CRAB*: C=Calcium, R=Renal failure, A=Anemia, B=bone lesion (Figure 1.17).

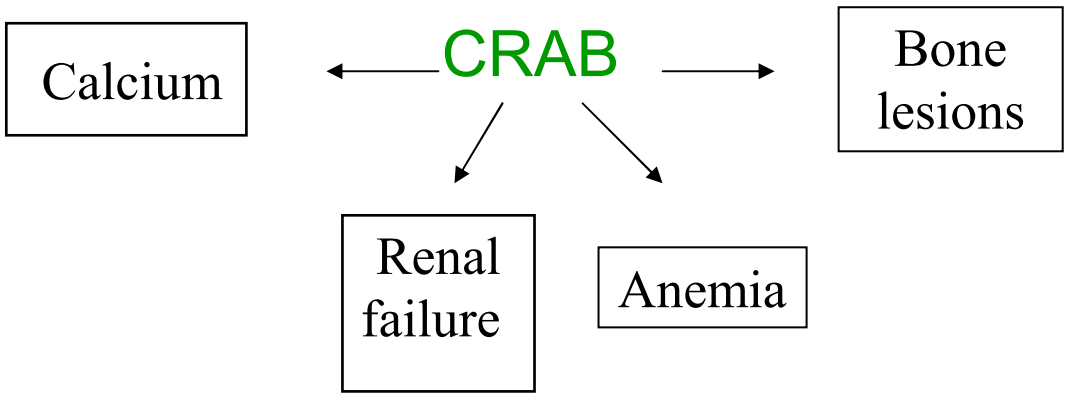

Figure 1.17 Representation of the most common symptoms of human multiple myeloma.

Multiple myeloma is characterised by uncontrolled proliferation of plasma cells within the marrow. Normal bone marrow contains no more than 4% of the plasma cells. In unhealthy bone marrow there are more than 10% of malignant plasma cells.

The uncontrolled proliferation of plasma cells leads to disruption of the balance between osteoblastosis and osteoclastosis within the bone, which leads to bone lesions. This is caused by overproduction of tumour necrosis factor-related induced cytokines (TRANCE) and inactivation of osteoprotegerin resulting in unrestricted osteoclastic activity. It generates lytic bone deposits on plain film radiography. Calcium, released from bones, is found in urine. Hypercalcemia may result in the development of renal failure. The anemia results from the replacement of normal bone marrow by infiltrating tumor cells and inhibition of normal red blood cell production.

In about 75% of all cases of multiple myeloma the paraprotein present (M protein) will correspond with one type of abnormal immunoglobulin. In about

60% of cases an abnormal protein, known as Bence-Jones protein may also be found in the urine.

Multiple myeloma cell growth is dependent on interactions between the multiple myeloma cells and the bone marrow cells. The mutiple myeloma cells bind to the bone marrow stroma cells *via* adhesion molecules, such as LFA-1 (leukocyte-associated antigen-1) (CD11a/CD18) and ICAM-1 (intracellular adhesion molecule-1) (CD54). Adhesion initiates a cascade of signalling events which result in cell proliferation, migration, angiogenesis, and ultimately enhanced cell survival. Multiple myeloma is one of the best studied disease states, in particular IL-6 has been shown to be a potent autocrine and paracrine growth factor which induces maturation of B cells into antibody-producing cells. IL-6 is a multifunctional cytokine which is responsible for regulating growth, differentiation and proliferation (Kishimoto *et al.*, 1995). IL-6 secreted from bone marrow stromal cells (BMSC) is integral for multiple myeloma cell proliferation *in vivo*. The stromal cell-derived IL-6 acts on the multiple myeloma cells, causing them to secrete their own IL-6. IL-6 signal trasduction commences with IL-6 receptor (IL6/gp80) binding, followed by interaction with the signal transducer gp130 and homodimerization (Schaper *et al.*, 1998).

There are three pathways downstream of the initial receptor-binding events that are likely to be involved in multiple myeloma growth (Figure 1.18). The first pathway is the jun-activated kinase (JAK) pathway, which activates STAT3 and STAT1 transcription factors that regulate cell survival (Catlett-Falcone *et al.,* 1999). The second is the mitogen-activated protein kinase (MAPK) pathway that is involved in multiple myeloma cell growth and

proliferation (Heinrich *et al.,* 1998). The third pathway is the phosphatidyl 3-kinase (PI3K)/Akt pathway, which leads to NF-κB activation. This facilitates multiple myeloma cell growth and survival by NF-κB-mediated transcription of pro-survival/anti-apoptotic mediators, *via* PI3K/Akt-induced cell-cycle activation, *via* JAK-STAT pathway (Tu *et al*., 2000).

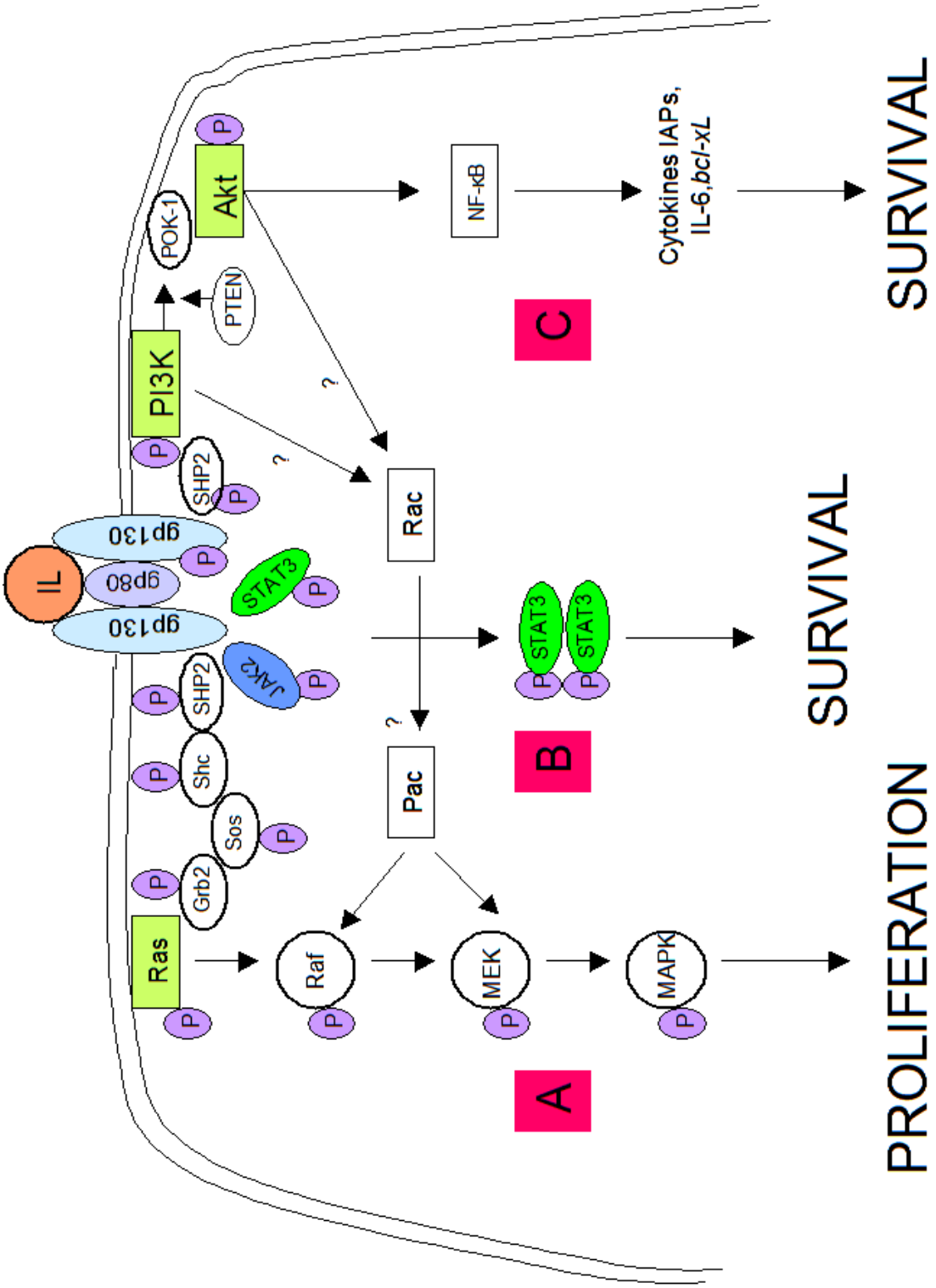

Figure 1.18 IL-6 signal transduction in multiple myeloma cells.
IL-6 is a growth and survival factor for multiple myeloma. Tis cytokine is regulating various aspects of growth, differentation and proliferation. There are three pathways downstratem of the initial receptor-binding event that are likely involved in multiple myeloma growth. A – the mitogen-activated protein kinase (MAPK) pathway; B – the jun-activated kinases (JAK) pathway; C – anti-apoptotic, pro-survival signals *via* activation of the phosphatidyl 3-kinase (PI3K)/Akt kinases pathway. Figure was created based on Greenstein *et al.* (2003).

Multiple myeloma (MM) malignancy appears during B cell maturation proccess in bone marrow. In bone marrow, syndecan-1 is only expressed on precursor B lymphocytes and lost before maturation (Sanderson *et al.*, 1989). Terminally differentiated plasma cells express relatively few surface antigens and do not express very common B cell markers, such as CD19 and CD20, CD38 and CD138 (Rawstron, 2006). Thus, syndecan-1 is a good marker for multiple myeloma cancer cells (Bernfield *et al*., 1992) and Reed-Sternberg cell identification (Wijdenes *et al.*, 1996).

CD138 or syndecan-1 is a glycoprotein expressed on simple epithelia (150-250 kDa), stratified epithelia (80-150 kDa), mesenchymal cells (220-300 kDa) and lymphocytes (80-150 kDa). The core of protein is composed of extracellular (251 residues), transmembrane (34 residues) and intracellular (25 residues) parts. The protein bears heparan and chondroitan sulfates. The ectodomain contains five putative glycosaminoglycan (GAG) attachment sites (Figure 1.19). Ridley *et al.* (1993) suggested that syndecan-1 plays major role in plasma cell adhesion to bone marrow stroma, especially to collagen type I.

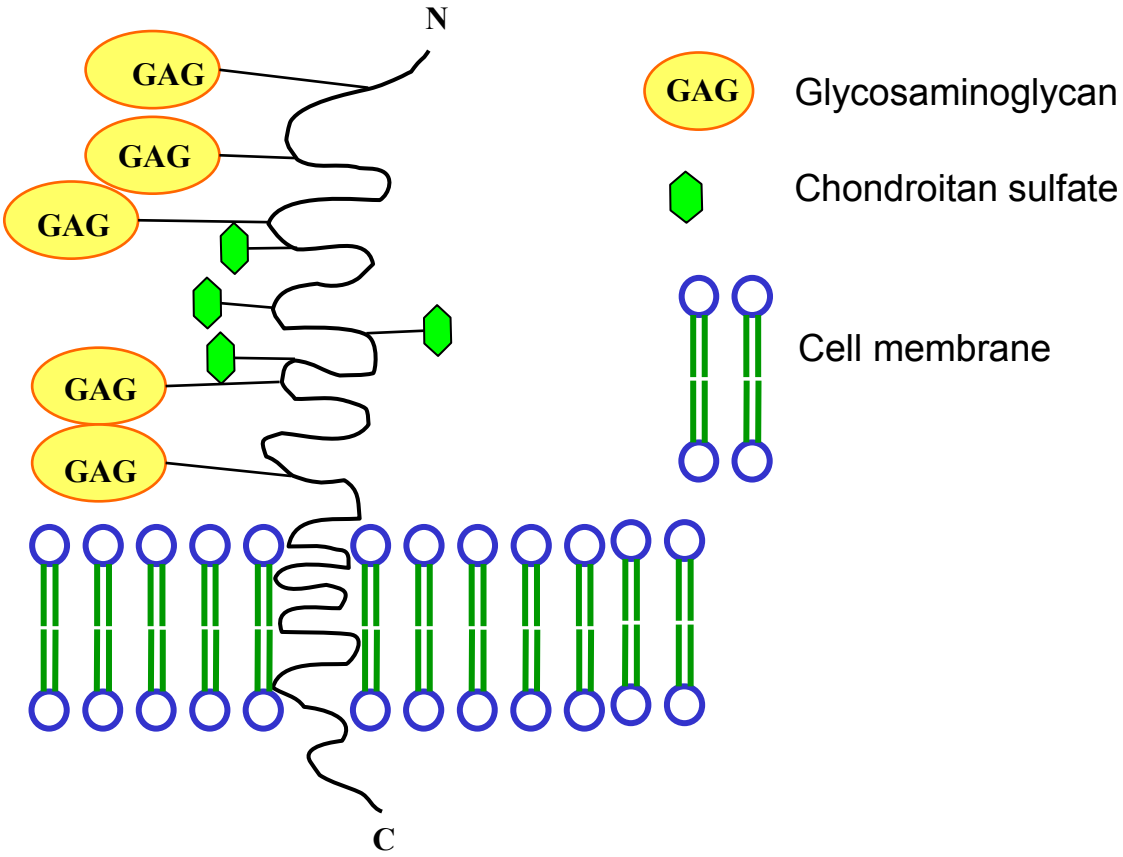

Figure 1.19 Schematic representation of CD138 (syndecan-1) transmembrane protein.
CD138 is composed of extracellular, transmembrane and intracellular parts. The protein has heparan, chondroitan sulfates and glycosaminoglycan (GAG) attachment sites.

Aims of research

The aims of the research described in this thesis were:

- To develop a targeted contrast agent (e.g. an antibody-modified liposome) for early and minimally non-invasive diagnosis of human multiple myeloma.

  Gadolinium (Gd) will be used as a paramagnetic contrast agent to enhance magnetic signals from imaged tissue. Immunoliposomes will be prepared and gadolinium ions will be incorporated onto the liposome surface for targeting CD138 (syndecan-1) glycoprotein overexpressed on human multiple myeloma cancer cells.

Nowadays, the diagnosis of this form of cancer usually requires the performance of a range of tests and the assessment of marrow specimens from invasive biopsy. Diagnosis of this disease is often delayed. Faster diagnosis of this disease can allow better prognosis for patients. The main aim of the project was to develop a minimally non-invasive diagnostic agent for non-curable malignancy.

- The ability of anti-CD138-conjugated-liposomes to target human multiple myeloma cell lines will be investigated *in vitro.*
- Contrast Gd-PAP-liposomes modified with anti-CD138 monoclonal antibodies will be targeted to human multiple myeloma cell lines.
- Visualization of targeted contrast anti-CD138-liposome interaction will be performed using magnetic resonance imaging (MRI) analyses at 1.5 T to assess its binding ability to cancer cells *in vitro* and contrast signal on MRI scans.

- The overall aim is to prepare sufficient targeted contrast agent to enhance visualization of multiple myeloma to allow effective minimally non-invasive diagnosis of this malignancy in humans.

Chapter 2

Materials and Methods

2.1 Materials

2.1.1 Equipment

Table 2.1 Equipment used and suppliers.

EQUIPMENT	SUPPLIER
Extruder (Mini model) Polycarbonate membranes (100 nm) Gas tight syringes (2) Extruder stand Stabilizer block O-rings Filter supports	Avanti Polar Lipids, Inc. Instruchemie B.V. Zwet 269932, AB Delfzyl, The Netherlands.
HPPS (High Performance Particle Sizer) (Nano S90)	Malvern/Zetasizer Nano 3000 HS, 10 Southville Road, Southborough, MA 01772, USA.
Desalting column	Pierce, Medical Supply Co. Ltd., Damastown, Mulhuddart, Dublin 15, Ireland.
pH meter (230V; 50/60Hz) (Orion3Star)	Fisher Scientific, Suite 3, Plaza 212, Blanchardstown Corporate Park 2, Ballycoolin, Dublin 15, Ireland.
CO_2 Tissue Culture Incubator (3111) Thermo Scientific	Bio-sciences, 3 Charlemont Terrace, Crofton Road, Dun Laoghaire, Co. Dublin, Ireland.
Microscope (Nikon Diaphot) (30/02381)	Micron Optical Co. Ltd., Ballybeg-Screen, Enniscorthy, Co. Wexford, Ireland.

EQUIPMENT	SUPPLIER
Laminar Flow Unit (Model: Holten Laminar A/S, HB2448K) Sonicator & Waterbath (120V 50/60Hz) (15-220)	A.G.B. Scientific Ltd., Orion Business Campus, Northwest Business Park, Ballycoolin, Dublin 15, Ireland.
Millipore Filtration Apparatus (Academic) DNA gel apparatus Bio-Rad (Wide-Mini-Sub®CellGT) Trans-Blot®SD Semi-Dry Transfer cell Bio-Rad	Alpha Technologies Ltd., The Leinster Technology Centre, Blessington Industrial Estate, Blessington, Co. Wicklow, Ireland.
Spectrophotometer UV Visible (UV-160A)	Allegheny-Singer Research Institute, 320 East North Avenue, 11th floor - South Tower, Pittsburgh, USA.
Centrifuge (2K15) Rotor 11192 (Sigma)	Sigma Centrifuges, 37507 Osterode am Harz, Germany.
Centrifuge (5804R) Rotor A-4-62 (Eppendorf)	Eppendorf UK Ltd., Endurance House Vision Park, Histon, Cambridge, CB24 9ZR, United Kingdom.
Centrifuge (2102, Z 233 MK-2) (HERMLE LaborTechnik)	BioExpress, 420 N. Kays Drive, Kaysville, UT 84037, USA.
Ultracentrifuge Optima™ L-100 K Rotor 70 Ti (Beckman Coulter)	Labplan, Allenwood Enterprise Park, Naas, Co. Kildare, Ireland.

EQUIPMENT	SUPPLIER
Buchi Vacuum Controller, Rotovapor R-200 New Brunschwick Scientific-Excella E24 Incubator Tomy Autoclave SX-700E High Pressure Steam Sterilizer	Mason Technology Ltd., Greenville Hall, 228 South Circular Road, Dublin 8, Ireland.
Biometra T $_{GRADIENT}$ PCR machine	LABREPCO, 101 Witmer Road, Suite 700, Horsham, PA19044, USA.
Nonodrop^{TM} ND-1000	NanoDrop Technologies, Inc., 3411 Silverside Road, 100BC, Wilmington, DE19810-4803, USA.
Gene Pulser Xcell^{TM} electroporation system	BioRad Laboratories, Inc., 2000 Alfred Nobel Drive, Hercules, CA94547, USA.
Safire 2 plate reader	Tecan Group Ltd., Seestrasse 103, CH-8708 Mannedorf, Switzerland.
Vibra Cell^{TM} sonicator	Sonics and Materials, Inc., 53 Church Hill Road, Newtown, CT06470-1614, USA.

EQUIPMENT	SUPPLIER
Freeze Dry System / Freezone 4.5	Labconco Corporation, 8811 Prospect Avenue, Kansas City, Missouri 64132-2696, USA.
UV trans-illuminator Model: 80-6246-82	Amersham Pharmacia Biotech, 800 Centennial Ave., Piscataway, NJ 08855, USA.
FACS Calibur	BD Biosciences, BD Pharminogen™, The Danby Building, Edmund Halley Road, Oxford Science Park, OX4 4DQ Oxford, United Kingdom.
Philips MRI scanners – 1.5T Gyroscan Intera	MagNET, Eindhoven, The Netherlands.
Fast Field-Cycling NMR relaxometer SpinMaster FFC2000 1T C/DC	STELAR s.r.l., 4 Enrico Fermi Street, 27035 Mede (PV), Italy.

2.1.2 Consumable items

2.1.2.1 Plastic and glass consumables

Table 2.2 Consumables used and suppliers.

ITEM	SOURCE
Eppendorf tubes, sterile universal containers, tips	Sarstedt Ltd., Sinnottstown Lane, Drinagh, Co. Wexford, Ireland.
2 mL glass tubes	Lennox, John F. Kennedy Drive, Naas Road, Dublin 12, Ireland.
Round bottom flasks Nunc Maxisorp ™ plates	Fisher Scientific, Suite 3, Plaza 212, Blanchardstown Corporate Park 2, Ballycoolin, Dublin 15, Ireland.
25 mL ultracentrifugation bottles, thick-wall polycarbonate	Labplan, Allenwood Enterprise Park, Naas, Co. Kildare, Ireland.

2.1.3 Reagents and chemicals

Table 2.3 Reagents and chemicals used and suppliers.

REAGENT	SUPPLIER
1,2-distearoyl-*sn*-glycero-3-phosphoethanolamine-N-[carboxy(polyethylene glycol)2000]-carboxylic acid (PEG-DSPE-carboxylic acid), Cholesterol, L-α-phosphatidylcholine, hydrogenated (egg, chicken) (egg PC), 1,2-distearoyl-*sn*-glycero-3-phosphoethanolamine-N-[metoxy(polyethylene glycol)-2000](ammonium salt) (DSPE-PEG-Metoxy), 1,2-dioleoyl-*sn*-glycero-3-phosphoethanolamine-N-(lissamine rhodamine B sulfonyl) (ammonium salt) (Rhodamine-PE), 1,2-dimyristoyl-*sn*-glycero-3-phosphoethanolamine-N-DTPA (Gadolinium salt), 1,2-dioleoyl-*sn*-glycero-3-phosphoethanolamine-N-(glutaryl) (sodium salt) (NGPE)	Avanti Polar Lipids, Inc. Instruchemie B.V. Zwet 269932, AB Delfzyl, The Netherlands.

REAGENT	SUPPLIER
Chloroform Methanol Dichloromethane Pyridine DMSO NaCl Trypan blue Trypsin Formaldehyde Penicillin/Streptomycin Gadolinium hexahydrate 1,2-distearoyl-*sn*-glycero-3-phosphocholine (DSPC) DMF DCC NHS Poly-ε-CBZ-$_{DL}$-lysine (MW 5,500) Hydrogen bromide (33 wt%) Diethyl ether Succinic anhydride $GdCl_3 \bullet 6H_2O$ Acetic acid Triethylamine Iodine MTT Silica plates Micro Lowry assay with Peterson's modification Alkaline phosphatase conjugated goat anti-mouse IgG	Sigma-Aldrich, Riedel de-Haen AG, Wunstorfer, Strabe 40, D-30926, Hannover, Germany.

REAGENT	SUPPLIER
Sephadex G-25	Pierce, Medical Supply Co. Ltd., Damastown, Mulhuddart, Dublin 15, Ireland.
Mouse anti-human CD138:FITC	AbD Serotec, MorphoSys UK Ltd., Endeavour House, Langford Business Park, Langford Lane, Kidlington, Oxford, OX5 1GF, United Kingdom.
FITC mouse IgG1κ isotype control Purified mouse anti-human CD138 FACS flow FACS rinse FACS clean FACS tubes	BD Bio-sciences, BD Pharminogen™, The Danby Building, Edmund Halley Road, Oxford Science Park, OX4 4DQ Oxford, United Kingdom.
Gd-DTPA-BSA monohydrate	Azopharma, 11810 Borman Drive, St. Louis, MO 63146, USA.
Rituxan® (human anti-CD20) Avastin® (human anti-VEGF-A) Herceptin® (human anti-HER2)	Mater Misericordiae University Hospital, Eccles Street, Dublin 7, Ireland.
Mouse 2C5 monoclonal antibody to nucleosomes	Pharmaceutical Biotechnology and Nanomedicine, Northeastern University, 360 Mugar Building, MA 02115, Boston, USA.

REAGENT	SUPPLIER
Dialysis tubing (300,000 Da) Dialysis tubing (50,000 Da) Dialysis tubing (3,500 Da) Page Ruler™ Plus Prestained Protein Ladder	AGB Scientific Ltd., Orion Business Campus, Northwest Business Park, Ballycoolin, Blanchardstown, Dublin 15, Ireland.
Vivaspin column (5,000 Da)	Sartorius Stedim Biotech GmbH, August-Spindler-Strasse 11, 37079 Goettingen, Germany.
Foetal bovine serum (FBS)	Invitrogen, 9704-CH-Groningen, The Netherlands.
PCR primers	Eurofins MWG Operon, 318 Worple Road, London, SW20 8QU, United Kingdom.
Bacteriological agar Yeast extract Tryptone	Cruinn Diagnostics Ltd., Hume Centre, Parkwest Business Park, Nanogor Road, Dublin 12, Ireland.
Restriction enzymes T4 DNA ligase	ISIS Ltd., Unit 1&2, Ballywaltrim Business Centre, Bogholl Road, Bray, Co. Wicklow, Ireland.
DNTP mix Go Taq® DNA Polymerase	Medical Supply Company Ltd., Damastown, Mulhuddart, Dublin 15, Ireland.
RPMI 1640 DMEM	Bio-sciences, 3 Charlemont Terrace, Crofton Road, Dun Laoghaire, Ireland.

2.1.4 Standard solutions

Table 2.4 Preparation of standard solutions.

SOLUTIONS	CONSTITUENTS
FACS buffer	0.1 M PBS, pH 7.4 2% (v/v) FCS 0.05% (w/v) NaN_3
Protein electrophoresis buffer	25 mM Tris base (3.0 g) 129 mM Glycine (14.4 g) 0.1% (w/v) SDS (1.0 g) adjust pH to 8.3 The components were dissolved in a 1L, pH was adjusted, and solution was stored RT
SDS Sample buffer	1 M Tris-HCl, pH 6.8 (0.6 mL) 50% (w/v) Glycerol (5.0 mL) 10% (w/v) SDS (2.0 mL) 2-Mercaptoethanol (0.5 mL) 1% (w/v) Bromophenol blue (1.0 mL) dH_2O (0.9 mL) The components were mixed thoroughly and stored at RT.
Ammonium Persulphate Solution	Ammonium persulphate (0.1 g) dH_2O (1.0 mL) The components were mixed thoroughly and stored at RT.
Transfer buffer	Trizma base (3.0 g) Glycine (14.4 g) Methanol (200 mL) dH_2O (make up to 1L)

SOLUTIONS	CONSTITUENTS
1M Phosphate Buffered Saline pH 7.3-7.4 (PBS) (1L)	NaCl (80 g) KCl (2 g) Na_2HPO_4 (14.4 g) KH_2PO_4 (2.4 g) adjust pH to 7.3 by addition of 1M HCl
1 x (0.1 M) Phosphate Buffered Saline – Tween PBST pH 7.3-7.4	0.1 M PBS, pH 7.3 0.05 % (v/v) Tween 20
MES buffer, pH 5.5	10 mM MES 20 mM NaCl adjust pH to 5.5 and store at RT
100 x 5O5	Glycerol 50% (v/v) Glucose 50% (v/v)

2.1.5 Constituents of buffers for SDS-PAGE (Sodium Dodecyl Sulphate-PolyAcrylamide Gel Electrophoresis) and Western blotting

Constituents of buffers for SDS-PAGE (Sodium Dodecyl Sulphate-PolyAcrylamide Gel Electrophoresis) and Western blotting are outlined in Table 2.5.

Stock Solutions:

(A) 30% (w/v) acrylamide containing 0.8% (w/v) bis-acrylamide

(B) 1.5 M Tris-HCl, pH 8.8, containing 0.4% (w/v) SDS

(C) 0.5 M Tris-HCl, pH 6.8, containing 0.4% (w/v) SDS

(D) 10% (w/v) ammonium persulfate

Table 2.5 The quantities of stock solutions required for the preparation of resolving and stacking gel used for a polyacrylamide gel electrophoresis.

SEPARATING GEL (12%)		STACKING GEL (5%)	
1 M Tris-HCl, pH 8.8	1.5 mL	1 M Tris-HCl, pH 6.8	0.63 mL
30% (v/v)Acrylamide	2.5 mL	30% (v/v)Acrylamide	0.84 mL
2% (v/v) Methylene bisacrylamide	1 mL	2% (v/v) Methylene bisacrylamide	0.34 mL
distilled water	0.93 mL	distilled water	3.10 mL
10% (w/v) SDS	0.03 mL	10% (w/v) SDS	0.05 mL
10% (w/v) ammonium persulfate	0.03 mL	10% (w/v) ammonium persulfate	0.05 mL
TEMED	6 µL	TEMED	5 µL

2.1.6 Culture media compositions

The recipes of various media used for culturing bacterial cells are presented in Table 2.6.

Table 2.6 Bacteriological media used in this study.

CULTURE MEDIA	CONSTITUENTS	
2x Tryptone and yeast extract (TY) medium	Tryptone Yeast Extract NaCl	16 g/L 10 g/L 5 g/L
Luria Bertani broth (LB) medium / agar	Tryptone Yeast Extract NaCl Agar	10 g/L 10 g/L 5 g/L 5 g/L
Super Broth (SB) Media	MOPS Tryptone Yeast extract	10 g/L 30 g/L 20 g/L

2.1.7 Bacterial strains

Two bacterial strains used for cloning and expression were purchased from Stratagene, LaJolla, California, USA are listed in Table 2.7.

Table 2.7 *E. coli* cells used for expression.

E. coli **XL10-GOLD strain:** endA1 glnV44 recA1 thi-1 gyrA96 relA1 lac Hte Δ(mcrA)183 Δ(mcrCB-hsdSMR-mrr)173 tet^R F'[proAB $lacI^qZ\Delta M15$ Tn10(Tet^R Amy Cm^R)]
E. coli **Rosetta(DE3)pLysS strain:** F^- ompT $hsdS_B(R_B^- m_B^-)$ gal dcm λ(DE3 [lacI lacUV5-T7 gene 1 ind1 sam7 nin5]) pLysSRARE (Cam^R)

2.1.8 Commercial kits and their suppliers

Different commercial kits along with their suppliers are listed in Table 2.8.

Table 2.8 Commercial kits used and their suppliers.

COMMERCIAL KITS	SUPPLIER
Superscript III reverse transcriptase kit	Invitrogen Corporation, 5791 Van Alley Way, Carlsbad, CA92008, USA.
QIAquick™ gel extraction kit	Qiagen, 28159 Avenue Stanford, Valencia, CA91355, USA.
Wizard Plus SV Miniprep™ kit	Promega, 2800 Woods Hollow Road, Madison, WI 53711, USA.

2.1.9 Cell lines

U266 and RPMI8226 human multiple myeloma cell lines were purchased from DSMZ (Deutsche Sammlung von Mikroorganismem und Zellkulturen GmbH, Inhoffenstrasse 7B, 38124 Braunschweig, Germany).

L428 and RAMOS cell lines were kindly donated by Dr. Dermot Walls, School of Biotechnology, Dublin City University, Ireland.

B16F10 cells were kindly donated by Prof. Vladimir Torchilin, Northeastern University, Boston, USA. Different cell lines used in this study are outlined in Table 2.9.

Table 2.9 List of cell lines and relevant culture media used in this study.

CELL LINE	DSZM NO. OR DONOR	DESCRIPTION	CULTURE MEDIUM
U266	ACC 9	Human Multiple Myeloma	RPMI 1640+ 10% (v/v) FBS
RPMI8226	ACC 402	Human Multiple Myeloma	RPMI 1640+ 10% (v/v) FBS
L428	Dr. Dermot Walls (Dublin City University)	Hodgkin's disease-derived	RPMI 1640+ 10% (v/v) FBS
RAMOS	Dr. Dermot Walls (Dublin City University)	Human Burkitt's Lymphoma	RPMI 1640+ 10% (v/v) FBS
B16F10	Prof. Vladimir Torchillin (Northeastern University, Boston, USA)	Murine Melanoma	DMEM+ 10% (v/v) FBS

2.2 Methods

2.2.1 Mammalian cell culture

2.2.1.1 Cell lines and media preparation

The cell lines used in the experimental work (Table 2.5) were cultured in RPMI 1640 or DMEM medium supplemented with 10% (v/v) FBS and 1% (v/v) antibiotics penicillin/streptomycin.

2.2.1.2 Recovery of frozen cells

Cells were recovered from liquid nitrogen with special care by thawing rapidly at 37°C and transferring to a sterile universal tube containing 10 mL of RPMI 1640 (with 10% (v/v) FBS). The cells were centrifuged at 342 g for 5 min (Sigma centrifuge) resuspended in fresh medium, transferred to culture flasks and incubated at 37°C in a humid 5% (v/v) CO_2 incubator.

2.2.1.3 Culture of cells in suspension and adherent cells

The cells were sub-cultured, using a split ratio of 1:2 every third day, maintaining a density of 1×10^6 cells/mL. Cells were flushed off the surface of the flask using a Pasteur pipette, collected and centrifuged at 342 g (Sigma centrifuge) at room temperature. The pellet was then resuspended in 2 mL of fresh culture medium. Cells were then transferred to T-75 flasks containing 14 mL of fresh RPMI 1640 medium

Adherent cells (B16F10) were detached with 1 mL 0.05 % (v/v) trypsin for 5 min at 37ºC. Trypsin was neutralized by adding 5 mL of medium supplemented with serum. Cells were then centrifuged at 342 g and resuspened in fresh medium. Cells were then transferred to flasks.

2.2.1.4 Cell counts and viability testing

Trypan Blue was used routinely to determine cell numbers and viability. Trypan Blue stain (Sigma, 0.25% (w/v)) was mixed 1:1 with 20 µL cell suspension and allowed to incubate for 2 min. A sample of this mixture was loaded onto the counting chamber of an improved Neubauer Haemocytometer slide and cell

numbers and viability were determined. Viable cells excluded the dye and remained white, while dead cells stained blue. The cell count was performed within 5 min after applying the Trypan Blue stain.

2.2.1.5 Long-term storage of cells

Cells required for long-term storage were frozen in liquid nitrogen. Harvested cells were pelleted and resuspended in freezing medium (90% (v/v) FBS, 10% (v/v) DMSO) to a concentration of 1 x 10^6 cells/mL. Aliquots of 1 mL were then transferred to sterile cryotubes and lowered slowly into the N_2 gas and liquid before being eventually immersed in liquid nitrogen.

2.2.2 Preparation of fluorescently-labelled liposomes

2.2.2.1 Preparation of lipid cake (film)

DSPE-PEG-COOH and cholesterol (1:1) were resuspended in 2 mL of 4:1 chloroform / methanol and throughly mixed by gentle vortexing. The solvent was removed by evaporation in a nitrogen gas flow for 1.5 h at room temperature to obtain a dry lipid cake (film).

2.2.2.2 Hydration of lipid film

The lipid film was resuspended in 1 mL 0.1 M PBS, pH 7.3, containing 25 μg/mL fluorescein isothiocyanate solution. The lipid solution was then freeze-thawed for 3-5 cycles between –80°C and 37°C, vortexed and sonicated for 15 min in a water-bath. The lipids were then extruded 15 times through a 100 nm polycarbonate membrane using an Avanti Polar Lipids mini-extruder to create uniform liposomes between 100 and 200 nm in diameter. The extruder was pre-

warmed to 50ºC before extrusion to allow the liposomes pass through the polycarbonate membrane.

2.2.2.3 Separation of fluorescent label-encapsulated liposomes from free fluorescent dye using size exclusion chromatography

Size exclusion chromatography with Sephadex G-25 (column size 0.5 × 6 cm) was used to separate fluorescent liposomes from free fluorescent dye. The column was equilibrated using 0.1 M PBS, pH 7.3, and the solution of lipid was added to the column. Fractions of 0.5 mL were collected and the fluorescence of the collected samples analysed in a Tecan Safire fluorescence reader (excitation 492 nm; emission 521 nm) to monitor the separation of fluorescent liposomes.

2.2.3 Fluorescently-labelled immunoliposome preparation

2.2.3.1 Attachment of antibodies to lipid *via* carboxylic groups

An amide bond was formed in two stages to achieve conjugation between DSPE-PEG-COOH phospholipid and antibody containing amine group. In the first stage, a free carboxylic group on the terminal end of a PEG chain in phospholipid was activated with water-soluble N,N'-dicyclohexyldiimide (DCC) and N-hydroxysulfosuccinimide (NHS). DSPE-PEG-COOH activation bases on carboxylic group esterification by DCC reagent. In the second stage, antibody was resuspended in 50 mM K_2HPO_4 buffer, pH 8.5, using a Vivaspin column (‘cut-off’ 5,000 Da) and was pooled together with phospholipid. A forty molar excess of this esterified lipid was conjugated to antibody by incubation in 50 mM K_2HPO_4 buffer, pH 8.5, overnight at 4°C. This lipid-antibody solution was dialyzed using 3,500 Da dialysis tubing against 0.1 M PBS, pH 7.4 for 2 h (‘cut-off’ 50,000 Da) to remove

DMSO in which esterified lipid was resuspended. The activated carboxyl groups reacted with amino groups on the antibody to create an amide bond (Figure 2.1). Subsequently, lipid-antibody linkage can be used for reverse-phase evaporation (REV) or co-incubation method.

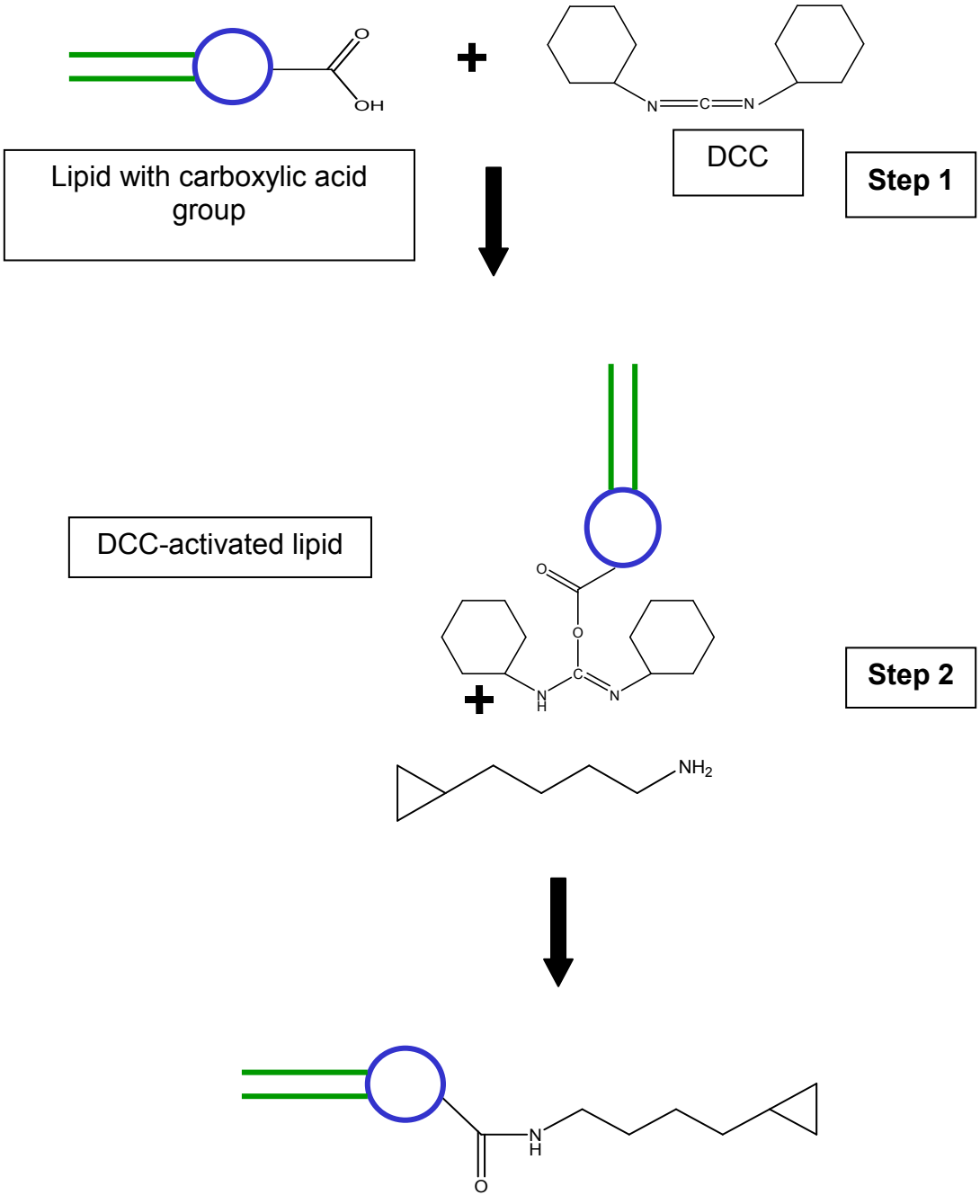

Figure 2.1 Amide bond reaction scheme
Carboxylic acid group activation (Step 1) facilitates conjugation with peptide containing amine group (Step 2).

2.2.3.2 Thin Layer Chromatography (TLC)

Esterification of DSPE-PEG-COOH was confirmed using thin layer chromatography (TLC). Confirmation of DSPE-PEG-COOH esterification was performed just before pooling this compound together with antibody for conjugation. Unmodified DSPE-PEG-COOH and esterified DSPE-PEG-COOH lipid were run on a Fluka silica plate (60 Å pore diameter) in chloroform/methanol (2:1) mobile phase and developed in iodine vapour. DSPE-PEG-COOH is a polar compound and is strongly attracted to the polar silica, whereas the non-polar esterified form of DSPE-PEG-COOH is less polar and runs further up the plate.

2.2.3.3 Immunoliposome preparation by Reverse Phase Evaporation (REV)

60 mol% DSPC, 30 mol% cholesterol, 9.9 mol% DSPE-PEG-COOH and 0.1 mol% rhodamine-PE phospholipids were resuspended in chloroform. DSPE-PEG-CO-NH-Ab conjugated (lipid-Ab), suspended in 0.1 M PBS, pH 7.3, was added to the chloroform lipid mixture. Aqueous and organic phases were observed. The lipid mixture was sonicated until it became a clear one-phase homogenous dispersion. Then, the mixture was placed on a rotary evaporator and organic solvent was slowly removed under reduced pressure at room temperature. The procedure was performed slowly taking care to avoid the formation of bubbles or foam. An excess of organic solvent allowed the creation of ‘inverted micelles’ (small water droplets) that were stabilized by the phospholipid monolayer. Slow removal of the organic solvent led to the transformation of these ‘inverted micelles’ into a viscous ‘gel-like’ state. At the critical point in this procedure, the gel state collapses and some of the inverted

micelles disintegrate. Subsequently, phospholipid concentration increases, due to evaporation of chloroform, which contributes to the formation of a complete bilayer of liposomes. Liposomes prepared by the REV method are mainly unilamellar, composed of one lipid bilayer (Szoka and Papahadjopoulos, 1978).

2.2.3.4 Immunoliposome preparation by co-incubation method

Briefly lipids were resuspended in chloroform and mixed together. The solvent was evaporated under nitrogen gas or with a Rotovap R-200 vacuum. The lipid film was hydrated in 1 mL 0.1 M PBS, pH 7.3, by vortexing. Liposomes were then extruded through a 100 nm polycarbonate membrane. Then, two mol% of DSPE-PEG-COOH was first esterified using DCC and NHS reagents. Forty molar excess of esterified DSPE-PEG-COOH was used for antibody conjugation (section 2.2.3.1). For immunoliposome preparation, DSPE-PEG-CO-NH-Ab in 100 µL 0.1 M PBS, pH 7.3, was co-incubated with previously prepared liposomes overnight at 4ºC while stirring.

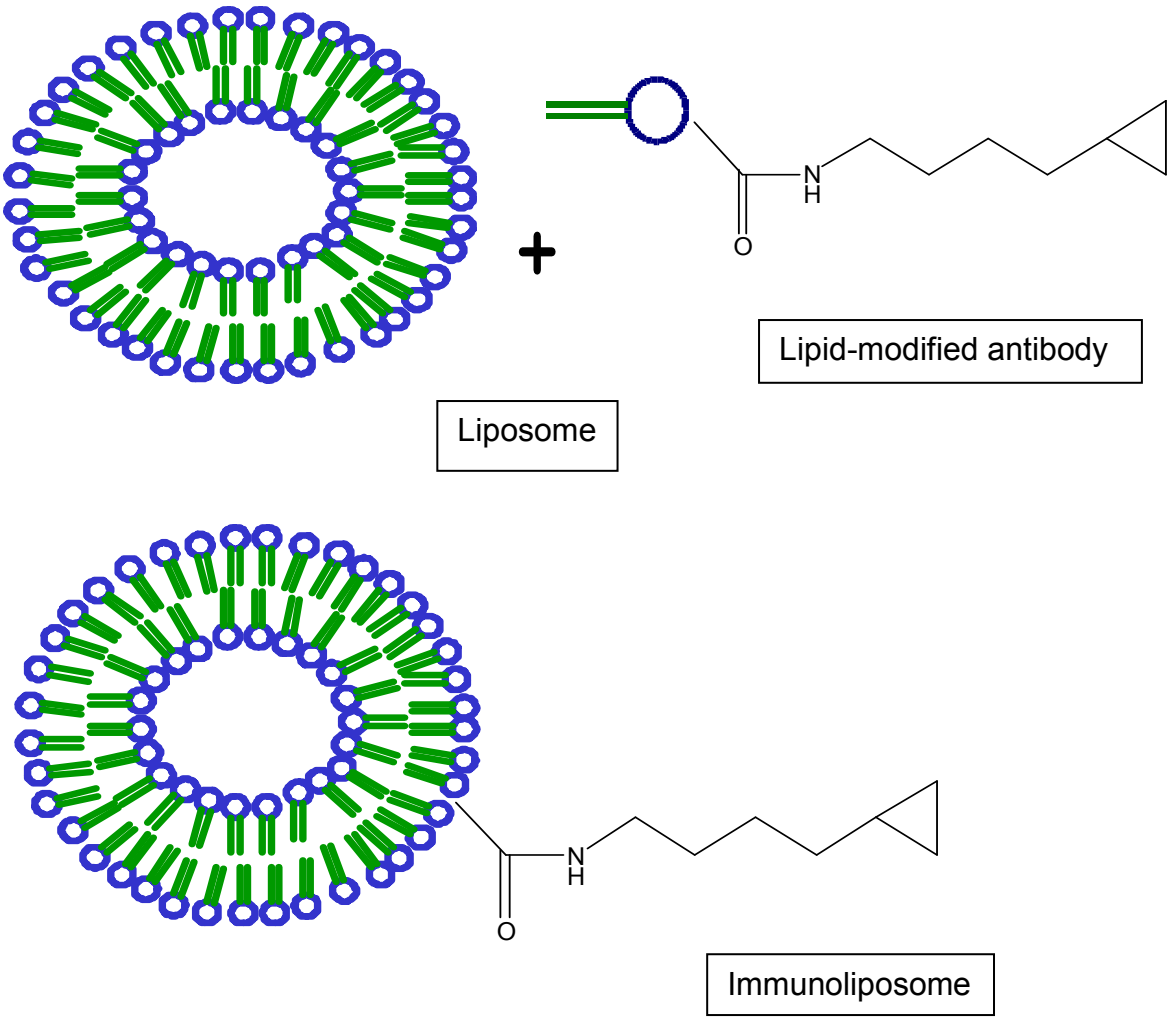

Figure 2.2 Co-incubation method for immunoliposome preparation.
Lipid-modified antibody was incorporated into the liposome membrane creating antibody-targeted liposomes (immunoliposomes).

2.2.3.5 Purification of immunoliposomes (IL) by ultracentrifugation

Separation of unbound antibodies from fluorescent immunoliposomes was performed by ultracentrifugation for 1 h at 149,008 g at 4°C. Ultracentrifugation of prepared 1 mL volumes of immunoliposomes was carried out twice and the supernatants collected. Following centrifugation and decanting of the supernatants the immunoliposome pellet was resuspended in 0.1 M PBS, pH 7.3 buffer.

2.2.3.6 Purification of immunoliposomes (IL) by dialysis

Separation of antibodies, which did not link to fluorescent liposomes from fluorescent immunoliposomes, was performed by dialysis against 0.1 M PBS, pH 7.3, for 2 days ('cut-off' 300,000 Da) at 4°C.

2.2.3.7 Liposomes and immunoliposome size determination and stability by Photon Correlation Spectroscopy (PCS)

Immunoliposomes were extruded through a polycarbonate membrane (100 nm pore size) and filtered (0.2 μm 'cut-off'). The hydrodynamic sizes of the immunoliposomes were determined using Photon Correlation Spectroscopy (Malvern / Zetasizer Nano 3000HS), HPPS, in the School of Chemical Sciences at Dublin City University. Liposomes (0.1 mg/mL of lipids) were placed in a plastic disposable 12.5 x 12.5 x 45 mm cuvette, and then inserted into the instrument.

Light from a 3mW He-Ne laser operating at a wavelenght of 633 nm was focused onto the sample held in a cuvette. A thermal equilibration time of 5-10 min preceded all measurements. Sample temperature was maintained constant at 25°C by the internal heating system of the instrument. The intensity of the scattered light was detected at a 173° angle to the incident beam. This is known as backscatter detection. This optical configuration results in an 8-fold increase in the detected scattering volume when compared with classical 90° scattering detection, resulting in an 8-fold increase in the count rate observed at the detector (Kaszuba *et al.,* 2008).

Photon Correlation Spectroscopy (PCS) can also provide information about the zeta potential of liposomes. The zeta potential is important in the assessment of

liposome stability and propensity for aggregation. Zeta potential indicates the degree of repulsion between adjacent, similarly charged particles in dispersion. For molecules and particles that are small enough, a high zeta potential will confer stability, e.g., the solution or dispersion will resist aggregation. When the potential is low, attraction exceeds repulsion and the dispersion will break and flocculate. Colloids with high zeta potential (negative or positive) are electrically stabilized while colloids with low zeta potentials tend to coagulate or flocculate (ASTM Standard, 1985).

2.2.3.8 Protein determination using the micro Lowry assay with Peterson's modification

Bovine Serum Albumin (BSA) protein standard solutions (50 - 400 µg/mL), blank (plain liposomes) and samples were prepared. 100 µL of the deoxycholate (DOC) 0.15% (v/v) was added to each solution and mixed thoroughly. After 10 min 100 µL of the 72% (v/v) TCA (trichloroacetic acid) solution was added. The solution was centrifuged in 15 mL tubes in an Eppendorf centrifuge for 5 min at 3220 g. The resulting pellet was resuspended in 1 mL of Lowry reagent solution and allowed to stand for 10 min at room temperature. Folin & Ciocalteu's phenol reagent (0.5 mL) was then added and the samples were mixed immediately. Colour was allowed to develop for 25 min and the absorbance was read at 600 nm using a Tecan Safire 2 spectrophotometer.

A calibration curve of BSA protein standards was prepared and used to determine the protein concentration in each sample.

This method was used for the quantification of soluble proteins. The procedure is based on Peterson's modification of the micro Lowry method and utilizes sodium dodecylsulfate (included in the Lowry reagent) to facilitate the dissolution of relatively insoluble lipoproteins. For many proteins, the Lowry reaction can be used directly with the protein solution. However, interference in the direct Lowry procedure is commonly caused by other chemicals in the protein solution, such as Tris, ammonium sulfate, EDTA, sucrose, citrate, amino acid and peptide buffers, and phenols. The protein precipitation procedure uses DOC (deoxycholate) and TCA (trichloroacetic acid), which eliminates all previously, mentioned interferences with the exception of phenols. The Lowry procedure is based on two chemical reactions. The first is the Biuret reaction, in which the alkaline cupric tartrate reagent complexes with the peptide bonds of the protein. This is followed by the reduction of the Folin & Ciocalteu's phenol reagent, which yields a purple colour. Absorbance of the coloured solution is read at a suitable wavelenght between 500-800 nm.

2.2.3.9 FLISA (Fluorophore-Linked ImmunoSorbent Assay) for immunoliposomes

Two human multiple myeloma cell lines (U266; RPMI8226) were co-incubated at 37°C for 1.5 h with 0.5 mg/mL of fluorescently-labelled immunoliposomes.

Tubes (1.5 mL) were pre-blocked with PBS-FCS (fetal calf serum)-sodium azide solution overnight at 4°C. One million (10^6) cells were incubated with immunoliposomes for 30 min at 4°C. Cells were then centrifuged down at 3,000 g. The cell pellet was resuspended in 200 µL of 0.1 M PBS, pH 7.4, and recentrifuged. Subsequently, cells were transferred to fresh tubes and washed

once with 0.1 M PBS, pH 7.4. Cells were then placed on a 96-well plate and the fluorescence was immediately determined (excitation 540 nm and emission 625 nm) using a Tecan Safire 2 Plate Reader.

2.2.4 FACS analyses for protein expression levels on cells

Analysis of surface expression of surface proteins was performed by standard direct immunofluorescence. One million cells were centrifuged at 3,000 g for 5 min using Z 233 MK-2 centrifuge and resuspended in FACS buffer (Table 2.4). Cells were then centrifuged at 3,000 g for 5 min and resuspended in 100 µL 25 µg/mL of mouse anti-human CD138 antibody. Non-specific binding of antibodies was assessed by labelling cells with an isotype control antibody. Samples were well mixed and incubated for 30 min at 4°C. Finally, cells were washed three times by centrifugation at 3,000 g for 5 min using Z 233 MK-2 centrifuge and resuspended in 200 µL 4% (v/v) formaldehyde/PBS. Samples were transferred to FACS tubes and were analyzed immediately. Antibody-labelled cells were identified and analysed for surface fluorescence at 488/530 nm on a FACSscan flow-cytometer (Becton-Dickinson). Fluorescence data were collected and analysed by the CellQuest software (Becton Dickinson).

2.2.5 FACS analyses - immunoliposome binding assay

One million cells were centrifuged at 3,000 g for 5 min using Z 233 MK-2 centrifuge and resuspended in 0.5 mg/mL of immunoliposomes in ‘serum-free’ medium. Cells were incubated with immunoliposomes for 1.5 h at 37ºC. Cells were subsequently washed three times at 3,000 g for 5 min with 0.1 M PBS, pH 7.3 using Z 233 MK-2 centrifuge, and then resuspended in 200 µL 4% (v/v)

paraformaldehyde/PBS. Samples were transferred to FACS tubes and immediately analyzed using the FACS Calibur. Immunoliposome-labelled cells were identified and analysed for surface fluorescence for FITC (excitation 488 nm; emission 530 nm) and for rhodamine B (excitation 540 nm; emission 625 nm) on a FACSscan flow-cytometer (Becton-Dickinson). Fluorescence data were collected and analysed by the CellQuest software (Becton Dickinson).

2.2.6 Synthesis of Polychelating Amphiphilic Polymer (PAP)

2.2.6.1 NGPE-PLL-CBZ synthesis

1 mL of 25 mg/mL NGPE (1, 2 – dioleoyl – *sn* – glycero – phosphoethanolamine – N - (glutaryl); Figure 2.3) in chloroform was activated with N - (3 - dimethylaminopropyl) - N' - ethylcarbodiimide hydrochloride (EDC) (20 mg) in the presence of N – hydroxysuccinimide (NHS) (13 mg) for 2-3 h at room temperature. Then, 40 µL of triethylamine was added to make the solution basic, to allow conjugation with poly – ε – CBZ (carbobenzyoxy) – $_{DL}$ – Lysine (PLL-CBZ).

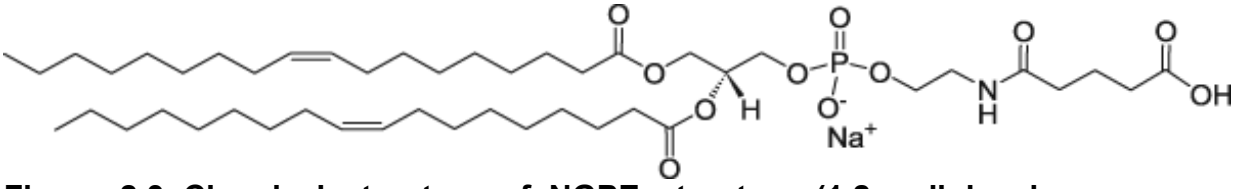

Figure 2.3 Chemical structure of NGPE structure (1,2 - dioleoyl - *sn* - glycero - 3 - phosphoethanolamine - N - (glutaryl)).

All NH_2 groups of PLL-CBZ are protected by CBZ groups, except one which will link to the activated carboxylic group of NGPE. For this reaction to occur, 186 mg of PLL-CBZ was dissolved in 4 mL of DMF solvent and pooled together with activated NGPE phospholipids. The reaction was performed at room temperature for 12 h with stirring. Any chloroform present was evaporated from the mixture

and the product was precipitated using distilled water. The NGPE-PLL-CBZ product was freeze-dried for 48 h. NGPE-PLL-CBZ polymer was obtained (193 mg by weight).

Poly-CBZ-lysine complex (10 mg) and NGPE-PLL-CBZ (10 mg) were dissolved in Cd_4Cl_3 and DMSO-d_4 and separated into two vials and NMR analyses were performed for confirmation that synthesis was successfully achieved.

2.2.6.2 NGPE-PLL-CBZ deprotection

The NGPE-PLL-CBZ complex was deprotected from the CBZ group using 2 mL of 33% (v/v) hydrogen bromide in acetic acid for 2 h at room temperature with stirring. The complex was precipitated using diethyl ether and freeze-dried for 12 h and 107 mg (by weight) of deprotected complex was obtained. Deprotection of the NGPE-PLL-CBZ complex generates up to 11 NH_2 groups which are available to undergo reaction with DTPA (Torchilin *et al.*, 1994).

2.2.6.3 NGPE-PLL-DTPA (PAP) synthesis

NGPE-PLL was treated with DTPA anhydride in the presence of triethylamine for 16 h at room temperature with stirring. Succinic anhydride was added and the reaction was allowed to run for 1 h at room temperature followed by dialysis against distilled water (‘cut-off’ 3,500 kDa).

All NH_2 groups which did not react with the DTPA anhydride were blocked by succinic anhydride.

2.2.6.4 Loading of PAP with Gd ions

$GdCl_3 \cdot 6H_2O$ was added to DTPA-PLL-NGPE suspended in 2 mL of pyridine and stirred for 4 h at room temperature**.** The reaction mixture was then dialyzed for 24 h against deionized water and vacuum dried at room temperature.

2.2.7 Preparation of contrast liposomes and immunoliposomes

Defined amount of lipids (described in 3.2.2, 4.2.2, 5.2.2, 5.2.3, 5.2.4, 5.2.6, 5.2.7, 5.2.8 sections) were resuspended in chloroform in a round bottomed flask and the solvent was evaporated under nitrogen for 30 min at room temperature. The lipid film was dried for 15 min in a freeze dryer. The lipid film was then hydrated in 0.5 mL 0.1 M PBS, pH 7.3. The mixture was heated to 50°C and vortexed. Liposomes were extruded through a 100 nm polycarbonate membrane.

For immunoliposome preparation liposomes were co-incubated with the DSPE-PEG_{2000}-antibody complex for 12 h at 4°C. Separation of unbound antibody from immunoliposomes was performed by dialysis against 0.1 M PBS, pH 7.3, for 2 days (‘cut-off’ 300,000 Da) at 4°C.

2.2.8 Cytotoxicity studies - MTT (1 - (4,5 – Dimethylthiazol – 2 - yl) - 3,5 - diphenylformazan) test

The MTT assay is a colorimetric test based on MTT’s (tetrazole) reduction to purple formazan by living cells. This assay can be used to determine cell viability (Mosmann, 1983). In this research the MTT assay was used to determine the cytotoxic effect of contrast liposomes on cells.

B16F10 melanoma cancer cells were seeded in a 96-well plate with $8x10^3$ cells/100µL/well and incubated overnight at 37°C, in 5% (v/v) CO_2. The medium was removed and the cells were treated with 100 µL of different concentrations of liposome formulations (1.4 – 0.01 mg/mL of lipids) in triplicate for 24 h at 37°C, 5% (v/v) CO_2. After 24 h, the cells were washed once with DMEM 'serum-free' medium and immediately the MTT reagent was added. The cells were further incubated for 1.5 h. Subsequently, the MTT solution was removed, 100 µL of DMSO was added and the fluorescence was determined (540 nm (excitation)/690 nm (emission)).

2.2.9 Gadolinium determination in contrast liposomes using Inductively Coupled Plasma-Atomic Emission Spectroscopy (ICP-AES)

The gadolinium concentration in contrast liposomes was determined using Inductively Coupled Plasma-Atomic Emission Spectroscopy (ICP-AES). This is a technique used for detection and analysis of trace metals in a liquid sample. The sample is aspirated and aerosolised and introduced into a high temperature (2100 – 2800ºC). The flame atomizes the sample (Figure 2.4). The atoms absorb radiation from the external light source at a characteristic wavelength, which stimulates a transition to an excited state energy level, allowing the quantitative measurement of the amount of emitted radiation.

Contrast liposomes were resuspended in 0.1 M PBS, pH 7.3, containing 0.2 % (v/v) Triton X-100. Then, liposomes were resuspended in 1 M HNO_3 for ICP-AES analysis.

A calibration curve was prepared using gadolinium standards in 1 M HNO_3.

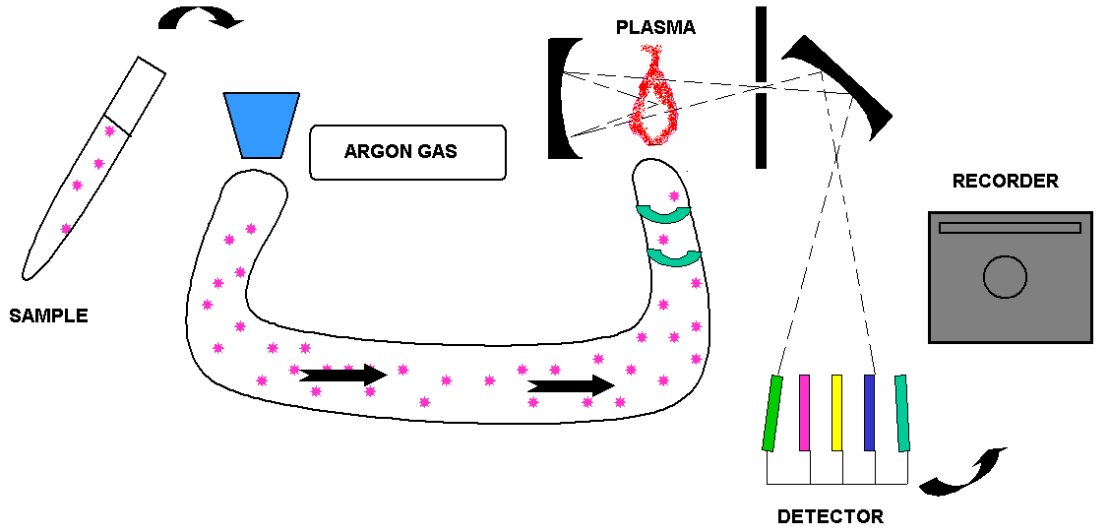

Figure 2.4 Schematic of Inductively Coupled Plasma-Atomic Emission Spectroscopy (ICP-AES).
The atomized sample absorbs radiation at a characteristic wavelength from the external light source and emittes light which can be quantitated.

2.2.10 Fast Field-Cycling NMR (FFC NMR)

Field-cycling NMR relaxometry involves the rapid switching of magnetic fields throughout the experiment in order to measure T_1 over a wide range of low magnetic field strenghts. A plot of the spin-lattice relaxation rate R_1 as a function of magnetic field, and hence resonance frequency, is known as a Nuclear Magnetic Resonance Dispersion (NMRD) profile. All field-cycling relaxometry experiments were performed on a Spinmaster FFC-2000 Fast Field-Cycling NMR Relaxometer (Stelar, Mede, Italy) using a sample volume of 0.5 – 1 mL. Measurements were carried out at 25°C. To measure T_1 at frequencies higher than 20 MHz, a reconditioned Bruker WP80 variable field magnet was used. This allowed measurements of T_1 from 35 – 75 MHz.

2.2.11 Magnetic Resonance Imaging (MRI)

The experiments were carried out on a 1.5 T whole-body clinical scanning system (Philips MRI Scanner, Gyroscan Intera) in Cappagh National Orthopaedic Hospital, Finglas, Dublin 11, Ireland.

Samples presented on the T_1-weighted image scan were analyzed using ZEN Carl Zeiss software. The same area of the sample picture was selected and the mean of pixel intensity was calculated.

2.2.12 CD138 protein fragment production

2.2.12.1 Cloning of CD138 gene elements into pQE60 and pQETriSystem II vectors

2.2.12.1.1 mRNA isolation from RPMI8226 cell line

Two T-75 flasks with the RPMI8226 human multiple myeloma cell line were centrifuged for 10 min at at 342 g (Sigma centrifuge). The cell pellet was resuspended in Trizol. RNA extraction was performed according to Fanning *et al.* (2002) protocol. Cells harvested from one T-75 flask were resuspended in 0.5 mL of Trizol in 'Rnase-free' tubes and left for 5 min at RT. Then, 100 µL of chloroform was added to tubes and they were shaked for 15 s and incubated for 2-3 min. Then, tubes were centrifuged at 14,000 g using Z 233 MK-2 centrifuge for 15 min at 4ºC. Three layers were observed. The upper (aqueous) layer was transferred to a fresh tube and 250 µL isopropanol was added and incubated for 10 min at RT. Then, samples were centrifuged at 14,000 g for 10 min at 4ºC. The supernatant was discarded and the precipitated RNA was washed with 75% (v/v) ethanol. The mixture was then centrifuged at 14,000 g for 10 min at 4ºC. Ethanol

was decanted and pellet was dried at 37ºC for 10 min. RNA was resuspended in 20 µL 'RNase-free' water. For storage, RNA was resuspended in 100% (v/v) ethanol supplemented with 0.3 M sodium acetate.

2.2.12.1.2 cDNA production from mRNA by reverse transcription

5 µg RNA was used for reverse transcription. cDNA was synthesized using the SuperScript III Preamplification System for First Strand cDNA Synthesis (Invitrogen, Cat# 18080-093).

Components used for reverse transcription are listed in Table 2.10 and Table 2.11.

First, 5 µg RNA was pooled together with primer oligo(dt) and dNTPs and co-incubated at 65ºC for 5 min and then placed on ice for 1 min (Table 2.10). Then, reverse-transcroption buffer was pooled with $MgCl_2$, DTT, RNaseOut inhibitor and SuperScript III reverse-transcriptase. Components, listed in Table 2.11, were pooled together with solutions prepared, as listed in Table 2.10, and then the mixture was incubated at 50ºC for 50 min. The reaction was terminated by heating at 85ºC for 5 min and then chilled on ice. One µL of RNaseH was then added and the reaction mixture was incubated for 20 min at 37ºC.

Table 2.10 List of components and their concentrations used in cDNA synthesis.

COMPONENT	VOLUME PER REACTION
RNA (5 µg)	
Primer oligo(dt) (50 mM)	1 µL
dNTPs (10 mM)	1 µL
Molecular Grade H_2O	Make up to 10 µL

Table 2.11 List of components and their concentrations used in cDNA synthesis.

COMPONENT	VOLUME PER REACTION
$MgCl_2$ (25 mM)	4 µL
10X Buffer	1X
RNaseOut™ ribonuclease	1 µL
Inhibitor (40 U/µL)	
DTT (0.1 M)	2 µL
Superscript III RT (200 U/µL)	1 µL
Molecular Grade H_2O	Make up to 20 µL

2.2.12.1.3 Design of CD138 fragments primers for pQE60 and pQETriSystem II vector

Primers were designed for further ligation into the pQE60vector (QIAGEN).

The multi-cloning region of the pQE60 vector contains a *Nco*I site at the amino end of the sequence and a *Bam*HI at the carboxyl end. Therefore, forward primers were designed to include the *Nco*I restriction site sequence and the

reverse primers were designed to contain the *Bam*HI sequence. The primer 3 programme was used for the design of primers.

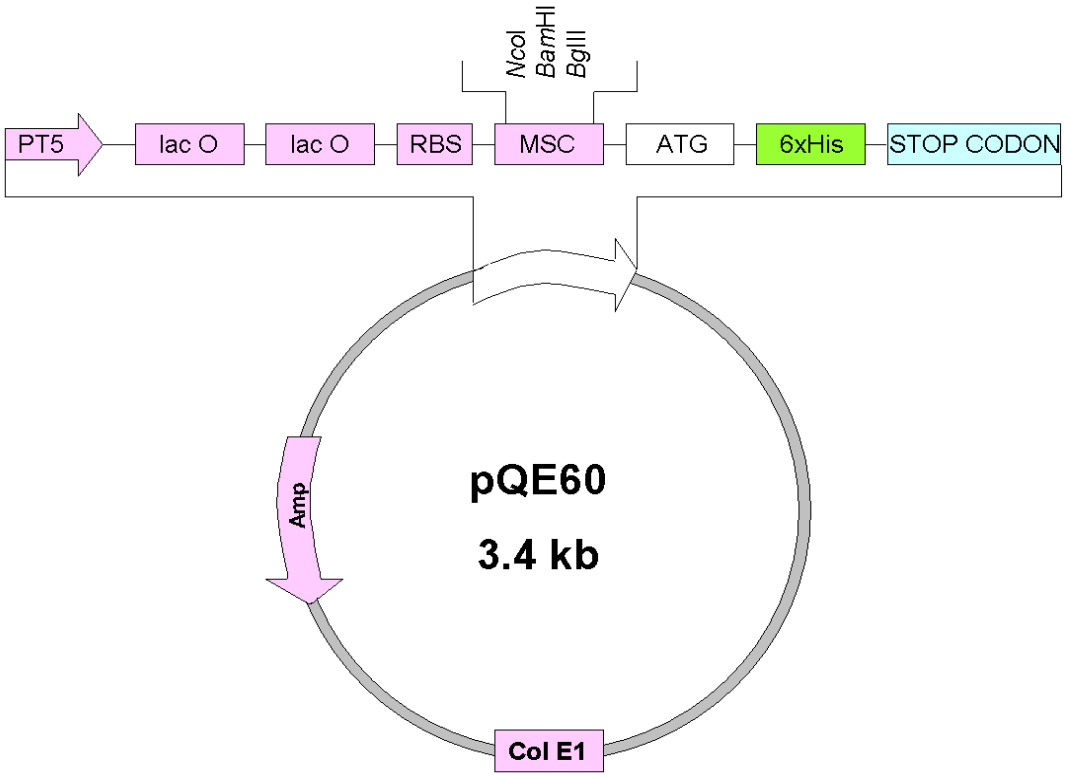

Figure 2.5 Diagram of the pQE60 vector used for the cloning of CD138. The plasmid contains a T5 promoter (PT5), lac operator (lac O), a ribosome binding site (RBS), a ATG start codon, a 6xHis tag sequence, a multiple cloning site (MCS) and a stop codon. The pQE60 vector has an amplicillin resistance gene and a Col E1 origin of replication.

The sense primer with the ***Nco*I** restriction site:

5' TAT CCA TGG AT AGG CGC GCG GCG CTC TG 3'

The anti-sense primer 1 (1-261 bp) with the ***Bam*HI** restriction site:

5' GAT GGA TCC AGC TGT AGC CTC CAG GCC GGT 3'

The anti-sense primer 2 (1-759 bp) with ***Bam*HI** restriction site:

5' GAT GGA TCC CAG CAC CTC TTT CCT GTC CA 3'

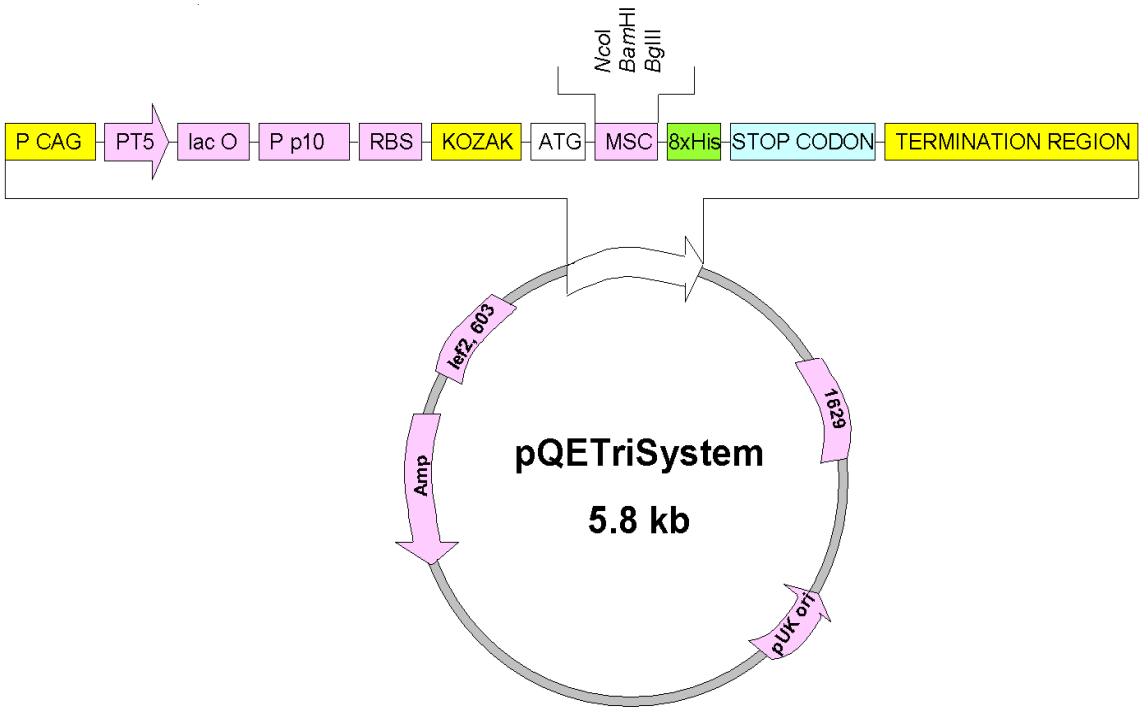

Figure 2.6 Diagram of the pQETriSystem vector used for the cloning of CD138.
The plasmid contains a T5 phage promoter (PT5), a P CAG promotor, a P p10 CMV/actin/globulin promotor, a lac operator (lac O), a ribosome binding site (RBS), a ATG start codon, a 8xHis tag sequence, a multiple cloning site (MSC), a stop codon and a pUK origin of replication.

The pQETriSystem vector contains a CAG, a T5, and p10 promoters that enable 6xHis-tagged protein expression in mammalian, *E. coli*, and baculovirus-infected insect cells, respectively. T5 promotor is recognized by RNA polymerase present in *E.coli* cells. The pQE vectors enable placement of the 6xHis tag at either the N- or C-terminus of the recombinant protein.

The multi-cloning region of the pQETriSystem II vector contains a *Sac*I site at the NH_2 end of the sequence and a *Hind*III at the COOH end. Therefore, forward primers were designed to include the *Sac*I restriction site sequence and the reverse primers were designed to contain the *Hind*III sequence.

The sense primer with the ***Sac*I** restriction site extra bases:

5' - TAT GAG CTC ATG AGG CGC GCG GCG CTC TG – 3'

The anti-sense primer (1 – 759 bp) with the ***Hind*III** restriction site:

5' - GAT AAG CTT CAG CAC CTC TTT CCT GTC CA – 3'

2.2.12.1.4 Plasmid isolation from bacterial cells

XL10 Blue *E. coli* cells containing the pQE60 or pQETriSystem II vector were inoculated in 2 x TY medium supplemented with 100 µg/mL of carbenicillin at 37°C overnight, while shaking (250 rpm using New Brunschwick Scientific-Excella E-24 Incubator).

The pQETriSystem II vector was isolated from cells according to the Promega Wizard Plus SV Miniprep protocol. A ten mL overnight culture was centrifuged at 3,220 g for 5 min in Eppendorf (5804R) centrifuge. The pellet was resuspended in 250 µL of cell resuspension solution. Next, 250 µL of cell lysis solution was added and microcentrifuge tube was inverted 4 times. It was left for 5 min and then alkaline protease solution was added to inactivate all endonucleases which could affect the quality of the isolated DNA. After adding 350 µL neutralization solution, and centrifugation (14,000 g for 10 min) in a microcentrifuge tube using the Hermle Z 233 MK-2 centrifuge the lysate supernatant was added to the silica minicolumn. Plasmid DNA, which bound to the silica minicolumn, was washed once with 95% (v/v) ethanol (to remove salt) at 14,000 g. The plasmid DNA was eluted from the silica minicolumn using 100 µL 'nuclease-free' water by centrifugation at 14,000 g for 1 min at RT.

2.2.12.1.5 Restriction analysis

A restriction analysis was performed at 37ºC for 1.5 h for the pQE60 and pQETriSystem II vectors containing CD138 gene fragments as follows:

REAGENT	VOLUME
DNA (5 µg)	depends on inserts and vector conc.
***Sac*I** (20 U / µL)	1 µL
***Hind*III** (20 U / µL)	1 µL
NE buffer (10x)	15 µL
10x BSA (100x)	1.5 µL
H_2O	made up to 150 µL

REAGENT	VOLUME
DNA (5 µg)	depends on inserts and vector conc.
***Hind*III** (20 U / µL)	1 µL
***Bam*HI** (20 U / µL)	1 µL
NE buffer (10x)	15 µL
10x BSA (100x)	1.5 µL
H_2O	made up to 150 µL

Each digest was run on a 1% (w/v) agarose gel (section 2.2.10.3).

2.2.12.1.6 Ligation of PCR products into pQE60 or pQETriSystem II vectors

The ligation reaction was set up as follows:

pQE60 vector			
1 –261 bp GENE		**1 – 759 bp GENE**	
ADDITIONS	**VOLUME**	**ADDITIONS**	**VOLUME**
• pQE60	11 µL (0.05 µg)	• pQE60	11 µL (0.05 µg)
• cut 1 –261 bp insert	1.6 µL (0.3 µg)	• cut 1 –759 bp insert	1.8 µL (0.1 µg)
• 5x buffer	4 µL	• 5x buffer	4 µL
• T4 DNA (40 U / µL)	2 µL	• T4 DNA (40 U / µL)	2 µL
• H_2O	1.4 µL	• H_2O	1.2 µL
• **Total volume**	20 µL	• **Total volume**	20 µL

pQETriSystem II vector			
1 –261 bp GENE		**1 – 759 bp GENE**	
ADDITIONS	**VOLUME**	**ADDITIONS**	**VOLUME**
• pQETriSystem II vector • cut 1 –261 bp insert • 5x buffer • T4 DNA (40 U / µL) • H_2O	8.2 µL (1 µg) 1.3 µL (1 µg) 4 µL 2 µL 4.5 µL	• pQETriSystem II vector • cut 1 –759 bp insert • 5x buffer • T4 DNA (40 U / µL) • H_2O	8.2 µL (1 µg) 3.4 µL (1 µg) 4 µL 2 µL 2.4 µL
• **Total volume**	20 µL	• **Total volume**	20 µL

The molar ratio of insert/vector was 3:1 for ligation.

The ligation reaction was incubated in room temperature overnight and then used for transformation.

2.2.12.1.7 DNA precipitation

Ligated DNA was precipitated to remove PCR reagents and for concentration. Precipitation was performed by adding 1/10 original volumes 3M sodium acetate, pH 5.2, followed by adding 2x total volume of 100% (v/v) ethanol. The solution was incubated at -20°C overnight. It was then centrifuged for 20 min at 19,500 g in Eppendorf centrifuge and the pellet was resuspended again using pre-chilled 75% (v/v) ethanol. The solution was centrifuged one more time for 10 min at 14,000 g and pellet was left to dry. After ethanol evaporation the DNA pellet was resuspended in sterile water.

2.2.12.2 Transformation of pQE60 and pQETriSystem II vector into XL10 Gold and Rosetta™ *E. coli* competent cells by electroporation

2.2.12.2.1 XL10 Gold, Rosetta™ *E.coli* competent cells - preparation and electroporation

Twenty µL of stock *E.coli* XL10 Gold cells was inoculated in SB medium supplemented with 5 µg/mL of tetracycline and incubated at 37°C overnight. Then, 3 mL of inoculated cells were transferred into two 250 mL volume of SB medium without any antibiotic. The culture was grown at 37°C with shaking (250 rpm) until an OD_{600} of 0.6 - 0.8 was reached. Next, the culture was chilled on ice and spun down in sterile tubes for 20 min at 4 °C (3,220 g) in an Eppendorf centrifuge. The pellets were resuspened in pre-chilled 10% (v/v) glycerol on ice and centrifuged as before. The supernatant was discarded and pellets resuspended in 10 % (v/v) glycerol, pooled together, made up to 250 mL with glycerol and spun down as before. The pellet was resuspended in 25 mL of glycerol and transferred to a 50 mL sterile tube. Cells were spun down as before (for 20 min at 3,220 g). The cell pellet was then gently resuspended in 5 mL of glycerol and immediately frozen in 0.5 mL aliquots in liquid nitrogen. Cells were also stored at -80°C.

DNA (pQETriSystem II and pQE60 vector) was transformed into *E. coli* XL10 Gold cells by electroporation to allow CD138 protein expression. Plain *E. coli* XL10 Gold competent cells (without plasmid) were thawed for transformation. Two µL of each ligation was added directly into the tube containing the competent cells and mixed by pipetting. Competent cells with the ligation

mixture were immediately put on the bottom of the pre-chilled cuvette (2 mm) and exposed to 2,500 V.

Afterwards cells were immediately transferred to prewarmed SB medium and placed to 37°C with shaking (250 rpm) for 1 h. Transformants were then spread onto LB agar plates containing100 µg/mL of carbenicillin. Plates were inverted and placed at 37°C overnight.

2.2.12.3 Agarose gel electrophoresis for DNA characterisation

DNA was analysed by agarose gel electrophoresis. Gels were prepared by dissolving agarose (usually 0.9-1.5% (w/v) in 1x TAE buffer) with 0.5 µg/mL of ethidium bromide. Gels were run at 100 V for 0.5 h, then visualized on a UV trans-illuminator and photographed using a UV image analyser (Amersham Pharmacia Biotech).

2.2.12.4 Colony PCR

Transformants were analysed by colony PCR as follows:

1-261 bp GENE FRAGMENT		1-759 bp GENE FRAGMENT	
VOLUME (µL)	**COMPONENTS**	**VOLUME (µL)**	**COMPONENTS**
	single colony		single colony
10 µL	Green GoTaq flexi buffer (5x)	10 µL	Green GoTaq flexi buffer(5x)
1 µL	dNTP (10 mM)	1 µL	dNTP (10 mM)
2 µL	$MgCl_2$ (25 mM)	2 µL	$MgCl_2$ (25 mM)
1 µL	Sense primer (100 pmol / µL)	1 µL	Sense primer (100 pmol / µL)
1 µL	Anti-sense (100 pmol / µL)	1 µL	Anti-sense (100 pmol / µL)
34.7 µL	sterile H_2O	34.7µL	sterile H_2O
0.25 µL	GoTaq polymerase (5 U / µL)	0.25 µL	GoTaq polymerase (5 U / µL)
Step 1: 95°C 2 min **Step 2:** 95°C 30 s **Step 3:** 58°C 30 s **Step 4:** 72°C 45 s **Step 5:** repeat Step 2 to Step 4 (30 times) **Step 6:** 72°C 5 min **Step 7:** 4°C pause		**Step 1:** 95°C 2 min **Step 2:** 95°C 30 s **Step 3:** 59°C 30 s **Step 4:** 72°C 45 s **Step 5:** repeat Step 2 to Step 4 (30 times) **Step 6:** 72°C 5 min **Step 7:** 4°C pause	

2.2.12.5 IPTG induced protein expression

Transformants were inoculated into 1 mL of SB medium supplemented with 100 µg/mL carbenicillin, After overnight incubation at 37°C, 100 µL of bacteria was subcultured into 10 mL fresh SB medium supplemented with 1X 5O5 medium (Table 2.4) and 100 µg/mL carbenicillin. Stock vials were prepared by adding glycerol (20% (v/v)) to the overnight grown culture and cells were then

stored at –80°C. The subcultured cells were grown until an OD of ~ 0.8 was reached followed by addition of isopropyl-β-D-thiogalactoside (IPTG) to a final concentration of 1 mM and inducing them overnight at 220 rpm at 30°C. The overnight culture was then spun down at 3,220 g for 20 min and the pellet was resuspended in 500 µL PBS. The resuspended culture was sonicated on ice for 90 s (with 3 s intervals between each step) at an amplitude of 50%, using a microtip Vibra Cell™ sonicator. Lysate was then centrifuged at 3,220 g for 20 min at 4°C to remove cell debris.

2.2.12.6 Polyacrylamide Gel Electrophoresis (PAGE)

Polyacrylamide gel electrophoresis (PAGE) was carried out using a discontinuous system, in the presence of sodium dodecyl sulphate (SDS), as described by Laemmli (1970). 12% (w/v) resolving and 5% (w/v) stacking gels were normally used and prepared from the following stock solutions as outlined in Table 2.5. Polymerisation of the separating gel acrylamide was catalysed by addition of ammonium persulfate solution and the accelerator TEMED (N,N,N',N'-tetramethyl-ethylenediamine) and the gel added to the space between the plates and covered with a layer of water. Once the gel had polymerised, the water was removed and the stacking gel placed was placed directly onto the separating gel. A plastic comb was placed in the gel to create the wells for sample application. When the gel had fully polymerised, the plates were placed in the elecrophoresis apparatus, the comb was removed and the chamber and wells filled with 1x electrophoresis buffer (25 mM Tris, 130 mM Glycine (electrophoresis grade), pH 8.3, and 0.1% (w/v) SDS) as outlined in Table 2.4. Excess sample buffer is essential to maintain reduction of protein

sulfhydryls and to prevent intra-molecular disulfide bond formation through oxidised cysteines. A 5 x stock solution of sample buffer was prepared to give the following final concentrations: 60 mM Tris-HCl, pH 6.8, 25% (w/v) glycerol, 2% (w/v) SDS, 14.4 mM 2-mercaptoethanol and 0.1% (w/v) bromophenol blue. Samples were mixed 1:5 with sample buffer and heated 5-10 min at 95°C. Appropriate protein molecular weight markers were run in parallel with samples. A total sample volume of 20 µL was added to the wells on the gel. The power unit was run at 90-130V.

2.2.12.7 Transfer of proteins from gels to nitrocellulose membranes and Western blotting

Following electrophoresis, a sheet of nitrocellulose membrane was placed on top of three sheets of Whatman filter paper pre-soaked in transfer buffer. The gel was carefully placed on top of the membrane and any air bubbles removed by rolling a clean 10 mL pipette over the sheets. Three more of pre-soaked filter paper were added on the top of the gel and air bubbles removed. The proteins were transferred from the gel to the membrane using a Bio-Rad Semi-dry Transfer system for 20 min at 15V at RT. After transfer the blotted membrane was blocked in 3% (w/v) milk Marvel in PBS for 1 h at RT. Following blocking, the blot was washed once with PBS and then incubated with mouse anti-human CD138 primary antibody at the 0.5 µg/mL in PBST containing 1% (w/v) milk Marvel solution for 1 h at RT. The blot was then washed three times with PBST then three times with PBS prior to incubation with 1:2,000 dilution of an enzyme-labelled secondary antibody (e.g. alkaline phosphatase-labelled goat anti-mouse IgG) in PBST containing 1% (w/v) milk Marvel for an 1 h at

RT. The blot was washed 3 times in PBST then PBS. Following this the membrane was developed using an appropriate substrate solution (e.g. 3,3',5,5'-Tetramethyl-Benzidine (TMB) for HRP-labelled and 5-bromo-4-chloro-3'-indolyphosphate / nitro blue tetrazolium chloride (BCIP/NBT) for alkaline phosphatase-labelled secondary antibodies). Color development was allowed to proceed at RT until the desired bands were apparent. The reaction was then stopped by washing extensively with distilled water.

2.2.12.8 Production of 1-253 aa CD138 protein fragment and purification using IMAC

Overnight cultures of selected clones were grown in LB medium, containing 100 µg/mL carbenicillin. This was carried out by inoculating with 10 µL of the stock culture and growth overnight at 37ºC. A 5 mL volume of the culture was then inoculated into 500 mL LB media containing 100 µg/mL carbenicillin and 1 x 5O5 media. The subcultured clone was incubated at 37ºC at 250 rpm until an OD ~0.8 (OD 800 nm) was achieved. The cultures were then induced by adding IPTG to a final concentration of 1 mM and incubating at 30ºC (250 rpm) overnight.

The overnight culture was then transferred to two 250 mL Sorval tubes and centrifuged at 18,500 x g in a GSA rotor for 20 min (‘brake on’) to pellet the bacterial cells. The supernatant was discarded. The pellet was thoroughly resuspended in 15 mL of sonication buffer (0.1 M PBS, pH 7.4, 0.5 M NaCl, 20 mM imidazole, 8 M urea) and aliquoted into 1 mL volumes in 2 mL microcentrifuge tubes. Each tube was sonicated on ice for 30 s (with 3 second intervals between each pulse) at an amplitude of 40, using a microtip Vibra Cell^{TM} sonicator and the cell debris removed by centrifuging at 22,000 x g for 10 min at 4C. The lysate supernatant was then

passed through a 0.2 µm filter to remove any residual cell debris that might clog the resin column later.

Purification of 1-253 aa CD138 protein fragment was performed using metal affinity chromatography (IMAC). It uses Ni^{+}-NTA agarose resin (QIAgen). A 4 mL aliquot of Ni^{+}-NTA agarose resin was added to a 20 mL column and allowed to settle down for 10 min. The column was equilibrated using 30 mL running buffer (0.1 M PBS, pH 7.4, 0.5 M NaCl, 20 mM imidazole, 8 M urea). The filtered lysate was then applied to the equilibrated column and the 'flow-through' was collected in a 50 mL tube. The column was then washed with 30 mL of washing buffer to remove loosely bound non-specific proteins and the wash collected in a 50 mL tube. The CD138 protein fragment was then eluted using 100 mM sodium acetate, pH 4.4, and collected in 400 µL aliquots in 1.5 mL micro-centrifuge tubes containing 100 µL of filtered neutralisation buffer (50 µL 100 mM NaOH and 50 µL of 1 mM PBS, pH 7.4.) The neutralised protein was then buffer exchange using a 5 kDa 'cut-off' Vivaspin^{TM} 6 column. The buffered exchanged proteins were then transfered to 15 mL tubes and stored at –20ºC.

Chapter 3

Optimization of Liposome and Immunoliposome Preparation

3.1 Introduction

The overall aim of this project was to prepare sufficient targeted contrast agent for the diagnosis of human multiple myeloma in humans using MRI.

There are different agents which can be used for this purpose e.g. solid lipid nanoparticles, liposomes, nanocrystals or carbon nanotubes. Liposomes were chosen to be used to target human multiple myeloma. Liposomes are artificially prepared vesicles consisting of phospholipid bilayers, which have been used extensively in drug and gene delivery. They are easily adapted for use *in vitro, ex vivo* and *in vivo*. The advantage of liposomal usage is that they remain in the circulation for a relatively long period of time and are not readily taken up by the macrophages in the RES, when containing either monosialoganglioside (GM1) (Allen *et al.*, 1987) or polyethylene glycol (5-10 mol%) derivatives of phosphatidylethanolamine (Klibanov *et al.,* 1990).

There are several methods for liposome preparation. The most common method used is lipid film hydration which leads to multilamellar vesicle (MLVs) formation. This method involves drying a solution of lipids so that a thin film is formed on the bottom of a round bottom flask and then hydrating the film by adding aqueous buffer and vortexing the dispersion for some time. MLVs are simple to prepare by this method and a variety of substances can be encapsulated. The drawbacks of this method are low internal volume, low encapsulation efficiency and the size distribution is heterogeneous (Bangham *et al.*, 1965, 1974). A different method for MLV generation was proposed by Kim *et al.* (1985). This solvent spherule method leads to preparation of liposomes of homogeneous size distribution. The process involves dispersing small spherules of volatile hydropohobic solvent in which lipids had been dissolved, in aqueous solution. MLVs are formed when controlled

evaporation of organic solvent is carried out e.g. in water bath at a required temperature.

MLVs can be used for preparation of large unilamellar vesicles (LUVs). Mayhew *et al*. (1984) called this approach microfluidization of liposomes. Devices are available commercially under trade names such as LUVET and EXTRUDER for passing MLVs through 100 nm polycarbonate membranes resulting in production of LUVs. Riaz *et al.* (1994) prepared liposomes by this technique and showed that the liposomes were unilamellar, using freeze fracture electron microscopy. Large unilamellar vesicles have high internal volume/encapsulation efficiency and can be used for the encapsulation of drugs and macromolecules. In this research, large unilamellar vesicles (LUVs) were created by lipid film hydration followed by extrusion.

A different method for preparation of LUVs is the reverse-phase evaporation (REV) method. First a two phase system containing phospholipids in organic solvent and aqueous buffer is formed and this is followed by a brief sonication. The organic solvent is removed under reduced pressure, resulting in the formation of a viscous gel. The liposomes are formed when residual solvent is removed by continued rotary evaporation under reduced pressure. In this study the REV method was used for immunoliposome preparation. Immunoliposomes, in which monoclonal antibody (mAb) fragments are conjugated to liposomes, represent the next generation of molecularly targeted systems. By combining the tumor targeting properties of mAbs with a contrast agent anchoring system, immunoliposomes can provide selective contrast agent accumulation on targeted tumor cells.

The main aim of this chapter was to describe optimization of liposome and immunoliposome preparation. Experiments were performed to establish the best

method for immunoliposome preparation using antibodies kindly donated by the Mater Misericordiae University Hospital, Dublin, for research purposes. To optimize the procedure for immunoliposome preparation, different antibodies (Herceptin®, 2C5 and Rituximab) were used. Herceptin® (Trastuzumab) is a humanized monoclonal antibody which interferes with HER2 receptors overexpressed on breast cancer cells. Cells treated with Herceptin® undergo arrest during the G1 phase of the cell cycle resulting in reduced proliferation. It was suggested that this antibody induces some of its effects by causing the downregulation of the HER2 receptor (Kute *et al.*, 1994). 2C5 is a monoclonal antibody (produced in Prof. V. Torchilin's group in Northeastern University, Boston, USA) which binds strongly to cancer cell lines which have higher number of nucleosomes attached to their outer cell membrane compared to normal non-cancer cells (Iakoubov *et al.,*1995). Rituximab is a chimeric antibody which binds to CD20, primarily found on the surface of B cells. This genetically engineered chimeric anti-CD20 monoclonal antibody containing human IgG1 kappa constant regions, with murine variable regions, mediates complement-dependent cell lysis and antibody-dependent cellular cytotoxicity (Reff *et al.*, 1994). It is used to treat leukaemias and lymphomas and in transplant rejection therapy.

Immunoliposomes have antibodies attached to the liposome surface. There are different chemical reactions which can be used to conjugate antibodies to liposomes. Modification of the antibody amine groups is the procedure most frequently use to produce antibody-liposome conjugates. Early procedures were described using crosslinking agents, such as l-ethyl-3-(3-dimethylaminopropyl) carbodiimide hydrochloride (EDC), in the presence of preformed liposomes containing a lipophilic carboxylic acid (Endoh *et al.,* 1981). DCC (N,N'-

dicyclohexylcarbodiimide) can also be used for crosslinking to carboxylic acid, because it has the same chemical features as EDC.

A different method for antibody-liposome conjugation involves the use of hetereobifunctional crosslinkers e.g. SATA (N-hydroxysuccinimide ester) which efficiently introduces a unique and selective reactive function, such as a protected thiol. Antibodies which have been activated by these crosslinkers can, after deprotection, where appropriate, react with a maleimide-activated lipid group in the liposome bilayers.

In this research, immunoliposomes were prepared using two different methods: (a) reverse-phase evaporation (REV) and (b) co-incubation methods. In both methods, antibody was firstly conjugated to phospholipid which was then used in immunoliposome preparation. Herceptin®-liposomes were prepared using reverse-phase evaporation (REV). The REV method was already described in detailed. In the co-incubation method liposomes were firstly prepared and then co-incubated with previously conjugated lipid-antibody linkage, leading to immunoliposomes generation. DSPE-PEG-COOH phospholipid was first esterified using DCC and NHS reagent and then conjugated with antibody. For example, 2C5 monoclonal antibody was conjugated to DSPE-PEG-COOH phospholipid and co-incubated with previously prepared liposomes to generate immunoliposomes. Rituximab-liposomes were also prepared using the co-incubation method. *In vitro* studies of Rituximab-liposomes with RAMOS (human Burkitt's lymphoma) and L428 (Hodgkin's disease-derived) cancer cell lines were performed. RAMOS and L428 cell lines were kindly donated by Dr. Dermot Walls, School of Biotechnology, Dublin City University. Avastin®, a humanized monoclonal antibody was used as a negative control for

Rituximab monoclonal antibodies. It recognizes and blocks VEGF-A (vascular endothelial growth factor-A) (Los *et al.*, 2007).

Once liposomes or immunoliposomes were formulated and generated they were characterized for their size and surface charge. Liposomes were investigated for their hydrodynamic diameter which was measured using scattered light off from the surface of the particles with photon correlation spectroscopy (PCS). The surface charge of the liposomes was obtained by measuring their zeta potential (electrokinetic potential).

Optimization of methods for the production of both liposomes and immunoliposomes was essential in order to develop the best liposomal nanoparticles for long-term usage in human multiple myeloma imaging.

3.2 Results

3.2.1 Generation and characterisation of fluorescently-labelled liposomes

Fluorescently-labelled liposomes were produced and purified as described in section 2.2.2.3. The free (i.e. non-encapsulated) fluorescent dye was separated from fluorescent liposomes using size exclusion chromatography on Sephadex G-25. Fractions were collected from the column and the fluorescence was measured using the Tecan Safire 2 plate reader (Figure 3.1).

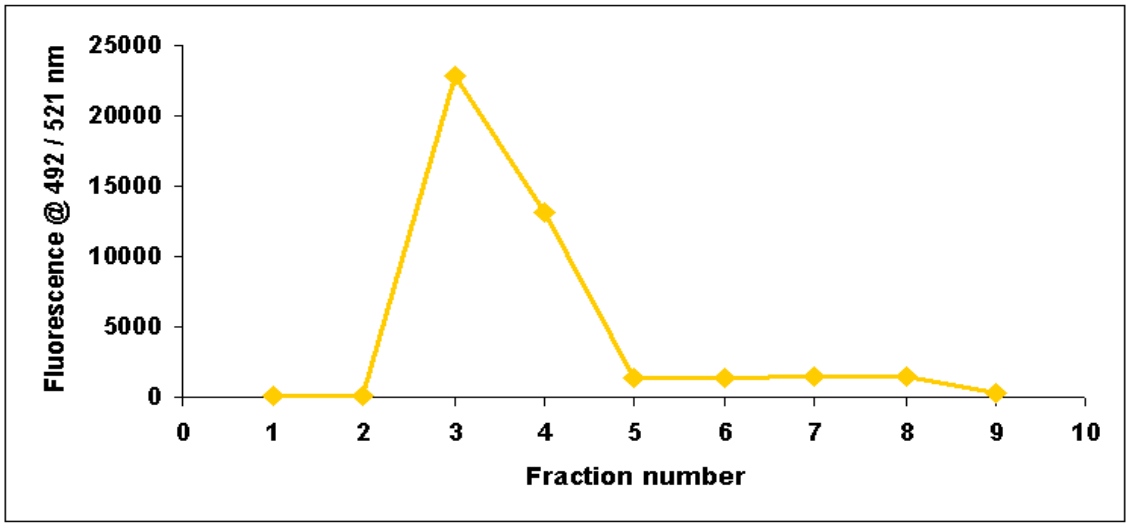

Figure 3.1 Elution profile of samples containing fluorescently-labelled liposomes after size exclusion chromatography on Sephadex G-25.
The column dimensions were 0.5 × 6 cm. Fractions of 0.5 mL were collected and the fluorescence recorded (excitation at 492 nm; emission at 521 nm).

The FITC dye penetrates the Sephadex G-25 beads due to its small size while the larger liposomes are excluded from the beads and were eluted in fractions 2-5. The diameter of fluorescently-labelled liposomes was estimated using Photon Correlation Specroscopy (PCS). An average diameter of 121 nm was determined for the liposomes, as shown in Figure 3.2.

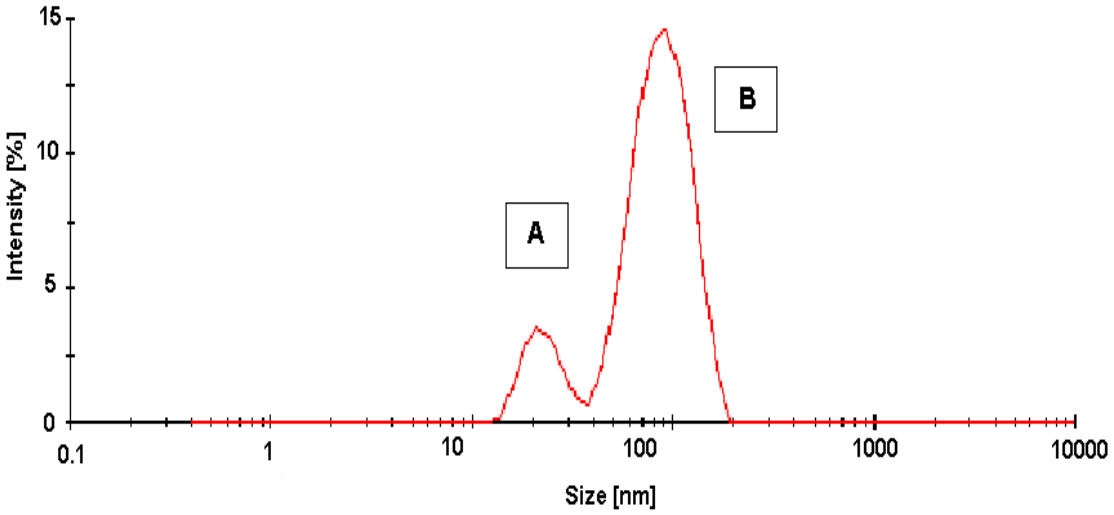

Figure 3.2 PCS analysis of fluorescently labelled liposomes.
Two major populations of particles with diameters of approximately 20 nm (A) for micelles and 121 nm (B) for liposomes.

3.2.2 Preparation and purification of fluorescently-labelled 2C5 antibody-conjugated-liposomes

This section contains a physical comparison between liposomes and antibody-conjugated-liposomes.

Liposomes were prepared by lipid film hydration, as described in section 2.2.2.2. The lipid film was hydrated using 1 mL of 0.1 M PBS, pH 7.4 (without any fluorescent dye). Briefly, a lipid film was prepared using 64.5 mol% of egg PC, 30 mol% of cholesterol, 5 mol% of DSPE-PEG-COOH and 0.5 mol% of rhodamine-PE. The lipid film was hydrated, heated to 50°C and vortexed to form liposomes anf then extruded through a 100 nm polycarbonate membrane. The size of these liposomes was estimated to be 182 nm with a zeta potential of -52.11 mV, which indicates that liposomes are stable. The zeta potential indicates the degree of repulsion between adjacent, similarly charged particles in dispersion. For molecules and particles that are small enough, a high zeta potential (higher than 30 mV or lower that –30 mV) will confer stability, e.g., the solution or dispersion will resist aggregation, whereas, when the potential is low, attraction exceeds repulsion and the dispersion flocculates.

Then, immunoliposome were prepared using co-incubation method. 2C5 monoclonal antibody was used for immunoliposome preparation. 2C5 antibody binds strongly to cancer cell lines which have higher number of nucleosomes attached to their outer cell membrane compared to normal non-cancer cells (Iakoubov *et al.*, 1995). Firstly, antibody was linked to DSPE-PEG-COOH phospholipid (section 2.2.3.4). In details, 2C5 antibody (0.6 mg) was conjugated to 2 mol% of DSPE-PEG-COOH and subsequently 2C5-antibody-conjugated-phospholipid was co-incubated with the previously prepared liposomes (composed

of 64.5 mol% of egg PC, 30 mol% of cholesterol, 3 mol% of DSPE-PEG-COOH and 0.5 mol% of rhodamine-PE) overnight at 4°C. Lipid composition for immunoliposome preparation is presented in Table 3.1.

Table 3.1 Lipids used for preparation of fluorescently-labelled 2C5-antibody-conjugated-liposomes.

Compound	Molecular weight [g]	Weight taken [mg]	Moles	Molar ratio of lipid to other lipids
Egg PC	790.12	4.00	$5.20*10^{-6}$	64.5 mol% (1)
Cholesterol	386.65	0.93	$2.42*10^{-6}$	30 mol% (0.47)
DSPE-PEG-COOH	2,847.78	0.67	$2.36*10^{-7}$	3 mol% (0.05)
Rhodamine-PE	1,176.93	0.05	$4.03*10^{-8}$	0.5 mol% (0.01)
DSPE-PEG-COOH	2,847.78	0.46	$1.61*10^{-7}$	2 mol% (0.03)
TOTAL		**6.11**		

After co-incubation the fluorescently-labelled 2C5-antibody-conjugated-liposomes were dialyzed against PBS, pH 7.4, ('cut-off' 300,000 Da) for 2 days at 4°C to remove unbound antibody. The size and zeta potential of fluorescent 2C5-antibody-conjugated-liposomes were determined by PCS.

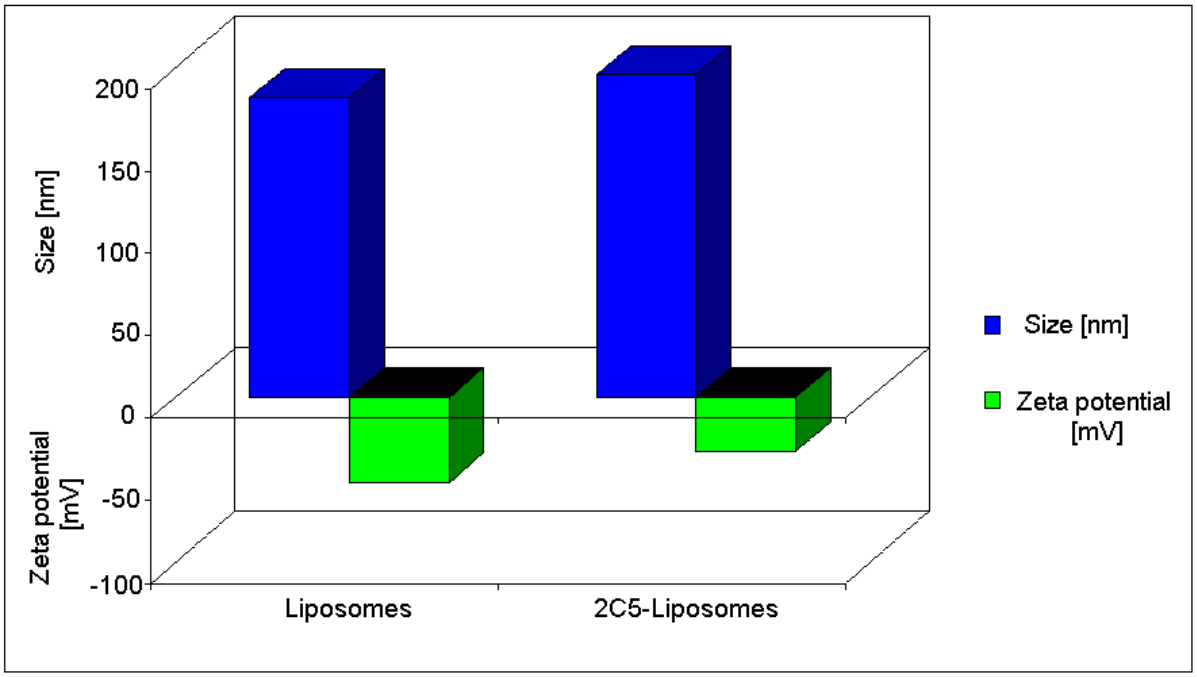

Figure 3.3 Comparison of size and zeta potential of fluorescently-labelled liposomes and fluorescently-labelled 2C5-conjugated-liposomes.
The diameter of prepared antibody-conjugated-liposomes increased from 182 nm to 195.9 nm and the zeta potential decreased from -52.11 to -32.65 mV. The diameter of 2C5-conjugated-liposomes increased compared to antibody-free-liposomes due to the antibody presence on the liposome surface. The zeta potential of 2C5-liposomes decreased compared to antibody-free-liposomes the former due to the positive charge from amine groups present on antibodies.

The size of prepared immunoliposomes was 196 nm with a zeta potential of -32.65 mV. The zeta potential of the liposomes decreased from -52.11 mV to -32.65 mV after immunoliposomes were generated, due to the positive charge of antibodies (Figure 3.3). It indicates that antibody attachment to liposome changes liposome properties in particle diameter and charge.

3.2.3 Preparation of fluorescently-labelled antibody-conjugated-liposomes – Reverse Phase Evaporation (REV) method

3.2.3.1 Fluorescently-labelled Herceptin®-antibody-conjugated-liposome preparation and purification

Firstly, Herceptin®-liposomes were prepared using the reverse phase evaporation method. The procedure for this method was described in section 2.2.3.

Briefly, DSPC, cholesterol and rhodamine-PE were resuspended in chloroform and the DSPE-PEG-COOH lipid was esterified and conjugated with 1.33 mg Herceptin® antibody. The Herceptin®-antibody-conjugated-phospholipid complex was buffered-ex-changed with 0.1 M PBS, pH 7.3. Then, Herceptin®-antibody-conjugated-phospholipid was put onto the lipid solution. An aqueous and an organic phase, were observed. Then the mixture was sonicated to generate an emulsion.

Any organic solvent remaining was slowly evaporated using a Rotovap R-200 apparatus and the aqueous solution was ultracentrifuged to separate immunoliposomes from free antibody. The immunoliposomes were then extruded through a 100 nm polycarbonate membrane. The protein concentration in the immunoliposome sample was estimated using the micro Lowry assay with Peterson's modification.

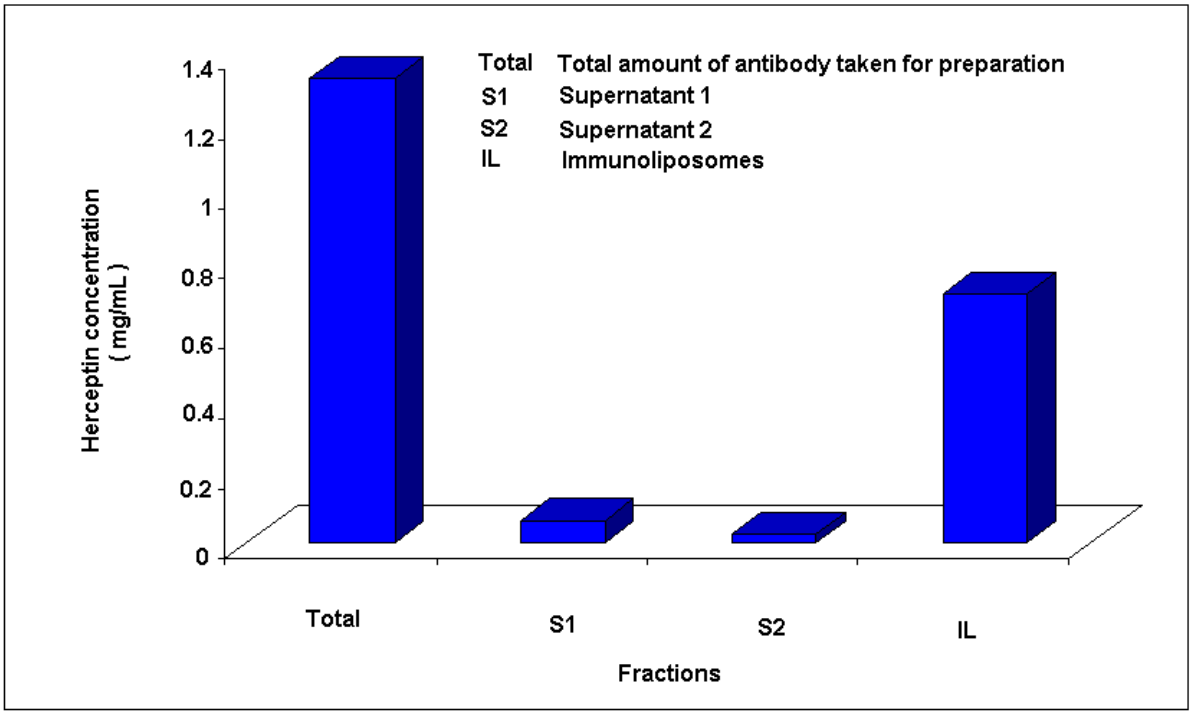

Figure 3.4 Determination of antibody concentration in Herceptin®-conjugated-liposomes after ultracentrifugation.
Immunoliposomes were ultracentrifuged twice and antibody concentration was estimated. 1.33 mg of Herceptin® monoclonal antibody was used for immuno-liposome preparation. Herceptin®-conjugated-liposomes were ultracentrifuged twice to separate them from unbound antibody and the supernatants were collected (S1-supernatant 1; S2-supernatant 2). It was estimated that there are 0.71 mg/mL of Herceptin® antibodies attached to liposomes; 0.06 mg/mL of unbound Herceptin® antibodies in S1 and 0.02 mg/mL of unbound Herceptin® antibodies in S2.

1.33 mg/mL of Herceptin® antibody was used for immunoliposome preparation and it was estimated that there was 0.71 mg/mL of antibody (Figure 3.4) in the immunoliposome sample. 0.06 mg/mL unbound antibody was found in supernatant 1 and 0.02 mg/mL is supernatant 2 after two steps of ultracentrifugation showing a 53% recovery of the antibody. Approximately 0.54 mg/mL of antibody was lost during the preparation procedure indicating that the reverse-phase evaporation (REV) method is not a very efficient method for immunoliposome preparation.

3.2.4 Fluorescently-labelled immunoliposomes – co-incubation method for immunoliposome preparation

The co-incubation method for immunoliposome preparation was performed (section 2.2.3.4) and compared with the reverse phase evaporation method. For optimization of this preparation procedure Rituximab monoclonal antibodies were used, as they were kindly donated by the Mater Misericordiae Hospital for use for research purposes. Rituximab is a chimeric monoclonal antibody that binds to CD20 which is primarily found on B cells (Reff *et al*., 1994). The interaction of Rituximab was first tested with RAMOS (human Burkitt's lymphoma) and L428 (Hodgkin's disease-derived) cell lines by flow cytometry to determine their suitability for use in immunoliposome binding studies.

3.2.4.1 Determination of positive/negative cell lines for Rituximab monoclonal antibody binding

Binding of the Rituximab monoclonal antibody to RAMOS (human Burkitt's lymphoma) and L428 (Hodgkin's disease-derived) cells were tested by flow cytometry, as described in section 2.2.4. RAMOS and L428 cells (10^6) were incubated with 1 µg/mL, 5 µg/mL, and 10 µg/mL of Rituximab for 30 min at 4ºC. The cells were then washed with PBS, pH 7.4, and incubated with a 1:2,000 dilution of Cy5 labelled-anti-human IgG secondary antibody for 30 min at 4ºC. Cells were washed three times with FACS buffer (0.1 M PBS, pH 7.4; 2% (v/v) FBS; 0.05% (w/v) NaN_3) and immediately analyzed on a FACS Calibur instrument

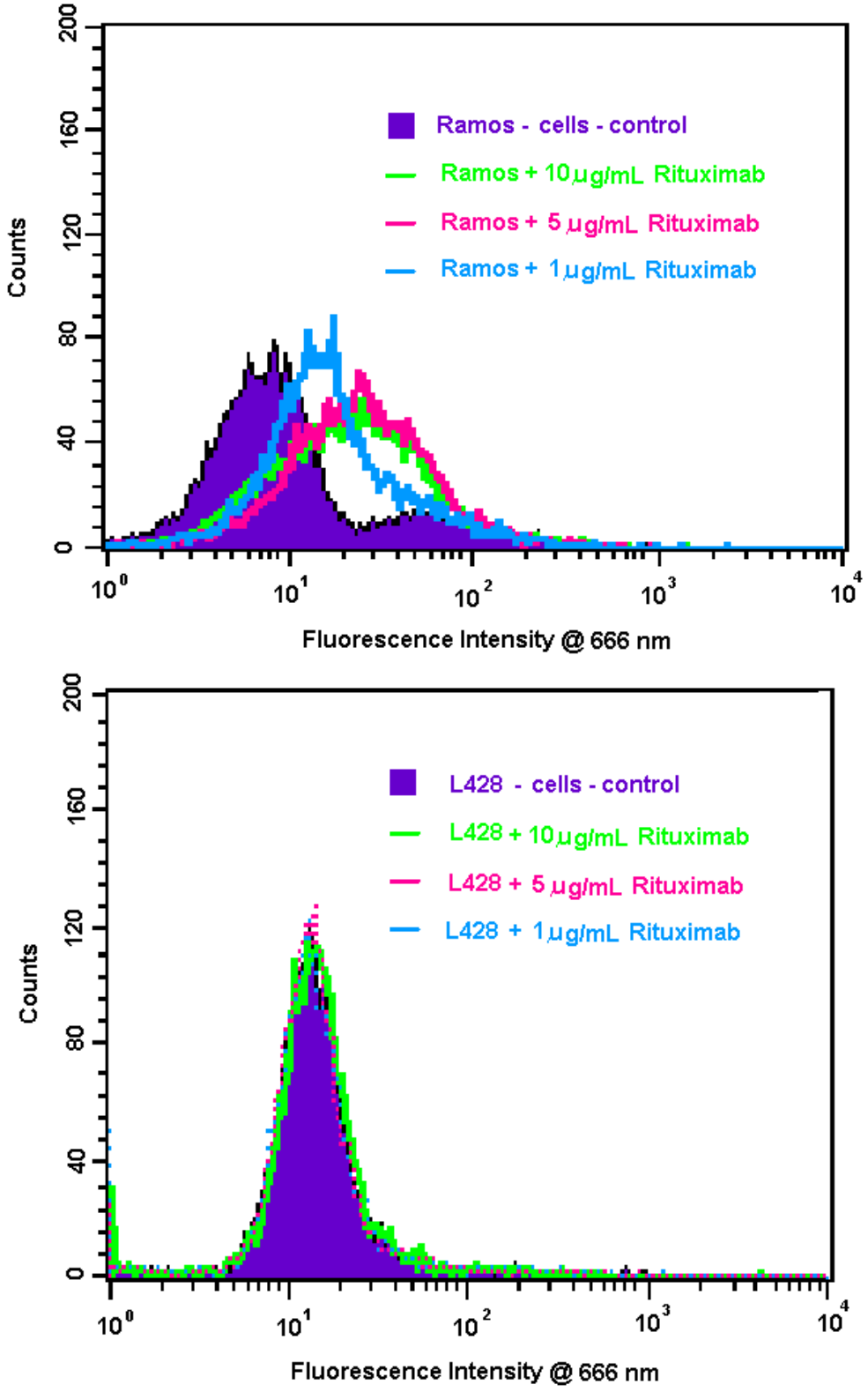

Figure 3.5 FACS analyses of RAMOS (human Burkitt's lymphoma) and L428 (Hodgkin's disease-derived) cell lines for CD20 protein expression.
RAMOS and L428 cell lines were treated with 10 µg/mL, 5 µg/mL, 1 µg/mL of Rituximab antibody. A 1:2,000 dilution of anti-human IgG-Cy5 conjugated was used as the secondary antibody.

No binding was observed using 1 µg/mL, 5 µg/mL or 10 µg/mL of Rituximab antibody with the L428 cell line (Figure 3.5). The RAMOS cell line was positively stained using these three different Rituximab concentrations. Thus, it was shown that the RAMOS cell line is CD20-positive and L428 is CD20-negative.

3.2.4.2 Preparation and purification of fluorescently-labelled Rituximab-conjugated-liposome

The procedure was in details described in detail in section 2.2.3.4. Briefly, 64.5 mol% of egg PC, 30 mol% of cholesterol, 3 mol% of DSPE-PEG-COOH and 0.5 mol% of rhodamine-PE was used to prepare a lipid film (Table 3.1). The lipid film was hydrated using 1 mL of 0.1 M PBS, pH 7.4 and vortexed. It was then extruded through a 100 nm polycarbonate membrane for liposome generation.

The Rituximab antibody (0.6 mg) was conjugated to 2 mol% of DSPE-PEG-COOH by firstly esterifing the DSPE-PEG-COOH using DCC and NHS. A forty molar excess of this esterified lipid was conjugated to the Rituximab monoclonal antibody by incubation in 0.1 M PBS, pH 8.5, overnight at 4°C. This Rituximab-conjugated-phospholipid solution was dialyzed using 3,500 Da dialysis tubing against 0.1 M PBS, pH 7.4 for 2 h to remove DMSO, in which esterified lipid was resuspended and subsequently co-incubation with the previously prepared liposomes overnight at 4°C. Liposomes were composed of 64.5 mol% egg PC, 30 mol% cholesterol, 3 mol% DSPE-PEG-COOH, 0.5 mol% rhodamine-PE and prepared by lipid film hydration followed by extrusion through 100 nm polycarbonate membrane

Fluorescently-labelled-liposomes were dialyzed against PBS, pH 7.4, (‘cut-off’ 300,000 Da) for 2 days at 4°C to remove unbound antibody.

3.2.4.3 FACS analyses of fluorescently-labelled Rituximab-conjugated-liposomes

Fluorescently-labelled Rituximab-conjugated-liposomes (0.1 mg/mL of lipids) were incubated with 10^6 RAMOS and L428 cells for 1 h at 37ºC in serum-free medium. Cells were washed 3 times with 0.1 M PBS, pH 7.3 and resuspended in FACS buffer (0.1 M PBS, pH 7.4; 2% (v/v) FBS; 0.05% (w/v) NaN_3) and immediately analyzed. Avastin®-conjugated-liposomes were used as a negative control and were prepared using the co-incubation method. Avastin® is a humanized monoclonal antibody which recognizes and blocks VEGF-A (vascular endothelial growth factor-A) (Los *et al.*, 2007).

It had previously been determined that Avastin® antibodies did not bind to either RAMOS or L428 cells (personal communication, Ferdia Bolster).

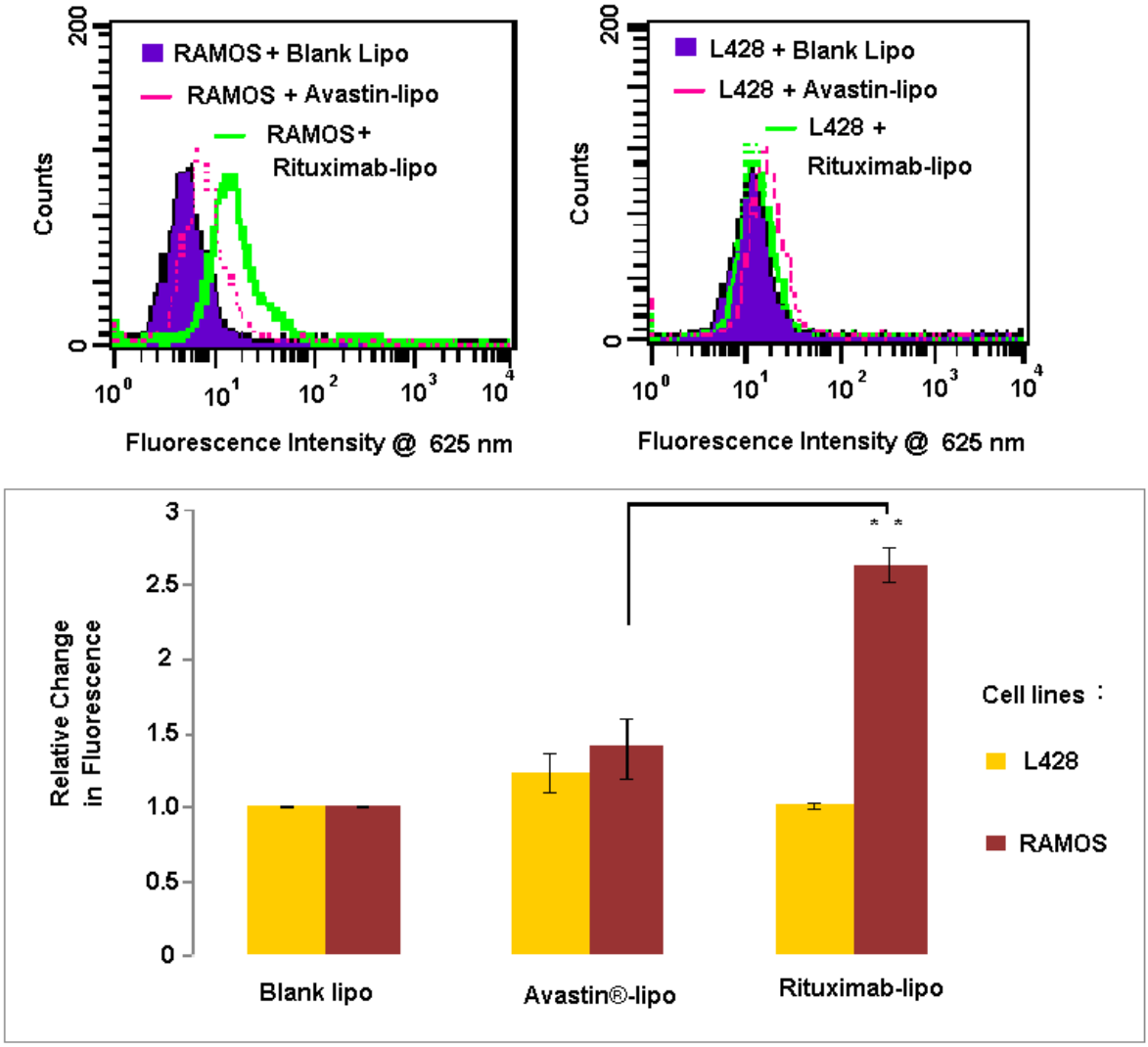

Figure 3.6 *In vitro* studies demonstrating specific binding of antibody-conjugated-liposomes to cells expressing the associated target antigen.
Fluorescent liposomes conjugated with either Rituximab, Avastin® (negative control antibody) or no antibody (blank lipo) was incubated with RAMOS and L428 cell lines. Analyses were performed in triplicate and the results were normalized for comparison purposes with blank liposomes and Avastin®-antibody-conjugated-liposomes.
The results are the mean ± the standard deviation and the experiment was performed in triplicate.
* Significantly different from control (Avastin®-conjugated-liposomes) (Student's *t*-test, 0.01<p<0.05

Fluorescence obtained from both cell lines after incubation with blank liposomes was taken as 1. Based on this, fluorescence of other samples was calculated (Figure 3.6). The RAMOS cell line bound Rituximab-conjugated-labelled-liposomes to 2.5 much larger degree than the L428 cell line. Using Student's *t*-test there was a

significant difference ($0.001<p<0.01$) in fluorescence between Avastin®-conjugated-liposomes (negative control) and Rituximab-conjugated-liposomes which bound to the RAMOS cell line. This shows that the Rituximab-labelled liposomes bound specifically to the RAMOS cell line.

Discussion

In this study, liposomes and antibody-conjugated (immuno)-liposomes were produced containing 5 mol% (w/v) PEGylated phospholipid. PEG content between 5-10 mol% was used as it was found to be sufficient to prolong circulation life-time *in vivo* and prevent liposome opsonization by the reticuloendothelial (RES) system (Klibanov *et al.*, 1990). The optimum cholesterol concentration for long-term circulating liposomes was 30 mol% or more. Therefore, 30 mol% of cholesterol was used for liposome and immunoliposome preparation (Bedu *et al*., 1996). Cholesterol acts as a spacer between the phospholipids of the liposome membrane thus reducing PEG chain-chain interactions (Strijkers *et al.,* 2005).

Immunoliposomes were prepared using two separate methods, reverse-phase evaporation and co-incubation. In both cases, antibody was coupled to the terminal end of the PEG chain, which contained a carboxylic acid group, to increase antibody accessibility to cancer cells. The term immunoliposome was coined to describe a liposome conjugated to an antibody or portions of an antibody (Siwak *et al.,* 2002). Maruyama *et al.* (1995) showed that liposomes which contained antibody attached to PEG demonstrated improved binding to their target when compared to liposomes combined with antibody attached directly to the lipid bilayer. The main aim of this research was to conjugate anti-CD138 antibodies to liposomes, because CD138 was determined to be a good marker for myeloma, due to its expression on majority of malignant plasma cells in bone marrow (Wijdenes *et al*., 2002). Ultimately, anti-CD138 antibodies will be used, however, due to the high cost of anti-CD138 antibodies, Herceptin, 2C5 and Rituximab were used during the optimisation steps for liposome generation.

During this project, the REV method was used for Herceptin®-conjugated-liposomes. This method allows the preparation of liposomes having by a high aqueous space to lipid ratio and facilitates entrapment of large quantities of material (Szoka and Parahadjopoulos, 1978). In Herceptin®-conjugated-liposomes prepared by the REV method 0.89 mg/mL of antibody was conjugated. Thus, it was found that the REV method was effective for immunoliposome preparation. The main drawback of this method is the exposure of the antibody to an organic solvent, which may lead to its denaturation. Secondly, the REV method leads to unpredictible and heterogenous size distribution of liposomes (between 100-1000 nm) (Duzgunes, 1983). However, this could be overcome by filtration through a 200 nm filter, which gives a more uniform vesicle population of between 120-300 nm with no loss of lipids (Szoka and Papahadjopoulos, 1978).

In comparison to the REV method, the co-incubation method does not involve any solvent usage, thus removing issues off potential antibody denaturation. Erdogan *et al.* (2006) successfully prepared 2C5-conjugated-liposomes using the co-incubation method and successfully targeted them for *in vitro* and *in vivo* studies (Erdogan *et al*., 2008). In this research, it was found that liposomes conjugated with 2C5 antibody showed an increase in size and a decrease in zeta potential. Singh *et al.* (1996) also noticed an increase in liposome size after antibody conjugation from 195 to 259 Å. Mayer *et al.* (1998) demonstrated that after adding PEG-PE in liposome preparation, the zeta potential decreased from 25-30 mV to 7-10 mV, due to the negative charge of the PEG-PE.

The binding ability of Rituximab-conjugated-liposomes (immunoliposomes), prepared by co-incubation method was tested *in vitro*. Rituximab is a monoclonal antibody which recognizes CD20 protein primarily found on B cells. Lapalombella *et*

al. (2008) prepared Rituximab-liposomes with encapsulated oligonucleotides to target CLL (chronic lymphocytic leukaemia). They found that the CD20 surface antigen internalization enhanced delivery of an oligonucleotide incorporated into anti-CD20-conjugated-liposomes.

In this study, FACS analyses were performed to assess the success of immunoliposome targeting. Rituximab-conjugated-liposomes were successfully targeted to the CD20-expressing RAMOS cell line to a significantly greater extent than to control liposomes with a non-specific antibody-conjugated and in comparison to blank liposomes (no-conjugated antibody-liposomes).

The results reported in this chapter signify that the methodology for immunoliposome preparation was successfully developed. Reverse phase evaporation and co-incubation methods are both efficient for targeted-liposome preparation. However, because of a few drawbacks associated with the REV method described above, the co-incubation method will be used for CD138-liposome preparation to be described in Chapters 4.

Chapter 4

Targeted anti-CD138

(Syndecan-1)-conjugated-liposomes

and

in vitro studies

4.1 Introduction

Human multiple myeloma is as yet an incurable malignancy of B plasma cells in bone marrow. The current diagnostic method of this cancer is invasive biopsy, which is painful for the patient. Also, diagnosis is often too late to enhance patient survival. The main aim of this project was to prepare an applicable minimally non-invasive diagnostic tool for faster diagnosis of multiple myeloma in humans, which would, in turn, improve patient prognosis. It should be a *novel* minimally non-invasive diagnostic method for multiple myeloma in humans.The principal aim of this chapter was to describe the binding ability of targeted nanoparticles (anti-CD138-fluorescently-labelled liposomes) to human multiple myeloma cancer cells *in vitro*.

Human multiple myeloma is a cancer of plasma cells. Myeloma starts when plasma cell becomes abnormal and starts to proliferate repeatedly. Over time, as the cancer develops, plasma cells become detectable in the blood and the cancer can spread to 'multiple' site in the body, hence the name multiple myeloma (MM). MM is a malignancy that accounts for slightly more than 10% of all haematological malignancies (Kyle *et al.,* 2004). It usually evolves from an asymptomatic pre-malignant stage of clonal plasma cell proliferation called 'monoclonal gammopathy of undetermined significance' (MGUS) (Kyle *et al.,* 2002). In some other patients, an intermediate asymptomatic but more advanced premalignant stage, referred to as 'smoldering multiple myeloma' (SMM) is clinically recognized (Kyle *et al.,* 2007).

Wijdenes *et al.,* (1996) reported that CD138 (syndecan-1) is a good marker for human multiple myeloma cancer using B-B4 monoclonal anti-CD138 antibodies in routine malignant bone marrow section. Luque *et al*. (1998) also reported the presence of overexpressed CD138 protein on malignant B cells in peripheral blood in multiple myeloma patients. The protein bears heparan sulfates and sometimes

chondroitan sulfates. The ectodomain contains five putative glycosaminoglycan (GAG) attachment sites, and a putative protease cleavage site at its C-terminus (Bernfield *et al.,* 1992). Hence, anti-CD138-targeted immunoliposomes were used as a diagnostic agent for human multiple myeloma malignancy. Immunoliposomes are commonly used particles to target different malignancies. Erdogan *et al.* (2006) successfully targeted pegylated 2C5-liposomes, containing gadolinium ions, to target murine Lewis lung carcinoma (LLC) and human mammary adenocarcinomas (MCF-7, BT20) *in vitro* and to LLC *in vivo* (Erdogan *et al*., 2008).

This chapter describes the physical characterisation of anti-CD138-conjugated-liposomes as well as the binding ability of anti-CD138-conjugated-liposomes to human multiple myeloma cell lines *in vitro*. The binding characteristics of targeted anti-CD138-conjugated-liposomes to cancer cell lines were studied using FACS and FLISA analyses.

To estimate the cell binding ability of immunoliposomes, *in vitro* binding studies were performed. Three cell lines (U266, RPMI8226 and L428) were used. U266 and RPMI8226 are human multiple myeloma cells and L428 is a Hodgkin's disease-derived cancer cell line. It was shown that the Hodgkin's disease-derived cell line, L428, does not express CD138 protein on its surface.

4.2 Results

4.2.1 Evaluation of CD138 surface expression on U266 and RPMI8226 human multiple myeloma cell lines and L428 Hodgkin's disease-derived cancer cells

In order to check CD138 protein expression level on U266 and RPMI8226 human multiple myeloma cancer cell lines, flow cytometry was performed. It was expected that both cell lines would express CD138 protein on the surface, because both are malignant plasma cells. U266 is an IgE- whereas RPMI8226 is an IgG-secreting myeloma. These two different human multiple myeloma cell lines ($2x10^6$ cells) were incubated with 0.25 µg/mL of FITC-labelled anti-human CD138 antibody from clone B-A38 (AbD Serotec). A FITC-labelled mouse IgG1κ isotype control, clone MOPC-21 (AbD Serotec) was also incorporated. Incubation was carried out for 30 min at 4°C. After washing with 0.1 M PBS, pH 7.4, samples were analyzed using the FACS Calibur instrument. Fluorescence data were collected and analysed using CellQuest software (Becton Dickinson).

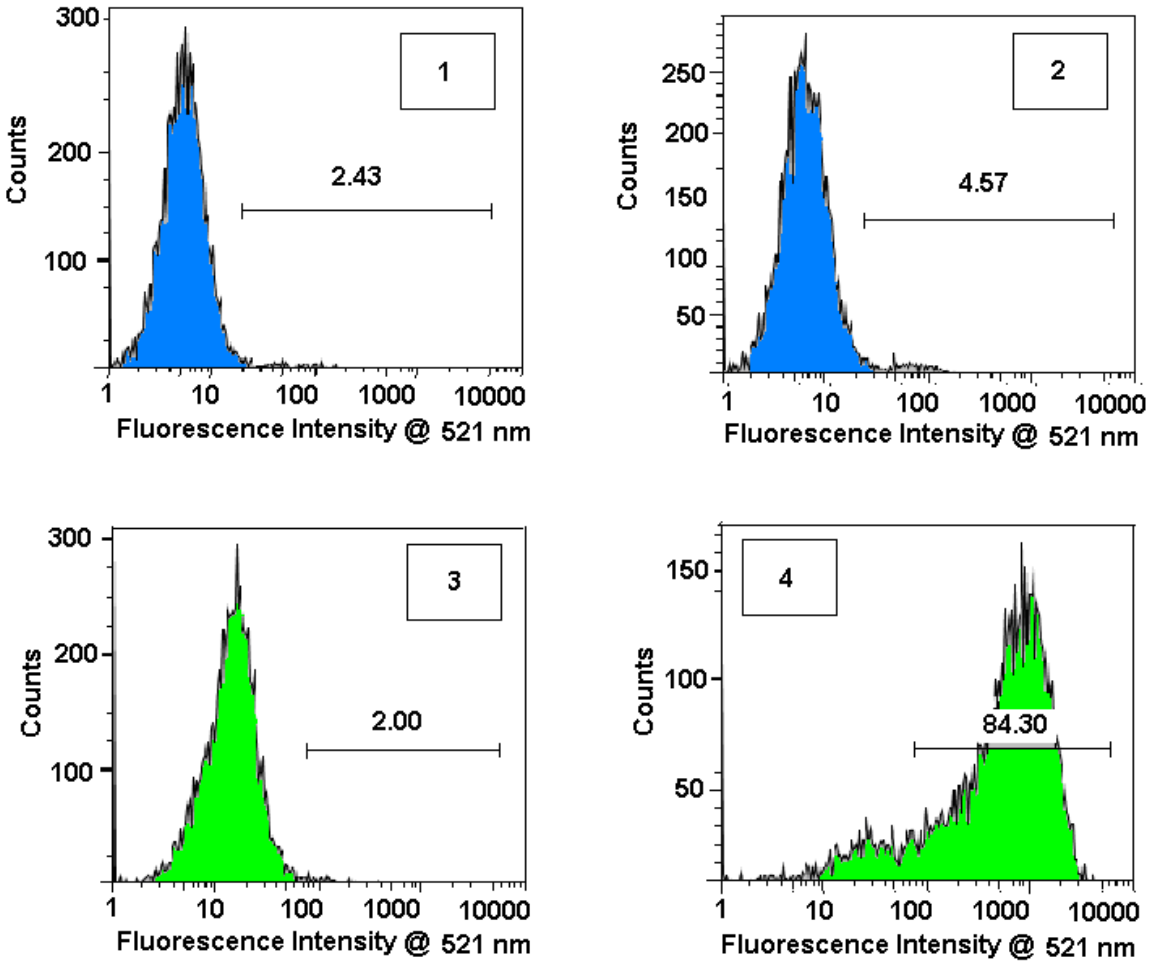

Figure 4.1 Estimation of CD138 protein expression levels on cells.
FACS analyses of U266 and RPMI8226 human multiple myeloma cell lines. 1) RPMI8226 + FITC-labelled IgGκ isotype control; 2) RPMI8226 + FITC-labelled-anti-human CD138 antibody 3) U266 + FITC-labelled IgGκ isotype control; 4) U266 + FITC-labelled-anti-human CD138 antibody. The U266 human multiple myeloma showed 84.3% staining with anti-human CD138 antibodies wherease RPMI8226 showed 4.6% of staining.

It was estimated that the expression levels of CD138 protein was 84.2 % on the U266 human multiple myeloma cell line and 4.6 % on the RPMI8226 cell line (Figure 4.1). The experiment was repeated with U266 and RPMI8226 human multiple myeloma cell lines and the L428 Hodgkin's disease-derived cell line. The aim of this experiment was to find a negative cell line which does not express CD138 protein on the surface. The same concentration of FITC-labelled anti-human CD138 antibody was tested on these cancer cell lines.

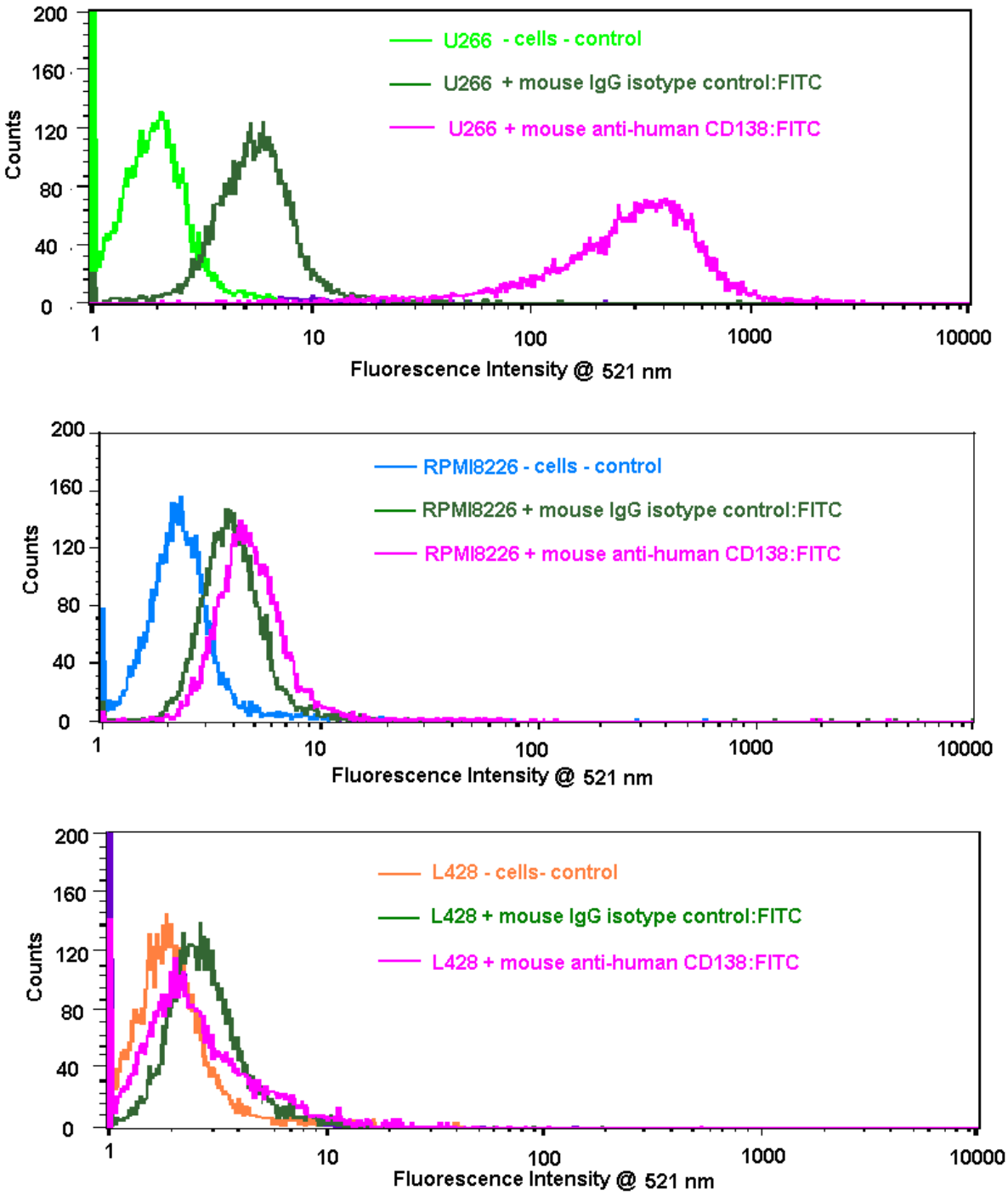

Figure 4.2 Estimation of CD138 protein level on cells (1).
U266, RPMI8226 and L428 cell lines were incubated with anti-human CD138:FITC labelled antibodies. Mouse IgG κ isotype:FITC antibody was used as a control. U266 multiple myeloma cells demonstrated much higher staining with anti-CD138 antibodies than RPMI8226 or L428 cell lines.

Cancer cell lines without incubation with any antibody and cells incubated with isotype control antibody were used as negative controls. Each cell line has its own

fluorescence (autofluorescence). However, cells incubated with isotype control antibody is the appropriate negative control. It was confirmed that U266 cell line expresses CD138 at a very high level, whereas RPMI8226 expresses CD138 in much lower amounts. The L428 Hodgkin's disease-derived cell line does not express any CD138 protein on its surface as no additional fluorescence was observed compared to cells incubated with isotype control antibodies (Figure 4.2). The results were normalized and are presented in Figure 4.3.

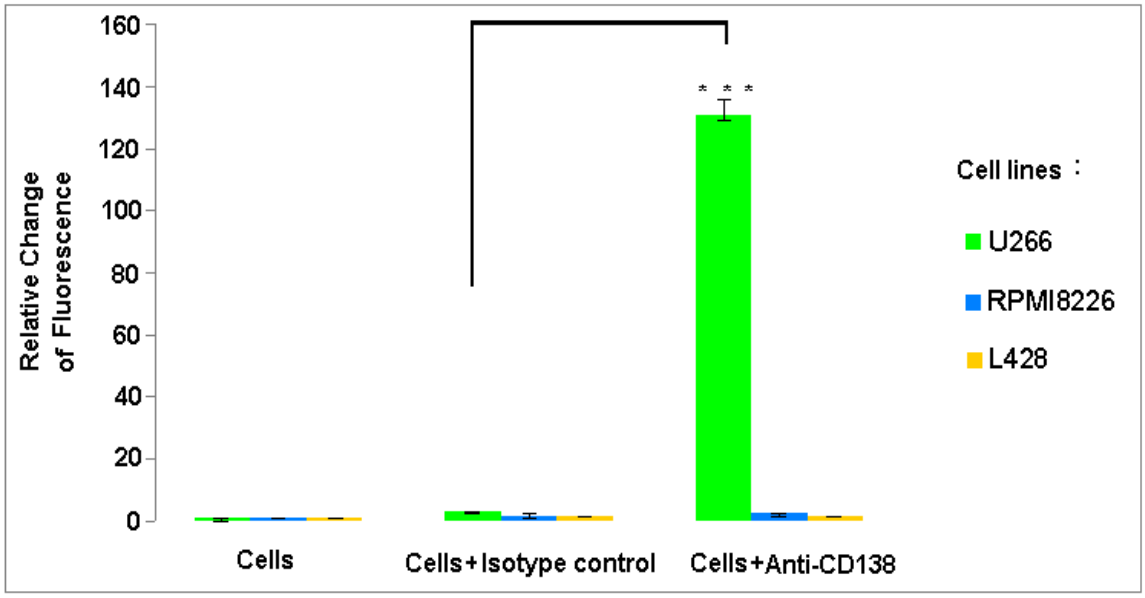

Figure 4.3 Estimation of CD138 protein level on cells (2).
U266, RPMI8226 and L428 cell lines were tested to determine CD138 protein expression levels. U266 cells express CD138 protein at a much higher level than RPMI8226. It was found that L428 does not express CD138 protein on the surface. Mouse IgG κ isotype:FITC antibody was used as an isotype control.
It was estimated using Student's *t*-test that there was a significant difference (p value<0.05) between U266 cells incubated with isotype control antibody and U266 cells incubated with anti-CD138:FITC antibody. The results are the mean ± the standard deviation and the experiment was performed in triplicate.
*** Significantly different from control (mouse IgG κ isotype:FITC antibody) (Student's *t*-test, p<0.001)

It was estimated that there was a significant difference (p<0.001) between U266 human multiple myeloma cancer cells incubated with mouse IgG κ isotype:FITC

antibody and with anti-CD138 antibody in the level of fluorescence detected. There was not a significant difference between other groups.

4.2.2 Preparation of fluorescently-labelled anti-CD138-conjugated-liposomes - Reverse Phase Evaporation (REV) method

Fluorescently labelled-anti-CD138-conjugated-liposomes were prepared using the reverse-phase evaporation (REV) method, as described in section 2.2.3.3.

The immunoliposome formulation used is outlined in Table 4.1. 60 mol% of DSPC, 30 mol% of cholesterol, 0.1 mol% of rhodamine-PE and 9.9 mol% of DSPE-PEG-COOH was used for the preparation of the fluorescently-labelled anti-CD138-conjugated-liposomes. An estimated 0.22 mg of esterified lipid was used for conjugation to 0.2 mg of anti-CD138 antibody. Immunoliposomes were ultracentrifuged two times to remove unbound antibody (section 2.2.3.5). After ultracentrifugation immunoliposomes were re-extruded.

Table 4.1 Lipids used for anti-CD138-conjugated-liposome preparation.

Compound	Molecular weight [g]	Weight used [mg]	Moles	Molar ratio of lipid to other lipids
DSPC	790.12	4.50	$5.70*10^{-6}$	60 mol% (1)
Cholesterol	386.65	1.10	$2.85*10^{-6}$	30 mol% (0.5)
DSPE-PEG-COOH	2847.78	2.68	$9.40*10^{-7}$	9.9 mol% (0.17)
Rhodamine-PE	1176.93	0.01	$9.46*10^{-9}$	0.1 mol% (0.002)
TOTAL		8.29		

4.2.2.1 Size and zeta potential determination using Photon Correlation Spectroscopy (PCS)

It was found that the average size of the prepared anti-CD138-conjugated-liposome was 99.05 nm in diameter with a polydispersity index (PDI) of 0.055 (Figure 4.4) using the HPPS Malvern/Zetasizer. Size measurement was determined in triplicate.

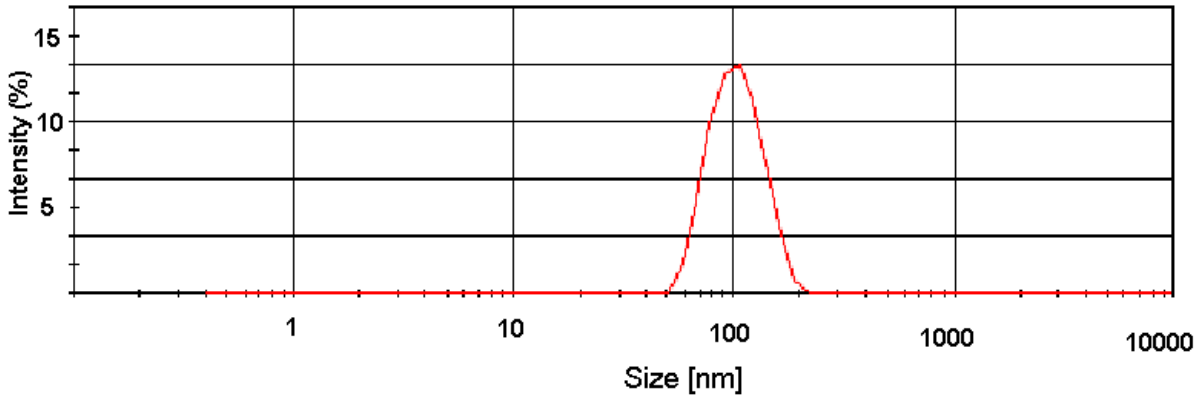

Figure 4.4 Size distribution by intensity plot for a liposome sample (Z-Avg = 99.05 nm, PDI = 0.055).
Average size of liposomes in solution was 99.05 nm with low polydispersity index (PDI), which indicates a monodisperse solution.

Photon Correlation Spectroscopy (PCS) also provides zeta potential information. The zeta potential number of anti-CD138-conjugated-liposomes was -38 mV, which indicates good particle stability (Figure 4.5). Colloids with high zeta potential (negative or positive; more than ±30) are electrically stabilized while colloids with low zeta potentials tend to coagulate or flocculate (ASTM Standard D, 1985).

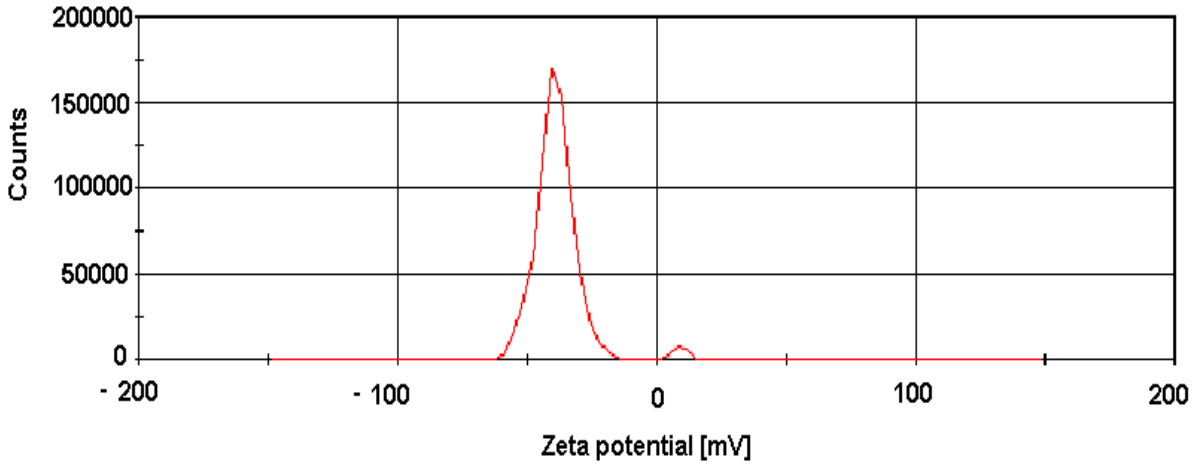

Figure 4.5 Zeta potential distribution of the anti-CD138 conjugated-liposomes. The zeta potential of anti-CD138-conjugated-liposomes was -38 mV.

4.2.2.2 Protein determination in anti-CD138-conjugated-liposomes

Anti-CD138-conjugated-liposomes were prepared using the reverse-phase evaporation method (REV). These immunoliposomes (IL) were purified from free antibodies by ultracentrifugation, as described in section 2.2.3.5. Samples were analyzed for protein content using the micro Lowry assay with Peterson's modification (section 2.2.3.8).

A calibration curve was drawn and used to determine protein concentration in the relevant samples. Approximately 103 µg/mL of antibody was found to be present on prepared immunoliposomes and approximately 24.32 µg/mL unbound anti-CD138 antibody was found in supernatant S1 (Figure 4.6).

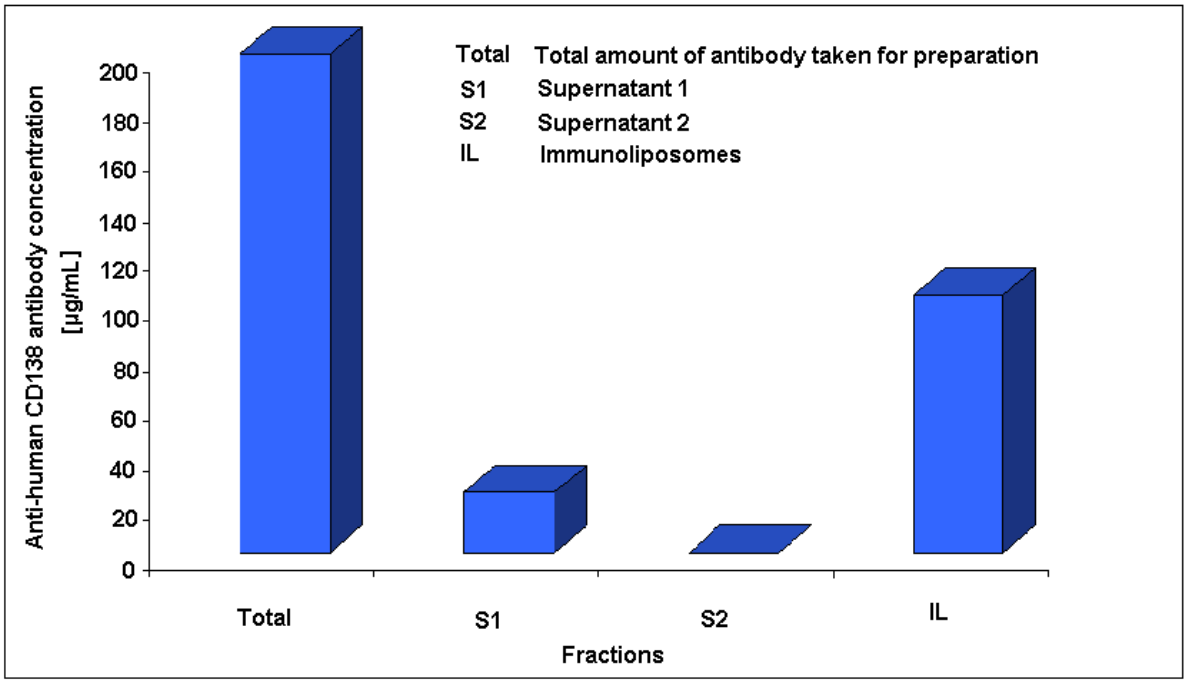

Figure 4.6 Determination of antibody concentration in anti-CD138-conjugated-liposomes after ultracentrifugation.
200 µg/mL of anti-CD138 antibody was used for immunoliposome preparation. Each preparation of anti-CD138-conjugated-liposomes was ultracentrifuged to remove free antibody and supernatants were collected (S1-supernatant 1; S2-supernatant 2). It was estimated that there was 103.18 µg/mL of anti-CD138 antibody attached to liposomes. It was found that there was 24.32 µg/mL of unbound anti-CD138 antibody in S1 and 0 µg/mL in S2.

4.2.2.3 Calculation of the number of antibody molecules per liposome

FIRST APPROACH:

The number of antibody molecules coupled per liposome was calculated based on the measured concentration (C_{AB}) of antibody (grams per mol of lipid) and diameter of the immunoliposomes (R). The assumption was that liposomes are approximately spherical. From this and literature values for specific volume (V_{Ls}) of 1.25 nm^3, bilayer thickness (d_{b1}) of 3.7 nm (Enoch and Strittmatter, 1979) and the molecular mass of the antibody (M_{Ab}) of 150 kDa, the number of antibodies-coupled to the liposome was calculated according to the formula below (Adrian *et al*., 2007):

$$n = \Pi/6 * C_{AB} * (3d_{b1} * R^2 - 3R * d_{b1}^2 + d_{b1}^3) * M_{AB}^{-1} * V_{Ls}^{-1}$$

where,

C_{AB} is the concentration of antibody in immunoliposomes [g/mol of lipids]

d_{b1} is the liposome bilayer thickness, which is 3.7 [nm]

R is the liposome diameter

M_{AB} is the molecular mass of antibody, which is 150,000 Da

V_{Ls} is the literature value for specific lipid volume, which is 1.25 nm^3

Anti-CD138-conjugated-liposomes were characterised by determining protein content using the micro Lowry assay with Peterson's modification. It was determined that in prepared immunoliposomes 103 µg/mL of antibody was present. The diameter of prepared immunoliposomes was found to be 99 nm.

To identify the C_{AB} value, antibody concentration was converted from µg/mL to antibody/mol of lipids. To do this, the molar concentration of lipids in liposomes was initially calculated as follows:

Egg PC $C_m = \frac{n}{V} = \frac{m_s/M}{V} = \frac{4.5*10^{-3}\ [g] / 790.12\ [g]}{2*10^{-3}\ [L]} = 2.85\ mM$

Cholesterol $C_m = \frac{n}{V} = \frac{m_s/M}{V} = \frac{1.1*10^{-3}\ [g] / 386.65\ [g]}{2*10^{-3}\ [L]} = 1.42\ mM$

DSPE-PEG-Metoxy $C_m = \frac{n}{V} = \frac{m_s/M}{V} = \frac{2.68*10^{-3}\ [g] / 2847.78\ [g]}{2*10^{-3}\ [L]} = 0.47\ mM$

Rhodamine-PE $C_m = \frac{n}{V} = \frac{m_s/M}{V} = \frac{0.01*10^{-3}\ [g] / 1176.93\ [g]}{2*10^{-3}\ [L]} = 0.005\ mM$

After adding all molar concentrations of lipids, it was found that the total molar lipid concentration was 4.75 mM.

To determine the amount of antibody present, the following calculations were carried out:

103.18 µg Ab → 1 mL

$103.18 * 10^{-3}$ g of Ab → 1,000 mL (1 L)

$103.18 * 10^{-3}$ g of Ab → $4.75 * 10^{-3}$ mole of lipids

21.72 g of Ab / 1 mole of lipids

In this way, the concentration of antibody (C_{AB}) was calculated to be 21.72 g of antibody per 1 mole of lipids.

The number of antibodies coupled to the liposome, according to formula mentioned above, was calculated as follows:

No. Ab / 1liposome = 3.14 / 6 * 21.72 (3 * 3.7 * $(99)^2$ – 3 * 99 * $(3.7)^2$ + $(3.7)^3$) * 1 / 150,000 * 1 / 1.25 = **6.3 Ab / liposome**

This is equivalent to ~6-7 antibodies per liposome.

SECOND APPROACH:

In this approach it was assumed that the size of an immunoliposome was 99 nm and that it was unilamellar.

To calculate antibody numbers per liposome, firstly the number of lipid molecules in the liposome and number of liposomes per 1 mL of solution has to be calculated (Hutchinson *et al.,* 1989).

The number of lipid molecules in the unilamellar liposome was calculated according to the Equation 1:

$$N_{tot} = \frac{[\,4\,\Pi\,(d/2)^2 + 4\,\Pi\,[\,d/2 - h\,]^2}{a} \qquad \text{Equation 1}$$

where,

4 Π (d / 2) $^{\mathbf{2}}$ is the surface area of the “monolayer” of the liposome, assuming it is spherical

d is the diameter of the liposome

a is the lipid head group area and

h is the thickness of the bilayer (~ 5 nm)

Table 4.2 Dimension of lipid head groups.

Lipid	Component	Area [nm^2]
DSPE-PEG	Head group	9
PC	Head group	0.75
Cholesterol	Head group	0.029

Cholesterol makes a negligible contribution to the surface area occupied by polar head groups because of its small size (0.029 nm^2) (Table 4.2). The only polar functional group on cholesterol is the single hydroxyl group.

It was decided to take 60 mol% DSPC and 9.9 mol% DSPE-PEG-DSPE-COOH for immunoliposome preparation.

$$a = \frac{0.75\ [nm^2] * 60\ mol\% + 9\ [nm^2] * 9.9\ mol\%}{100\ mol\%}$$

$a = 1.34\ [nm^2]$

In the above equation the surface area of both monolayers in a unilamellar liposome are added together. Then the total lipid area is divided to the average of head group area of DSPC and DSPE-PEG-COOH lipid molecule.

For unilamellar liposomes, which are 100 nm in diameter and with 5 nm of bilayer thickness, above equation is simplified to:

$$N_{tot} = \frac{4\ \Pi * 2500\ [nm^2] + 4\ \Pi * 2025\ [nm^2]}{1.35\ [nm^2]} = 42{,}381\ \text{lipids / liposome}$$

It was estimated based on Equation 1 that there are 42,381 lipids per single liposome.

N_{tot} = 42,381 lipids / liposome

The number of liposomes in 1 ml of solution was calculated according to Equation 2:

$$N_{liposomes} = \frac{M_{lipid} \times N_A}{N_{tot} \times 1000} \qquad \text{Equation 2}$$

where,

$N_{liposomes}$ is the number of liposomes in 1 mL of solution

M_{lipid} is the molar concentration of lipid

N_{tot} is the total number of lipids per liposome (section 3.2.5)

N_A is Avogadro's number which is equal to $6.02*10^{23}$ particles

For immunoliposome preparation, 60 mol% of DSPC, 30 mol% of cholesterol, 9.9 mol% of DSPE-PEG-COOH and 0.1 mol% of Rhodamine-PE were used. The total amount of lipids used was 8.29 mg (Table 2.8 in section 2.6.3.2). Finally, liposomes were suspended in 2 mL of 0.1 M PBS, pH 7.4.

To find out, how many liposomes are in 1 mL of solution, the molar concentration of lipids had to be calculated first, as follows:

DSPC $C_m = \frac{n}{V} = \frac{m_s/M}{V} = \frac{4.5*10^{-3}\ [g] / 790\ [g]}{2*10^{-3}\ [L]} = 2.85\ mM$

Cholesterol $C_m = \frac{n}{V} = \frac{m_s/M}{V} = \frac{1.1*10^{-3}\ [g] / 386\ [g]}{2*10^{-3}\ [L]} = 1.42\ mM$

DSPE-PEG-COOH $C_m = \frac{n}{V} = \frac{m_s/M}{V} = \frac{2.68*10^{-3}\ [g] / 2847.78\ [g]}{2*10^{-3}\ [L]} = 0.47\ mM$

Rhodamine-PE $C_m = \frac{n}{V} = \frac{m_s/M}{V} = \frac{0.01*10^{-3}\ [g] / 1176.93\ [g]}{2*10^{-3}\ [L]} = 0.005\ mM$

where,

C_m is the molar concentration

n is the moles number

m_s is amount of lipid taken for preparation

M is the molecular weight of lipid

V is the volume of the suspension

After adding all lipid molar concentrations, a total molar lipid concentration of 4.75 mM was determined.

The amount of liposomes in 1 mL of solution ($N_{liposomes}$) was calculated as follows:

$$N_{liposomes} = \frac{4.75 * 10^{-3} * 6.02 * 10^{23}}{42{,}381.1 * 1000} = 6.74 * 10^{13}\ \text{liposomes / mL}$$

One molecule of whole antibody has a molecular weight of 150 kDa. Antibody concentration in purified immunoliposomes was previously determined to be 141.88

µg/mL. Based on this, it can be calculated that in the anti-CD138-conjugated liposomes solution there was $9.5*10^{-10}$ moles of antibody.

1 mole of Ab is equivalent to 150,000 g/L, therefore

$103.18*10^{-6}$ g/L = x moles of Ab in immunoliposomes

x = $6.8 * 10^{-10}$ mole of Ab in immunoliposomes

This number has to be multipled by Avogadro's number. It was estimated that in 1L solution there are $5.69*10^{14}$ antibodies.

$6.8 * 10^{-10}$ mole of Ab * $6.02*10^{23}$ = $4.09 * 10^{14}$ antibody molecules

To find out how many antibody molecules are present on one liposome, $4.09 * 10^{14}$ antibody molecule number has to be divided by number of liposomes in solution ($6.07 * 10^{13}$ liposomes; section 3.2.6).

$$\frac{4.09 * 10^{14} \text{ (number of antibodies)}}{6.07 * 10^{13} \text{ (number of liposomes)}} = \textbf{6.74 Ab / 1 liposome}$$

Based on this, it was calculated that there were ~ 6-7 antibody molecules per liposome. This is similar to the previous number calculated using another approach.

This confirms that the two approaches produce the same value and hence that it does not matter if the calculation is based on the volume or on the surface area of the bilayer. The AB/liposome value obtained is effectively determined by C_{AB} and is subject to the assumption that the preparation is quantitative.

4.2.2.4 Cell binding experiment - FLISA (Fluorophore - Linked Immunosorbent Assay) for fluorescently-labelled anti-CD138-conjugated-liposomes (REV method)

Fluorophore-Linked Immunosorbent Assay (FLISA) was performed to characterise fluorescently-labelled anti-CD138-conjugated-liposomes, prepared by the REV method.

Fluorescently-labelled immunoliposomes were incubated with a human multiple myeloma cell lines (U266 and RPMI8226) according to the procedure described in section 2.2.3.9. Different concentrations of immunoliposomes were incubated with 10^6 human multiple myeloma cells.

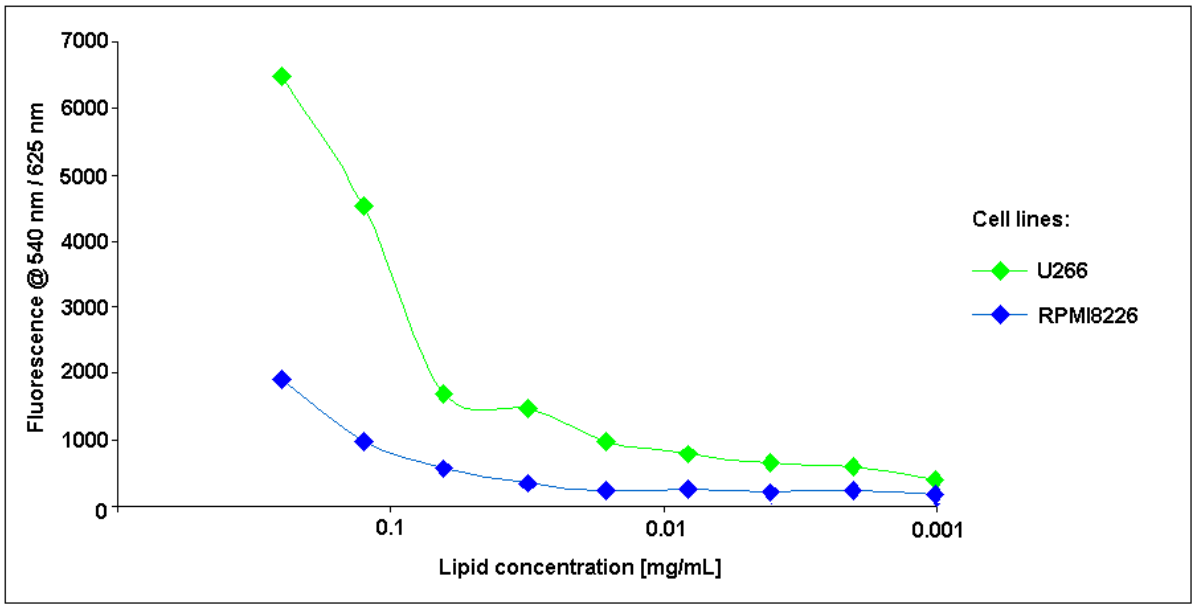

Figure 4.7 Binding of fluorescently-labelled anti-CD138-conjugated liposomes to human multiple myeloma cell lines (U266 and RPMI8226).
The anti-CD138-conjugated-liposomes used in this assay were prepared using the REV method. Different dilutions of anti-CD138-conjugated-liposomes were incubated with the cancer cell lines *in vitro*.

The higher fluorescence observed after incubation of immunoliposomes with U266 human multiple myeloma cells, shows better binding compared to the RPMI8226 cell line. It was calculated that there were ~ 6-7 anti-CD138 antibodies present on

each liposome. As a negative control multiple myeloma cell lines (U266 and RPMI8226) were incubated with fluorescently-labelled blank liposomes (plain liposomes; without antibody). Fluorescence obtained from cell lines incubated with plain liposomes was subtracted from fluorescence obtained from cell lines incubated with fluorescently-labelled anti-CD138-conjugated-liposomes. Fluorescence was measured using the Tecan Safire 2 spectrophotometer (excitation 540 nm; emission 625 nm).

4.2.3 Fluorescently-labelled anti-CD138-conjugated-liposomes - co-incubation method for immunoliposome of production

Fluorescently-labelled anti-CD138-conjugated-liposomes were prepared using the co-incubation method, as described in section 2.2.3.4. This method of immunoliposome preparation was performed to compare it with the reverse-phase evaporation method.

A lipid film was created using 64.5 mol% of egg PC, 30 mol% of cholesterol, 3 mol% of DSPE-PEG-Metoxy and 0.5 mol% of rhodamine-PE (Table 4.3). The lipid film was hydrated with 1 mL 0.1 M PBS, pH 7.4, by vortexing and sonicating for 30 min in a water-bath at 25ºC. The liposomes were extruded through a 100 nm polycarbonate membrane and co-incubated with DSPE-PEG-CO-NH-anti-CD138 antibody overnight at 4ºC. Monoclonal anti-CD138 antibody (0.2 mg) and a 40 molar excess of esterified DSPE-PEG-COOH lipid (2 mol%) were used. The total amount of lipids used for anti-CD138-conjugated-liposome preparation was 2.04 mg.

Table 4.3 Anti-CD138-conjugated-liposome lipid formulation.
The following lipids were used in defined molar ratios for immunoliposome preparation.

Compound	Molecular weight [g]	Weight used [mg]	Moles	Molar ratio of lipid to other lipids
Egg PC	790.12	1.33	$1.68*10^{-6}$	64.5 mol% (1)
Cholesterol	386.65	0.31	$8.02*10^{-7}$	30 mol% (0.47)
DSPE-PEG-Metoxy	2805.54	0.23	$8.20*10^{-8}$	3 mol% (0.05)
Rhodamine-PE	1176.93	0.02	$1.70*10^{-8}$	0.5 mol% (0.01)
DSPE-PEG-COOH	2847.78	0.16	$5.62*10^{-8}$	2 mol% (0.03)
TOTAL		2.04		

First fluorescently-labelled liposomes were prepared and then co-incubated with 2 mol% of DSPE-PEG-COOH conjugated with anti-CD138 monoclonal antibody. Fluorescently-labelled liposomes (blank liposomes; with no-conjugated antibody) were prepared as a negative control. The following lipids were used in defined molar ratios for liposome preparation. Liposomes were prepared by lipid film formation and hydration using 1 mL 0.1 M PBS, pH 7.4. 64.5 mol% of egg PC, 30 mol% of cholestrol, 5 mol% of DSPE-PEG-Metoxy and 0.5 mol% of rhodamine-PE were used for the two described formulations (Tables 4.3 and 4.4).

Table 4.4 Formulation for generation of fluorescently-labelled liposomes.

Compound	Molecular weight [g]	Weight used [mg]	Moles	Molar ratio of lipid to other lipids
Egg PC	790.12	4.00	$5.06*10^{-6}$	64.5 mol% (1)
Cholesterol	386.65	0.94	$2.35*10^{-6}$	30 mol% (0.47)
DSPE-PEG-Metoxy	2805.54	1.14	$4.07*10^{-7}$	5 mol% (0.01)
Rhodamine-PE	1176.93	0.05	$4.33*10^{-8}$	0.5 mol% (0.01)
TOTAL		6.14		

4.2.3.1 Protein determination in anti-CD138-conjugated-liposomes

Anti-CD138-conjugated-liposomes were prepared using the co-incubation method. Immunoliposomes (IL) were purified from free antibodies by dialysis, through 300,000 Da membrane, as described in section 2.2.3.6. Samples were analyzed using the micro Lowry assay with Peterson's modification (section 2.2.3.8).

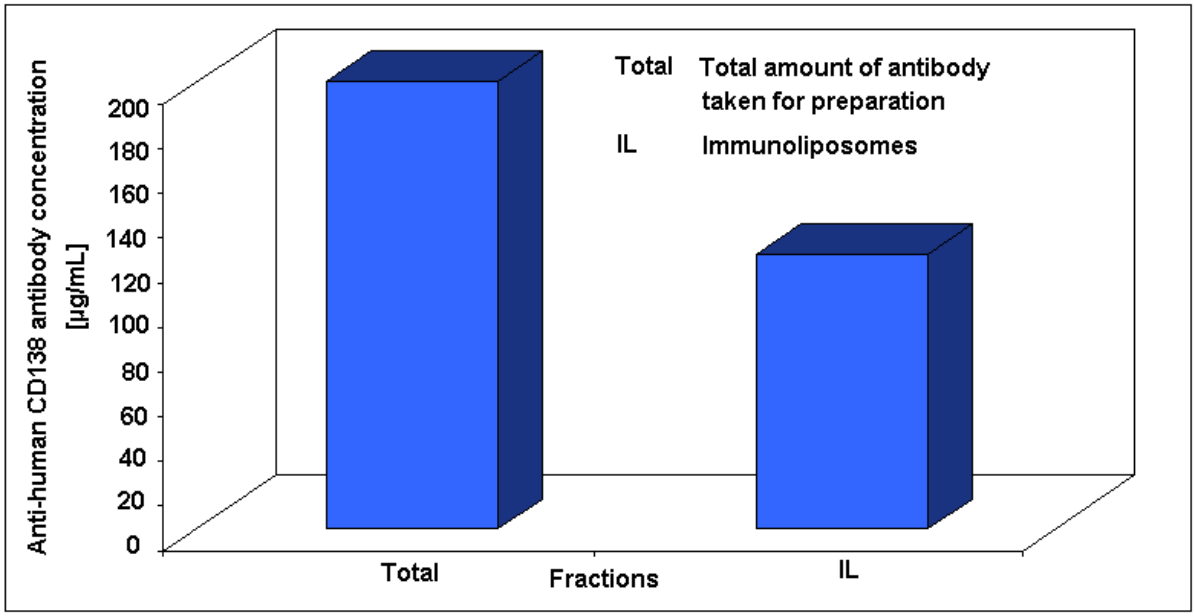

Figure 4.8 Determination of antibody concentration in anti-CD138-conjugated-liposomes after dialysis.
200 µg/mL of anti-CD138 antibody was used for immunoliposome preparation using the co-incubation method. It was estimated that there was 122.5 µg/mL of anti-CD138 antibody attached to liposomes.

A calibration curve was drawn and used to determine protein concentration in the samples. Approximately, 122.5 µg/mL of antibody was found to be present on the prepared immunoliposomes (Figure 4.8). It was found that 77.5 µg/mL of anti-CD138 antibody did not bind to liposomes and was removed from the immunoliposome sample by dialysis. The effectiveness of antibody coupling was 61.25%.

4.2.3.2 Calculation of the number of lipid molecules per liposome

Previously, the number of antibodies bound to liposomes prepared using REV method was calculated (section 4.2). This process was repeated for the co-incubation approach.

In this approach it was assumed that the size of an immunoliposome was 100 nm and that it was unilamellar.

To calculate antibody numbers per liposome, firstly the number of lipid molecules in the liposome and number of liposomes per 1 mL of solution had to be calculated (Hutchinson *et al.,* 1989).

The number of lipid molecules in the unilamellar liposome was calculated according to Equation 1:

$$N_{tot} = \frac{[\,4\,\Pi\,(d/2)^2 + 4\,\Pi\,[\,d/2 - h\,]^2}{a} \qquad \text{Equation 1}$$

where,

4 Π (d / 2) ^{2} is the surface area of the "monolayer" of the liposome, assuming it is spherical

d is the diameter of the liposome

a is the lipid head group area and

h is the thickness of the bilayer (~ 5 nm)

Table 4.5 Dimension of lipid head groups.

Lipid	Component	Area [nm^2]
Egg PC	Head group	0.75
DSPE-PEG	Head group	9
PE	Head group	0.37
Cholesterol	Head group	0.029

Cholesterol makes a negligible contribution to the surface area occupied by polar head groups because of its small size (0.029 nm^2) (Table 4.5). The only polar functional group on cholesterol is the single hydroxyl group.

64.5 mol% of egg PC, 30 mol% of cholestrol, 5 mol% of DSPE-PEG-Metoxy and 0.5 mol% of rhodamine-PE were used for immunoliposome preparation.

$$a = \frac{0.75\ [nm^2] * 64.5\ mol\% + 9\ [nm^2] * 5\ mol\% + 0.37\ [nm^2] * 0.5\ mol\%}{100\ mol\%}$$

$a = 0.94\ [nm^2]$

In the above equation the surface area of both monolayers in a unilamellar liposome are added together. Then the total lipid area is divided to the average of head group area of DSPC and DSPE-PEG-COOH lipid molecules.

For unilamellar liposomes, which are 100 nm in diameter with a 5 nm bilayer thickness, the above equation is simplified to:

$$N_{tot} = \frac{4\ \Pi * 2500\ [nm^2] + 4\ \Pi * 2025\ [nm^2]}{0.94\ [nm^2]} = 60{,}461\ \text{lipids / liposome}$$

It was estimated, based on Equation 1, that there are 60,461 lipids per single liposome.

N_{tot} = 60,461 lipids / liposome

The number of liposomes in 1 ml of solution was calculated according to Equation 2:

$$N_{liposomes} = \frac{M_{lipid} \times N_A}{N_{tot} \times 1000} \qquad \text{Equation 2}$$

where,

$N_{liposomes}$ is the number of liposomes in 1 mL of solution

M_{lipid} is the molar concentration of lipid

N_{tot} is the total number of lipids per liposome (section 3.2.5)

N_A is Avogadro's number which is equal to $6.02*10^{23}$ particles

For immunoliposome preparation, 64.5 mol% of egg PC, 30 mol% of cholestrol, 5 mol% of DSPE-PEG-Metoxy and 0.5 mol% of rhodamine-PE were used. The total amount of lipids used was 2.05 mg (Table 4.3 in section 4.2.7). Finally, liposomes were suspended in 0.5 mL of PBS buffer, pH 7.3.

To find out, how many liposomes are 1 mL of solution, the molar concentration of lipids had to be first calculated, as follows:

Egg PC $C_m = \frac{n}{V} = \frac{m_s/M}{V} = \frac{1.33*10^{-3}\ [g] / 790.12\ [g]}{0.5*10^{-3}\ [L]} = 3.37\ mM$

Cholesterol $C_m = \frac{n}{V} = \frac{m_s/M}{V} = \frac{0.31*10^{-3}\ [g] / 386.65\ [g]}{0.5*10^{-3}\ [L]} = 1.60\ mM$

DSPE-PEG-Metoxy $C_m = \frac{n}{V} = \frac{m_s/M}{V} = \frac{0.23*10^{-3}\ [g] / 2805.54\ [g]}{0.5*10^{-3}\ [L]} = 0.16\ mM$

Rhodamine-PE $C_m = \frac{n}{V} = \frac{m_s/M}{V} = \frac{0.01*10^{-3}\ [g] / 1176.93\ [g]}{0.5*10^{-3}\ [L]} = 0.02\ mM$

DSPE-PEG-COOH $C_m = \frac{n}{V} = \frac{m_s/M}{V} = \frac{0.16*10^{-3}\ [g] / 2847.78\ [g]}{0.5*10^{-3}\ [L]} = 0.11\ mM$

where,

C_m is the molar concentration

n is the number of moles of lipid

m_s is amount of lipid taken for preparation

M is the molecular weight of lipid

V is the volume of the suspension

After adding all lipids molar concentrations, a total lipid concentration of 5.32 mM was found.

Then, the amount of liposomes in 1 mL of solution ($N_{liposomes}$) is calculated as follows:

$$N_{liposomes} = \frac{5.32 * 10^{-3} * 6.02 * 10^{23}}{60{,}461 * 1000} = 5.3\ 10^{13}\ \text{liposomes / mL}$$

One molecule of whole antibody has a molecular weight of 150 kDa. Antibody concentration in purified immunoliposomes solution was previously determined to be 122.5 µg/mL. Based on this, it can be calculated that in an anti-CD138-conjugated-liposome solution $8.2*10^{-10}$ moles of antibody are present.

1 mole of Ab is equivalent to 150,000 g/L, therefore

$122.5*10^{-6}$ g/L = x moles of Ab in immunoliposomes

x = $0.82 * 10^{-9}$ mole of Ab in immunoliposomes

This number has to be multipled by Avogadro's number. It was estimated that in 1L solution there are $5.69*10^{14}$ antibodies.

$8.2 * 10^{-10}$ mole of Ab * $6.02*10^{23}$ = $49.36 * 10^{13}$ antibody molecules

To find out how many antibody molecules are present on one liposome, $4.94 * 10^{14}$ antibody moles has to be divided by number of liposomes in solution ($5.30 * 10^{13}$ liposomes).

$$\frac{4.94 * 10^{14} \text{ (number of antibodies)}}{5.30 * 10^{13} \text{ (number of liposomes)}} = \textbf{9.3 Ab / liposome}$$

Based on this, it was calculated that there were ~ 9-10 antibody molecules per liposome.

4.2.3.3 Cell binding experiment – FACS analyses for fluorescently-labelled anti-CD138-conjugated-liposomes (co-incubation method) of production

To characterise fluorescently-labelled anti-CD138-conjugated-liposomes, FACS analyses were performed. Anti-CD138-conjugated-liposomes were prepared, as described in section 2.2.3.4. A lipid film was prepared from egg PC, cholesterol, DSPE-PEG-Metoxy and Rhodamine-PE lipid, hydrated with 1 mL 0.1 M PBS, pH 7.3, and extruded through a 100 nm polycarbonate membrane. The liposome solution was co-incubated with previously prepared DSPE-PEG-CO-NH-anti-CD138. Immunoliposomes were dialysed against 0.1 M PBS, pH 7.3, for 2 days ('cut-off' 300,000 Da) to remove free antibody.

Five hundred thousand cells from each of the cell lines, RPMI8226, U266 and L428, were treated with 0.5 mg/mL of liposomes for 1.5 h at 37 ºC in 'serum-free' medium. Cells were washed three times with 0.1 M PBS, pH 7.3, and immediately analyzed on the FACS Calibur instrument (Figure 4.9).

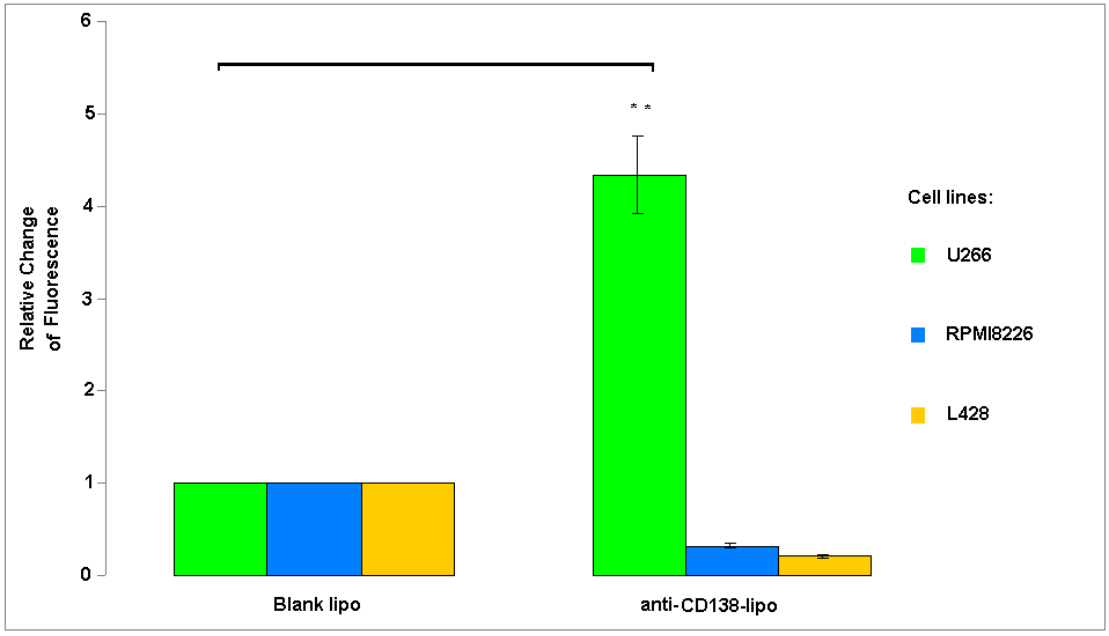

Figure 4.9 Binding assay of fluorescently-labelled anti-CD138-conjugated-liposomes *in vitro*.
Blank liposomes (Plain lipo; without antibody). Previously, it was estimated that U266 expresses CD138 protein at 84.3%. Anti-CD138-conjugated-liposomes (anti-CD138-lipo) used for this binding experiment were prepared using the co-incubation method. The results are the mean ± the standard deviation and the experiment was performed in triplicate.
** Significantly different from control (Blank liposomes) (Student's *t*-test, $0.001<p<0.01$)

This experiment clearly demonstrated that fluorescently-labelled anti-CD138-conjugated liposomes bind to a much greater degree to the U266 myeloma than to controls or the other cell lines tested. Results were normalized. Fluorescence levels obtained from the three cell lines used after incubation with blank liposomes was adjusted to 1. The fluorescence obtained from the other samples was expressed relative to this value. It was estimated, using Student's *t*-test, that there was a significant difference (p value<0.05) between U266 cells incubated with blank liposomes and U266 cells incubated with anti-CD138-conjugated-liposomes.

Discussion

The overall objective of this project was to prepare anti-CD138 targeted nanoparticles (e.g. anti-CD138-conjugated-liposomes) for use in minimally non-invasive diagnosis of multiple myeloma using MRI.

The main aim of this chapter was to describe the preparation of targeted anti-CD138 (syndecan-1)-conjugated-liposomes by two different methods and determination their physical characteristics (size, zeta potential and number of antibody molecules linked per liposome). This chapter described also the binding ability of anti-CD138-conjugated-liposomes to human multiple myeloma cancer cells *in vitro*.

It was found that the U266 human multiple myeloma cell line was positively stained (84.3%) using anti-CD138, clone B-A38, compared to 2% with the mouse IgG1 isotype. This is with agreement with other researchers. Sun *et al.* (2008) performed U266 staining with the anti-CD138, clone B-B4, and reported 95.2% positively stained cells compared to 5.3% in the mouse IgG1 isotype control. It was found that the U266 cell line was an ideal line to examine anti-CD138-conjugated-liposome interactions. The specific association of immunoliposomes with their target cells is a necessary requirement for the required active targeting strategy.

Two methods were used for anti-CD138-conjugated-liposomes preparation (reverse phase evaporation (REV) and co-incubation method). It was shown using the FLISA assay that fluorescent anti-CD138-conjugated-liposomes prepared by the REV method bound to the U266 cell line to a significantly greater extent than to the RPMI8226 cell line.

Maruyama *et al.* (1990) successfully prepared 34A-liposomes for *in vivo* targeting in mice using the REV method. They tested PEGylated immunoliposomes with antibody attached to the distal terminus of PEG chain. They assessed that 30

antibody molecules were conjugated per liposome. In this study, anti-CD138 antibody was also conjugated to the terminus of the PEG chain and it was determined that 6-7 antibody molecules was linked per liposome (Adrian *et al.*, 2007). It was determined by the micro Lowry assay with Peterson's modification (Peterson, 1977) that 142 µg/mL of anti-CD138 antibody was conjugated to liposomes after initially taking 200 µg/mL of antibody per reaction.

The co-incubation method was also tested for immunoliposome preparation. Erdogan *et al.* (2006) successfully used the co-incubation method to prepare targeted 2C5-liposomes-Gd-loaded PAP to murine Lewis lung carcinoma (LLC) *in vitro* as well as *in vivo* (Erdogan *et al.*, 2008). Using ELISA, they demonstrated that targeted 2C5-conjugated-liposomes bound to a greater extent (more than 2 fold) to cancer cells than plain liposomes.

In this study, it was found that fluorescently-labelled anti-CD138-conjugated-liposomes bound at a 4.5-fold significantly greater extent to the U266 cell line compared to fluorescently-labelled non-targeted liposomes. (i.e. blank liposomes; plain liposomes; without antibody) using flow cytometry. It was found that ~ 9-10 antibody molecules of anti-CD138 antibody were linked per liposome in the co-incubation method of production.

Both production methods were effective for immunoliposome preparation which was shown by the ability of the antibody-conjugated-liposomes to bind cancer cells *in vitro* (FLISA assay and FACS analyses). However, the main drawback of the REV method is the exposure of the antibody to an organic solvent which may lead to denaruration of the protein. Secondly, losses of the material during immunoliposome preparation are high, which decreases the amount of final product. The co-incubation method does not involve any solvent usage which prevents significantly

antibody denaturation. Preliminary studies indicate that it also results in higher levels of antibody attachment.

FACS analyses were also carried out by other researchers to observe the binding ability of immunoliposomes with cells *in vitro* (Roth *el al.*, 2007; Lopes de Menezes *et al.* 2000; Beduneau *et al.* 2007; Mamot *et al.*, 2005) indicating the approach used is accepted and is recommended as a method used to ensure the association between conjugated-liposomes with a relevant antibody and the targeted cells.

In conclusion, the research in this chapter shows that multiple myeloma cells can be targeted by anti-CD138 antibody-conjugated-liposomes to a significant extent. This valuable information now leads us to the next step, in which targeted anti-CD138-conjugated-liposomes can be loaded with paramagnetic contrast agent (e.g. gadolinium) and used for a minimally non-invasive diagnostic purpose for human multiple myeloma. Both methods (REV and co-incubation) were effective for targeted liposome preparation, but because of a few drawbacks associated with the REV method, it was decided to work with co-incubation in further experiments.

The development of this potentially *novel* diagnostic method will be further described in Chapter 5.

Chapter 5

Magnetic resonance relaxation studies on magnetoliposomes

5.1 Introduction

The main aim of this chapter was to prepare sufficient contrast agent for minimally non-invasive diagnosis of multiple myeloma in humans. The current diagnostic method for this cancer involves invasive biopsy, which is painful for the patient. The bone marrow section is then immunochemically examined using anti-CD138 antibodies. Currently, magnetic resonance imaging (MRI) is an established minimally non-invasive clinical imaging modality which is capable of producing three-dimentional images of tissues containing water with a high degree of spatial resolution. MRI relies primarily on registering and interpreting differences in image contrast between tissues, normal or pathological, which represent the anatomical expression of disease. However, MRI can be also achieved through a combination of imaging and active targeting of a contrast agent to disease-specific markers enabling minimally non-invasive, specific detection of biochemical markers. Thus, molecular, magnetic resonance imaging seeks to improve diagnostic accuracy through the visualization of processes or components that cause disease (Lanza *et al.*, 2003). There are also different imaging methods like PET (position emission tomography) and SPECT (single position emission computed tomography) (Kairemo *et al.*, 2008). Each modality has advantages and disadvantages. SPECT and PET have high sensitivity (10^{-11}-10^{-12} mol/L for PET and 10^{-10}-10^{-11} mol/L for SPECT) but low spacial resolution and poor anatomical definition. MRI, in contrast, exhibits good spatial resolution but low sensitivity of 10^{-3}-10^{-5} mol/L. The low sensitivity of MRI scans can be overcome by using contrast agents with high relaxivity. These agents consist of molecules which incorporate a paramagnetic metal ion, most commonly gadolinium (Gd) or iron (Fe). The former class includes a paramagnetic agent, mainly Gd, which increase R_1 and R_2 relaxation rates. However, the best

visualization is obtained using T_1-weighted images because the percentage change in R_1 in tissue is much greater than in R_2. Superparamagnetic contrast agents (e.g. Fe) generally lead to a much larger increase in R_2 than in R_1 and are best seen with T_2-weighted scans. Paramagnetic agents directly affect water protons in their close vicinity and are highly dependent on local water flux. Hence, the influence of these agents is very local and they should ideally be in contact with water with adequate exchange rates. In contrast, superparamagnetic agents affect the magnetic field independent of their environment and, thus, their influence in terms of contrast extends well beyond their immediate surroundings (Lanza *et al.,* 2004). The gadolinium-loaded contrast agents currently on the market require a tissue concentration of 10^{-7} mol/g to obtain sufficient contrast in the resulting image (Gupta and Weissleder, 1996; Lanza *et al.,* 2004). This level is too high for imaging sparse molecular biomarkers expressed in the living body since typical receptors are normally present in low concentrations of 10^{-9} to 10^{-13} mol/g (Strijkers *et al.,* 2005). Therefore, method development is needed to increase the number of Gd moieties bound per contrast agent molecule. There have been a number of reports concerning the conjugation of Gd chelates to macromolecules such as dendrimers, linear polymers, and proteins, as well as the use of liposomes as Gd-chelate carriers (Kobayashi *et al*. 2001; Hueber *et al.,* 1998; Langereis *et al*. 2004). There are different agents which can be used for this purpose e.g. solid lipid nanoparticles, liposomes, micelles, nanocrystals, carbon nanotubes. Liposomes were chosen to be nanoparticles used to target human multiple myeloma because they are a versatile tool used traditionally in drug and gene delivery, and are easly adapted for use *in vitro*, *ex vivo* and *in vivo*. The overall liposome properties can be adjusted using parameters such as lipid composition, head group charge, and lipid tail size.

The traditional method of encapsulating contrast agents, such as the clinically used Gd chelates, has the disadvantage that the entrapped agents easily 'leak' out of liposomes prior to reaching the target site. This problem can be avoided by chelation of Gd with molecules like DTPA-BSA, DOTA-DSA or DTPA-PLL-NGPE that can easily be inserted into the bilayer of liposomes. In this way, Gd can be anchored to the liposome surface instead of being entrapped in the liposome lumen.

Kamaly *et al.* (2008) used bimodal paramagnetic and fluorescent liposomes for cellular and human ovarian cancer imaging by enhanced permeation and retention (EPR) mechanisms due to the porous nature of the endothelial cell layer. Similarly, Mulder *et al.* (2005) prepared bimodal (paramagnetic and fluorescent) liposomes actively targeted to $\alpha_v\beta_3$ integrin site on HUVEC (human umbilical vein endothelial cells) human endothelial cells *in vitro* and *in vivo*. Erdogan *et al.* (2008) successfully targeted pegylated 2C5-liposomes, containing gadolinium-loaded polychelating amphiphilic polymer (PAP), to murine Lewis lung carcinoma (LLC) *in vivo* and human mammary adenocarcinomas (MCF-7, BT20) *in vitro* (Erdogan *et al*., 2006). They also demonstrated that these targeted liposomes showed better and faster targeting in *in vivo* imaging than non-targeted contrast liposomes. PAP contains several groups which can chelate several Gd ions per polymer molecule and can be firmly incorporated into the liposomal membrane. Torchilin *et al.* (1994) showed that the PAP complex generates up to 11 NH_2 groups, which are available to undergo reaction with DTPA which can subsequently be loaded with Gd ions. Erdogan *et al*. (2006) confirmed that PAP-loaded pegylated liposomes are capable of carrying higher amounts of ^{111}In radiotracer than similar liposomes loaded with the monomeric chelate, DTPA-PE.

In this project, two compounds were used: Gd-DTPA-BSA and Gd-PAP. Gd-DTPA-BSA chelates one Gd ion per molecule and is an amphiphilic phospholipid composed of a hydrophilic head and a hydrophobic tail, which allow phospholipid incorporation into liposome membranes. Contrast liposomes (containing Gd-DTPA-BSA and Gd-PAP) were prepared and analyzed. In theory liposomes containing Gd-PAP should show higher signals than liposomes containing Gd-DTPA-BSA, due to the ability of PAP to carry more metal ions.

Anti-CD138-Gd-conjugated-liposomes were then used as a targeted contrast agent for imaging human multiple myeloma *in vitro*.

5.2 Results

5.2.1 Synthesis of polychelating amphiphilic polymer (PAP)

Before preparation of contrast liposomes, polychelataing amphiphilic polymer (PAP) was first synthesized, as described in section 2.2.6. Briefly, poly(ε-carbobenzyoxy-l-lysine) (poly(CBZ)-lysine) was conjugated to 1,2-dioleoyl-*sn*-glycero-3-phosphoethanolamine-N-(glutaryl) (NGPE) using EDC and NHS. NGPE-PLL-CBZ was deprotected from CBZ to expose NH_2 groups for conjugation with DTPA anhydride (Figure 5.1). Subsequently, NGPE-PLL (Poly(l-lysine)-DTPA was chelated by gadolinium ions and dialysed to separate it from free ions.

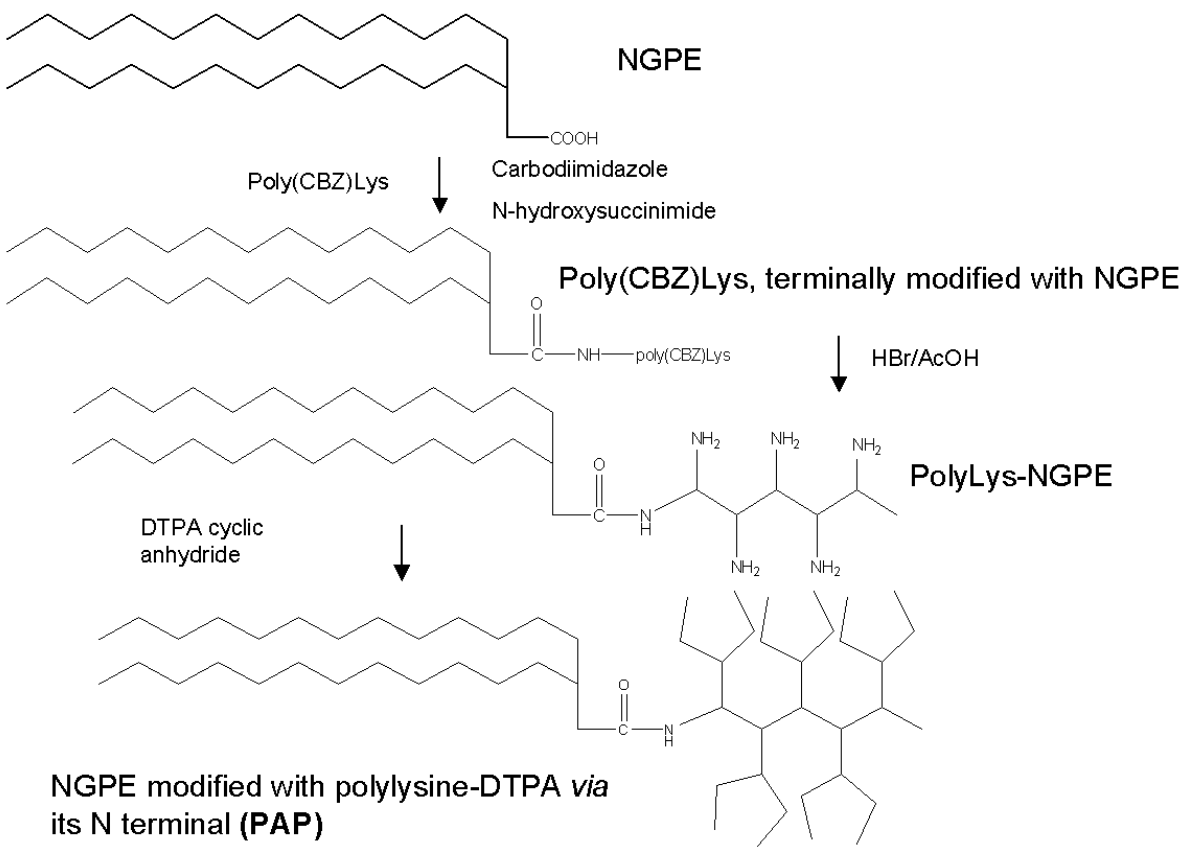

Figure 5.1 Polychelating amphiphilic polymer (PAP) synthesis.
Poly(CBZ)Lys was conjugated with NGPE and then CBZ was deprotected from NGPE-Poly(CBZ)Lys. The deprotected compound was then linked with DTPA.

5.2.2 Relaxometric analysis of contrast Gd-DTPA-BSA-liposomes and Gd-PAP-liposomes based on estimated gadolinium concentration

Contrast liposomes were prepared using lipid formulations of 63.25 mol% (w/v) of egg PC, 30 mol% (w/v) of cholesterol, 5 mol% (w/v) PEG_{2000}-PE and 1.75 mol% (w/v) of Gd-DTPA-BSA or 1.75 mol% (w/v) of Gd-PAP, as described in section 2.2.7 (Table 5.1 and Table 5.2). A lipid film was prepared and hydrated with 1 mL of 0.1 M PBS, pH 7.3.

Table 5.1 Lipid formulation used to prepare contrast liposomes (1.75 mol% (w/v) Gd-DTPA-BSA).

Compound	Molecular weight [g]	Weight taken [mg]	Moles	Molar ratio of lipid to other lipids
Egg PC	790.12	4.00	$5.19*10^{-6}$	63.25 mol% (1)
Cholesterol	386.65	0.95	$2.46*10^{-6}$	30 mol% (0.47)
PEG_{2000}-PE	2,805.50	1.15	$4.10*10^{-7}$	5 mol% (0.08)
Gd-DTPA-BSA	1,068.60	0.15	$1.40*10^{-7}$	1.75 mol% (0.03)
TOTAL		6.25		

Table 5.2 Lipids used for contrast liposomes (1.75 mol% (w/v) Gd-PAP) preparation.

Compound	Molecular weight [g]	Weight taken [mg]	Moles	Molar ratio of lipid to other lipids
Egg PC	790.12	4.00	$5.19*10^{-6}$	63.25 mol% (1)
Cholesterol	386.65	0.95	$2.46*10^{-6}$	30 mol% (0.47)
PEG_{2000}-PE	2,805.50	1.15	$4.10*10^{-7}$	5 mol% (0.08)
Gd-PAP	11,370.0	1.59	$1.40*10^{-7}$	1.75 mol% (0.03)
TOTAL		7.70		

Dilutions of both types of contrast liposomes were prepared and T_1 relaxation times measured using a 5 mHz RADX NMR Analyzer. The relaxation time (T_1) is the time needed for the ^1H magnetisation to return from its non-equilibrium state to equilibrium. Paramagnetic contrast agents like gadolinium have an ability to shorten the T_1 relaxation time of surrounding water ^1H nuclei, resulting a bright signal on the image. Relaxation rate (R_1) is the reciprocal of relaxation time ($1/T_1$). It was expected that liposomes containing Gd-PAP-liposomes will show a higher R_1 relaxation rate than Gd-DTPA-BSA-liposomes, because DTPA-BSA phospholipid chelates one gadolinium ion per molecule (Figure 5.2), whereas PAP can chelate up to 11 gadolinium ions per molecule (Torchilin *et al.* 1994).

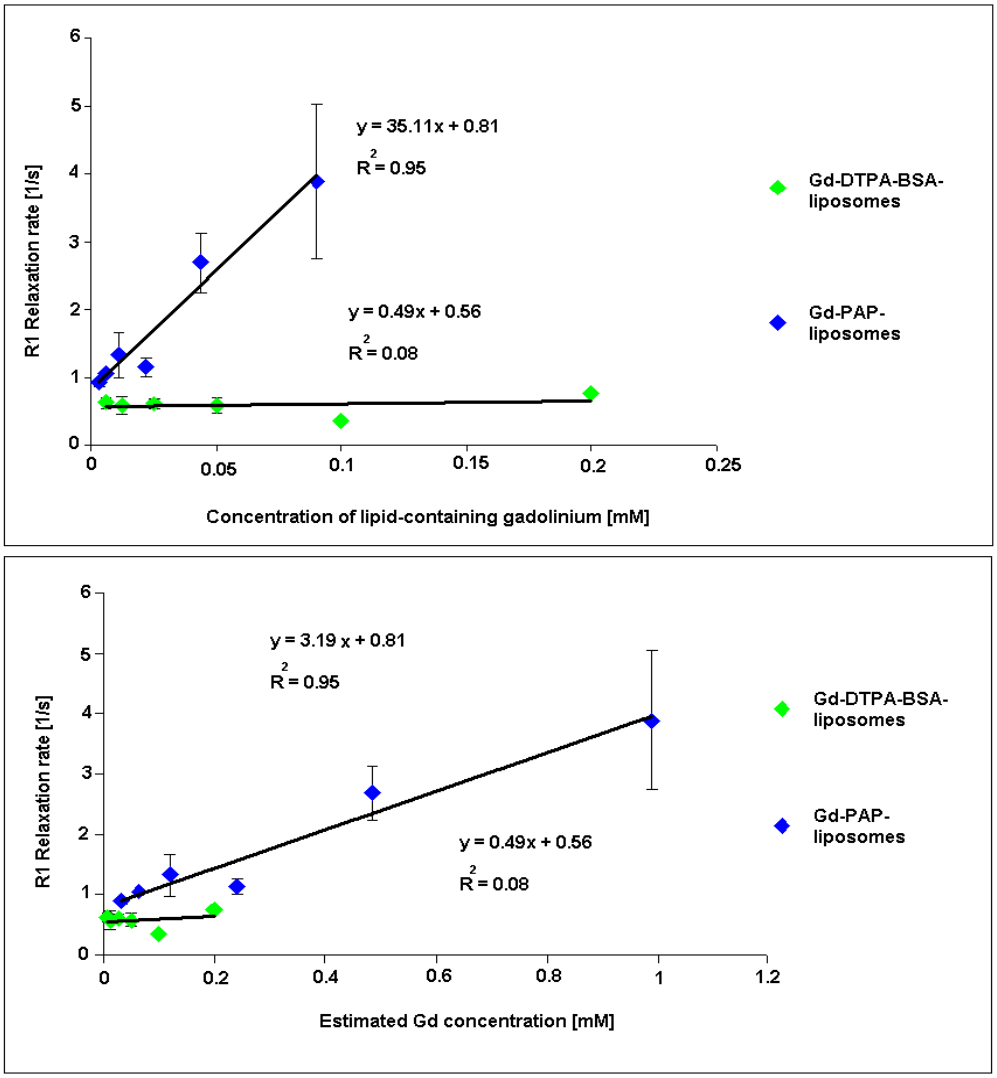

Figure 5.2 Relaxivity studies of contrast liposomes.
Different concentrations of contrast liposomes (Gd-PAP-liposomes and Gd-DTPA-BSA-loaded monochelated liposomes) were analyzed using the 5 mHz RADX NMR Analyzer. T_1 relaxation times [ms] were measured. Relaxation rate (R_1) [1/s] was plotted against lipid-containing gadolinium concentration [mM] (top graph). On the bottom graph, relaxation rate (R_1) was plotted against estimated gadolinium concentration in analysed samples. Gd-PAP-liposomes showed a higher relaxation rate than Gd-DTPA-BSA liposomes. The results are the mean ± the standard deviation and the experiment was performed in triplicate.

The effectiveness of the gadolinium as a contrast agent to shorten the T_1 or T_2 relaxation times of the water protons can be quantified by the concentration independent relaxivity, r_1 or r_2, which is defined as the change in R_1 or R_2 relaxation rate per unit concentration of the contrast agent. In this case, r_1 relaxivity was assessed based on R_1 relaxation rate and estimated gadolinium concentration. The r_1 relaxivity is a slope of curve presented on the bottom plot (Figure 5.2) (R_1

relaxation rate *vs* estimated gadolinium concentration). It was showed that r_1 relaxivity of Gd-PAP-liposomes is higher (3.19 $mM^{-1}s^{-1}$) than the r_1 relaxivity of Gd-DTPA-BSA-liposomes (0.49 $mM^{-1}s^{-1}$). The r_1 relaxivity value in this experiment was calculated based on the premise that the PAP molecule chelates 11 ions of gadolinium and is probably inaccurate. A more accurate measurement of relaxometry using a known concentration of Gd, was then carried out, as described in section 5.2.3.

5.2.3 Relaxometric analysis of Gd-DTPA-BSA-liposomes and Gd-PAP-liposomes based on the determined gadolinium concentration

5.2.3.1 Determination of gadolinium content in Gd-DTPA-BSA-liposomes and Gd-PAP-liposomes

Contrast liposomes were prepared using a formulation of 63.25 mol% (w/v) of egg PC, 30 mol% of cholesterol, 5 mol% (w/v) PEG_{2000}-PE and 1.75 mol% (w/v) of Gd-DTPA-BSA or 1.75 mol% (w/v) of Gd-PAP, as described in section 2.2.7 (Tables 5.3 and 5.4). A lipid film was prepared and hydrated with 2.2 mL of distilled water for Gd-DTPA-BSA-liposomes and 0.7 mL distilled water for Gd-PAP-liposomes. The liposomes were extruded through a 100 nm polycarbonate membrane and their size was determined using Photon Correlation Spectroscopy (PCS). The size of the Gd-DTPA-BSA liposomes was determined to be 171.2 nm PDI (0.23) while Gd-PAP-liposomes were 175.1 nm (PDI 0.22).

Table 5.3 Lipid formulation used to prepare contrast liposomes (1.75 mol% (w/v) Gd-DTPA-BSA).

Compound	Molecular weight [g]	Weight taken [mg]	Moles	Molar ratio of lipid to other lipids
Egg PC	790.12	240.00	$3.1*10^{-4}$	63.25 mol% (1)
Cholesterol	386.65	56.80	$1.46*10^{-4}$	30 mol% (0.47)
PEG_{2000}-PE	2,805.50	70.00	$2.5*10^{-5}$	5 mol% (0.08)
Gd-DTPA-BSA	1,068.60	9.32	$8.72*10^{-5}$	1.75 mol% (0.03)
TOTAL		376.12		

Table 5.4 Lipids used for contrast liposomes (1.75 mol% (w/v) Gd-PAP) preparation.

Compound	Molecular weight [g]	Weight taken [mg]	Moles	Molar ratio of lipid to other lipids
Egg PC	790.12	24.00	$3.12*10^{-5}$	63.25 mol% (1)
Cholesterol	386.65	5.68	$1.46*10^{-5}$	30 mol% (0.47)
PEG_{2000}-PE	2,805.50	7.00	$2.49*10^{-6}$	5 mol% (0.08)
Gd-PAP	11,370.0	9.92	$0.87*10^{-6}$	1.75 mol% (0.03)
TOTAL		46.6		

Inductively Coupled Plasma-Atomic Emission Spectroscopy (ICP-AES) was performed for a precise determination of gadolinium. The gadolinium content in contrast liposomes (Gd-DTPA-BSA-liposomes and Gd-PAP-liposomes) was then determined using Inductively Coupled Plasma-Atomic Emission Spectroscopy (ICP-AES). Firstly, a calibration curve of $GdCl_3$ was made (Figure 5.3). ICP-AES analyses

of both contrast liposomes resuspended in 0.2 % (v/v) Triton X-100 (to break down liposome vesicles) were carried out.

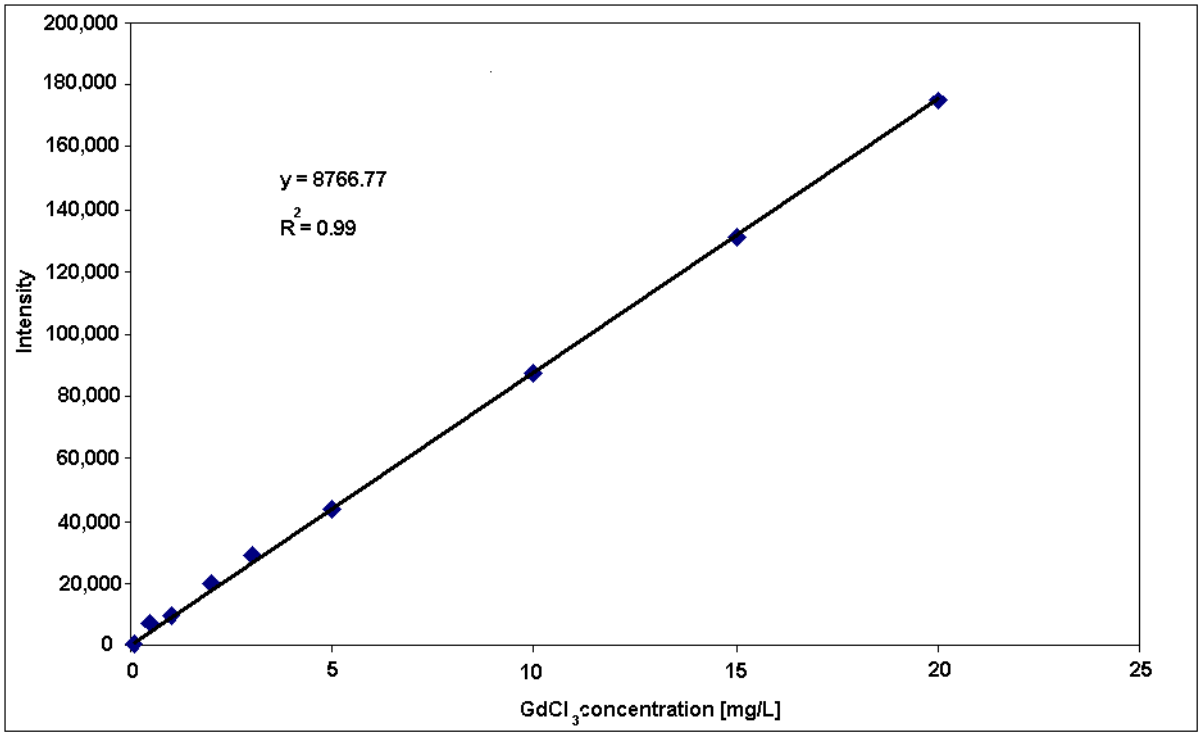

Figure 5.3 Calibration curve based on gadolinium chloride ($GdCl_3$) salt standards solutions (0 – 20 mg/L).

The gadolinium content of the contrast liposomes were determined using the calibration curve and it was calculated that there are 2.7 mM of Gd in Gd-DTPA-BSA-liposomes and 16.5 mM in Gd-PAP-liposomes. The difference in gadolinium concentration found was as expected since PAP can carry more gadolinium ions per molecule compared to the DTPA-BSA molecule.

Additionally, to calculate r_1 relaxivity value, NMR analyses of contrast liposomes were carried out to determine T_1 relaxation time of water protons.

5.2.3.2 Calculation of relaxivity value of contrast liposomes

The effectiveness of the gadolinium as a contrast agent to shorten the T_1 or T_2 relaxation times of the water protons can be quantified by the concentration

independent relaxivities, r_1 or r_2, which are defined as the change in R_1 or R_2 relaxation rate per unit concentration of the contrast agent. NMR analyses of contrast liposomes were carried out to determine T_1 relaxation time of water protons. Taking into account T_1 relaxation time measurments and gadolinium concentration, relaxivity of contrast liposomes was calculated using the following equation:

$$r_1 = \frac{R_{1\,obs} - R_{1\,H_2O}}{[Gd]}$$

where,

$\mathbf{r_1}$ is the relaxivity of contrast agent (nominal value-concentration independent)

$\mathbf{R_{1\ obs}}$ is the observed relaxation rate in the presence of enhancement

$\mathbf{R_{1\ H_2O}}$ is the relaxation rate of water protons

[Gd] is the concentration of gadolinium contrast agent in [mM]

Relaxivity is expressed in [$mM^{-1}s^{-1}$] unit.

The relaxivity (r_1) value was calculated, based on gadolinium content determination. An important quality criterion for MRI contrast agents is their molar relaxivity. A Nuclear Magnetic Resonance Dispersion (NMRD) profile was drawn (relaxivity (r_1) in relation to Larmour Frequency (MHz)). The r_1 relaxivity is a nominal value, independent of gadolinium concentration, which demonstrates contrast agents as sensitive enough for potential use in real samples.

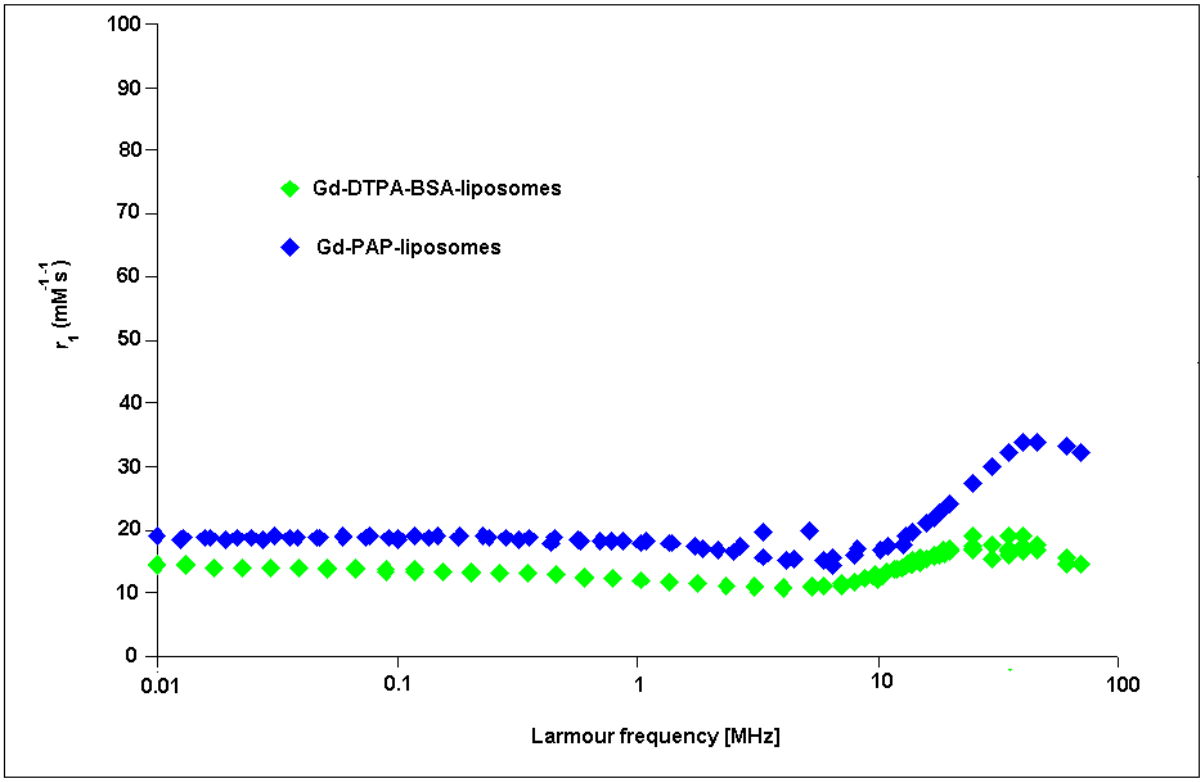

Figure 5.4 Relaxivity profile of Gd-DTPA-BSA-liposomes and Gd-PAP-liposomes.
Diameter of Gd-DTPA-BSA-liposomes was 171.2 nm (PDI 0.23) and of Gd-PAP-liposomes was 175.1 nm (PDI 0.22).

It was shown that r_1 relaxivity of Gd-PAP-liposomes is significantly higher that r_1 relaxivity of Gd-DTPA-BSA-liposomes. Based on Figure 5.4 it was determined that the r_1 relaxivity of Gd-PAP-liposomes is approximately 20 $mM^{-1}s^{-1}$ over a Larmour frequency range of 0.01-10 MHz and approximately 37 $mM^{-1}s^{-1}$ at the most common clincal magnetic field (of 60 MHz). The relaxivity of Gd-DTPA-BSA-liposomes was found to be approximately 15 $mM^{-1}s^{-1}$ over a Larmour frequency range of 0.01-10 [MHz] and approximately 20 $mM^{-1}s^{-1}$] at 60 MHz. These results indicated that liposomes containing Gd-PAP are better contrast agents than liposomes containing Gd-DTPA-BSA.

5.2.4 Magnetic resonance imaging of Gd-DTPA-BSA-liposomes and Gd-PAP-liposomes

Contrast liposomes were prepared using lipid formulations of 63.25 mol% (w/v) of egg PC, 30 mol% of cholesterol, 5 mol% (w/v) PEG_{2000}-PE and 1.75 mol% (w/v) of Gd-DTPA-BSA or 1.75 mol% (w/v) of Gd-PAP (Tables 5.5 and 5.6). The lipid film was hydrated in 1 mL of 0.1 M PBS, pH 7.3, and the liposomes were extruded through a 100 nm polycarbonate membrane. The average size of prepared contrast liposomes was determined using PCS to be 150 nm (PDI 0.23) for Gd-DTPA-BSA-liposomes and 118 nm (PDI 0.10) for Gd-PAP-liposomes.

Table 5.5 Lipid formulation used to prepare contrast liposomes (1.75 mol% (w/v) Gd-DTPA-BSA).

Compound	Molecular weight [g]	Weight taken [mg]	Moles	Molar ratio of lipid to other lipids
Egg PC	790.12	60.00	$7.79*10^{-5}$	63.25 mol% (1)
Cholesterol	386.65	14.20	$3.66*10^{-5}$	30 mol% (0.47)
PEG_{2000}-PE	2,805.50	17.50	$6.23*10^{-6}$	5 mol% (0.08)
Gd-DTPA-BSA	1,068.60	2.33	$2.18*10^{-6}$	1.75 mol% (0.03)
TOTAL		94.03		

Table 5.6 Lipids used for contrast liposomes (1.75 mol% (w/v) Gd-PAP) preparation.

Compound	Molecular weight [g]	Weight taken [mg]	Moles	Molar ratio of lipid to other lipids
Egg PC	790.12	60.00	$7.79*10^{-5}$	63.25 mol% (1)
Cholesterol	386.65	14.20	$3.66*10^{-5}$	30 mol% (0.47)
PEG_{2000}-PE	2,805.50	17.50	$6.23*10^{-6}$	5 mol% (0.08)
Gd-PAP	11,370.0	24.80	$2.18*10^{-6}$	1.75 mol% (0.03)
TOTAL		116.50		

Ten µL of each preparation was resuspended in 2 mL distilled water and magnetic resonance imaging was carried out in a 1.5 T of electromagnetic field scanner (Gyroscan Intera; Philips, Netherlands) at Cappagh Hospital, Dublin, Ireland (Figure 5.5).

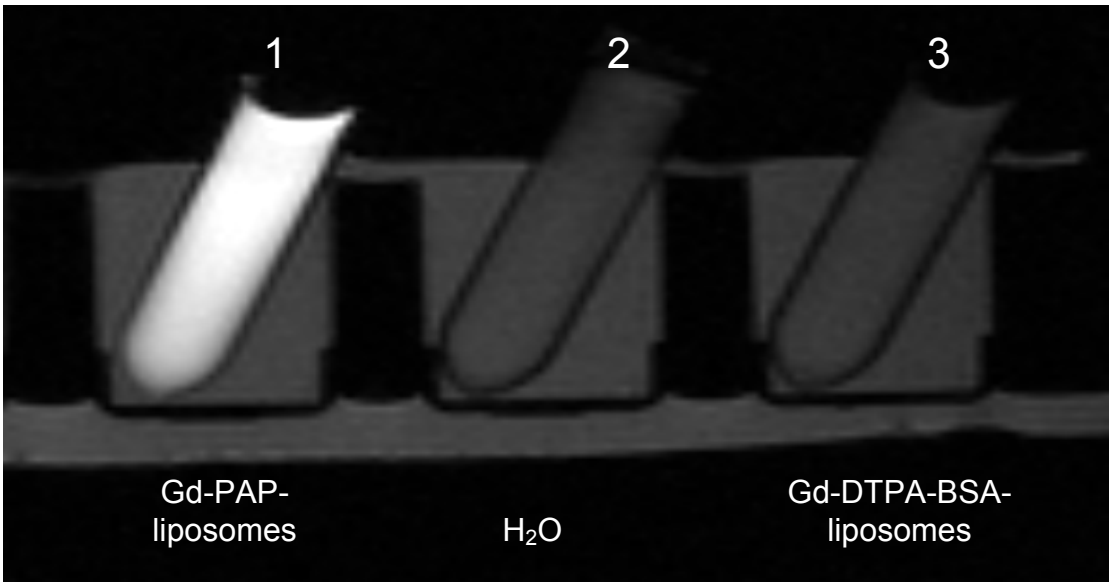

Figure 5.5 T_1-weighted images of contrast liposomes (containing 1.75 mol% (w/v) Gd-DTPA-BSA or Gd-PAP phospholipid) using Magnetic resonance imaging (MRI) in a 1.5T electromagnetic field.

As can be seen in Figure 5.5 Gd-PAP-containing liposomes are significantly brighter compared to Gd-DTPA-BSA-liposomes on the MRI scan. Gd-DTPA-BSA-liposomes showed a similar MR image to water protons indicating that these liposomes do not contain a sufficient amount of Gd ions to give a measurable signal on T_1-weighted images. In contrast, Gd-PAP-liposomes contain a sufficient amount of Gd in order to give a measurable signal in a MRI instrument used for patient analysis indicating that Gd-PAP-liposomes are sensitive enough for potential use in real clinical samples.

5.2.5 Stability studies of contrast liposomes

Contrast liposomes containing 1.75 mol% Gd-DTPA-BSA and Gd-PAP were prepared as described in section 2.2.7 (Table 5.1 and 5.2). Size measurements were performed over 14 days using PCS for Gd-DTPA-BSA-liposomes and over 19 days for Gd-PAP-liposomes using PCS (Figure 5.6).

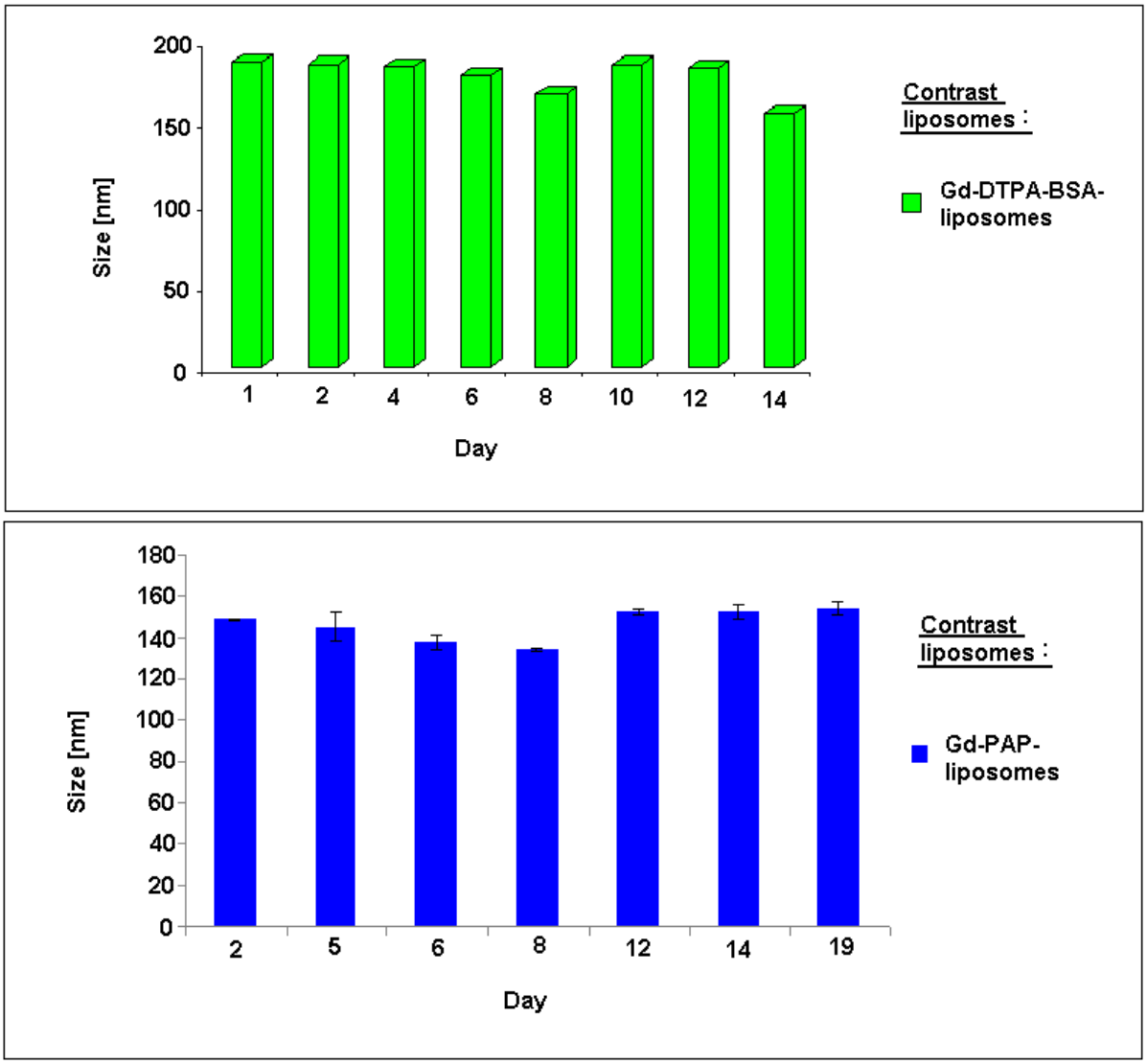

Figure 5.6 Size distribution of Gd-DTPA-BSA-liposomes and of Gd-PAP-liposomes.
It was found that contrast liposomes containing 1.75 mol% (w/v) Gd-DTPA-B-BSA or Gd-PAP were stable over 14 days and 19 days, respectively.

The diameter of contrast Gd-DTPA-BSA-liposomes was 187 nm on day 1 and did not significantly change over the 14 days of the study. For Gd-PAP-liposomes the diameter was 149 nm on day 2 after preparation and did not change over 19 days.

The charge of prepared contrast Gd-DTPA-BSA-liposomes was also measured by PCS. It was estimated that zeta potential of prepared contrast liposomes was -40.15 mV and was stable over 12 days indicating that Gd-DTPA-BSA-loaded liposomes are stable (Figure 5.7).

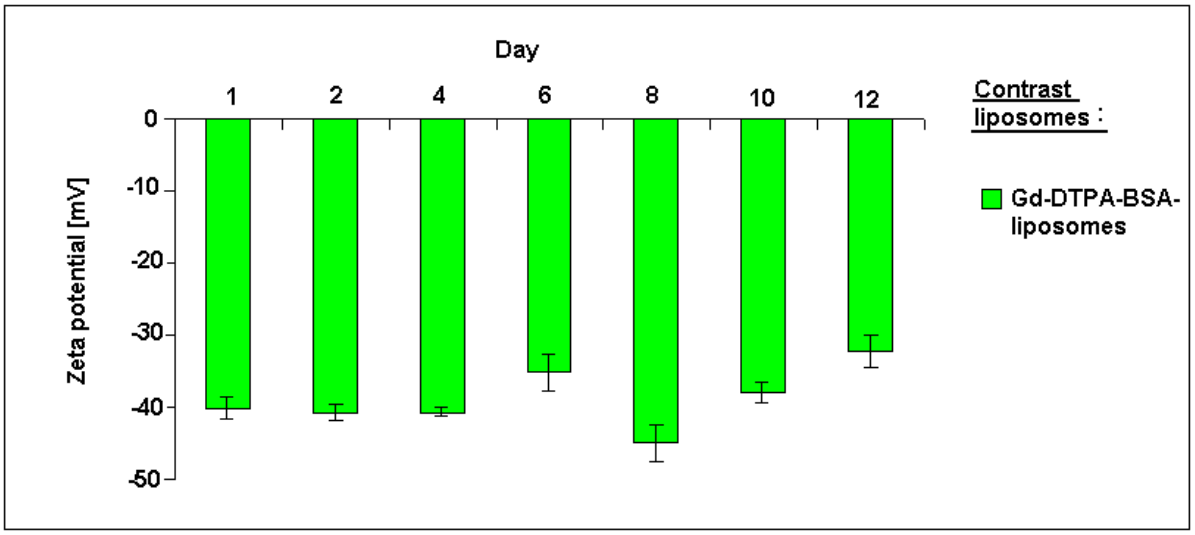

Figure 5.7 Zeta potential of contrast liposomes containing 1.75 mol% (w/v) Gd-DTPA-BSA.
The charge of contrast liposomes was stable over 12 days. The zeta potential of Gd-DTPA-BSA-liposomes was approximately –40 mV with variations in the 5-7 mV range. The results are the mean ± the standard deviation and the experiments were performed in triplicate. There was no significant difference between the values over the time frame of the experiment.

Based on size and zeta potential, no aggregation of contrast liposomes was observed.

5.2.6 *In vitro* studies of targeted contrast anti-CD138-conjugated-liposomes

Contrast anti-CD138-conjugated-liposomes (containing 1.75 mol% Gd-DTPA-BSA or 1.75 mol% Gd-PAP phospholipid) were prepared, using 63.25 mol% (w/v) of egg PC, 30 mol% of cholesterol, 5 mol% (w/v) PEG_{2000}-PE and 1.75 mol% (w/v) of Gd-DTPA-BSA or 1.75 mol% (w/v) of Gd-PAP (Tables 5.7 and 5.8).

Table 5.7 Formulation for generation of fluorescently-labelled anti-CD138 contrast Gd-DTPA-BSA-liposomes.

Compound	Molecular weight [g]	Weight used [mg]	Moles	Molar ratio of lipid to other lipids
Egg PC	790.123	1.33	$1.68*10^{-6}$	62.75 mol% (1)
Cholesterol	386.65	0.31	$8.10*10^{-7}$	30 mol% (0.48)
DSPE-PEG-Metoxy	2,805.54	0.23	$8.10*10^{-8}$	3 mol% (0.048)
FITC-PE	1,136.41	0.015	$1.30*10^{-8}$	0.5 mol% (0.008)
Gd-DTPA-BSA	1,068.6	0.05	$4.70*10^{-8}$	1.75 mol% (0.03)
DSPE-PEG-COOH	2,847.78	0.15	$5.40*10^{-8}$	2 mol% (0.032)
TOTAL		2.09		

Table 5.8 Formulation for generation of fluorescently-labelled anti-CD138 contrast Gd-PAP-liposomes.

Compound	Molecular weight [g]	Weight used [mg]	Moles	Molar ratio of lipid to other lipids
Egg PC	790.123	1.33	$1.68*10^{-6}$	62.75 mol% (1)
Cholesterol	386.65	0.31	$8.10*10^{-7}$	30 mol% (0.48)
DSPE-PEG-Metoxy	2,805.54	1.14	$8.10*10^{-8}$	3 mol% (0.048)
FITC-PE	1,136.41	0.015	$1.30*10^{-8}$	0.5 mol% (0.008)
Gd-PAP	11,370.0	0.53	$4.70*10^{-8}$	1.75 mol% (0.03)
DSPE-PEG-COOH	2,847.78	0.15	$5.40*10^{-8}$	2 mol% (0.032)
TOTAL		2.57		

Blank liposomes were also prepared as a negative control.

Anti-CD138 contrast liposomes (0.5 mg/mL) were incubated with human multiple myeloma cancer cells (U266; RPMI8226*)* and L428 Hodgkin's disease-derived cancer cell line for 1.5 hours at 37°C *in vitro*. FACS analyses of contrast liposomes were carried out as described in section 2.2.5 and the results are shown in Figures 5.8 and 5.9.

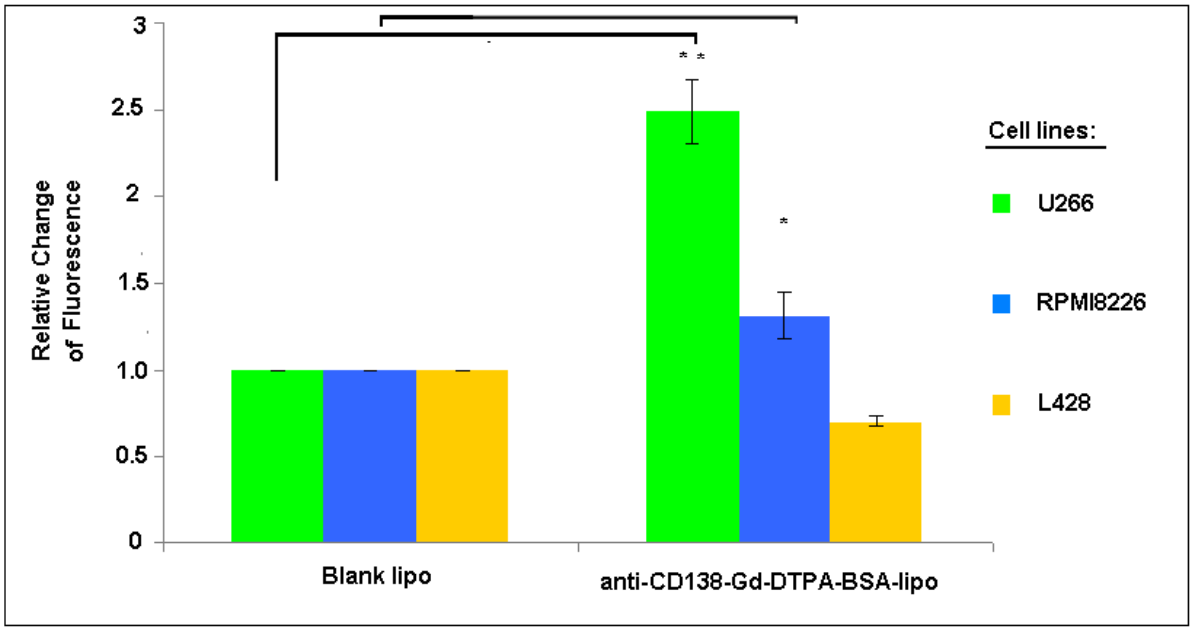

Figure 5.8 *In vitro* studies of contrast anti-CD138-conjugated-Gd-DTPA-BSA-loaded liposomes.
Blank liposomes (plain liposomes, Blank lipo); liposomes without antibody attached) were incubated with multiple myeloma cells lines (U266; RPMI8226) and a Hodgkin's disease-derived cancer cell line (L428). Previously, it was estimated that U266 expresses CD138 protein at 84.3%. The L428 cell line does not express CD138. Anti-CD138-conjugated-Gd-DTPA-BSA-loaded liposomes (anti-CD138-Gd-PAP-lipo) used for this binding experiment were prepared using the co-incubation method. The results are the mean ± the standard deviation and the experiment was performed in triplicate.
* Significantly different from control (Blank-liposomes) (Student's *t*-test, $0.01<p<0.05$)
** Significantly different from control (Blank-liposomes) (Student's *t*-test, $0.001<p<0.01$)

Contrast anti-CD138-conjugated-Gd-DTPA-BSA-liposomes bound significantly to human multiple myeloma cell lines (U266; RPMI8226) in comparison to plain liposomes. Figure 5.8 indicates that they did not bind to L428, the Hodgkin's disease-derived cancer cell line.

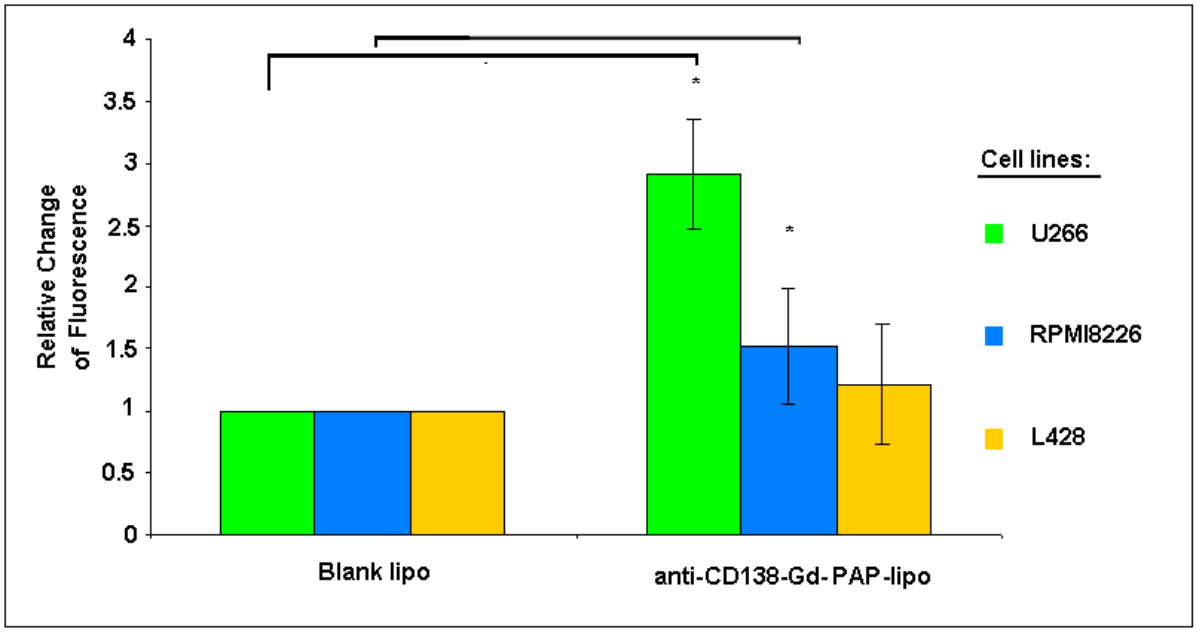

Figure 5.9 *In vitro* studies on contrast anti-CD138-conjugated-Gd-PAP-loaded liposomes.
Blank liposomes (plain liposomes, Blank lipo); liposomes without antibody attached) were incubated with multiple myeloma cells lines (U266; RPMI8226) and Hodgkin's disease derived cancer cell line (L428). Previously, it was estimated that U266 expresses CD138 protein at 84.3%. L428 Hodgkin's disease derived cancer cell line is a negative cell line for CD138 protein. Anti-CD138-conjugated-Gd-PAP-loaded liposomes (Anti-CD138-Gd-PAP-lipo) used for this binding experiment were prepared using the co-incubation method. The results are the mean ± the standard deviation and the experiment was performed in triplicate.
* Significantly different from control (Blank-liposomes) (Student's *t*-test, $0.01<p<0.05$)

Similar to results shown in Figure 5.8 the contrast anti-CD138-conjugated-Gd-PAP-liposomes bound significantly to human multiple myeloma cell lines (U266; RPMI8226) when compared to plain liposomes but did not bind to L428 Hodgkin's disease-derived cancer cell line (Figure 5.9). Anti-CD138-conjugated-Gd-DTPA-BSA-loaded and anti-CD138-conjugated-Gd-PAP-loaded-liposomes bound approximately 2.5 fold and 3 fold, respectively, more strongly to U266 human multiple myeloma cells than did plain liposomes.

A significant difference was not observed in the binding of anti-CD138-conjugated-Gd-DTPA-BSA and anti-CD138-conjugated-Gd-PAP-liposomes to the U266 human multiple myeloma cell line based on FACS analysis (Figure 5.8 and Figure 5.9).

5.2.7 Magnetic resonance imaging of anti-CD138-conjugated-Gd-DTPA-BSA-liposomes and anti-CD138-conjugated-Gd-PAP-liposomes

Contrast anti-CD138-conjugated-liposomes (containing 1.75 mol% Gd-DTPA-BSA or 1.75 mol% Gd-PAP phospholipid) were prepared in 1 mL 0.1 M PBS, pH 7.3, (Tables 5.9 and 5.10). Anti-CD138-conjugated-liposomes were prepared by the co-incubation method and extruded trough a 100 nm polycarbonate membrane.

Table 5.9 Formulation for generation of contrast anti-CD138-conjugated-Gd-DTPA-BSA-liposomes.

Compound	Molecular weight [g]	Weight used [mg]	Moles	Molar ratio of lipid to other lipids
Egg PC	790.123	10	$1.68*10^{-6}$	63.75 mol% (1)
Cholesterol	386.65	2.4	$8.10*10^{-7}$	30 mol% (0.48)
DSPE-PEG-Metoxy	2,805.54	1.7	$8.10*10^{-8}$	3 mol% (0.048)
Gd-DTPA-BSA	1,068.6	0.39	$4.70*10^{-8}$	1.75 mol% (0.03)
DSPE-PEG-COOH	2,847.78	1.2	$5.40*10^{-8}$	2 mol% (0.032)
TOTAL		15.69		

Table 5.10 Formulation for generation of fluorescently-labelled anti-CD138 contrast Gd-PAP-liposomes.

Compound	Molecular weight [g]	Weight used [mg]	Moles	Molar ratio of lipid to other lipids
Egg PC	790.123	10	$1.68*10^{-6}$	62.75 mol% (1)
Cholesterol	386.65	2.4	$8.10*10^{-7}$	30 mol% (0.48)
DSPE-PEG-Metoxy	2,847.78	1.7	$8.10*10^{-8}$	3 mol% (0.048)
Gd-PAP	11,370.0	4.1	$4.70*10^{-8}$	1.75 mol% (0.03)
DSPE-PEG-COOH	2,847.78	1.2	$5.40*10^{-8}$	2 mol% (0.032)
TOTAL		19.4		

The size of prepared contrast immunoliposomes was 151.1 nm (PDI 0.098) for anti-CD138-conjugated-Gd-DTPA-BSA-liposomes and 112.5 nm (PDI 0.251) for anti-CD138-conjugated-Gd-PAP-liposomes. 50 µL of each immunoliposome preparation was diluted in 1.8 mL of distilled water and analyzed using MRI, at 1.5 T.

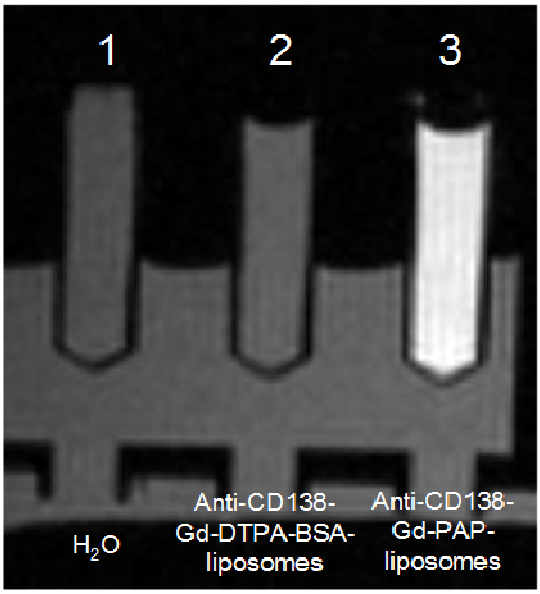

Figure 5.10 T_1-weighted images of contrast anti-CD138-conjugated-liposomes (containing 1.75 % (w/v) Gd-DTPA-BSA or Gd-PAP phospholipid) using Magnetic resonance imaging (MRI).
Imaging was performed in an electromagnetic field of 1.5 T.

Figure 5.10 indicates that anti-CD138-conjugated-Gd-PAP-containing liposomes are brighter compared to anti-CD138-conjugated-Gd-DTPA-BSA-liposomes on MRI scanning. Anti-CD138-conjugated-Gd-DTPA-BSA-liposomes showed a similar MR image to water protons. Anti-CD138-conjugated-Gd-PAP-liposomes contain sufficient quantities of Gd to give measurable signals in a clinical MRI system. Anti-CD138-conjugated-Gd-DTPA-BSA-liposomes do not contain sufficient Gd ions to give a measurable signal on T_1-weighted images. Magnetic resonance scans visualized that anti-CD138-conjugated-liposomes containing Gd-PAP are better contrast agents than anti-CD138-conjugated-liposomes containing Gd-DTPA-BSA phospholipid. This indicates that anti-CD138-conjugated-Gd-PAP-liposomes are sensitive enough for potential use in real clinical samples.

5.2.8 Magnetic resonance imaging of anti-CD138-conjugated-Gd-DTPA-BSA-liposomes and anti-CD138-conjugated-Gd-PAP-liposomes – *in vitro* studies

Contrast anti-CD138-conjugated-liposomes (containing 1.75 mol% Gd-DTPA-BSA or 1.75 mol% Gd-PAP phospholipid) were prepared, using 63.25 mol% (w/v) of egg PC, 30 mol% of cholesterol, 5 mol% (w/v) PEG_{2000}-PE and 1.75 mol% (w/v) of Gd-DTPA-BSA or 1.75 mol% (w/v) of Gd-PAP (Tables 5.8 and 5.9).

In vitro studies of contrast anti-CD138-conjugated-liposomes with human multiple myeloma cancer cell lines were carried out in order to examine immunoliposome binding ability. Contrast immunoliposomes (containing 1 mg/mL lipids) were incubated with cancer cell lines for 1 hour in 'serum-free' medium at 37°C. Cells were subsequently washed three times at 3,000 g for 5 min with 0.1 M PBS, pH 7.3 using Z 233 MK-2 centrifuge, and finally resuspended in 0.5 mL 0.1 M PBS, pH 7.3. Interaction of contrast anti-CD138-liposomes was visualized using MR imaging at 1.5 T (Figure 5.11).

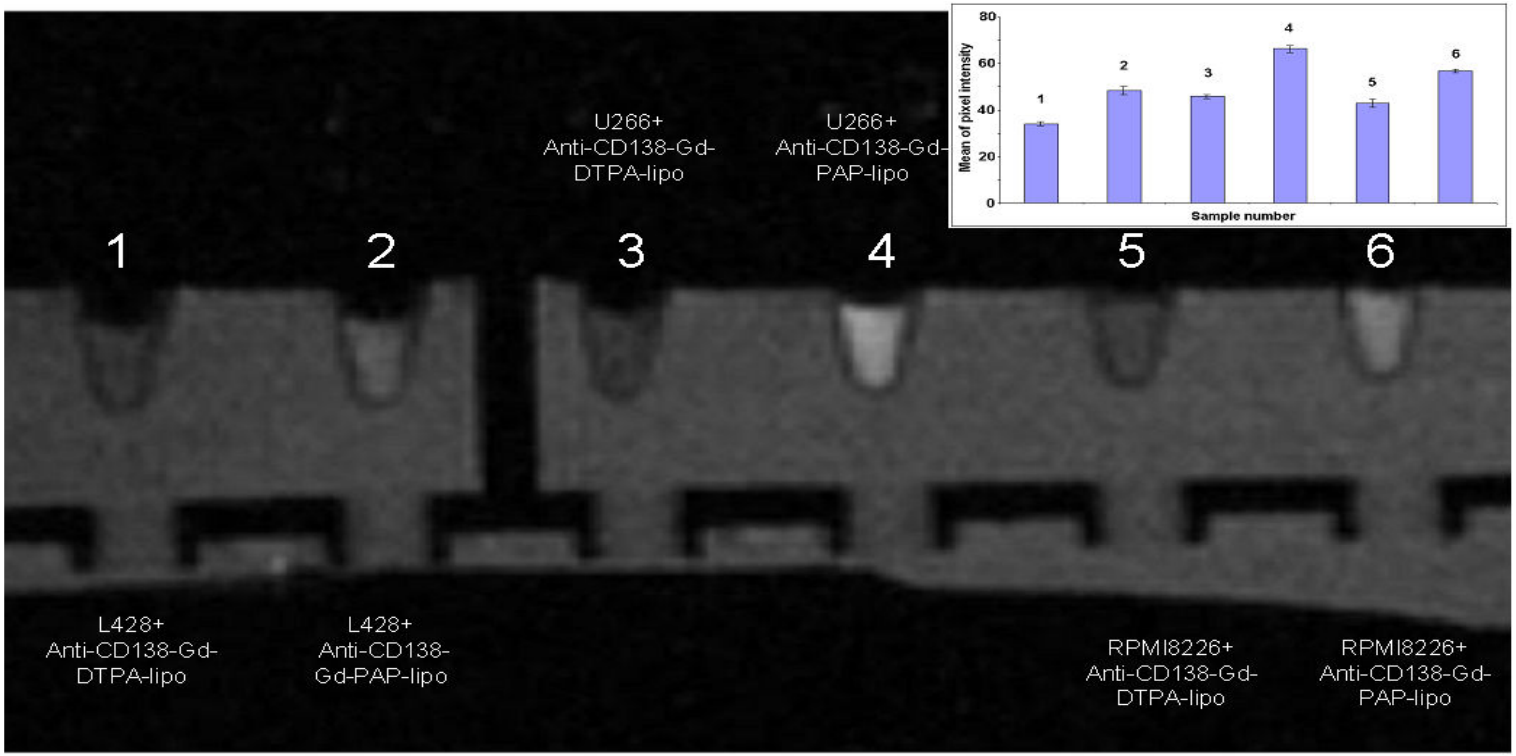

Figure 5.11 T_1-weighted image studies of contrast anti-CD138-liposomes (containing 1.75 % (w/v) Gd-DTPA-BSA or Gd-PAP phospholipid) using magnetic resonance imaging (MRI) *in vitro.*
Lane 1: L428 Hodgkin's disease-derived cells incubated with anti-CD138-Gd-DTPA-BSA-liposomes (mean pixel intensity of 34, as shown in insert); Lane 2: L428 Hodgkin's disease-derived incubated with anti-CD138-Gd-PAP-liposomes (mean pixel intensity of 48, as shown in insert); Lane 3: U266 human multiple myeloma cell line incubated with anti-CD138-Gd-DTPA-BSA-liposomes (mean pixel intensity of 45, as shown in insert); Lane 4: U266 human multiple myeloma cell line incubated with anti-CD138-Gd-PAP-liposomes (mean pixel intensity of 66, as shown in insert); Lane 5: RPMI8226 human multiple myeloma cell line incubated with anti-CD138-Gd-DTPA-BSA-liposomes (mean pixel intensity of 42, as shown in insert); Lane 6: RPMI8226 human multiple myeloma cell line incubated with anti-CD138-Gd-PAP-liposomes (mean pixel intensity of 57, as shown in insert).

These scans (Figure 5.11) indicated that contrast anti-CD138-conjugated-liposomes containing Gd-PAP gave stronger contrasts than anti-CD138-conjugated-liposomes containing Gd-DTPA-BSA. Anti-CD138-conjugated-Gd-PAP-liposomes bound more strongly to the U266 human multiple myeloma cancer cell line than to the L428 Hodgkin's disease-derived cell line. Anti-CD138-conjugated-Gd-DTPA-BSA-liposomes do not contain sufficient Gd ions to give a measurable signal on T_1-weighted images. Magnetic resonance scan indicated that anti-CD138-conjugated-liposomes containing Gd-PAP are better contrast agents than anti-CD138-conjugated-liposomes containing Gd-DTPA-BSA phospholipids. This implies that anti-CD138-conjugated-Gd-PAP-liposomes are sufficiently sensitive for potential use in real clinical samples.

Discussion

Currently, magnetic resonance imaging (MRI) is an established minimally non-invasive clinical imaging modality which is capable of producing three-dimensional images of tissues containing water with a high spacial resolution. The main drawback of MRI is very low sentitivity which can be overcome by contrast agent usage. Paramagnetic agents directly affect water protons in their close vicinity and are highly dependent on local water flux. Hence, the influence of these agents is very local and they should ideally be in contact with water with adequate exchange rates. Such contrast agents shorten the T_1 relaxation time and thus increase longitudinal and transverse relaxation rates (R_1 and R_2) (Aime *et al.,* 2002).

In this study, contrast liposomes were prepared using Gd-loaded-DTPA-PLL-NGPE (PAP) and Gd-loaded-DTPA-BSA. Due to the presence of a larger number of Gd ions (one Gd ion per DTPA-BSA to 11 Gd ions per PAP), Gd-loaded-PAP-liposomes showed increased relaxation rates when compared to Gd-DTPA-BSA-liposomes. These results are in agreement with studies carried out by Erdogan *et al.* (2006). They demonstrated that liposomes loaded with Gd *via* membrane-incorporated polychelating amphiphilic polymer (PAP) significantly increased the Gd content and relaxation rate R_1 of PEGylated liposomes.

T_1 relaxation times were measured using a 5 MHz RADX NMR Analyzer. It was shown that liposomes containing Gd-PAP showed a higher relaxivity value (3.19 [$mM^{-1}s^{-1}$]) compared to liposomes containing Gd-DTPA-BSA phospholipid (0.49 [$mM^{-1}s^{-1}$]). The r_1 relaxivity value in this experiment was calculated based on the premise that the PAP molecule chelates 11 ions of gadolinium. Subsequently, more detailed NMR studies were performed, and the gadolinium concentration in the liposomes was determijned using Inductively Coupled Plasma – Atomic Emission

Spectroscopy (ICP-AES). Based on this approach, the r_1 relaxivity of Gd-PAP-liposomes was found to be 37 $mM^{-1}s^{-1}$ compared to 20 $mM^{-1}s^{-1}$ for Gd-DTPA-BSA-liposomes, at 60 MHz. Hence, liposomes containing Gd-PAP phospholipid are better contrast agent than liposomes containing Gd-DTPA-BSA, per Gd ion, an effect that is amplified if the relaxivity per lipid is considered. It is likely that the values fro the second study is more reliable as the Gd concentration was determined directly.

Stability tests on contrast liposomes (containing Gd-DTPA-BSA) found that they are stable in solution for 14 days while liposomes containing Gd-PAP are stable for 19 days.

In a related study Weissig *et al.* (2000) reported that 1.75 mol% (w/v) is an optimal Gd-PAP molar fraction for preparing contrast liposomes. Further increases in Gd-PAP did not increase the molecular relaxivity. They explained that a higher polychelate concentration brings molecules of amphiphilic polychelators close to each other thus decreasing the degree of exposure of Gd atoms to water.

The interaction of contrast anti-CD138-conjugated-liposomes with human multiple myeloma cells was visualized on a T_1-weighted image by MRI. Kamaly *et al.* (2008) also performed T_1-weighted images of Gd-loaded-DOTA-DSA-liposomes and HeLa cells after liposome internalization. They observed successful Gd-labelling which was indicated by reduction of T_1 values, relative to controls.

In conclusion, the results reported in this chapter show that polychelating amphiphilic polymer (PAP) is capable of chelating many gadolinium ions per molecule which increase the relaxation rate (R_1) of surrounding water protons. This phenomenom was first shown by Torchilin's group (Weissig *et al.*, 2000), and can potentially strongly increase the sensitivity of human multiple myeloma images obtained in humans. The findings described in this chapter will hopefully contribute

to the preparation of *novel* minimally non-invasive contrast agents for the diagnosis of this malignancy.

Chapter 6

Cloning and Production of a Recombinant CD138 (Syndecan-1) Fragment

6.1 Introduction

The main aim of this project was to prepare minimally non-invasive diagnostic test for human multiple myeloma (MM). Multiple myeloma is characterised by uncontrolled proliferation of malignant plasma cells within the marrow. Normal bone marrow consists of no more than 4% of plasma cells, whereas in unhealthy bone marrow there can be more than 10% plasma cells.

Wijdenes *et al.* (2002) identified CD138 (syndecan-1) as a marker for multiple myeloma cancer cells, due to its expression in the majority of malignant plasma cells in bone marrow. However, in healthy bone marrow, syndecan-1 is only expressed on precursor B lymphocytes and is lost before maturation (Sanderson *et al.*, 1989). Terminally differentiated plasma cells express relatively few surface antigens and do not express very common B cell markers, such as CD19 and CD20. Multiple myeloma can appear during plasma cell maturation, when CD38 and CD138 are not lost and are expressed at high levels (Rawstron *et al.*, 2006).

Ridley *et al.* (1993) suggested that CD138 plays a major role in plasma cell adhesion to bone marrow stroma, especially to collagen type I. It is a glycoprotein expressed on simple epithelia (150-250 kDa), stratified epithelia (80-150 kDa), mesenchymal cells (220-300 kDa) and lymphocytes (80-150 kDa). The size of the CD138 protein depends on the glycosaminoglycan pattern of the molecule. In particular, the smallest isoform, with an avarage molecular size of about 92 kDa, has been described on stratified keratinocytes (Sanderson and Bernfield, 1988; Bernfield, 1993). The protein is composed of three domains (Figure 6.1), the extracellular domain - ectodomain (251 residues), transmembrane domain (25 residues) and intracellular domain (34 residues). The transmembrane domain and part of the extracellular domain contain hydrophobic sequences. The expected

molecular weight of monomeric syndecan-1 is 35 kDa (non-glycosylated form of syndecan-1; core protein). Additionally, a high molecular weight form of the protein may often be seen, and may be the mature form of syndecan-1 with all of its glycosaminoglycan (GAG), heparan and chondroitan sulfate additions.

The extracellular domain contains five putative glycosaminoglycan (GAG) attachment sites. A glycosaminoglycan is a mucopolysaccharide, which is a long unbranched polysaccharide consisting of a repeating disaccharide unit (hexose or hexuronic acid and hexosamine). The protein bears heparan sulfate and sometimes chondroitan sulfates residues. Heparan sulfate is a linear polysaccharide, which interacts with a number of ligands like growth factors, components of the extracellular matrix, cell-cell adhesion molecules, protease inhibitors, lipid binding proteins, blood-coagulation factors and pathogens (Bernfield *et al.*, 1992; Carey *et al.*, 1997). It was shown that the extracellular domain of CD138 protein diverged rapidly when comparing CD138 sequences of different species. There are some constant regions of the extracellular sites, e.g. the position of the potential GAG attachment and cleavage sites. The transmebrane and intracellular domains are conserved (Bernfield *et al.* 1992).

There are different clones of anti-CD138 antibodies recognising human syndecan-1 e.g. mouse B-B2, B-B4, MI15, 1D4, 104-9 and DL-101. Gattei *et al.* (1998) investigated the reactivity of anti-CD138 monoclonal antibodies with either intact native proteoglycans or a recombinant non-glycosylated form of syndecan-1 (core protein). They reported the capability of a number of anti-CD138 monoclonal antibodies to recognize the human syndecan-1 molecule by way of epitopes localized at the core protein level. They identified that B-B4, 1D4 and MI15 recognize the same or closely related epitopes within the ectodomain of syndecan-1

core protein. Dore *et al.* (1998) identified different epitopes recognized by B-B2 monoclonal antibodies (Figure 6.1).

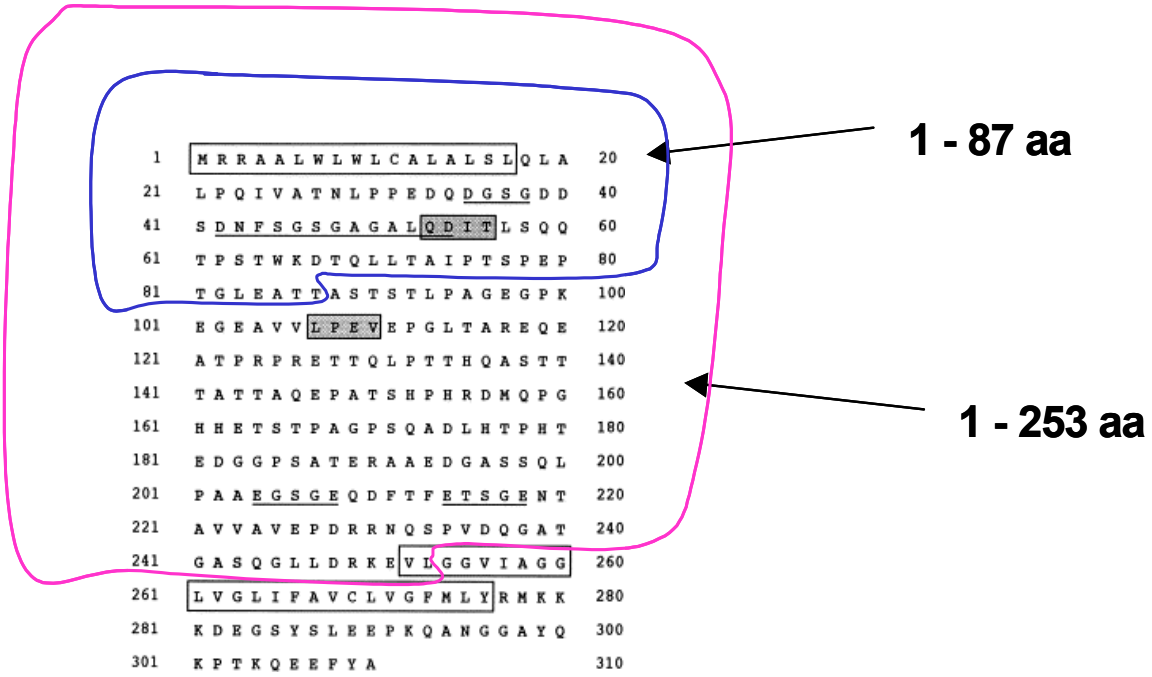

Figure 6.1 Epitopes on the syndecan-1 amino acid sequence (Adapted from Dore *et al.*, 1998).
Hydrophobic sequences of the extracellular part of syndecan-1 and transmembrane region are boxed in white. Glycosaminoglycan sites are underlined and B-B2 and B-B4 antibody epitopes are boxed in grey.

This chapter descibes the production of a recombinant CD138 protein fragment composed of 1-87 or 1-253 amino acids, because human CD138 antigen is not available commercially (Figure 6.2). A 253 aa (1-253 aa) CD138 protein fragment was produced because the extracellular part of the protein contains two different epitopes recognized either by B-B2 or B-B4 monoclonal antibodies. It was decided to work with the MI15 clone of monoclonal anti-CD138 antibodies because it is able to recognize native and recombinant forms of syndecan-1. The MI15 monoclonal anti-CD138 antibody recognizes the same or closely related epitope to the B-B4 antibody and does not recognize the B-B2 epitope located on the 1-87 aa protein fragment. This antibody was, therefore, used to detect the expression of the

recombinant CD138 protein fragment. An eighty seven (1-87 aa) CD138 protein fragment was also produced as a negative control for MI15 monoclonal antibodies. Expression of a recombinant CD138 protein will enable large-scale production of the antigen which can then be used for immunisation to generate polyclonal, monoclonal or recombinant antibodies. Moreover, CD138 antigen can be used to evaluate the specific binding ability of anti-CD138-conjugated-liposomes to the CD138 antigen.

6.2 Results

6.2.1 Cloning and expression of the CD138 gene fragment in pQE60 vector

The pQE60 vector allows high level protein expression with a His-tag located on the C-terminus. The primers were designed, as described in section 6.2.1.1, so that they contain a restriction site for *Nco*I and *Bam*HI enzymes for cloning into pQE60 vector.

6.2.1.1 Optimisation and amplification of CD138 fragments using cDNA as a template

mRNA isolated from RPMI8226 cells, as described in section 2.2.10.1.1, was used to obtain cDNA by reverse transcription (section 2.2.10.1.2). Briefly, 211 ng RNA was isolated from RPMI8226 human multiple myeloma cancer cells using Trizol reagent and chloroform. Then total RNA was reverse transcriped to cDNA. RNA was combined with oligo(dt) primers and dNTPs. They were co-incubated for 5 min at 65ºC and then on ice for 1 min. Oligo(dt) primers consist of short strands (12-18 bases) of thymine deoxynucleotides that hybridize to the mRNA poly A tail and prime reverse transcription. Then, reverse-transcription buffer, $MgCl_2$, DTT, RNaseOut inhibitor and Superscript III reverse-transcriptase were added to the previously prepared mixture. Reverse-transcription was performed for 50 min at 50ºC and

terminated at 85ºC for 5 min and 63 ng of cDNA was used as a template for amplification of CD138 gene fragments (261 bp and 759 bp gene fragments) using:

Sense primer with ***Nco*I** restriction site

5' TAT CCA TGG AT AGG CGC GCG GCG CTC TG 3'

Anti-sense primer 1 (1-261 bp) with ***Bam*HI** restriction site

5' GAT GGA TCC AGC TGT AGC CTC CAG GCC GGT 3'

Anti-sense primer 2 (1-759 bp) with ***Bam*HI** restriction site

5' GAT GGA TCC CAG CAC CTC TTT CCT GTC CA 3'

The CD138 gene fragment was amplified, as described in section 2.2.10.1.3, using sense primer and anti-sense primer 1 for amplification of 261 bp gene fragment (87 aa) and sense primer and anti-sense primer 2 for amplification of the 759 bp (253 aa) fragment.

Optimization of CD138 gene fragment amplification was carried out. Different temperatures (58ºC and 59ºC) for the PCR annealing step were tested.

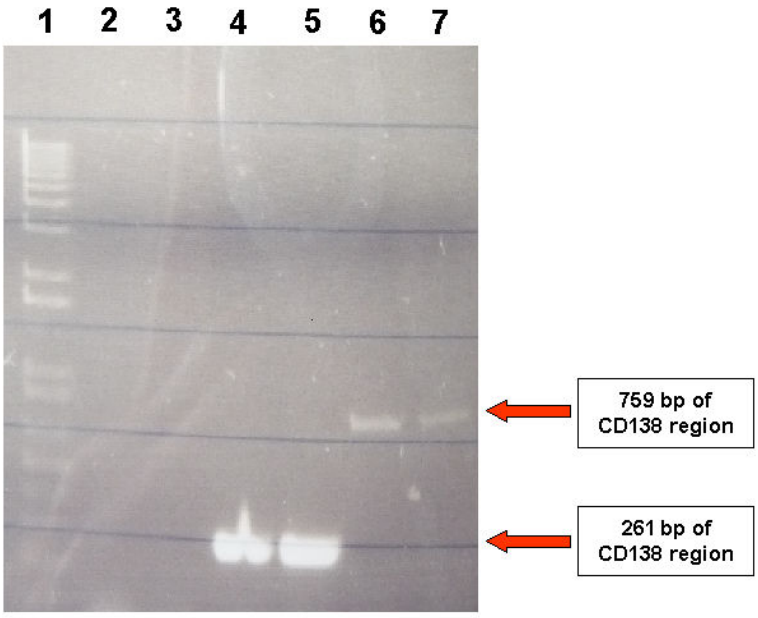

Figure 6.2 Optimization of CD138 protein fragment amplification by PCR.
Lane 1 contains a 1 kB marker for determination of gene sizes; Lanes 2 and 3 are negative controls (without DNA); Lane 2 contains primers for 1-261 bp gene amplification; Lane 3 contains primers for 1-759 bp gene amplification; Lanes 4 and 5 consist of amplified 1-261 bp (consistent with a 87 aa protein) CD138 gene fragment; Lanes 6 and 7 consist of amplified 1-759 bp CD138 gene fragments. Both gene fragment amplifications were performed at 95ºC / 30 s for DNA denaturation, 58ºC / 30 s for annealing and 72ºC / 45 s for elongation.

It was observed that 95ºC / 30 s for DNA denaturation, 58ºC / 30 s for annealing and 72ºC / 45 s for elongation were optimal for 1-261 bp of the CD138 gene amplification. These conditions were not optimal for amplification of 1-759 bp of the CD138 gene fragment, due to the small amount of final product observed in lane 6 and 7 (Figure 6.2).

Different temperatures were tested for 1-759 bp of CD138 gene amplification.

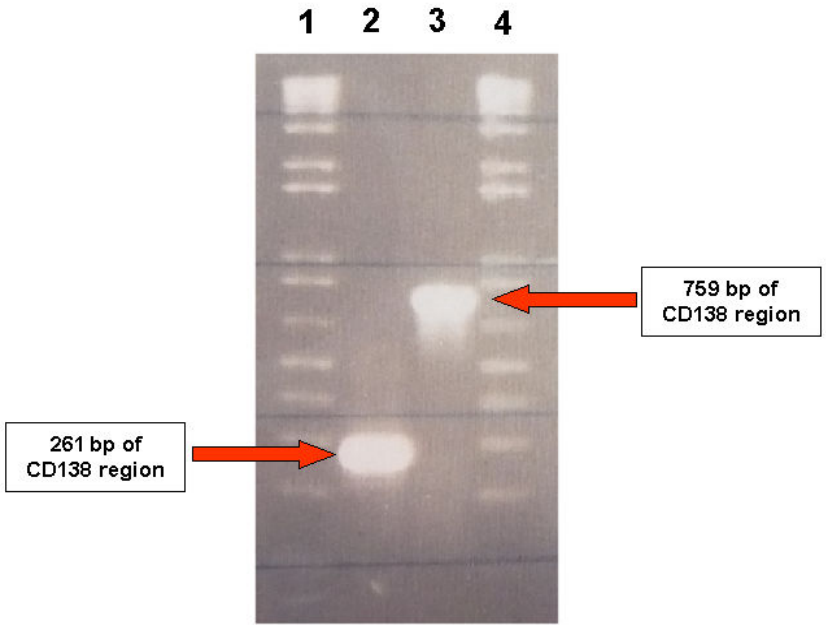

Figure 6.3 Optimization of CD138 protein fragment amplification using cDNA as a template.
Lanes 1 and 4 contain a 1 kB marker for determination of gene sizes; Lane 2 contains an amplified 1-261 bp CD138 gene fragment (consistent with a 87 aa derivative of CD138); Lane 3 contains an amplified 1-759 bp (consistent with a 253 aa protein) CD138 gene fragment. The CD138 gene fragment (1-261 bp) was amplified at 95ºC / 30 s for DNA denaturation, 58ºC / 30 s for annealing and 72ºC / 45 s for elongation and the CD138 gene fragment (1-759 bp) was amplified at 95ºC / 30 s for DNA denaturation, 59ºC / 30 s for annealing and 72ºC / 45 s for elongation.

Finally, it was determined that 59ºC / 30 s for annealing and then 72ºC / 45 s for elongation for the 1-759 bp gene fragment was effective. This cycle was repeated 30 times.

PCR products were run on a 1% (w/v) agarose gel (Figure 6.3) and both products yielded bands of the correct size. After the optimization step, CD138 gene fragments were amplified on a large-scale, as shown in Figure 6.4.

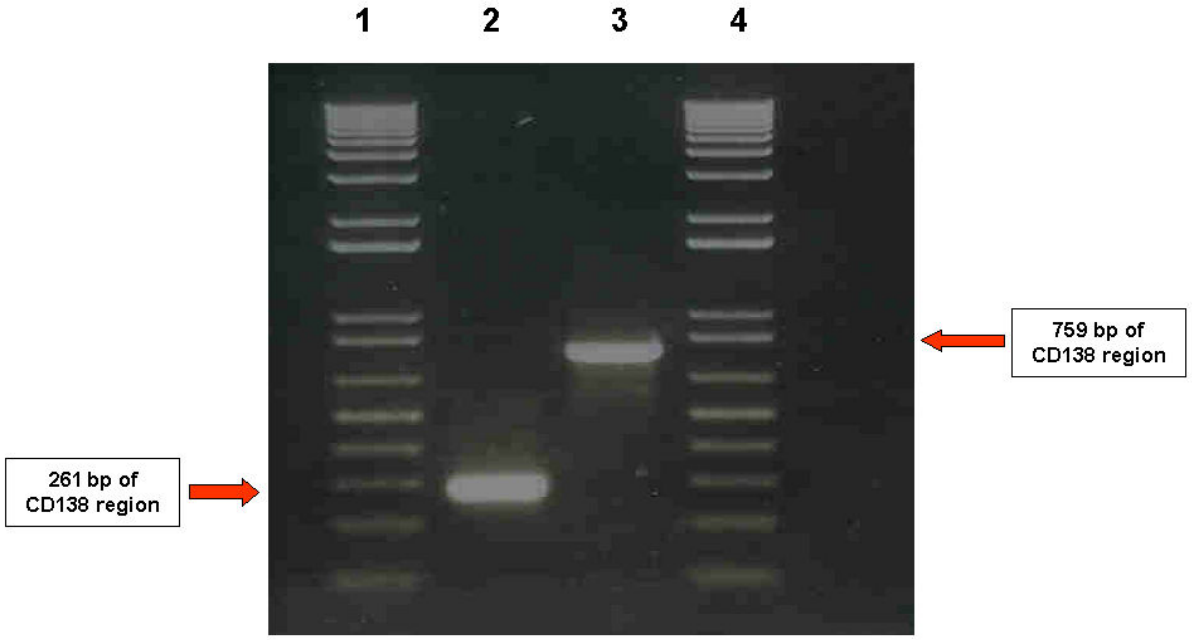

Figure 6.4 Amplification of CD138 (syndecan-1) gene fragments using cDNA as a template.
Lanes 1 and 4 contain a 1 kB marker for determination of gene sizes; Lane 2 consists of a PCR product with 1-261 bp (consistent with a 87 aa protein fragment) and Lane 3 consists of a PCR product with a 1-759 bp gene fragment (consistent with a 253 aa protein fragment).

6.2.1.2 CD138 gene fragment cloning process

The CD138 gene fragment was digested using *Nco*I and *Bam*HI and cloned into predigested pQE60 using T4 DNA ligase, as described in sections 2.2.10.1.5 and 2.2.10.1.6. Ligation was performed at room temperature and the final ligated product was ethanol-precipitated before use in transformation. pQE60 vectors, containing the insert, were transformed into XL10-Gold or Rosetta™ bacterial cells. XL10-Gold cells were used because of their ability to transform large DNA molecules with high efficiency. They are deficient in all known restriction systems thus keeping the insert stable and improving the quality of miniprep DNA isolation. Rosetta™ *E.coli* was used for CD138 protein fragment expression as this strain enhances the expression of eukaryotic proteins because it contains the pRARE plasmid with rare codons.

6.2.1.3 Analysis of CD138 cloning process by colony pick PCR or plasmid amplification

Colony pick PCR was performed on 7 clones to verify the presence or absence of the CD138 gene fragment in the pQE60 vector in XL-10 Gold *E. coli* cells. The PCR product was run on a 1% (w/v) agarose gel (Figure 6.5).

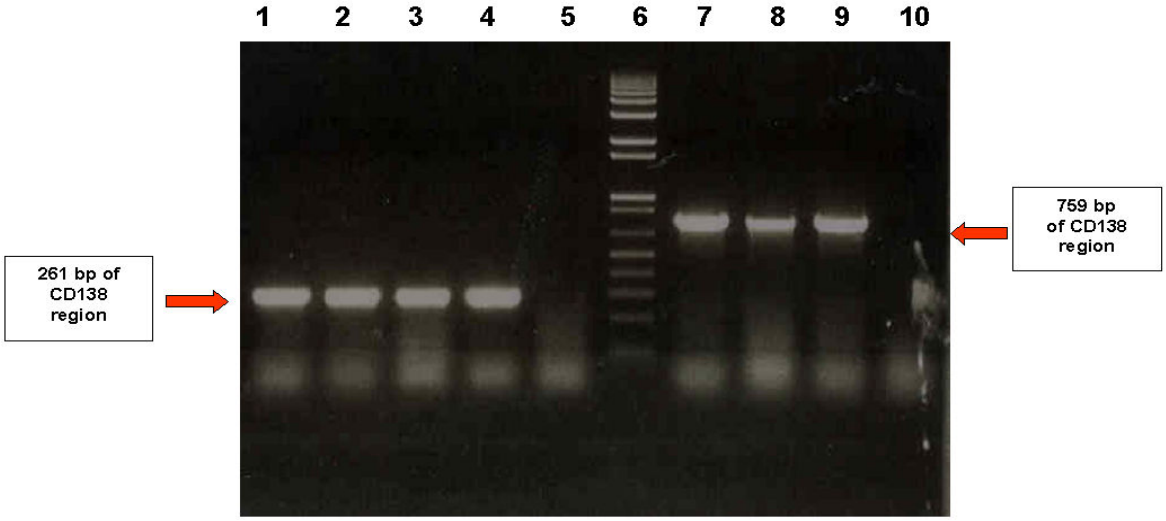

Figure 6.5 Screening of clones for CD138 gene fragment by colony pick PCR. Lanes 1-4 include different clones (1,2,3,4) of transformed *E. coli* XL10-Gold cells with the pQE60 vector / 1-261 bp gene fragment; Lane 5 contains transformed *E.coli* XL10-Gold cells with the empty pQE60 vector; Lane 6 contains 1 kB ladder for determination of gene fragment size; Lanes 7-9 contain clones (1,4,5) of transformed *E.coli* XL10-Gold cells with pQE60 vector with the 1-759 bp gene fragment; Lane 10 contains transformed *E.coli* XL10-Gold cells with an empty pQE60 vector.

It was shown that clones 1,2,3 and 4 were positive for the 1-261 bp of CD138 gene fragment and 1,4,5 were positive for the 1-759 bp CD138 gene fragment.

Plasmid DNA was isolated from ten clones of XL10-Gold transformants, containing 1-261 bp or 1-759 bp CD138 gene fragments, as detailed in section 2.2.10.1.4. 1 µg of plasmid DNA was used in PCR on these clones.

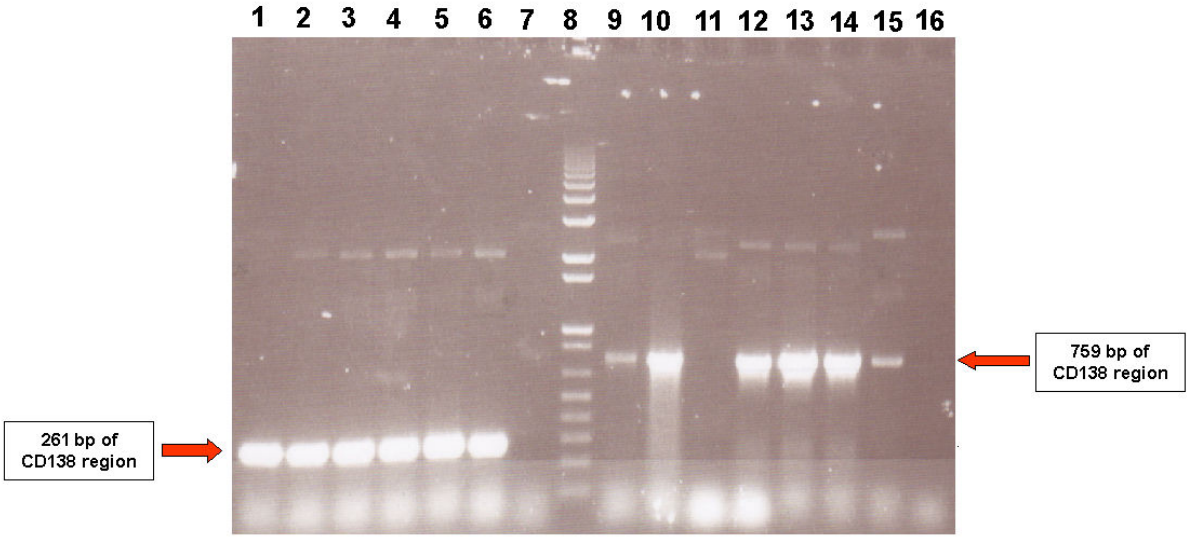

Figure 6.6 Amplification of CD138 gene fragment using pQE60 plasmid DNA as a template.
Lanes 1 and 2 are PCR products with 1-261 bp (consistent with a 87 aa derivative of CD138) CD138 gene fragment (clones 1 and 2 were isolated from the transformed *E.coli* Rosetta™ cell line); Lanes 3-6 consist of amplified 1-261 bp CD138 gene fragments (clones 1,2,3 and 4 from *E.coli* XL10-Gold cells); Lane 7 consists of a negative control (pQE60 vector without the CD138 insert); Lane 8 contains 1 kB ladder for determination of gene fragment size; Lanes 9-11 consist of a 1-759 bp (consistent with a 253 aa derivative of CD138) CD138 gene fragment (clones 1,2 and 3 were isolated from the transformed *E.coli* Rosetta™ cell line); Lanes 12-15 consist of an amplified 1-759 bp CD138 gene fragments (clones 1,2,3 and 4 isolated from *E.coli* XL10-Gold cells); Lane 16 is a negative control (pQE60 vector without CD138 insert).

It was found that clones 1,2,3 and 4 of the XL10-Gold *E.coli* cells contained the pQE60 vector with the 1-261 bp gene fragment and clones 1,2,3 and 4 of the XL10-Gold *E.coli* cells contained the 1-759 bp CD138 gene fragment.

It was also found that clones 1 and 2 of the Rosetta™ *E.coli* cells contained the pQE60 vector with the 1-261 bp CD138 gene fragment, and clones 1 and 2 of the Rosetta™ *E.coli* cells contained the pQE60 vector with the 1-759 bp gene (Figure 6.6).

Lane 15 consists of an amplified 1-759 bp CD138 gene fragment but the amount of the amplified gene is much smaller than in other samples. This is because of the differences in expression level between clones. Additional gene bands appeared

between 2,000 and 5,000 bp. The band which relates to the plasmid which was used as a template for CD138 gene fragment amplification is found at 3,431 bp.

6.2.1.4 Expression of the CD138 protein fragment in bacterial cells

Both CD138 (syndecan-1) protein fragments were expressed in *E.coli* XL10-Gold and Rosetta^{TM} cells following induction with 1 mM IPTG, as described in section 2.2.10.5. The cells were lysed and the presence of CD138 was determined by Western blotting using the monoclonal anti-human CD138 clone MI15 antibody, as detailed in section 2.2.10.7.

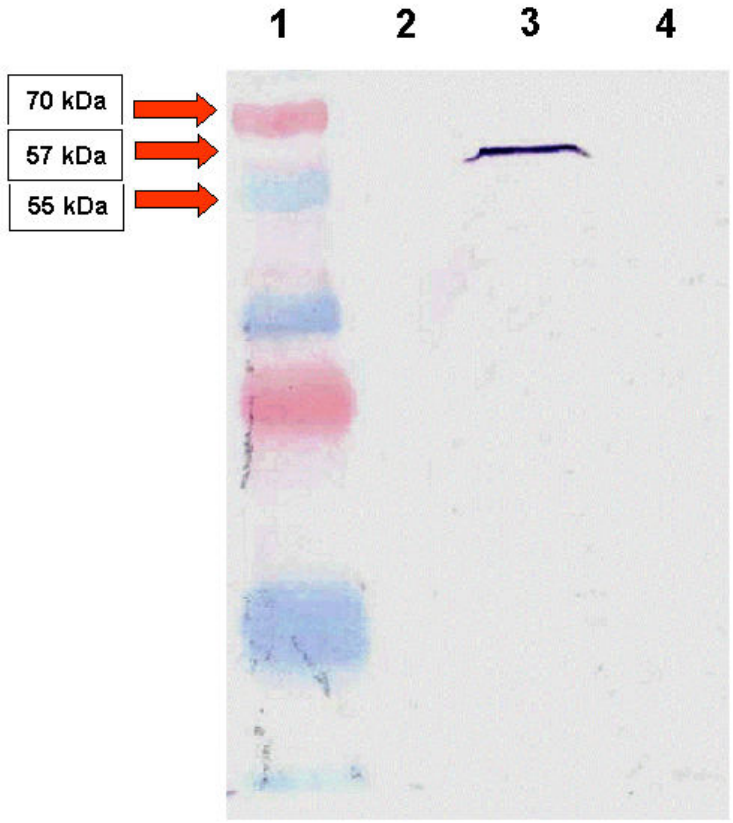

Figure 6.7 Screening for CD138 protein fragment expression by Western blotting.
The presence of CD138 protein fragment was determined by Western blotting using monoclonal anti-human CD138 primary antibodies and alkaline phosphatase conjugated goat anti-mouse IgG secondary antibody. Lane 1: PageRuler^{TM} Plus Prestained Protein Ladder for determination of protein size; Lane 2: negative control, *E.coli* Rosetta^{TM} cells without transformed plasmid; Lane 3: *E.coli* Rosetta^{TM} cells with transformed pQE60 vector with the 1-759 bp CD138 gene fragment (consistent with a 253 aa derivative of CD138) clone 1; Lane 4: *E.coli* Rosetta^{TM} cells with transformed the pQE60 vector with the 1-261 bp CD138 gene fragment (consistent with a 87 aa derivative of CD138) clone 1.

Expression of CD138 protein fragment (253 aa) was unsuccessful in *E.coli* XL10-Gold cells. However, the CD138 protein fragment was detected in the lysate after induction with 1 mM IPTG, in the *E.coli* Rosetta^{TM} cell line containing the XL10-Gold with the 1-759 bp CD138 gene fragment (Figure 6.7). The CD138 gene fragment (1-759 bp) generates a 253 aa protein and it was calculated that the molecular weight of that CD138 protein fragment is approximately 28 kDa, with theorectical pI of 4.36. The Western blot showed that CD138 protein fragment was detected using a

monoclonal anti-human CD138 antibody (clone MI15) but the molecular weight of the detected protein was ~57 kDa. It appears that the 253 aa CD138 protein fragment dimerized. For a better understanding, characterisation of the CD138 protein was performed using ExPASy program (ProtParam tool). ExPASy (Expert Protein Analysis System) is maintained by the Swiss Institute of Bioinformatics and serves as a main resource for proteomics tools and databases. This programme analyzes protein sequences, structures and two-dimensional gel electrophoresis. It was determined that the 253 aa CD138 protein fragment is unstable. Studies on instabilities indicate that when an instability index is smaller than 40 the protein is designated as stable and when value is above 40 it infers that the protein may be unstable. The instability index computed for the CD138 protein, consisting of 253 aa, was 49.76 so the protein fragment was assessed as unstable. Dimerization may transform the CD138 protein fragment from an unstable to a stable form.

After expression of the 87 aa CD138 protein, it was shown that the 87 aa CD138 protein fragment was not detected by the anti-human CD138 monoclonal antibody clone, MI15, after protein induction of Rosetta™ *E.coli* cells containing 1-261 bp gene fragment (consistent with a 87 aa), because epitope recognized by MI15 monoclonal anti-CD138 antibody is not among CD138 protein fragment composed of 1-87 aa.

6.2.1.5 Purification of 253 aa CD138 protein fragment

Expression of the CD138 protein fragment (consistent with a 253 aa derivative of CD138) in *E. coli* Rosetta™ cells, containing the pQE60 vector with an insert, was induced using 1 mM IPTG. The CD138 protein fragment was purified using affinity chromatography (Ni^{+}-NTA), as described in section 2.2.10.8. The CD138 protein fragment contained a His-tag on the C-terminus, which enabled the protein to bind

to the nickel resin. The His-tag fused to the CD138 recombinant protein has a high affinity for nickel ions which are immobilized on sepharose beads. Sodium acetate (pH 4.4) was used to elute His-tagged proteins from the column.

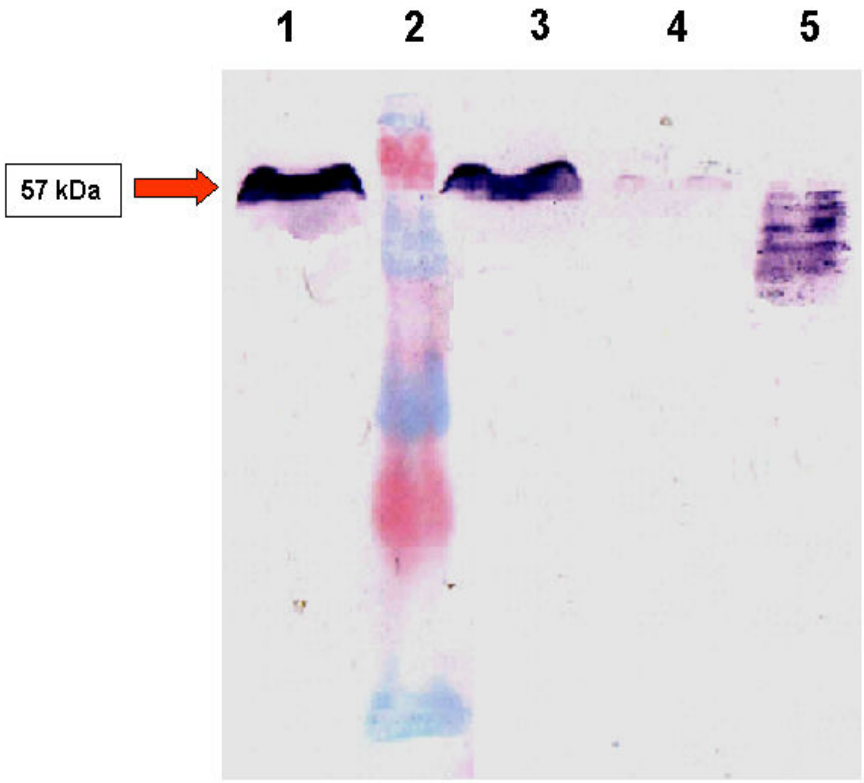

Figure 6.8 Western blotting of the 253 aa CD138 protein fragment.
Purification of expressed CD138 protein fragment in RosettaTM
Lane 1: Lysate - CD138 protein fragment not purified; Lane 2: PageRuler^{TM}Plus Prestained Protein Ladder for determination of protein fragment size; Lane 3: 'flow-through' 1; Lane 4: 'flow-through' 2; Lane 5: eluted 253 aa CD138 protein fragment.

The majority of the CD138 protein fragment was found in the 'flow-through', which means that protein did not bind to the resin. Some of the CD138 protein fragment bound to the nickel resin and was eluted, but several bands were formed on Western blotting with the MI15 monoclonal anti-CD138 antibody (Figure 6.8). This may be due to proteolytic breakdown. Purification of the CD138 protein fragment was performed using 0.1 M PBS, pH 7.4 / 0.5 M NaCl / 20 mM imidazole / 8mM urea, in the sonication and running buffers. NaCl was used to eliminate any protein-

protein interactions and to avoid any ion exchange effects. Urea was used to maintain denaturating conditions for His-tagged proteins to enable protein linearization. Sodium acetate at low pH was used for the elution step. Some of CD138 protein fragment was found in the elution fraction but the majority of the protein was found in the 'flow-through' which means that the protein was not binding to the Ni^{+-}NTA resin. Therefore, purification procedure of CD138 protein fragment was unsuccessful using the conditions described above.

6.2.2 Cloning of CD138 gene fragment in pQETriSystem

The pQE60 vector can only be used in prokaryotic cells and protein expression in prokaryotic cells does not allow for any post-translational modification (e.g. glycosylation). Production of the native, glycosylated form of CD138 protein is very important as it is the best form to use for immunization and, subsequently, for antibody generation. This enables comparison with the non-glycosylated form of CD138. Eukaryotic expression systems give post-translational modification of proteins and would enable comparison of anti-CD138 antibody binding characteristics to non-glycosylated and glycosylated forms of the CD138 protein.

The pQETriSystem vector enables protein expression in insect or mammalian cells and can be use to obtain post-translational modifications.

The pQETriSystem II vector also has a C-terminal His-tag sequence for ease of purification. To perform the cloning into the pQETriSystem II vector, primers were designed so that the sense primer contains a restriction site for *SacI* and anti-sense for *Hind III* enzyme.

Sense primer with ***Sac*I** restriction site extra bases

5' - TAT GAG CTC ATG AGG CGC GCG GCG CTC TG – 3'

Anti-sense primer (1-759 bp) with ***Hind*III** restriction site

5' - GAT AAG CTT CAG CAC CTC TTT CCT GTC CA – 3'

Gene fragment amplification was carried out, as described in section 2.2.10.1.3. Briefly, the PCR conditions used were 95ºC / 30 s for DNA denaturation, 59ºC / 30 s for annealing and 72ºC / 45 s for elongation for the 1-759 bp CD138 gene fragment. This cycle was repeated 30 times.

The CD138 gene fragment was cloned into a *Sac*I *Hind*III digested pQETriSystem II vector and transformed into XL10-Gold *E.coli* cells.

6.2.2.1 Analysis of CD138 cloning process by colony pick PCR and enzymatic digestion

The CD138 gene fragment was cloned into pQETriSystem II vector and transformed into *E. coli* XL10-Gold cells. Colony pick PCR was carried out on 7 clones to assess the success of the cloning process. The PCR product was run on a 1% (w/v) agarose gel (Figure 6.9).

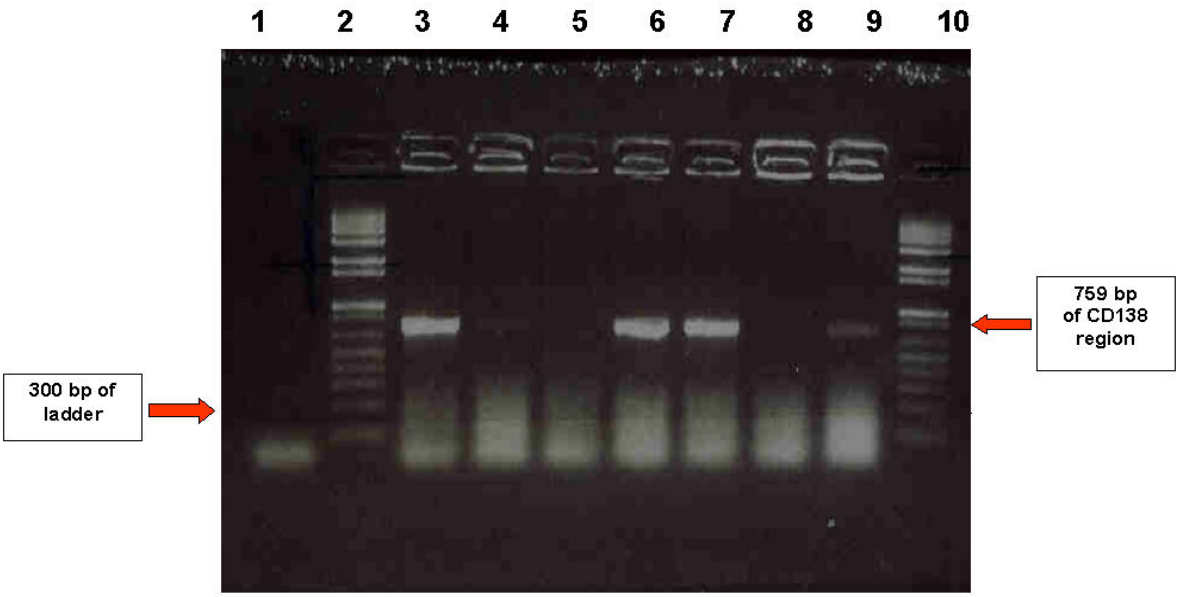

Figure 6.9 Screening of clones for the CD138 gene fragment by colony pick PCR.
Lane 1 contains a negative contol (PCR without cells); Lanes 2 and 10 contain 1 kB ladder for determination of gene fragment size; Lanes 3-9 contain clones (1,2,3,4,5,6 and 7) of transformed *E. coli* XL10-Gold cells with the pQETriSystem II with the1-759 bp CD138 gene fragment.

It was shown that clones 1,4 and 5 of pQETriSystem II vector / 759 bp were positive for the 1-759 bp gene fragment (Figure 6.9).

Restriction analysis of the pQETriSystem II vector was performed, as a second confirmation of the cloning process. Briefly, plasmid DNA was isolated from 4 clones of XL10-Gold transformants, containing the 1-759 bp CD138 gene fragment, as described in section 2.2.10.1.4. The plasmid was digested using *Sac*I and *Hind*III enzymes for 1.5 h at 37°C to confirm presence or absence of the CD138 fragment (Figure 6.10).

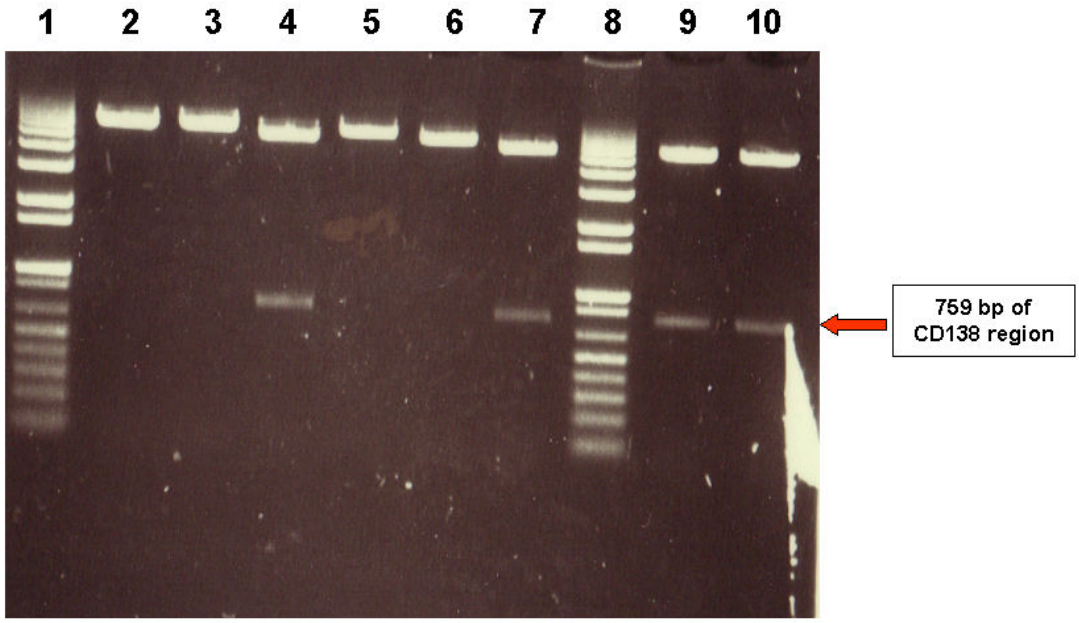

Figure 6.10 Restriction analyses of pQETriSystem II vector containing an inserted 1-759 bp CD138 gene fragment.
Lanes 1 and 8 contain 1 kB ladder for determination of gene fragment size; Lanes 2-4 contain digested the pQETriSystem II vector with the 1-759 bp CD138 gene fragment clone 1; Lane 2 contains the pQETriSystem II vector with the 1-759 bp CD138 gene fragment clone 1 digested with *Sac*I only; Lane 3 contains the pQETriSystem II vector with the 1-759 bp CD138 gene fragment - digested with *Hind*III only; Lane 4 contains the pQETriSystem II vector with the 1-759 bp CD138 gene fragment digested with both *Sac*I and *Hind*III enzymes; Lanes 5-7 include the pQETriSystem II with the 1-759 bp CD138 gene fragment clone 2 digested as before using both *Sac*I and *Hind*III enzymes; Lane 9 contains the pQETriSystem II with the 1-759 bp CD138 gene fragment clone 4 digested with both enzymes; Lane 10 contains the pQETriSystem II with the 1-759 bp CD138 gene fragment clone 5 digested with both enzymes.

It was found that clones 1,2,4 and 5 of XL10-Gold cells contain the pQETriSystem II vector with the insert composed of the 759 bp gene fragment of CD138.

Thus, the CD138 gene fragment, composed of 1-759 bp, was successfully cloned into pQETriSystem II vector and this vector can be now used for transfection into mammalian cells for the expression of the glycosylated form of CD138.

Discussion

The main aim of the research, described in this chapter, was to produce the CD138 (syndecan-1) protein fragment in a recombinant form as the protein is not available commercially. Large-scale production of the CD138 protein fragment would enable immunization which could lead to the generation of polyclonal, monoclonal or recombinant antibodies. Production of both the non-glycosylated and glycosylated forms of the CD138 protein would enable comparisons between anti-CD138 antibodies generated to both forms and would be useful for targeting multiple myeloma.

This is the first attempt at the production of CD138 protein fragment in a prokaryotic cell system. Gattei *at al.* (1998) previously produced the glycosylated form using a ‘cell-free’ system. Their 'cell-free' system resulted in a cleaner lysate compared to the bacterial system used in this study. They produced the glycosylated form whereas the prokaryotic system only allowed protein core production with no modifications. However, protein production in a 'cell-free' system is time consuming and expensive compared to the use of prokaryotic cells, which is easy and cheap. The CD138 protein fragment could also be used for the evaluation of anti-CD138-liposome binding capacity. At the moment human multiple myeloma cancer cells are used as a target to determine the ability of these liposomes to bind CD138. CD138 protein fragment production would allow the performance of kinetic studies with anti-human CD138-liposomes using Biacore1000. Using this approach estimation of the lowest concentration for anti-CD138-conjugated-liposomes to be used for imaging can be determined.

Gattei *et al.* (1998) found that B-B4, MI15 and 104-9 anti-CD138 antibodies recognize the recombinant non-glycosylated form of the CD138 protein. The

molecular mass of the detected recombinant CD138 protein (310 aa) was 70 kDa. These clones of anti-human CD138 antibodies also recognize the glycosylated form of the CD138 protein.

The extracellular portion of the CD138 protein fragment, composed of 253 aa, is recognized by MI15 monoclonal antibody. Epitopes recognized by the MI15 monoclonal anti-CD138 antibody are between amino acids 107-110 (Dore *et al*., 1998). A second fragment of CD138 of 1-87 aa was produced as a negative control, because this fragment does not contain the epitope recognized by the monoclonal CD138 antibody, MI15.

Advances in genetic engineering have greatly facilitated the expression of mammalian proteins in prokaryotic systems such as *E.coli* (Makrides, 1996; Tolia and Joshua-Tor, 2006). Expression of CD138 protein fragment was unsuccessful in XL10-Gold *E.coli* cells, however, CD138 protein fragment was detected after induction in the Rosetta^{TM} *E.coli* strain, using Western blotting. The choice of *E.coli* strain plays an important role in expression of recombinant proteins. The Rosetta^{TM} *E.coli* strain was designed to enhance the expression of eukaryotic proteins. This strain contains the pRARE plasmid with rare codons. The Rosetta^{TM} strain possess tRNAs for AGG, AGA, AUA, CUA, CCC, GGA codons. Thus, Rosetta^{TM} strains provide for ‘universal’ translation, which might otherwise be limited by the codon usage of *E. coli*. The pRARE plasmid, in the Rosetta^{TM} stain, can co-exist with the expression plasmid. However, the highly concentrated proteases of the intracellular environment may also alter some characteristics of the final expressed product, prohibiting the expression of some bioactive proteins in *E.coli*. The Rosetta^{TM} strain does not contain the Lon protease, and another outer membrane protease, OmptT.

The absence of these two key proteases reduces degradation of proteins expressed (Sorensen and Mortensen, 2005; Ratelade *at al.*, 2009).

The calculated mass of the CD138 protein fragment, composed of 253 aa, should be around 28 kDa, but the mass observed on Western blotting was approximately 57 kDa. This is probably as a result of dimerisation. This finding is in the agreement with other researchers, who observed a 70 kDa molecular mass for the CD138 protein product (310 aa) on Western blotting while 35 kDa was the predicted mass (Bernfield *et al.*, 1992; Carey, 1997). CD138 forms SDS-resistant dimers. However, dimerization was not a problem with CD138 protein fragment production, because the relevant epitope was still recognized by the MI15 monoclonal anti-CD138 antibody.

CD138 protein fragment (253 aa) was successfully cloned into the pQE60 vector and expressed in the Rosetta^{TM} strain. Problems occurred during purification. Studies indicated that the CD138 protein fragment generates a stable dimer in a denaturating environment, but dimer formation does not prevent binding of the MI15 anti-CD138 monoclonal antibody. Purification of the CD138 protein fragment, however, still needs to be further optimized. Dimerisation of the recombinant CD138 fragments could result in the unavailability of the His-tag for binding to the Nickel resin. For IMAC purification, decreasing the pH of the running buffer, as the pI of CD138 protein fragment is 4.36, would help avoid ionic interactions between proteins. It was also observed that the protein detected was cleaved into different fragments of varying sizes, possibly due to proteases present in the lysate. This could be prevented by the use of specific protease inhibitors.

These preliminary studies showed the successful production of the non-glycosylated form of CD138 in bacterial cells. It was shown that the MI15 anti-CD138 monoclonal

antibody recognizes the form of the CD138 protein. However, further optimization of purification steps are necessary to facilitate larger yields to be obtained which are necessary for protein characterisation, kinetic studies, binding studies and immunization in multiple hosts (mouse, rabbit and chicken) for recombinant and monoclonal antibody production. Production of the CD138 protein fragment would be very useful for anti-CD138-conjugated-liposome binding studies.

Chapter 7

Conclusions and Future Work

Conclusions

The main aim of this project was to prepare contrast (gadolinium-loaded) nanoparticles which would target the CD138 (syndecan-1) transmembrane glycoprotein overexpressed on the surface of human multiple myeloma cells in bone marrow. These contrast targeted nanoparticles were designed to be used for diagnostic purposes. The main advantage of this approach would be to develop a diagnostic agent which can be used for minimally-invasive detection of cancer.

Immunoliposomes were chosen as nanoparticles for use in this project. Anti-human CD138 monoclonal antibodies were successfully conjugated to the carboxylic acid group of phospholipids. Two different methods of immunoliposome preparation (reverse phase evaporation and the co-incubation method) were optimized and used. The size and zeta potential of the immunoliposomes generated were measured. The average sizes of liposomes and of immunoliposomes which were extruded through 100 nm polycarbonate membranes, were approximately 100 nm. The number of antibodies per liposome was calculated to be 6-7 using the reverse phase evaporation method and 9 using co-incubation method. *In vitro* binding assays (FACS analyses and FLISA) were carried out to characterise the liposome binding to cancer cells. It was found that anti-CD138-conjugated-liposomes were targeting significantly more strongly to the U266 human multiple myeloma cancer cell line than control liposomes.

Part of this work was carried out in the Pharmaceutical Biotechnology and Nanomedicine Centre in Prof. Vladimir Torchilin's group at Northeastern University in Boston, USA. Polychelating amphiphilic polymer (PAP) was synthesized there and loaded with gadolinium ions. PAP can chelate several Gd ions per single amphiphilic polymer molecule thus increasing the relaxation effect resulting in

improved potential for tissue imaging. Gadolinium ions were first loaded into the PAP molecule and contrast liposomes (containing Gd-DTPA-BSA and Gd-PAP) were then prepared. Detailed NMR analysis showed that not only does the higher Gd content of Gd-PAP aid in enhancing the relaxation in water containing liposomes, but that Gd-PAP is also more effective per Gd ion than Gd-DTPA-BSA. Stability tests on contrast liposomes (containing Gd-DTPA-BSA) found that they are stable in solution for 14 days while liposomes containing Gd-PAP are stable for 19 days. T_1-weighted images of contrast liposomes showed that Gd-PAP-containing liposomes are significantly brighter compared to Gd-DTPA-BSA-liposomes on MRI scanning.

Anti-CD138-conjugated contrast liposomes were prepared and binding tested against human multiple myeloma cell lines *in vitro*. Anti-CD138-Gd-DTPA-BSA- and anti-CD138-Gd-PAP-liposomes bound approximately 2.5 fold and 3 fold more strongly, respectively, to the U266 human multiple myeloma than did control liposomes. T_1-weighted images of contrast immunoliposomes showed that anti-CD138-Gd-PAP-liposomes are significantly brighter compared to anti-CD138-Gd-DTPA-BSA-liposomes on MRI scanning. *In vitro* interactions of contrast anti-CD138-conjugated liposomes with cancer cell lines were also performed. MRI scanning of these interactions showed that anti-CD138-Gd-PAP-liposomes gave stronger contrast than anti-CD138-conjugated-liposomes containing Gd-DTPA-BSA after incubation with U266 human multiple myeloma cell line.

The findings described in this thesis will hopefully contribute to the preparation of *novel* minimally-invasive contrast agents for the diagnosis of human multiple myeloma.

Future work

An exact molecular mass assessment of gadolinium-loaded polychelating amphiphilic polymer (PAP) will be carried out using Matrix-Assisted Laser Desorption / Ionization (MALDI) mass spectrometer. It will allow accurate relaxometry analysis of contrast anti-CD138-Gd-PAP-liposomes.

Contrast anti-CD138-conjugated-liposomes (containing Gd-PAP or Gd-DTPA-BSA) will be used in *in vivo* studies in a multiple myeloma mouse model. Interactions of contrast immunoliposomes with cancer cells will be visualized using magnetic resonance (MR) scanning in Cappagh Hospital, Radiology Department. In addition, significant amounts of glycosylated and non-glycosylated forms of CD138 protein fragments will be produced which would enable animal immunization for polyclonal, monoclonal and recombinant antibody generation. The generation of better and more specific antibodies, in large quantities, would be required for the next phase of this work which will require both *in vitro* and *in vivo* imaging studies

Chapter 8

References

Adrian J.E., Kamps J.A., Scherphof G.L., Meijer D.K., van Loenen-Weemaes A.M., Reker-Smit C., Terpstra P. and Poelstra K. (2007). A novel lipid-based drug carrier targeted to the non-parenchymal cells, including hepatic stellate cells, in the fibrotic livers of bile duct ligated rats. *Biochimica et Biophysica Acta.* **1768**(6): 1430-9.

Aime S., Dastru W. and Crich S.G. (2002). Innovative magnetic resonance imaging diagnostic agents based on paramagnetic Gd(III) complexes. *Biopolymers*. **66**(6): 419-428.

Allen T.M., Brandeis E., Hansen C.B., Kao G.Y. and Zalipsky S. (1995). A new strategy for attachment of antibodies to sterically stabilized liposomes resulting in efficient targeting to cancer cells. *Biochimica et Biophysica Acta.* **1237**(2): 99-108.

Allen T.M. and Chonn A. (1987). Large unilamellar liposomes with low uptake by the reticuloendothelial system. *FEBS Letters*. **223**: 42–46.

Allport J.R. and Weissleder R. (2001). *In vivo* imaging of gene and cell therapies. *Experimental Hematology*. **29**(11): 1237-1246.

Aragnol D. and Leserman L.D. (1986). Immune clearance of liposomes inhibited by an anti-Fc receptor antibody *in vivo*. *Proceedings National Academy of Science (U S A).* **83**(8): 2699-703.

ASTM Standard D. (1985). Zeta Potential of Colloids in Water and Waste Water *American Society for Testing and Materials.* 4182-4187.

Baeten J., Haller J., Shih H. and Ntziachristos V. (2009). *In vivo* investigation of breast cancer progression by use of an internal control. *Neoplasia (New York, N.Y.)*. **11**(3): 220-227.

Bangham A.D., Standish M.M. and Watkins J.C. (1965). Diffusion of univalent ions across the lamellae of swollen phospholipids. *Molecular Biology Journal*. **13**(1): 238-252.

Bangham A.D., Hill M.W. and Miller N.G.A. (1974). Methods in Membrane Biology (Korn N.D., ed.). Plenum. N.Y., **1**:1-68.

Barenholz Y. (2003). Relevancy of drug loading to liposomal formulation therapeutic efficacy. *Liposome Research*. **13**(1): 1-8.

Bedu-Addo F.K., Tang P., Xu Y. and Huang L. Interaction of polyethyleneglycol-phospholipid conjugates with cholesterol-phosphatidylocholine mixture sterically stabilized liposome formulations. *Pharmaceutical Research.* **13**(5) : 718-24.

Beduneau A., Saulnier P., Hindre F., Clavreul A., Leroux J.C. and Benoit J.P. (2007). Design of targeted lipid nanocapsules by conjugation of whole antibody and antibody Fab' fragments. *Biomaterials.* **28**: 4978-4990.

Bernfield M., Hinkes M.T. and Gallo R.L. (1993). Developmental expression of the syndecans:possible function and regulation. *Development*, Suppl. **119**: 205-212.

Bernfield M., Kokenyesi R., Kato M., Hinkes M.T., Spring J., Gallo R.L. and Lose E.J. (1992). Biology of the syndecans: a family of transmembrane heparan sulfate proteoglycans. *Annual Review Cell Biology.* **8**: 365-393.

Bertini I., Bianchini F., Calorini L., Colagrande S., Fragai M., Franchi A., Gallo O., Gavazzi C. and Luchinat C. (2004). Persistent contrast enhancement by sterically stabilized paramagnetic liposomes in murine melanoma. *Magnetic Resonance Medicine.* **52**(3): 669-72.

Bianco A., Kostarelos K. and Prato M. (2005). Applications of carbon nanotubes in drug delivery. *Current Opinion in Chemical Biology.* **9**(6): 674-9.

Bona C.A. and Bonilla F.A. (1996). *Textbook of Immunology.* (2 ed). CRC Press. ISBN 9783718605965 p.102.

Caravan P., Ellison J.J., McMurry T.J. and Lauffer R.B. (1999). Gadolinium(III) chelates as MRI contrast agents: structure, dynamics and applications. *Chemical Reviews*. **99**(9): 2293-352.

Carey D.J. (1997). Syndecans: multifuncional cell-surface co-receptors. *Biochemical Journal.* **327**: 1-16.

Caride V.J., Sostman H.D., Winchell R.J. and Gore J.C. (1984). Relaxation enhancement using liposomes carrying paramagnetic species. *Magnetic Resonance Imaging.* **2**(2): 107-12.

Catlett-Falcone R., Landowski T. and Oshiro M.M. (1999). Constitutive activation of Stat3 signaling confers resistance to apoptosis in human U266 myeloma cells. *Immunity*. **10**(1): 105-115.

Chang D.K., Lin C.T., Wu C.H. and Wu H.C. (2009). A novel peptide enhances therapeutic efficacy of liposomal anti-cancer drugs in mice models of human lung cancer. *Public Library Science One*. **4**(1): e4171.

Corot C., Robert P., Idée J.M. and Port M. (2006). Recent advances in iron oxide nanocrystal technology for medical imaging. *Advance Drug Delivery Reviews.* **58**(14): 1471-504.

Dass C.R. and Choong P.F. (2006). Targeting of small molecule anticancer drugs to the tumour and its vasculature using cationic liposomes: lessons from gene therapy. *Cancer Cell International*. **6**: 17.

Debbage P. and Jaschke W. (2008). Molecular imaging with nanoparticles: giant roles for dwarf actors. *Histochemistry of Cell Biology.* **130**(5): 845-75.

Devoisselle J.M., Vion-Dury J., Galons J.P., Confort-Gouny S., Coustaut D., Canioni P. and Cozzone P.J. (1988). Entrapment of gadolinium-DTPA in liposomes. Characterization of vesicles by P-31 NMR spectroscopy. *Investigative Radiology.* **23**(10): 719-24.

Dore J.M., Morard F., Vita N. and Wijdenes J. (1998). Identification and location on syndecan-1 core protein of the epitopes of B-B2 and B-B4 monoclonal antibodies. *FEBS Letters*. **426**: 67-70.

Dreborg S. and Akerblom E.B. (1990). Immunotherapy with monomethoxypoly-ethylene glycol modified allergens. *Critical Reviews of Therapeutic Drug Carrier Systems.* **6**(4): 315-65.

Drummond D.C., Meyer O., Hong K., Kirpotin D.B. and Papahadjopoulos D. (1999). Optimizing liposomes for delivery of chemotherapeutic agents to solid tumors. *Pharmacological Reviews.* **51**(4): 691-743.

Drummond D.C., Noble C.O., Hayes M.E., Park J.W. and Kirpotin D.B. (2008). Pharmacokinetics and *in vivo* drug release rates in liposomal nanocarrier development. *Pharmaceutical Sciences.* **97**(11): 4696-740.

Drummond D.C., Meyer O. and Hong K. (1999). Optimizing liposomes for delivery of chemotherapeutic agents to solid tumors. *Pharmacological Reviews*. **51**(4): 691-743.

Drummond D.C., Noble C.O. and Hayes M.E. (2008). Pharmacokinetics and *in vivo* drug release rates in liposomal nanocarrier development. *Pharmaceutical Sciences*. **97**(11): 4696-4740.

Duzgunes N., Wilschut J., Hong K., Fraley R., Perry C., Friend D.S., James T.L. and Papahadjopoulos D. (1983). Physicochemical characterization of large unilamellar phospholipid vesicles prepared by reverse-phase evaporation. *Biochimica Biophysica Acta.* **732**(1): 289-299.

Endoh H., Suzuki Y. and Hashimoto Y. (1981). Antibody coating of liposomes with l-ethyl-3-(3-dimethylaminopropyl)carbodiimide and the effect on target specificity. *Immunological Methods*. **44**: 79-85.

Enoch H.G. and Strittmatter P. (1979). Formation and properties of 1000-A-diameter, single-bilayer phospholipid vesicles. *Biochemistry*. **76**(1): 145-149.

Erdogan S., Medarova Z.O., Roby A., Moore A. and Torchilin V.P. (2008). Enhanced tumor MR imaging with gadolinium-loaded polychelating polymer-containing tumor-targeted liposomes. *Magnetic Resonance Imaging.* **27**(3): 574-80.

Erdogan S., Roby A., Sawant R., Hurley J. and Torchilin V.P. (2006). Gadolinium-loaded polychelating polymer-containing cancer cell-specific immunoliposomes. *Liposome Research.* **16**(1): 45-55.

Erdogan S., Roby A. and Torchilin V. (2006). Enhanced tumor visualization by gamma-scintigraphy with 111In-labelled polychelating-polymer-containing mmunoliposomes. *Molecular Pharmaceutics*. **3**(5): 525-30.

Fanning A.S., Ma T.Y. and Anderson J.M. (2002). Isolation and functional characterization of the actin binding region in the tight junction protein ZO-1. *FASEB Journal.* **16**(13): 1835-7.

Gabizon A. and Papahadjopoulos D. (1988). Liposome formulations with prolonged circulation time in blood and enhanced uptake by tumors. *Proceedings National Academy of Sciences (U S A).* **85**(18): 6949-53.

Gattei V., Godeas C., Degan M., Rossi F.M., Aldinucci D. and Pinto A. (1998). Characterization of anti-CD138 monoclonal antibodies as tools for investigating the molecular polymorphism of syndecan-1 in human lymphoma cell. *British Journal of Hematology*. **104**: 152-162.

Glogard C., Stensrud G. and Hovland R. (2002). Liposomes as carriers of amphiphilic gadolinium chelates: the effect of membrane composition on incorporation efficacy and *in vitro* relaxivity. *International Journal of Pharmaceutics*. **233**(1-2): 131-140.

Gref R., Lück M., Quellec P., Marchand M., Dellacherie E., Harnisch S., Blunk T. and Müller R.H. (2000). 'Stealth' corona-core nanoparticles surface modified by polyethylene glycol (PEG): influences of the corona (PEG chain length and surface density) and of the core composition on phagocytic uptake and plasma protein adsorption. *Colloids Surface B Biointerfaces.* **18**(3-4): 301-313.

Greenstein S., Krett N.K., Kurosawa Y., Ma Ch., Chauhan D., Hideshima T., Anderson K.C. and Rosen S.T. (2003). Characterisation of MM.1 human multiple myeloma (MM) cell lines: A model system to elucidate the characteristics, behavior, and signaling of steroid-sensitive and -resistant MM cells. *Experimental Hematology*. **31**: 271-282.

Gupta H. and Weissleder R. (1996). Targeted contrast agents in MR imaging. *Magnetic Resonance Imaging Clinics of North America*. **4**(1): 171-184.

Hak S., Sanders H.M., Agrawal P., Langereis S., Grüll H., Keizer H.M., Arena F., Terreno E., Strijkers G.J. and Nicolay K. (2009). A high relaxivity Gd(III)DOTA-DSPE-based liposomal contrast agent for magnetic resonance imaging. *European Journal of Pharmaceutics and Biopharmaceutics.* **72**(2): 397-404.

Heinrich P.C., Behrmann I., Muller-Newen G., Schaper F. and Graeve L. (1998). Interleukin-6-type cytokine signalling through the gp130/Jak/STAT pathway *Biochemical Journal*. **334**(2): 297-314.

Hosokawa S., Tagawa T., Niki H., Nohga K. and Nagaike K. (2003). Efficacy of immunoliposomes on cancer models in a cell-surface-antigen-density-dependent manner. *British Journal of Cancer*. **89**: 1545-1551.

Harashima H., Sakata K., Funato K. and Kiwada H. (1994). Enhanced hepatic uptake of liposomes through complement activation depending on the size of liposomes. *Pharmaceutical Research*. **11**(3): 402-406.

Harding J.A., Engbers C.M., Newman M.S., Goldstein N.I. and Zalipsky S. (1997). Immunogenicity and pharmacokinetic attributes of poly(ethylene glycol)-grafted immunoliposomes. *Biochimica et Biophysica Acta.* **1327**(2): 181-92.

Heitzmann H. and Richards F.M. (1974). Use of the avidin-biotin complex for specific staining of biological membranes in electron microscopy. *Proceeding National Academy of Science U.S.A.* **71**: 3537.

Hilgenbrink A.R. and Low P.S. (2005). Folate receptor-mediated drug targeting: from therapeutics to diagnostics. *Pharmaceutical Sciences*. **94**(10): 2135-2146.

Huang S.K., Mayhew E. and Gilani S. (1992). Pharmacokinetics and therapeutics of sterically stabilized liposomes in mice bearing C-26 colon carcinoma. *Cancer Research*. **52**(24): 6774-6781.

Hueber M.M., Staubli A.B., Kustedjo K., Gray M.H.B., Shih J., Fraser S.E., Jacobs R.E. and Meade T.J. (1998). Fluorescently detectable magnetic resonance imaging agents. *Bioconjugate Chemistry*. **2**: 242-249.

Hutchinson F.J., Francis S.E., Lyle I.G. and Jones M.N. (1989). The characterisation of liposomes with covalently attached proteins. *Biochimica et Biophysica Acta.* **978(**1): 17-24.

Iakoubov L., Rokhlin O. and Torchilin V. (1995). Anti-nuclear autoantibodies of the aged reactive against the surface of tumor but not normal cells. *Immunology Letters*. **47**: 147-149.

Ishida O., Maruyama K. and Tanahashi H. (2001). Liposomes bearing polyethyleneglycol - coupled transferrin with intracellular targeting property to the solid tumors *in vivo. Pharmaceutical Research*. **18**(7): 1042-1048.

Kabalka G.W., Davis M.A., Moss T.H., Buonocore E., Hubner K., Holmberg E., Maruyama K. and Huang L. (1991). Gadolinium-labelled liposomes containing various amphiphilic Gd-DTPA derivatives: targeted MRI contrast enhancement agents for the liver. *Magnetic Resonance Medicine.* **19**(2): 406-15.

Kabalka G., Buonocore E. and Hubner K. (1987). Gadolinium-labelled liposomes: targeted MR contrast agents for the liver and spleen. *Radiology*. **163**(1): 255-258.

Kairemo K., Erba P., Bergstrom K. and Pauwels E.K.J. (2008). Nanoparticles in cancer. *Radiopharmaceuticals.* **1**: 30-36.

Kamaly N., Kalber T., Ahmad A., Oliver M.H., So P.W., Herlihy A.H., Bell J.D., Jorgensen M.R. and Miller A.D. (2008). Bimodal paramagnetic and fluorescent liposomes for cellular and tumor magnetic resonace imaging. *Bioconjugate Chemistry*. **19**: 118-129.

Kaszuba M., McKnight D., Connah M.T., McNeil-Watson F.K. and Nobbmann U. (2008). Measuring sub nanometre sizes using dynamic light scattering. *Nanoparticles Research*. **10**: 823-829.

Kim S., Jacobs R.E. and White S.H. (1985). Preparation of multilamellar vesicles of defined size-distribution by solvent-spherule evaporation. *Biochimica et Biophysica Acta.* **812**(3): 793-801.

Kishimoto T., Akira S. and Taga T. (1995). Interleukin-6 family of cytokines and gp130. *Blood*. **86**(4): 1243-1254.

Klibanov A., Maruyama K., Torchilin V. and Huang L. (1990). Amphipatic polyethyleneglycols effectively prolong the circulation time of liposomes. *FEBS Letters.* **268**: 235-237.

Kobayashi H., Sato N., Kawamoto S., Saga T., Hiraga A., Haque T.L. Ishimori T., Konishi J., Togashi K. and Brechbiel M.W. (2001). Comparison of the macromolecular MR contrast agents with ethylenediamine-core versus ammonia-core generation-6 polyamidoamine dendrimer. *Bioconjugate Chemistry.* **12**: 100-107.

Kute T., Lack C.M., Willingham M., Bishwokama B., Williams H., Barrett K., Mitchell T. and Vaughn J.P. (1994). Development of Herceptin resistance in breast cancer cells. *Cytometry.* **57**(2): 86-93.

Kyle R.A. and Rajkumar S.V. (2004). Multiple myeloma. *New England Journal Medicine.* **351**: 1860-1873.

Kyle R.A., Therneau T.M., Rajkumar S.V., Offord J.R., Larson D.R., Plevak M.F. and Melton L.J. 3rd. (2002). A long-term study of prognosis in monoclonal gammopathy of undetermined significance. *New England Journal Medicine.* **346**(8): 564-569.

Kyle R.A., Remstein E.D., Therneau T.M., Dispenzieri A., Kurtin P.J., Hodnefield J.M., Larson D.R., Plevak M.F., Jelinek D.F., Fonseca R., Melton L.J. and Rajkumar S.V. (2007). Clinical course and prognosis of smoldering (asymptomatic) multiple myeloma. *New England Journal Medicine.* **356**(25): 2582- 2590.

Kyte J. and Doolittle R.F. (1982). A simple method for displaying the hydropathic character of a protein. *Journal of Molecular Biology*. **157**(1): 105-132.

Laemmli U.K. (1970). Cleavage of structural proteins during the assembly of the head of bacteriophage T4. *Nature.* **227**(5259):680-685.

Langereis S., Kooistra H.A.T., van Genderen M.H.P. and Meijer E.W. (2004). Probing the interaction of the biotin avidin complex with the relaxivity of biotinylated Gd DTPA. *Organic Biomolecular Chemistry*. **2**: 1271-1273.

Lanza G.M., Lamerichs R., Caruthers S. and Wickline S.A. (2003). Molecular Imaging in MR with targeted paramagnetic nanoparticles. **47**(1): 34.

Lanza G.M., Winter P.M. and Caruthers S.D. (2004). Magnetic resonance molecular imaging with nanoparticles. *Nuclear Cardiology.* **11**(6): 733-743.

Lapalombella R., Yu B., Triantafillou G., Liu Q., Butchar J.P., Lozanski G., Ramanunni A., Smith L.L., Blum W., Andritsos L., Wang D.S., Lehman A., Chen C.S., Johnson A.J., Marcucci G., Lee R.J., Lee L.J., Tridandapani S., Muthusamy N. and Byrd J.C. (2008). Lenalidomide down-regulates the CD20 antigen and antagonizes direct and antibody-dependent cellular cytotoxicity of rituximab on primary chronic lymphocytic leukaemia cells. *Blood.* **112**: 5180-5189.

Leclercq F., Cohen-Ohana M., Mignet N., Sbarbati A., Herscovici J., Scherman D. and Byk G. (2003). Design, synthesis, and evaluation of gadolinium cationic lipids as tools for biodistribution studies of gene delivery complexes. *Bioconjugate Chemistry.* **14**(1): 112-9.

Leclercq F., Cohen-Ohana M. and Mignet N. (2003). Design, synthesis, and evaluation of gadolinium cationic lipids as tools for biodistribution studies of gene delivery complexes. *Bioconjugate Chemistry*. **14**(1): 112-119.

Liang H.D. and Blomley M.J. (2003). The role of ultrasound in molecular imaging. *British Journal of Radiology*. **76**(2): 140-50.

Lopes de Menezes D.E., Pilarski L.M., Belch A.R. and Allen T.M. (2000). Selective targeting of immunoliposomal doxorubicin against human multiple myeloma *in vitro* and *ex vivo*. *Biochimica et Biophysica Acta*. **1466**: 205-220.

Los M., Roodhart J.M. and Voest E.E. (2007). Target practice: lessons from phase III trials with bevacizumab and vatalanib in the treatment of advanced colorectal cancer. *Oncologist.* **12**(4): 443-50.

Luque R., Brieva J.A., Moreno A., Manzanal A., Escribano L., Villarrubia J., Velasco J.L., López-Jiménez J., Cerveró C., Otero M.J., Martínez J., Bellas C. and Roldán E. (1998). Normal and clonal B lineage cells can be distinguished by their differential expression of B cell antigens and adhesion molecules in peripheral blood from multiple myeloma (MM) patients--diagnostic and clinical implications. *Clinical Experimental Immunology.* **112**(3): 410-8.

Machy P. and Leserman L.D. (1984). Elimination or rescue of cells in culture by specifically targeted liposomes containing methotrexate or formyl-tetrahydrofolate. *EMBO.* **3**(9): 1971-7.

Maeda H., Sawa T. and Konno T. (2001). Mechanism of tumor-targeted delivery of macromolecular drugs, including the EPR effect in solid tumor and clinical overview of the prototype polymeric drug SMANCS. *Controlled Release*. **74**(1-3): 47-61.

Makrides S. (1996). Strategies for achieving high-level expression of genes in *Escherichia coli*. *Microbiology and Molecular Biology Reviews*. **60**: 512-426.

Mamot C., Drummond D., Noble C.O., Kallab V., Guo Z., Hong K., Kirpotin D. and Park J. (2005). Epidermal growth factor receptor-targeted immunoliposomes

significantly enhance the efficiency of multiple anticancer drug in vivo. *Cancer Research.* **65**(24): 11631-11638.

Martin C.R. and Kohli P. (2003). The emerging field of nanotube biotechnology. *National Review of Drug Discovery.* **2**(1): 29-37.

Maruyama K., Takahashi N., Tagawa T., Nagaike K. and Iwatsuru M. (1997). Immunoliposomes bearing polyethyleneglycol-coupled Fab' fragment show prolonged circulation time and high extravasation into targeted solid tumors *in vivo*. *FEBS Letters.* **413**(1): 177-80.

Maruyama K., Takizawa T., Yuda T., Kennel S.J., Huang L. and Iwatsuru M. (1995). Targetability of novel immunoliposomes modified with amphipathic poly(ethylene glycol)s conjugated at their distal terminals to monoclonal antibodies. *Biochimica et Biophysica Acta.* **1234**(1): 74-80.

Maruyama K., Holmberg E., Kennel S.J., Klibanov A., Torchilin V.P. and Huang L. (1990). Characterization of *in vivo* immunoliposome targeting to pulmonary endothelium. *Pharmaceutical Sciences*. **79**(11): 978-84.

Matsumura Y., Gotoh M., Muro K., Yamada Y., Shirao K., Shimada Y., Okuwa M., Matsumoto S., Miyata Y., Ohkura H., Chin K., Baba S., Yamao T., Kannami A., Takamatsu Y., Ito K. and Takahashi K. (2004). Phase I and pharmacokinetic study of MCC-465, a doxorubicin (DXR) encapsulated in PEG immunoliposome, in patients with metastatic stomach cancer. *Annual Oncology.* **15**(3): 517-25.

Mayhew E., Nikolopoulos G.T., King J.J. and Siciliano A.A. (1985). A practical method for the large scale manufacture of liposomes. *Pharmaceutical Manufacturing.* **2**(8): 18-22.

Meldrum K.K., Burnett A.L. and Meng X. (2003). Liposomal delivery of heat shock protein 72 into renal tubular cells blocks nuclear factor-kappaB activation, tumor necrosis factor-alpha production, and subsequent ischemia-induced apoptosis. *Circulation Research*. **92**(3): 293-299.

Meyer O., Kirpotin D., Hong K., Sternberg B., Park J.W., Woodle M.C. and Papahadjopoulos D. (1998). Cationic liposomes coated with polyethylene glycol as carriers for oligonucleotides. *Biological Chemistry*. **273**(25): 15621–15627.

Mody V.V., Nounou M.I. and Bikram M. (2009). Novel nanomedicine-based MRI contrast agents for gynecological malignancies. *Advanced Drug Delivery Reviews*. **61**(10): 795-807.

Möschwitzer J. and Muller R.H. (2006). New method for the effective production of ultrafine drug nanocrystals. *Nanosciences Nanotechnology.* **6**(9-10): 3145-53.

Mosmann T. (1983). Rapid colorimetric assay for cellular growth and survival: Application to proliferation and cytotoxicity assays. *Immunological Methods*. **65**(1-2): 55-63.

Mulder W.J., Strijkers G.J. and Griffioen A.W. (2004). A liposomal system for contrast-enhanced magnetic resonance imaging of molecular targets. *Bioconjugate Chemistry*. **15**(4): 799-806.

Mulder W.J., Strijkers G.J., Habets J., Bleeker E.J.W., van der Schaft D.W.J., Storm G., Koning G.A., Griffioen A.W. and Nicolay K. (2005). MR molecular imaging and fluorescence microscopy for identification of activated tumor endothelium using bimodal lipidic nanoparticles. *FASEB*. **19**: 2008-2010.

Mulder W.J., Strijkers G.J., van Tilborg G.A., Griffioen A.W. and Nicolay K. (2006). Lipid-based nanoparticles for contrast-enhanced MRI and molecular imaging. *NMR Biomedicine.* **19**(1): 142-64.

Müller R.H., Mäder K. and Gohla S. (2000). Solid lipid nanoparticles (SLN) for controlled drug delivery - a review of the state of the art. *European Journal of Pharmaceutics and Biopharmaceutics.* **50**(1): 161-77.

Nasongkla N., Bey E., Ren J., Ai H., Khemtong C., Guthi J.S., Chin S.F., Sherry A.D., Boothman D.A. and Gao J. (2006). Multifunctional polymeric micelles as cancer-targeted, MRI-ultrasensitive drug delivery systems. *Nano Letters.* **6**(11): 2427-30.

Navon G., Panigel R. and Valensin G. (1986). Liposomes containing paramagnetic macromolecules as MRI contrast agents. *Magnetic Resonance Medicine.* **3**(6): 876-80.

Needham D., McIntosh T.J. and Lasic D.D. (1992). Repulsive interactions and mechanical stability of polymer-grafted lipid membranes. *Biochimica et Biophysica Acta.* **1108**(1): 40-8.

Pan H., Han L. and Chen W. (2008). Targeting to tumor necrotic regions with biotinylated antibody and streptavidin modified liposomes. *Controlled Release*. **125**(3): 228-235.

Pardeike J., Hommoss A. and Muller R.H. (2009). Lipid nanoparticles (SLN, NLC) in cosmetic and pharmaceutical dermal products. *International Journal of Pharmaceutics*. **366**(1-2): 170-184.

Park J.W., Hong K. and Kirpotin D.B. (2002). Anti-HER2 immunoliposomes: enhanced efficacy attributable to targeted delivery. *Clinical Cancer Research*. **8**(4): 1172-1181.

Park J.W., Hong K. and Kirpotin D.B. (1997). Immunoliposomes for cancer treatment. *Advances in Pharmacology.* **40**: 399-435.

Peterson G.L. (1977). A simplification of the protein assay method of Lowry et al., which is generally more applicable. *Analitical Biochemistry.* **83**(2):346-356.

Phelps M.E. (2000). PET: the merging of biology and imaging into molecular imaging. N*uclear Medicine.* **41**(4): 661-681.

Poucková P., Zadinová M., Hlousková D., Strohalm J., Plocová D., Spunda M., Olejár T., Zitko M., Matousek J., Ulbrich K. and Soucek J. (2004). Polymer-conjugated bovine pancreatic and seminal ribonucleases inhibit growth of human tumors in nude mice. *Controlled Release.* **95**(1): 83-92.

Ratelade J., Miot M., Johnson E., Betton J., Mazodier P. and Benaroudj N. (2009). Production of recombinant proteins in the lon-deficient BL21(DE3) strain of *Escherichia coli* in the absence of the DnaK chaperone. *Applied and Environmental Microbiology.* **75**: 3803-3807.

Rawstron A.C. (2006). Immunophenotyping of plasma cells. *Current Protocoles in Cytometry*. ISBN 0471142956. Chapter **6**:Unit 6.23.

Reff M.E., Carner K., Chambers K.S., Chinn P.C., Leonard J.E., Raab R., Newman R.A., Hanna N. and Anderson D.R. (1994). Depletion of B cells *in vivo* by a chimeric mouse human monoclonal antibody to CD20. *Blood.* **83**(2): 435-45.

Reimer D.L., Kong S. and Monck M. (1999). Liposomal lipid and plasmid DNA delivery to B16/BL6 tumors after intraperitoneal administration of cationic liposome DNA aggregates. P*harmacology and Experimental Therapeutics*. **289**(2): 807-815.

Riaz M. and Weiner N.D. (1994). Stability of phosphoinosaitdes containing liposomes: effect of Triton X-100, temperature and 68 rpm. *Pakistan Journal of Pharmaceutical Sciences.* **7**(2): 61-68.

Ridley R.C., Xiao H., Hata H., Woodiff J., Epstein J. and Sanderson R.D. (1993). Expression of syndecan regulates human myeloma plasma cell adhesion to type I colagen. *Blood*. **81**: 767-74.

Roth A., Drummond D.C. and Conra, F. (2007). Anti-CD166 single chain antibody-mediated intracellular delivery of liposomal drugs to prostate cancer cells. *Molecular Cancer Therapeutics*. **6**(10): 2737-2746.

Roth P., Hammer C. and Piguet A.C. (2007). Effects on hepatocellular carcinoma of doxorubicin-loaded immunoliposomes designed to target the VEGFR-2. *Drug Targeting*. **15**(9): 623-631.

Sahoo S.K., Ma W. and Labhasetwar V. (2004). Efficacy of transferrin-conjugated paclitaxel-loaded nanoparticles in a murine model of prostate cancer. *International Journal of Cancer.* **112**(2): 335-340.

Sanderson R.D., Lalor P. and Bernfield M. (1989). B lymphocytes express and lose syndecan at specific stages of differentiation. *Cell Regulation*. **1**: 27-35.

Sanderson R.D. and Bernfield M. (1988) Molecular polymorphism of a cell surface proteoglycan: distinct structures on simple and stratified epithelia. *Proceedings of the National Academy of Science of the United States of America.* **85**: 9562-9566.

Sapra P. and Allen T.M. (2002). Internalizing antibodies are necessary for improved therapeutic efficacy of antibody-targeted liposomal drugs. *Cancer Research*. **62**: 7190-7194.

Schaper F., Gendo C. and Eck M. (1998). Activation of the protein tyrosine phosphatase SHP2 *via* the interleukin-6 signal tranducig receptor protein gp130 requires tyrosine kinase Jak1 and limits acute-phase protein expression. *Biochemical Journal*. **335**(3): 557-565.

Schwendener R.A., Wüthrich R., Duewell S., Wehrli E. and von Schulthess G.K. (1990). A pharmacokinetic and MRI study of unilamellar gadolinium-, manganese-, and iron-DTPA-stearate liposomes as organ-specific contrast agents. *Investigative Radiology.* **25**(8): 922-32.

Senior J. and Gregoriadis G. (1982). Is half-life of circulating liposomes determined by changes in their permeability? *FEBS Letters.* **145**(1): 109-14.

Seymour L.W. (1992). Passive tumor targeting of soluble macromolecules and drug conjugates. *Critical Reviews in Therapeutic Drug Carrier Systems*. **9**(2): 135-187.

Sihorkar V. and Vyas S.P. (2001). Potential of polysaccharide anchored liposomes in drug delivery, targeting and immunization. P*harmacy & Pharmaceutical Sciences*. **4**(2): 138-158.

Singh A.K., Kilpatrick P.K. and Carbonell R.G. (1996). Application of antibody and fluorophore-derivatized liposomes to heterogeneous immunoassays for d-dimer. *Biotechnology Progress.* **12**: 272−280.

Siwak D.R., Tari A.M. and Lopez-Berestein G. (2002). The potential of drug-carrying immunoliposomes as anticancer agents. Commentary re: J. W. Park et al., Anti-HER2 immunoliposomes: enhanced efficacy due to targeted delivery. *Clinical Cancer Research.* **8**(4): 955-6.

Smith B.R., Johnson G.A., Groman E.V. and Linney, E. (1994). Magnetic resonance microscopy of mouse embryos. *Proceedings National Academy of Sciences (U S A).* **91**(9): 3530-3533.

Sokolov K., Aaron J. and Kumar S. (2004). Molecular imaging of carcinogenesis with immuno-targeted nanoparticles. *Conference proceedings: Annual International Conference of the IEEE Engineering in Medicine and Biology Society.IEEE Engineering in Medicine and Biology Society.Conference*. **7**: 5292-5295.

Sorensen H.P. and Mortensen K.K. (2005). Advanced genetic strategies for recombinant protein expression in *Escherichia coli*. *Journal of Biotechnology*. **115**: 113-128.

Soucek J., Poucková P., Zadinová M., Hlousková D., Plocová D., Strohalm J., Hrkal Z., Oleár T. and Ulbrich K. (2001). Polymer conjugated bovine seminal ribonuclease

inhibits growth of solid tumors and development of metastases in mice. *Neoplasma.* **48**(2): 127-32.

Soucek J., Pouckova P. and Strohalm J. (2002). Poly[N-(2-hydroxypropyl) methacrylamide] conjugates of bovine pancreatic ribonuclease (RNase A) inhibit growth of human melanoma in nude mice. D*rug Targeting*. **10**(3): 175-183.

Strijkers G.J., Mulder W.J., van Heeswijk R.B., Frederik P.M., Bomans P., Magusin P.C. and Nicolay K. (2005). Relaxivity of liposomal paramagnetic MRI contrast agents. *MAGMA.* **18**(4): 186-92.

Sulkowski W., Pentak D., Nowa, K. and Sulkowska A. (2005). The influence of temperature and pH on the structure of liposomes formed from DMPC. *Molecular Structure.* **792**: 257.

Sun C., Lee J.S. and Zhang M. (2008). Magnetic nanoparticles in MR imaging and drug delivery. *Advanced Drug Delivery Reviews*. **60**(11): 1252-1265.

Szoka Jr. and Paphadjopoulos D. (1978). Procedure for preparation of liposomes with large internal aqueous space and high capture by reverse-phase evaporation. *Proceeding National Academy Science U S A.* **75**(9): 4194-8.

Tolia N.H. and Joshua-Tor L. (2006). Strategies for protein coexpression in *Escherichia coli*. *Nature Methods*. **3**: 55-64.

Tomalia D.A., Reyna L.A. and Svenson S. (2007). Dendrimers as multi-purpose nanodevices for oncology drug delivery and diagnostic imaging. *Biochemical Society Transactions*. **35**: 61-67.

Torchilin V.P. (2007). Targeted pharmaceutical nanocarriers for cancer therapy and imaging. *AAPS Journal*. **9**(2) 128-47.

Torchilin V.P. (2005). Recent advances with liposomes as pharmaceutical carriers. *Nature reviews. Drug Discovery*. **4**(2) 145-160.

Torchilin V.P. (2000). Polymeric contrast agents for medical imaging. *Current Pharmaceutical Biotechnology*. **1**(2): 183-215.

Torchilin V.P., Rammohan R., Weissig V. and Levchenko T.S. (2001). TAT peptide on the surface of liposomes affords their efficient intracellular delivery even at low temperature and in the presence of metabolic inhibitors. *Proceedings of the National Academy of Sciences of the United States of America*. **98**(15): 8786-8791.

Torchilin V.P., Trubetskoy V.S., Milshteyn A.M., Canillo J., Wolf G.L., Papisov M.I. and Bogdanov A.A., Narula A.A., Khawc B.A., Omelyanenko V. (1994). Targeted delivery of diagnostic agents by surface-modified liposomes. *Controlled Release*. **28**(1-3):45-58.

Trubetskoy V.S., Cannillo J.A., Milshtein A., Wolf G.L. and Torchilin V.P. (1995). Controlled delivery of Gd-containing liposomes to lymph nodes: surface modification may enhance MRI contrast properties. *Magnetic Resonance Imaging.* **13**(1): 31-7.

Trubetskoy V.S., Torchilin V.P., Kennel S.J. and Huang L. (1992). Use of N-terminal modified poly(L-lysine)-antibody conjugate as a carrier for targeted gene delivery in mouse lung endothelial cells. *Bioconjugate chemistry*. **3**(4): 323-227.

Tu Y., Gardner A. and Lichtenstein A. (2000). The phosphatidylinositol 3-kinase/AKT kinase pathway in multiple myeloma plasma cells: roles in cytokine-dependent survival and proliferative responses. *Cancer Research.* **60**(23): 6763-6770.

Unger E.C., Winokur T., MacDougall P., Rosenblum J., Clair M., Gatenby R. and Tilcock C. (1989). Hepatic metastases: liposomal Gd-DTPA-enhanced MR imaging. *Radiology.* **171**(1): 81-5.

Unger E., Fritz T., Shen D.K. and Wu G. (1993). Manganese-based liposomes. Comparative approaches. *Investigative radiology*. **28**(10): 933-938.

Vasey P.A., Kaye S.B., Morrison R., Twelves C., Wilson P., Duncan R., Thomson A.H., Murray L.S., Hilditch T.E., Murray T., Burtles S., Fraier D., Frigerio E. and Cassidy J. (1999). Phase I clinical and pharmacokinetic study of PK1 [N- (2 - hydroxypropyl) methacrylamide copolymer doxorubicin]: first member of a new class

of chemotherapeutic agents-drug-polymer conjugates. Cancer Research Campaign Phase I/II Committee. *Clinical Cancer Research.* **5**(1): 83-94.

Qiao J., Li S.L., Wei L., Jiang J., Long R., Mao H., Wei L., Wang L., Yang H., Grossniklaus H.E., Liu Z.R., Yang J.J. (2011). HER2 targeted molecular MR imaging using a *de novo* designed protein contrast agent. *PloS ONE*. **6**(3): e18103.

Wang K., Ruan J., Qian Q., Song H., Bao C., Zhang X., Kong Y., Zhang C., Hu G., Ni J., Cui D. (2011). BRCAA1 monoclonal antibody conjugated fluorescent magnetic nanoparticles for *in vivo* targeted magnetofluorescent imaging of gastic cancer. *Journal of Nanobiotechnology*. **9**: 23.

Wang X., Yang .L, Chen Z.G. and Shin D.M. (2008). Application of nanotechnology in cancer therapy and imaging. *Cancer Journal of Clinicians.* **58**(2): 97-110.

Weissig V.V., Babich J. and Torchilin V.V. (2000). Long-circulating gadolinium-loaded liposomes: potential use for magnetic resonance imaging of the blood pool. *Colloids Surface B: Biointerfaces.* 18(3-4): 293-299.

Weissleder R., Simonova M. and Bogdanova A. (1997). MR imaging and scintigraphy of gene expression through melanin induction. *Radiology*. **204**(2): 425-429.

Wijdenes J., Dore J.M., Clement C. and Vermot-Desroches C. (2002). CD138. *Journal of Biological Regulators and Homeostatic Agents.* **16**(2):152-5.

Wijdenes J., Vooijs W.C., Clément C., Post J., Morard F., Vita N., Laurent P., Sun R.X., Klein B. and Dore J.M. (1996). A plasmocyte selective monoclonal antibody (B-B4) recognizes syndecan-1. *British Journal Haematology*. **94**(2):318- 323.

Winter G. and Harris W. J. (1993). Humanized antibodies. *Immunology Today*. **14**(6): 243-246.

Yang Z., Yang M. and Xiahou G. (2009). Targeted delivery of insulin-modified immunoliposomes *in vivo*. *Liposome Research*. **19**(2): 116-121.

Yoo H.S. and Park T.G. (2004). Folate receptor targeted biodegradable polymeric doxorubicin mic elles. C*ontrolled Release.* **96**(2): 273-283.

Zarabi B., Borgman M.P. and Zhuo J. (2009). Non-invasive monitoring of HPMA copolymer-RGDfK conjugates by magnetic resonance imaging. *Pharmaceutical Research*. **26**(5): 1121-1129.

Zhen Z., Xie J. (2012). Development of manganese-based nanoparticles as contrast probes for magnetic resonance imaging. *Theranostics.* **2**(1): 45-54.